

**SYNTHESIS AND CHARACTERIZATION OF
POLYMERIC COMPOSITE ADSORBENTS FOR THE
REMOVAL OF RADIOACTIVE MATERIALS FROM
WASTEWATER**

MICHAEL ADEKUNLE OLATUNJI

**FACULTY OF SCIENCE
UNIVERSITY OF MALAYA
KUALA LUMPUR**

2017

**SYNTHESIS AND CHARACTERIZATION OF
POLYMERIC COMPOSITE ADSORBENTS FOR THE
REMOVAL OF RADIOACTIVE MATERIALS FROM
WASTEWATER**

MICHAEL ADEKUNLE OLATUNJI

**THESIS SUBMITTED IN FULFILMENT OF THE
REQUIREMENTS FOR THE DEGREE OF DOCTOR OF
PHILOSOPHY**

**DEPARTMENT OF PHYSICS
FACULTY OF SCIENCE
UNIVERSITY OF MALAYA
KUALA LUMPUR**

2017

UNIVERSITY OF MALAYA
ORIGINAL LITERARY WORK DECLARATION

Name of Candidate: **Michael Adekunle Olatunji**

Matric No: **SHC130083**

Name of Degree: **Doctor of Philosophy**

Title of Thesis: **Synthesis and Characterization of Polymeric Composite Adsorbents for the Removal of Radioactive Materials from Wastewater**

Field of Study: **Experimental Physics**

I do solemnly and sincerely declare that:

- (1) I am the sole author/writer of this Work;
- (2) This Work is original;
- (3) Any use of any work in which copyright exists was done by way of fair dealing and for permitted purposes and any excerpt or extract from, or reference to or reproduction of any copyright work has been disclosed expressly and sufficiently and the title of the Work and its authorship have been acknowledged in this Work;
- (4) I do not have any actual knowledge nor do I ought reasonably to know that the making of this work constitutes an infringement of any copyright work;
- (5) I hereby assign all and every rights in the copyright to this Work to the University of Malaya ("UM"), who henceforth shall be owner of the copyright in this Work and that any reproduction or use in any form or by any means whatsoever is prohibited without the written consent of UM having been first had and obtained;
- (6) I am fully aware that if in the course of making this Work I have infringed any copyright whether intentionally or otherwise, I may be subject to legal action or any other action as may be determined by UM.

Candidate's Signature

Date:

Subscribed and solemnly declared before,

Witness's Signature

Date:

Name: Dr. Mayeen Uddin Khandaker

Designation: Associate Professor

ABSTRACT

The research focused on the synthesis of polypyrrole conducting polymer derivatives for the removal of ^{109}Cd , ^{137}Cs and ^{60}Co radionuclides. The polypyrrole-based adsorbents (pure polypyrrole, surfactant-doped polypyrrole, polypyrrole/sawdust composite and polypyrrole/activated carbon composite) were characterized by FESEM, HR-TEM, BET, FTIR, XRD, TG-DTG and Boehm titration methods. All the polypyrrole materials were successfully tested to remove ^{109}Cd , ^{137}Cs and ^{60}Co radionuclides from aqueous solutions. The preliminary investigations revealed that the composite materials have higher removal percentage for the radionuclides than the pure polypyrrole. Comparison of the removal by the composites revealed that the polypyrrole/ activated carbon composite prepared in the presence of anionic surfactant had higher removal percentage for all the radionuclides than the polypyrrole/sawdust composite prepared with or without the anionic surfactant. Consequently, the effect of the experimental variables on adsorption of the radioactive materials were investigated by using composites of surfactant-doped polypyrrole (PPy/SDBS) and surfactant-doped polypyrrole/activated carbon (PPy/SDBS/AC) and the results were compared with that of pure polypyrrole (PPy). For all polypyrrole adsorbents, the effect shows increasing the uptake of the radionuclides with increasing solution pH, initial ion concentration, contact time and temperature, except for ^{109}Cd radionuclide that decreased with increasing the temperature. In all cases, equilibrium adsorption was achieved within 240 min contact time and at a pH of 6. The maximum adsorption capacities were realized with PPy/SDBS/AC composite in order of 35.3 mgCd.g^{-1} , 23.0 mgCs.g^{-1} and 18.1 mgCo.g^{-1} , followed by PPy/SDBS adsorbent in the order of 16.0 mgCd.g^{-1} , 14.2 mgCs.g^{-1} and 13.5 mgCo.g^{-1} and PPy adsorbent in the order of 9.78 mgCo.g^{-1} , 8.96 mgCd.g^{-1} and 6.40 mgCs.g^{-1} , respectively. In the bi-solute adsorption system, the maximum adsorption capacities for the competitive adsorption are ranked as $^{137}\text{Cs} > ^{109}\text{Cd} > ^{60}\text{Co}$. The effect of random irradiation of the as-prepared polypyrrole

adsorbents with 100 and 200 kGy gamma doses on the adsorption capacity showed to be practically negligible, except for the surfactant-doped polypyrrole/activated carbon composite which showed relatively higher sorption capacity. The desorption of the spent polypyrrole-based adsorbents was successful with 0.1 – 1 M HCl, but adsorption by the recycled adsorbents was not successful after 4 cycles.

University of Malaya

ABSTRAK

Kajian ini khusus untuk sintesis polimer polypyrrole derivatif untuk penyingkiran radionuklid ^{109}Cd , ^{137}Cs dan ^{60}Co . Bahan-bahan berasaskan polypyrrole (polypyrrole tulen, polypyrrole didopkan surfaktan, polypyrrole/ komposit habuk papan dan polypyrrole/ diaktifkan komposit karbon) telah disahkan berjaya dihasilkan melalui pencirian oleh FESEM, HR-TEM, BET, FTIR, XRD, TG-DTG dan Boehm kaedah titratan. Semua bahan polypyrrole telah berjaya diuji untuk membuang ^{109}Cd , ^{137}Cs dan ^{60}Co radionuklid daripada air sisa. Siasatan awal mendapati bahawa bahan-bahan komposit mempunyai peratusan penyingkiran yang lebih tinggi bagi radionuklid berbanding polypyrrole tulen. Perbandingan penyingkiran oleh komposit mendedahkan bahawa polypyrrole/ komposit karbon diaktifkan bersama surfaktan anionik mempunyai peratusan penyingkiran yang lebih tinggi untuk semua radionuklid berbanding polypyrrole/ habuk papan yang disediakan dengan atau tanpa surfaktan anionik. Oleh itu, kesan pembolehubah eksperimen pada penyerapan bahan radioaktif telah disiasat dengan menggunakan komposit polypyrrole didopkan surfaktan (PPy/SDBS) dan polypyrrole didopkan surfaktan/ karbon diaktifkan (PPy/SDBS/AC) dan keputusan dibandingkan dengan daripada polypyrrole tulen (PPy). Untuk semua bahan polypyrrole, diperhatikan bahawa pengambilan radionuklid meningkat apabila pH, kepekatan awal ion, putaran / kelajuan pergolakan, masa sentuhan dan suhu meningkat, kecuali ^{109}Cd radionuklid yang menunjukkan penurunan apabila suhu ditingkatkan. Dalam semua kes, penjerapan seimbang telah dicapai dalam 240 minit masa sentuhan dan pada pH 6. Kapasiti penyerapan maksimum dicapai oleh PPy/SDBS/AC komposit dalam susunan 35.3 mgCd.g^{-1} , 23.0 mgCs.g^{-1} dan 18.1 mgCo.g^{-1} , diikuti oleh PPy/SDBS dalam susunan 16.0 mgCd.g^{-1} , 14.2 mgCs.g^{-1} dan 13.5 mgCo.g^{-1} dan PPy dalam susunan 9.78 mgCo.g^{-1} , 8.96 mgCd.g^{-1} dan 6.40 mgCs.g^{-1} . Dalam sistem penjerapan dwi-bahan larut, penjerapan ^{137}Cs telah meningkat dengan kehadiran ^{109}Cd dan ^{60}Co , sedangkan yang kedua-dua itu telah

dihalang dengan kehadiran ^{137}Cs . Kapasiti penjerapan maksimum bagi penjerapan kompetitif disusun sebagai $^{137}\text{Cs} > ^{109}\text{Cd} > ^{60}\text{Co}$. Kesan penyinaran rawak bahan polypyrrole dengan 100 dan 200 kGy dos gamma kepada kapasiti penyerapan secara praktikalnya boleh diabaikan, kecuali polypyrrole didopkan surfaktan/karbon diaktifkan yang menunjukkan kapasiti penyerapan yang lebih tinggi. Penyahjerapan bahan polypyrrole berjaya dilakukan dengan menggunakan 0.1 – 1 M HCl, tetapi penjerapan oleh adsorben dikitar semula tidak berjaya selepas 4 pusingan.

University of Malaya

ACKNOWLEDGEMENTS

All glory to God Almighty for this great achievement. To Him alone be praised forever.

So many people have been involved in getting this far. First in the list is my Supervisor, Assoc. Prof. Dr. Mayeen Uddin Khandaker. I really appreciate your efforts, understanding, love, concern and help in building up my dream to this level. You are indeed great. Special thanks to my Co-supervisor, Assoc. Prof. Dr. Ekramul Mahmud for your unparalleled supports and discussions in understanding the subject matter. Your suggestions and trust in me are really unforgettable. My gratitude also goes to my other Co-supervisor, Prof. Dr. Mohd Yusoff Amin for your care. I cannot forget your kind advice, courage you instilled in me and in particular, the errand you ran in ensuring my working safety with radioactive materials. I say thank you, Prof.

Many thanks to all my colleagues namely: Dr. Asaduzzman Khandoker, Dr. Matthew, Dr. Ahmad Usman, Mr. Farhad Moradi, Dr. Obidul Huq and Mrs. Bemigho Uwatse. Without your understanding and cooperation, it would have been practically impossible to use the radiation detector and other equipment at the right time. Thank you also for the time of useful discussions we shared towards completing our respective research studies.

I want to laud the contributions of the University of Malaya for the research grant giving to me. This research study was conducted under the research grant number PG027-2014A. It would have been very difficult if not for the financial support. Thank you.

My sincere thanks go to my mother, brothers and sisters for their love and understanding throughout this study. In particular, I want to specially thank my brother Engr. Kayode Olatunji for your prayers and financial support during this programme. May God reward you accordingly. To Dr. Felix Adekunjo, I will always be thankful to you for the errand you ran during the admission process. Little did you know that you were my inspiration back then in undergraduate days and it is always a surprise to me that

God continued to use you all through my higher education programmes. You are such an angel of help sent my way in life. One thing I am very sure is that God will not forget the labour of your love. Finally, my special appreciation goes to Dr. Amos Adaraniwon for your role in my life. This column cannot be sufficient to express your contributions to my moral, financial and spiritual life throughout our staying together. You are just wonderful!

University of Malaya

TABLE OF CONTENTS

ABSTRACT	iii
ABSTRAK	v
ACKNOWLEDGEMENTS	vii
TABLE OF CONTENTS	ix
LIST OF FIGURES	xv
LIST OF TABLES	xix
LIST OF SYMBOLS AND ABBREVIATIONS	xxi
LIST OF APPENDICES	xxii
CHAPTER 1: INTRODUCTION	1
1.1 Overview.....	1
1.1.1 Water Pollution.....	2
1.2 Health Risks of Consumption of Radioactive Materials contaminated Water and Foodstuffs	3
1.3 Efforts Towards Remediation of Radionuclides from Environmental Materials	4
1.4 Adsorption technique.....	5
1.5 Polymer-based Adsorbents	5
1.6 Conducting polymers and their composites.....	6
1.7 Research Objectives.....	6
CHAPTER 2: LITERATURE REVIEW	9
2.1 Radioactivity and its Origin in Water	9
2.2 Biological Effects of Human Exposure to Radiation	11
2.2.1 Specific Effects and Properties of Radioactive Materials	12
2.2.1.1 Radioactive cesium	13

2.2.1.2	Radioactive cobalt	14
2.2.1.3	Radioactive cadmium	14
2.3	Liquid radioactive waste treatment techniques.....	15
2.3.1	Adsorption	16
2.4	Factors affecting adsorption process	20
2.4.1	Solution pH.....	20
2.4.2	Temperature.....	21
2.4.3	Initial adsorbate concentration.....	22
2.4.4	Contact time.....	23
2.4.5	Presence of interfering ions	23
2.4.6	Adsorbent dosage	24
2.4.7	Adsorbent surface area and pore size	24
2.5	Categories of adsorbent materials.....	25
2.5.1	Inorganic materials	26
2.5.1.1	Metal oxides	26
2.5.1.2	Clay minerals.....	27
2.5.1.3	Zeolites	28
2.5.1.4	Siliceous materials.....	29
2.5.1.5	Miscellaneous inorganic materials	30
2.5.1.6	Activated carbons (AC).....	31
2.5.1.7	Carbon nanotubes (CNT) adsorbents	32
2.5.2	Agricultural wastes and by-products	33
2.5.3	Biological wastes	34
2.5.4	Industrial wastes	35
2.5.5	Polymeric adsorbents.....	35
2.5.5.1	Natural polymeric adsorbents.....	36

2.5.5.2	Synthetic polymeric adsorbents	38
2.5.6	Polymer composite adsorbents	39
2.5.6.1	Polyethyleneimine-based (PEI) composites.....	39
2.5.6.2	Polyacrylonitrile-based (PAN-based) composites.....	40
2.5.6.3	Conducting polymer-based composites	41
2.6	Desorption and reusability of spent-adsorbent	45
2.7	Adsorption isotherms.....	46
2.7.1	Langmuir isotherm model	47
2.7.2	Freundlich isotherm model.....	48
2.7.3	Dubinin-Radushkevich (D-R) isotherm model.....	49
2.7.4	Temkin isotherm model.....	49
2.7.5	Sips isotherm model	50
2.7.6	Redlich-Peterson (R-P) isotherm model.....	51
2.8	Adsorption kinetic models.....	52
2.8.1	Lagergren First-order/ Pseudo First-order model.....	53
2.8.2	Pseudo Second-order model	53
2.8.3	Intra-particle diffusion model.....	54
2.8.4	Elovich model.....	54
2.9	Adsorption thermodynamics.....	55
2.10	Adsorbent characterization methods.....	56
2.10.1	Fourier Transform Infra-Red (FTIR).....	56
2.10.2	Scanning Electron Microscopy (SEM).....	57
2.10.3	Field Emission Scanning Electron Microscopy (FESEM)	57
2.10.4	Energy-dispersive X-ray Spectroscopy (EDX/EDS).....	58
2.10.5	Transmission Electron Microscopy (TEM).....	59
2.10.6	X-ray diffraction (XRD).....	60

2.10.7	Thermogravimetric (TG) and Differential thermogravimetry (DTG) analysis	61
2.11	Review of adsorption of radioactive materials	63
2.11.1	Multi-solute adsorption	63
2.11.2	Single-solute adsorption	67
CHAPTER 3: RESEARCH METHODOLOGY		72
3.1	Chemicals and Materials.....	72
3.2	Synthesis of polymeric materials.....	73
3.3	Composites of polypyrrole	74
3.4	Characterization of polymeric adsorbent materials	76
3.4.1	Surface characterization and thermal stability.....	77
3.4.2	Surface charge identification	78
3.5	Preparation of radioactive solutions	79
3.6	Adsorption experiments.....	80
3.7	Gamma-ray spectroscopy system	81
3.7.1	Functions of the gamma-ray spectrometer components	83
3.7.2	Shielding.....	84
3.7.3	Detection system calibration	85
3.7.3.1	Energy calibration	86
3.7.3.2	Efficiency calibration	86
3.8	Evaluation of adsorption parameters	88
CHAPTER 4: ADSORBENT CHARACTERIZATION.....		92
4.1	Nitrogen physisorption measurements	92
4.1.1	BET surface area and pore volume.....	92
4.1.2	Nitrogen adsorption/desorption curves.....	94

4.2	Surface morphology by FESEM and HR-TEM.....	98
4.2.1	FESEM analysis	98
4.2.2	HR-TEM analysis	101
4.3	X-ray diffraction (XRD) analysis	102
4.4	FTIR analysis.....	104
4.4.1	PPy104	
4.4.2	PPy/SD composite	106
4.4.3	PPy/AC composite.....	107
4.4.4	PPy/SDBS.....	108
4.4.5	PPy/SDBS/SD and PPy/SDBS/AC composites	110
4.4.6	FTIR of irradiated polypyrrole-based materials	111
4.5	Thermogravimetric analysis	115
4.6	Surface charge titration.....	118

CHAPTER 5: APPLICATION OF POLYPYRROLE-BASED ADSORBENTS

	IN ADSORPTION STUDIES.....	121
5.0	Introduction.....	121
5.1	Preliminary investigation.....	122
5.1.1	Pyrrole to oxidant mole ratios	122
5.1.2	Selection of SDBS concentration for PPy/SDBS	123
5.1.3	Effect of SD/AC mass on adsorption performance of polypyrrole composites	124
5.2	Single-solute adsorption of ¹⁰⁹ Cd, ¹³⁷ Cs and ⁶⁰ Co radionuclides by PPy, PPy/SDBS and PPy/SDBS/AC composites.....	127
5.2.1	Results on effects of pH and contact time	130
5.2.2	Results on effects of initial concentration, temperature and interfering metal ions	137

5.2.3	Results on adsorption kinetic model analysis.....	143
5.2.4	Results on adsorption isotherm model analysis.....	147
5.2.4.1	The plots and results of isotherm models for adsorption of ^{109}Cd radionuclide	148
5.2.4.2	The plots and results of isotherm models for adsorption of ^{137}Cs radionuclide	150
5.2.4.3	The plots and results of isotherm models for adsorption of ^{60}Co radionuclide	152
5.2.5	Thermodynamic parameters for adsorption.....	155
5.2.6	Results of desorption and reusability of spent adsorbents.....	160
5.2.6.1	Desorption	160
5.2.6.2	Reusability of recycled polypyrrole-based adsorbents.....	162
5.2.7	Radiation hardness of polypyrrole-based materials.....	164
5.3	Bi-solute competitive adsorption of radionuclides by PPy/SDBS and PPy/SDBS/AC composites	167
5.4	Evidence of adsorption of radionuclides by polypyrrole-based adsorbents	173
5.4.1	FTIR analysis of polypyrrole-based adsorbents after adsorption.....	174
5.4.2	XRD analysis of polypyrrole-based adsorbents after adsorption	177
CHAPTER 6: CONCLUSIONS AND SUGGESTIONS		181
6.1	Conclusion	181
6.2	Suggestion for further work.....	183
REFERENCES		185
LIST OF PUBLICATIONS AND PAPERS PRESENTED		208
APPENDICES		210

LIST OF FIGURES

Figure 2.1: Basic terms associated with adsorption (Worch, 2012).	19
Figure 2.2: Gas adsorption and pore filling.	19
Figure 2.3: Operating mode of TEM with all its component parts (Al-Nasri, 2013).	60
Figure 2.4: Schematic diagram of TGA (a) and top view of sample pan being loaded into furnace (b) (Al-Nasri, 2013).	63
Figure 3.1: Block diagrams for the chemical synthesis of polypyrrole and its composites used in this study.	76
Figure 3.2: A block diagram of a basic gamma-ray spectroscopy.	82
Figure 3.3: Radiation detector showing lead shielding and interaction that occur from radioactive source.	85
Figure 3.4: Energy of adsorption parameters.	88
Figure 4.1: N ₂ adsorption/desorption isotherms and pore size distribution (inset) of PPy.	96
Figure 4.2: N ₂ adsorption/desorption isotherms and pore size distribution (inset) of PPy/SD composite.	96
Figure 4.3: N ₂ adsorption/desorption isotherms and pore size distribution (inset) of PPy/SDBS.	97
Figure 4.4: N ₂ adsorption/desorption isotherms and pore size distribution (inset) of PPy/SDBS/AC composite.	97
Figure 4.5: FESEM image of pure polypyrrole (PPy) adsorbent.	99
Figure 4.6: FESEM image of polypyrrole/sawdust (PPy/SD) composite.	100
Figure 4.7: FESEM image of SDBS-doped polypyrrole (PPy/SDBS).	100
Figure 4.8: FESEM image of SDBS-doped polypyrrole/activated carbon (PPy/SDBS/AC) composite.	101
Figure 4.9: HR-TEM images of (a) PPy, (b) PPy/SDBS, (c) PPy/SD and (d) PPy/SDBS/AC composite.	102
Figure 4.10: XRD patterns of different polypyrrole-based materials.	104

Figure 4.11: FTIR spectra of PPy for different ratios.	105
Figure 4.12: FTIR spectrum of PPy/SD composite.	107
Figure 4.13: FTIR spectrum of PPy/AC composite.	108
Figure 4.14: FTIR spectra of PPy/SDBS prepared with different concentration of SDBS as in Table 4.1.	109
Figure 4.15: FTIR spectrum of PPy/SDBS/SD composite.	111
Figure 4.16: FTIR spectrum of PPy/SDBS/AC composite.	111
Figure 4.17: FTIR spectra of irradiated PPy at different gamma doses.	114
Figure 4.18: FTIR spectra of irradiated PPy/SD composite at different gamma doses.	114
Figure 4.19: FTIR spectra of irradiated PPy/AC composite at different gamma doses.	115
Figure 4.20: FTIR spectra of irradiated PPy/SDBS/AC composite at different gamma doses.	115
Figure 4.21: TG (green) and DTG (red) results for thermal decomposition of as-prepared polypyrrole-based materials as a function of temperature. ..	118
Figure 5.1: Effect of adsorbent dosage on concentration of (a) ^{109}Cd , (b) ^{137}Cs and (c) ^{60}Co radionuclides.	129
Figure 5.2: Speciation diagrams for radioactive metal ions (a) cadmium, (b) cesium (c) cobalt distribution in the solution as a function of pH.	131
Figure 5.3: Effect of pH on adsorption capacity of ^{109}Cd	134
Figure 5.4: Effect of pH on adsorption capacity of ^{137}Cs	134
Figure 5.5: Effect of pH on adsorption capacity of ^{60}Co	135
Figure 5.6: Effect of contact time on amount of ^{109}Cd adsorbed.	136
Figure 5.7: Effect of contact time on amount of ^{137}Cs adsorbed.	136
Figure 5.8: Effect of contact time on amount of ^{60}Co adsorbed.	137
Figure 5.9: Effect of initial concentration on amount of ^{109}Cd adsorbed.	138
Figure 5.10: Effect of initial concentration on amount of ^{137}Cs adsorbed.	138

Figure 5.11: Effect of initial concentration on amount of ^{60}Co adsorbed.....	138
Figure 5.12: Effect of temperature on amount of ^{109}Cd adsorbed.....	140
Figure 5.13: Effect of temperature on amount of ^{137}Cs adsorbed.....	140
Figure 5.14: Effect of temperature on amount of ^{60}Co adsorbed.....	140
Figure 5.15: Effect of interfering metal ions on amount of ^{109}Cd adsorbed.....	142
Figure 5.16: Effect of interfering metal ions on amount of ^{137}Cs adsorbed.....	142
Figure 5.17: Effect of interfering metal ions on amount of ^{60}Co adsorbed.....	142
Figure 5.18: Plots of adsorption kinetics for ^{109}Cd . The solid and dotted lines show the fitting of theoretical and experimental data.	145
Figure 5.19: Plots of adsorption kinetics for ^{137}Cs . The solid and dotted lines show the fitting of theoretical and experimental data.	146
Figure 5.20: Plots of adsorption kinetics for ^{60}Co . The solid and dotted lines show the fitting of theoretical and experimental data.....	147
Figure 5.21: Plots of adsorption isotherms for ^{109}Cd . The solid and dotted lines show the fitting of theoretical and experimental data.	149
Figure 5.22: Plots of adsorption isotherms for ^{137}Cs . The solid and dotted lines show the fitting of theoretical and experimental data.	151
Figure 5.23: Plots of adsorption isotherms for ^{60}Co . The solid and dotted lines show the fitting of theoretical and experimental data.	153
Figure 5.24: Plot of $\ln K_d$ against T^{-1} for adsorption of radionuclides by PPy.....	158
Figure 5.25: Plot of $\ln K_d$ against T^{-1} for adsorption of radionuclides by PPy/SDBS..	159
Figure 5.26: Plot of $\ln K_d$ against T^{-1} for adsorption of radionuclides by PPy/SDBS/AC.	159
Figure 5.27: Effect of HCl concentration and temperature on the desorption of ^{109}Cd radionuclide.	161
Figure 5.28: Effect of HCl concentration and temperature on the desorption of ^{137}Cs radionuclide.....	162
Figure 5.29: Effect of HCl concentration and temperature on the desorption of ^{60}Co radionuclide.	162

Figure 5.30: Effect of recyclability and reusability of the adsorbents on ^{109}Cd adsorption.....	163
Figure 5.31: Effect of recyclability and reusability of the adsorbents on ^{137}Cs adsorption.....	164
Figure 5.32: Effect of recyclability and reusability of the adsorbents on ^{60}Co adsorption.....	164
Figure 5.33: Effect of gamma-irradiation of polypyrrole-based adsorbents on ^{109}Cd adsorption.	166
Figure 5.34: Effect of gamma-irradiation of polypyrrole-based adsorbents on ^{137}Cs adsorption.....	166
Figure 5.35: Effect of gamma-irradiation of polypyrrole-based adsorbents on ^{60}Co adsorption.....	166
Figure 5.36: Plots of bi-solute competitive adsorption of (a) $^{109}\text{Cd}/^{137}\text{Cs}$, (b) $^{109}\text{Cd}/^{60}\text{Co}$ and (c) $^{137}\text{Cs}/^{60}\text{Co}$ by PPy/SDBS.....	169
Figure 5.37: Plots of bi-solute competitive adsorption of (a) $^{109}\text{Cd}/^{137}\text{Cs}$, (b) $^{109}\text{Cd}/^{60}\text{Co}$ and (c) $^{137}\text{Cs}/^{60}\text{Co}$ by PPy/SDBS/AC.	170
Figure 5.38: The relationship between measured and predicted equilibrium sorption capacities from competitive Langmuir model (a) PPy/SDBS and (b) PPy/SDBS/AC.	173
Figure 5.39: FTIR of PPy after adsorption.....	174
Figure 5.40: FTIR analysis of PPy/SDBS after adsorption.	176
Figure 5.41: FTIR analysis of PPy/SDBS/AC after adsorption.....	177
Figure 5.42: XRD patterns of PPy adsorbent (a) before adsorption, (b) after ^{109}Cd adsorption, (c) after ^{137}Cs adsorption and (d) after ^{60}Co adsorption.....	178
Figure 5.43: XRD patterns of PPy/SDBS (a) before adsorption, (b) after ^{109}Cd adsorption, (c) after ^{137}Cs adsorption and (d) after ^{60}Co adsorption.....	179
Figure 5.44: XRD patterns of PPy/SDBS/AC (a) before adsorption, (b) after ^{109}Cd , (c) after ^{137}Cs adsorption and (d) after ^{60}Co adsorption.....	180

LIST OF TABLES

Table 1.1: Categories of water pollutants and their forms.	3
Table 2.1: Radioactive Waste Classification (IAEA, 1999).	11
Table 3.1: Energy of the radionuclides with corresponding efficiency.	87
Table 4.1: Preparation of polypyrrole and composites, pore volume distribution and surface area measurements.....	94
Table 4.2: The acidity and basicity of surface functional groups on AC and PPy/SDBS/AC composite.	120
Table 5.1: Adsorption performance of PPy prepared with different ratios of pyrrole to oxidant.....	123
Table 5.2: Effect of SDBS concentration on % removal of ¹⁰⁹ Cd, ¹³⁷ Cs and ⁶⁰ Co radionuclides by PPy/SDBS.....	124
Table 5.3: Adsorption performance of polypyrrole composites prepared with SD, AC and SDBS.	126
Table 5.4: Optimized adsorbents production conditions for higher adsorption performance.....	126
Table 5.5: Adsorption kinetic model parameters for ¹⁰⁹ Cd radionuclide.....	144
Table 5.6: Adsorption kinetic model parameters for ¹³⁷ Cs radionuclide.	144
Table 5.7: Adsorption kinetic model parameters for ⁶⁰ Co radionuclide.....	144
Table 5.8: Langmuir and Freundlich parameters for adsorption of ¹⁰⁹ Cd radionuclide.....	149
Table 5.9: Langmuir and Freundlich parameters for adsorption of ¹³⁷ Cs radionuclide.....	151
Table 5.10: Langmuir and Freundlich parameters for adsorption of ⁶⁰ Co radionuclide.	153
Table 5.11: Estimated values of thermodynamic parameters for adsorption of radionuclides by PPy at different temperature.	157
Table 5.12: Estimated values of thermodynamic parameters for adsorption of radionuclides by PPy/SDBS at different temperature.	157

Table 5.13: Estimated values of thermodynamic parameters for adsorption of radionuclides by PPy/SDBS/AC at different temperature.....	158
Table 5.14: Desorption results of ^{109}Cd , ^{137}Cs and ^{60}Co radionuclides from spent polypyrrole-based adsorbents.	161
Table 5.15: Langmuir model parameters for bi-solute competitive adsorption of ^{109}Cd , ^{137}Cs and ^{60}Co radionuclides.	168
Table 5.16: Comparison of q and b values for single-solute and bi-solute competitive adsorption.	171
Table 5.17: Statistical parameters for bi-solute competitive adsorption predictions for competitive Langmuir model (CLM) proposed by Butler-Ockrent.....	173

University of Malaya

LIST OF SYMBOLS AND ABBREVIATIONS

γ	:	Gamma-ray
D	:	Crystallite size
λ	:	Wavelength
β	:	Line broadening at half the maximum intensity (FWHM)
θ	:	Bragg angle (in degree)
nm	:	Nanometer
m	:	Meter
pm	:	Picometer
ml	:	Milliliter
L	:	Liter
g	:	Gram
mg	:	Milligram
Bq	:	Becquerel
s	:	Second
Å	:	Armstrong
Pa	:	Pascal
K	:	Kelvin
°C	:	Degree Celsius
J	:	Joule
c	:	Speed of light

LIST OF APPENDICES

Appendix A: Certificate of γ -ray calibration standard source.....	210
Appendix B: Calculation of initial radioactivity of ^{109}Cd , ^{137}Cs and ^{60}Co radionuclides in wastewater.....	211
Appendix C: Examples of adsorption efficiency (%) and sorption capacity (mg/g) estimation using PPy adsorbent.....	214
Appendix D: Boehm's titration curves and calculations.....	219
Appendix E: FESEM and HR-TEM images of adsorbents.....	227
Appendix F: Plots of free energy against temperature.....	232

CHAPTER 1: INTRODUCTION

1.1 Overview

Water is an essential element for life and forms about 65 % of human body constituents (Saad, 2013). In the planet earth, water is the most abundant natural resource covering up to 70 % of its surface and that makes the earth as the only planet that has the right to sustain life on its own. Surprisingly, as abundant as water is on the earth, lack of access to safe and drinking water is the most long-time challenge the world is facing. In 1817, Samuel Taylor Coleridge referred to the problem of safe water in his famous poem (The Rime of the Ancient Mariner) by saying “*water, water, everywhere, nor any drop to drink,*”. Among many factors, rapid population growth, climate change and intensive industrial development are some of the leading causes of clean water shortage today (UN, 2012; Juilong, 2014). This is due to the fact that water resource is almost present everywhere, close to us, but only 3 % of this is available as clean and that can be used. Unfortunately, this percentage (3 %) is also not readily available for usage, it exists either as ice or snow. Till date, less than 1 % of the world’s fresh water e.g. rivers and lakes (that is about 0.007 % of the earth’s water) is available for direct usage (Juilong, 2014) and around 90 % of the earth’s water is in the form of salty water (Schwarz et al., 1990). The available water cannot meet the demand pose by the growing population which is currently over seven billion and estimated to reach ten billion in 2040 (UN, 2004) and, water need of the industries. The world is currently experiencing over utilization of available water. As it stands, the highest percentage of natural water resource found in ocean is not suitable for direct use because of pollution. And it was recently reported that more than half of the world population will be faced with the problem of safe water scarcity by 2025 (Zhao et al., 2010). This is where issues of water pollution, waste treatment and/ or storage started gaining great attentions to researchers from the health

point of view for environmental protection and conservation, if life must be sustained in the earth.

1.1.1 Water Pollution

Water pollution is the major issue confronting the use of abundant natural freshwater in the world for decades. Various ecological and societal activities of the modern age comprising of economics, industrial and agricultural developments form the basis for huge volume of wastes that pollute our water bodies. Chemical producing industries such as petrochemical, metallurgy, fertilizer etc produce a large volume of organic and inorganic wastes during production of synthetic chemicals, storage and consumption (Juilong, 2014). Oil spillage by petroleum industries during transportation contributes substantially to water pollution of the present world. Other activities involving applications of radioisotopes in medicine, agriculture and scientific research such as testing of nuclear weapons, nuclear power generation, reprocessing or nuclear fuel cycle, mining and milling of mineral ores, leather tanning, combustion of fossil fuels form another pathway to water pollution today (UNSCEAR, 2000). Many of the wastes generated from these industrial activities are still being released indirectly into the environment without treatment or by accidental discharge. Underground storage of waste solutions has also contributed significantly to water pollution, because some of the storage tanks are usually leaked and thereby release their contents into the underground water. For instance, about 53 million gallons of high-level radioactive wastes generated by the United States department of energy which is stored underground at the Hanford site are believed to have leaked, contributing to water and environmental pollution (Steeffel et al., 2003). The various water pollutants are classified into three categories based on their forms as seen in Table 1.1. These are the main contributors to natural ecosystem degradation. However, the research focuses on the contribution of radioactive wastes to water pollution and their removal from the aqueous solution.

Table 1.1: Categories of water pollutants and their forms.

Category of pollutants	Effluents	Main Source
Organic	Contain solutions such as dye, grease, plasticizers, drug residues, phenols, oil, dissolved organic matter, sediment, excess nutrients, fossil fuel combustion by-products, detergent, hydrocarbons etc	Industries such as Painting, rubber production, agriculture, textile, dyeing, leather tanning, printing, plastics, food processing, domestic sewage, pharmaceutical
Inorganic	Various industrial wastes such as heavy metals, bromate, surfactants, ammonia, perchlorate etc	Synthetic chemical industries, mineral ores exploitation, petroleum industries
Radioactive	Primarily exist as fission products of nuclear effluents, medical/ patient effluents, electronic waste solution etc	Scientific research, nuclear plants, medical diagnosis, laundry, military activities, petroleum industries, reprocessing of spent fuel

1.2 Health Risks of Consumption of Radioactive Materials contaminated Water and Foodstuffs

Radioactive substances are toxic, hazardous and non-biodegradable once they are released into the environment. Both radioactive and non-radioactive forms of cesium, cobalt, cadmium, strontium and europium are of particular concern because they are common in waste effluents from different industrial activities. Their easy migration within the liquid, soil and airborne dust particles makes them difficult to control or manage and hence, can easily harm human health, animal, vegetal life and even affect our economy (Eisenbud and Gesell, 1997; Real et al., 2004). Food chain is the main pathway through which these elements get to human and animals and once they are consumed, they can build up to a higher concentration in the human body causing many health dysfunctions. Their radioactive forms are fission products from the use of nuclear fuels

and are directly released during diagnoses and treatments of patients in nuclear medicine. Apart from these sources, accidents such as the earthquake and tsunami also could cause huge damage to the nuclear plants, which results into the release of these radionuclides into the environment (example is the recent Fukushima nuclear accident of March 11, 2011 that released a huge amount of ^{134}Cs , ^{137}Cs and so on). They are also released during industrial and agricultural applications. Their health effects can be carcinogenic and mutagenic in nature. In addition to radioactive contamination, they cause heavy metal contamination and poisoning, because radionuclides convert to stable heavy metal ions when they decay to steady states. Due to their specific properties, such as high characteristic energies, long half-lives and their interaction with biological systems, the public exposure to these radioactive elements from all sources have been limited to 0.01 mSv/yr (UNSCEAR, 2008).

1.3 Efforts Towards Remediation of Radionuclides from Environmental Materials

The practice of keeping the radioactive waste materials in lead covered rooms until the radioactive materials decay to stable forms has become outdated, following the increasing rate of radioactive waste accumulation in environment (Eroglu et al., 2009). Today, it is acknowledged that removal from waste streams is the only effective approach to prevent degradation of our natural ecosystem by radioactive materials.

Hence, ion-exchange, precipitation, reverse osmosis, coagulation/flocculation, liquid extraction, electric-field-assisted and adsorption techniques have been developed and used. However, some of these techniques have been impeded by a lot of factors including complexity of operation requirements, longevity of operation time, secondary contamination, cost of operation and maintenance, high cost of materials, and mostly lack of efficiencies for low-level radioactivity removal. Instead, adsorption technique is

considered as more feasible, economic and environmental friendly for large volume reduction of low-level liquid wastes.

1.4 Adsorption technique

Adsorption technique is a worldwide and acceptable technique, credited with excellent decontamination of low-level liquid radioactive wastes (LLRW). The fact that, there are many available materials for adsorbents unlike in other techniques, makes it a choicer technique for different stakeholders. Materials such as inorganic, biological, industrial wastes, agricultural wastes and polymers have enjoyed wider applications as adsorbents for radioactive and heavy metal removal from waste streams. However, the fine particulate nature and inconvenient separation procedures of most adsorbents from solutions limit their extensive use. On the other hand, polymers are easy to separate and also regarded as low-cost, and have been gaining attention as adsorbents in LLRW treatment, due to their non-toxicity and long-term stability. In the current study, adsorption by polymer-based materials has been investigated for the removal of radioactive materials from the wastewater.

1.5 Polymer-based Adsorbents

Several polymers are in use as adsorbents for adsorption of radioactive and heavy metal ions from wastewater. These polymers can be broadly classified into two groups, which are natural and synthetic polymers. The main challenge with the use of natural polymers as adsorbents is that they dissolve in both organic and inorganic acids to become viscous and hence, they are limited in use for metal ion removal from solution (Wang et al., 2009). On the contrast, the synthetic polymers which can also be classified into non-conducting polymers and conducting polymers are convenient to use, because they are stable in both organic and inorganic acids and in environment. Among the synthetic polymers, conducting polymers have found an increasing research attention, due to their

particular physico-chemical properties, they are considered as a new dimension in environmental remediation of pollutants and besides, they are easy to separate from solution after use with simple filtration method (Huang et al., 2014).

1.6 Conducting polymers and their composites

Polyaniline, polypyrrole, polyacetylene and polythiophene are the most common conducting polymers, but in terms of synthesis, doping and dedoping process, polypyrrole is economical and eco-friendly over other conducting polymers. Although contain surface amino functional groups which have possibility to coordinate with different metal ions, pure polypyrrole particles have low sorption capacity for metal ions, due to the easy agglomeration and less water dispersion (Bai et al., 2015; Chen et al., 2016). However, different surface functional materials can be used with polypyrrole to form composite materials that can yield higher sorption capacity for metal ions. In recent time, materials such as sawdust, natural and synthetic zeolite, clays, silica, coal and agricultural or biological byproducts are the commonly used components with polypyrrole or other conducting polymers (Huang et al., 2014). Despite the previous efforts, till now, development of polypyrrole composite adsorbents that have high surface area and rich surface functional groups, such that can result in higher sorption capacities and convenient separation procedures are still much anticipated for metal ions removal.

1.7 Research Objectives

As mentioned in the foregoing, water pollution is a major challenge facing adequate safe water supply to the world population and also responsible in parts, to the degradation of natural ecosystem. When industrial waste effluents are discharged into the ocean, sea, river and soil without prior treatment, it disrupts the self-cleansing capacity of these natural water resources and thereby causing the collapse of the aqueous ecosystem. In particular, to health of man and animal, when the contents of these waste-effluents are

released into the water bodies and soil, they become accessible via food chain. Both radioactive and non-radioactive elements are among the most significant pollutants constituting major problems to life and therefore, must be removed from their aqueous solution because they are toxic, harmful and non-biodegradable. The fact that these radioactive elements decay to stable metal ions which is another source of serious water pollution makes another reason for their urgent removal from solution. To do this, novel conducting polymer-based materials were developed and investigated as adsorbents for the removal of ^{109}Cd , ^{137}Cs and ^{60}Co radionuclides from wastewater, as a model for the removal of radioactive materials from low-level radioactive waste solutions.

The main objectives of the study are to:

1. Synthesize polypyrrole and polypyrrole-based composite materials in the presence of anionic surfactant, sawdust and activated carbon using ferric chloride hexahydrate as oxidant.
2. Characterize the as-prepared polypyrrole-based materials using BET, FESEM, FTIR, TG-DTG and XRD techniques.
3. Study the single-solute adsorption of ^{109}Cd , ^{137}Cs and ^{60}Co radionuclides under various experimental conditions such as adsorbent precursors' ratio, adsorbent dose, solution pH, contact time, temperature and interfering metal ions.
4. Model the adsorption process (that is, isotherm, kinetics and thermodynamics) based on the third objective.
5. Study the bi-solute adsorption of $^{109}\text{Cd}/^{137}\text{Cs}$, $^{109}\text{Cd}/^{60}\text{Co}$ and $^{137}\text{Cs}/^{60}\text{Co}$ radionuclides using Competitive Langmuir Model (CLM).
6. Investigate the effect of gamma-ray exposures on the adsorption capacity of the polypyrrole composite materials.

7. Perform desorption and reusability studies on the used polypyrrole composite adsorbents.

University of Malaya

CHAPTER 2: LITERATURE REVIEW

2.1 Radioactivity and its Origin in Water

The term radiation applies to the emission and propagation of energy through space or a material medium. In other words, radiation is a packet of photons which travel from one point to another in the form of electromagnetic waves. It is natural and all around us; it comes up from the ground, down through the atmosphere, and even from within our own bodies, it can be man-made too (US EPA, 2007).

Matter is composed of atoms; some atoms are unstable. As unstable atoms change and become more stable, they give off invisible energy in the form of waves or particles called radiation. This process is called radioactivity, which can be defined as a phenomenon in which radiation is given off by the nuclei of the element. Radioactivity could be natural or artificial. The elements formed by the process are called radionuclides.

In a pristine environment, it is estimated that 87% of the radiation to which humans are exposed is from natural sources and the remaining is due to human encroachment, otherwise known as artificial radiation (UNSCEAR, 2008). The natural radioactivity being from the very long-lived (in order of about 10^{10} years) naturally occurring radioisotopes of uranium, thorium and potassium. There are different sources of radiation; the earth is the very primary source of radiation. The natural radioactivity of the earth is in different categories. The first is the primordial radionuclides and they are very much abundant in the marine environment and in the mineral ores in the rock. Their existence is traceable to the origin of earth with sufficiently long half-lives that they have remained since their creation. Nearly all of the radioactive material in the ocean is natural, and represents material that has been on earth since its formation. The second category is termed cosmogenic radionuclides, which are continuously produced by the bombardment

of stable nuclides by cosmic rays, primarily in the atmosphere. Secondary radionuclides are derived from radioactive decay of the primordial.

On the other hand, industrialization and technological advancement of the modern age, involving applications of radioisotopes in medicine, agriculture, scientific investigations, nuclear power generation, reprocessing or nuclear fuel recycle represent the artificial sources of radioactivity in human environment (UNSCEAR, 2000). The rate of radioactive wastes generated by countries varied depending on the scale of applications and range of activity associated with nuclear and radioactive material utilization (Abdel-Rahman et al., 2011a). Basically, there is no exact data on the amount of radioactive wastes released by various processes in the environment and so, affects the selection of its different management options owing to its shielding demands. At present, radioactive wastes are classified according to activity and half-life, based on a lot of perspectives such as safety, physical/ chemical characteristics, process engineering demand and regulatory issues (Abdel-Rahman et al, 2011b). This classification is very helpful throughout of their management phases from the generation through collection, segregation, treatment, conditioning, storage to transportation to final disposal (Abdel-Rahman et al., 2011a). The classification is shown in the Table 2.1. Once these radioactive wastes are discharged into the water bodies and soils, they become very difficult to clean up because of their behaviors in the environmental compartments, and that is why treatment assumes a very important place in radioactive wastes management.

Table 2.1: Radioactive Waste Classification (IAEA, 1999).

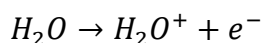
Waste classes	Typical characteristics
Exempt waste (EW)	Activity levels at or below clearance levels, based on an annual dose to members of the public of less than 0.01 mSv
Low- and intermediate-level waste (LILW)	Activity levels above clearance levels and thermal power below about 2 kW/m ³
Low- and intermediate-level waste short-lived (LILW-SL)	Restricted long-lived radionuclide concentrations (limitation of long-lived alpha emitting radionuclides to 4,000 Bq/g in individual waste packages and to an overall average of 400 Bq/g per waste package)
Low- and intermediate-level waste long lived (LILW-LL)	Long-lived radionuclide concentrations exceeding limitations for short lived wastes
High-level wastes (HLW)	Thermal power above 2 kW/m ³ and long-lived radionuclide concentrations exceeding limitations for short lived waste.

2.2 Biological Effects of Human Exposure to Radiation

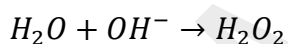
When radiation passes through a cell, a change of event takes place. The first stage known as the physical stage occurs through interaction with cells and tissues. Chemical changes are produced through the processes of excitation and ionization, which cause subsequent molecular damage in a short period of time. It is after a long period of time (hours, days or months) that the molecular or biological damage becomes evident. The destructive effects of radiation are through direct damage to critical bio-molecule and indirectly through the production of a sequence of toxic reactive species that are not in equilibrium. The cell DNA is the critical target for radiation damage since it is the molecule that is responsible for cellular integrity and there's no substitute for DNA in the cell.

Majority of the reactive species responsible for indirect damage to DNA are formed from radiolysis of water, since 80 % of the cell constitutes water. When a cell is irradiated,

it emits a free electron and produces a positively charged water ion, which immediately decomposes into hydrogen ion (H^+) and hydroxyl free radical (OH^-).



The hydroxyl free radical is a highly reactive and powerful oxidation agent, which produces chemical modifications in soluble organic molecules. There may be recombination within the tract to either produce new damaging molecules such as hydrogen peroxide (H_2O_2) or harmless molecules such as water or hydrogen gas.



The radicals produced have the ability to move away from the track by diffusion and can initiate chemical reactions that cause cellular damage.

The cell damage can occur either by producing lesion in solute molecules directly (for example, by rupturing the covalent bond) or by indirect action between the solute molecules and the free radicals produced during ionization of water. This can lead to cell death (it may be deterministic or non-stochastic effect) or cellular transformation (stochastic effect— some of the damaged cells may be repaired).

2.2.1 Specific Effects and Properties of Radioactive Materials

There are many radioactive materials that can be found in the environment, particularly in aqueous media. Their level of radioactivity depends on many factors including the background radioactivity level and the human activities involving production and

applications of radioactive materials. Since this study focuses on radioactive cesium, cobalt and cadmium hence, their specific properties, sources and health effects are considered briefly in the subsequent sections.

2.2.1.1 Radioactive cesium

Cesium represents one of the common hazardous substances creating adverse effects on human health and environment. Its stable form can be transferred to liquid wastes especially those emanated from extractive oil industry. It is a very reactive alkaline metal and can easily be adsorbed to the body like potassium and distributed into the soft tissues of the whole body (Holleman et al., 1985; Lin et al., 2001; Nilchi et al., 2011a). Thyroid cancer is one of the terrible consequences of this metal adsorption (Sangvanich et al., 2010). Its acute poisoning causes medullar dystrophy, asthma, allergy, heart problems, disorders in reproductive function and bone mineralization, liver damages and mutagenic effects (Olatunji et al., 2015). Out of its 39 known isotopes, ^{134}Cs , ^{135}Cs and ^{137}Cs are of significant concern which form major fission products contained in the wastes released into the environment from the leaks of nuclear reactors (which has resulted into dangerous nuclear disaster such as Fukushima Daiichi of 2011), reprocessing of nuclear fuels or PUREX (Plutonium Uranium Reduction Extraction) process, nuclear weapon testing and radionuclides production facilities for medical applications. In particular, ^{137}Cs a gamma-emitter due to its physical (long half-life, $T_{1/2} = 30.17$ y; intense gamma ray's emission, $E_{\gamma} = 661.7$ keV and heat output of 0.42 W/g) characteristics, is responsible for large source of radioactivity in spent nuclear fuel from several years of cooling up to several hundred years after use (Raut et al., 2013; Zerriffi, 2000). And, due to its chemical (high solubility/ mobility) characteristics, could easily be transferred to the food chain when use in agriculture and medicine for food and medical accessories sterilization and in sewage sludge treatment. The decay of ^{137}Cs radionuclide produces barium, forming

another source of pollution by heavy metal. As a result, the admissible level of ^{137}Cs in drinking water has been set at 10 Bq/L to reduce exposure (WHO, 2008).

2.2.1.2 Radioactive cobalt

Although cobalt possesses some importance in diet, its increasing applications in various industries such as petrochemical, metallurgical, electroplating, and electronic industries could bring about contamination of both underground and surface waters, which may result into overexposure. It has been linked to cardiomyopathy, asthma, pneumonia, diarrhea, paralysis, low blood pressure, neurotoxicological symptoms etc. (Shahat et al., 2015; Parab et al., 2010; Lauwerys & Lison, 1994). Excluding the 4 meta-stable states, a total of 22 radioisotopes of cobalt have been characterized so far. Among them, ^{60}Co forms the major hazardous radionuclide that can easily be transferred to the medium of our environment from its various usage such as in medical therapy, x-ray welding and flaw detections in industries. Considering its long half-life ($T_{1/2}=5.2714$ y), specific activity (1100 Ci/g) and intense gamma emissions ($E_{\gamma}=1173.2$ and 1332.5 keV), it can induce cancer upon absorption by liver, kidney or any body tissues. When ^{60}Co decays, it releases nickel, forming a secondary source of contamination. As a result, different national and international Organizations have set admissible limits for cobalt ion in drinking water, US EPA sets limit at 0.1 mg/L and 1 mg/L by New Zealand (Gebrekidan & Samuel, 2011), while WHO sets limits of ^{60}Co at 100 Bq/L (WHO, 2008).

2.2.1.3 Radioactive cadmium

Nuclear plant operation, painting, fertilizer, smelting and refining of zinc, copper and lead ores, plastic stabilizers, nickel-cadmium batteries and electroplating industries form parts of the sources of cadmium contamination in the water. Cadmium is readily accumulated in many organisms, notably molluscs and crustaceans and in vegetables, cereals and starchy roots (WHO, 2010). Upon consumption above limiting index, it can

cause high blood pressure, osteoporosis and destruction of testicular tissue. Itai-itai, a bone degeneration disease outbreak of 1955 in Japan was attributed to cadmium consumption in food (Taty-Costodes et al., 2003; Kalkan et al., 2013). Cadmium has nine major radioactive isotopes, of which only three: cadmium-109, cadmium-113 and cadmium-113m have half-lives long enough to warrant potential concern (Olatunji et al., 2016). Among them, ^{109}Cd is a short-lived radioisotope ($T_{1/2} = 1.3$ yrs), and once produced, it decays to the stable ^{109}Ag via an $\text{EC} + \beta^-$ process followed by the emission of energetic gamma rays ($E_\gamma = 88.0336$ keV; $I_\gamma = 3.70\%$). So, when it is dispersed into the environment from any sources, its activity will be remaining for at least 10 yrs (~ equal to 8 half-lives). Moreover, the very high specific activity (2600 Ci/g) of ^{109}Cd made it more concern for health when ingested. Hence, the admissible level of ^{109}Cd in drinking water is set at 100 Bq/L for health safety (WHO, 2008).

All these justify the need for expedite action in order to remove the harmful contents of liquid radioactive wastes before disposal to environment or other repositories.

2.3 Liquid radioactive waste treatment techniques

Previously in nuclear science and medicine, the common precautionary approach to remove the harmful effects of radioactive materials from the environment is to keep them in lead safe. However, this method is rather unsuitable or not very much practical because it is slow, expensive and time-consuming (Eroglu et al., 2009).

Considering the longtime requirement for a radionuclide to become stable and cost involvement in building lead covered rooms for enormous radioactive waste-effluents being generated, it is much preferred to remove radioactive materials from their waste-effluents. Because of the strict requirements connected with the limits of radioactive substances and other impurities (suspended particulates, bio-foulants and organic or inorganic chemicals) before the waste-effluents can be safely discharged to the

environment, different treatment techniques including volume reduction and reduction of radioactive compounds and other solutes are normally implemented. The following are some of the techniques that have been found suitable for liquid radioactive waste treatment:

- ❖ Chemical precipitation
- ❖ Coagulation and flocculation
- ❖ Ion exchange
- ❖ Solvent extraction
- ❖ Membrane technologies which include reverse osmosis and microfiltration
- ❖ Electrosorption
- ❖ Adsorption

Depending on the nuclear activities, national regulatory framework demands and economic status of the various countries, the techniques can be combined to ensure total removal of the radioactive substances before disposal (IAEA, 2003). However, among the various techniques, adsorption technique is a worldwide and acceptable technique, credited with excellent decontamination performance. In the current study, adsorption technique has been investigated for the removal of radioactive materials from the wastewater.

2.3.1 Adsorption

The present study concerns the use of adsorption technique. This is a technique by which a substance is removed or accumulated on the immobile solid from its fluid phase surrounding, and usually referred to as liquid-solid or gas-solid interaction depending on the type of substance. The solid material that provides the surface for the adsorption of the substance is called the adsorbent while the substance is referred to as the adsorbate. These and other terms associated with adsorption process are represented in Figure 2.1.

Because the process occurs at the surface of the adsorbent, it is sometimes called a surface-phase transfer phenomenon (Gupta & Suhas, 2009). Adsorption occurs also as a natural process in different environmental compartments when natural solid materials is in contact with aqueous phase.

Adsorption can take different dimensions, if the process is initiated as a result of weak intermolecular forces (such as Van der Waals interactions, π - π stacking interactions, dispersion forces etc.) (Pignatello, 2011), then it is specifically called physisorption or physical adsorption. The fact that the intermolecular forces are weak in nature, makes adsorption process reversible, which means that the adsorbate can be obtained by a reverse process called desorption under suitable conditions (eluent agents, pH, temperature and so on). Based on its features, physisorption process ensure the preservation of the adsorbate identity on desorption, which also makes the process an important consideration where the adsorbates are required to be recovered from the aqueous solution.

Gas adsorption is a typical of physical adsorption which was initially described in 1930s in Langmuir's theory of monolayer adsorption but latter extended to multilayer adsorption by Brunauer, Emmett and Teller (BET), due to the influence of increased gas pressure on adsorption of gas by the adsorbent. Low activation energy is required to control physical adsorption. Figure 2.2 illustrates gas adsorption on the surface of the adsorbent and the filling of the pores. On the other hand, removal of adsorbate by the adsorbent can occur due to the formation of chemical bonds between the molecules of the adsorbate and the adsorbent and that is called chemisorption or chemical adsorption. In such a case, the adsorbate cannot freely move due to many functional groups in the active sites interacting with the adsorbate and most times, the interaction produces new chemical bonds with the adsorbate, which makes the identity of the latter to be lost. Chemical

adsorption proceeds favourably only at elevated temperatures owing to the activation barriers, but the attraction forces binding the adsorbate to the adsorbent are very strong, which makes desorption very difficult (Pignatello, 2011). Chemical adsorption is closely related to ion exchange process. On its part, ion exchange is a reversible chemical process in which an ion from solution exchanges with similarly charged ion attached to the adsorbent, the solid particle. Due to their common features, adsorption and ion exchange are sometimes grouped together as sorption processes for effective sequestration of toxins from waste/drinking waters (LeVan et al., 1997; Clifford, 1999). The two processes are frequently encountered in environmental systems than does the chemical process.

Adsorption is recognized as an effective and economic method for the removal of a multiplicity of solutes compared to the other approaches, owing to a number of reasons. These include; the ease of design and operation, adsorbate-specificity, better treatment with no/little secondary waste generation, it is the only effective method for low-level radioactive and non-radioactive wastewater treatment, high efficient performance, ease of regeneration and reuse of adsorbent, suitability for both batch and column studies, the availability of the adsorbents and low-cost of the operation (Zakharchenko et al., 2012). All these and many other advantages make adsorption a leading technique in wastewater treatment and the same reasons, justify its application in the current study.

Normally, a good adsorbent must have good kinetic properties. This means that, it should be able to transfer large adsorbing molecules rapidly to the adsorbent sites. In addition, a suitable adsorbent must also have good macroporous structure and be stable under chemical, mechanical, radiation and thermal reaction conditions. The adsorbent materials and/ or adsorbent precursors should be readily available and the cost of procurement should be very reasonably low, to be considered as good adsorbents. However, the behaviour and efficiency of adsorbents can also be influenced by the

condition of the wastewater to be treated and that can affect the sorption characteristics of the adsorbate by a particular adsorbent.

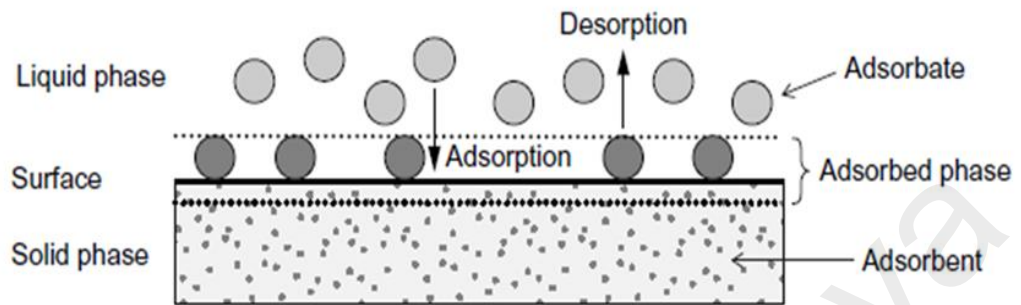


Figure 2.1: Basic terms associated with adsorption (Worch, 2012).

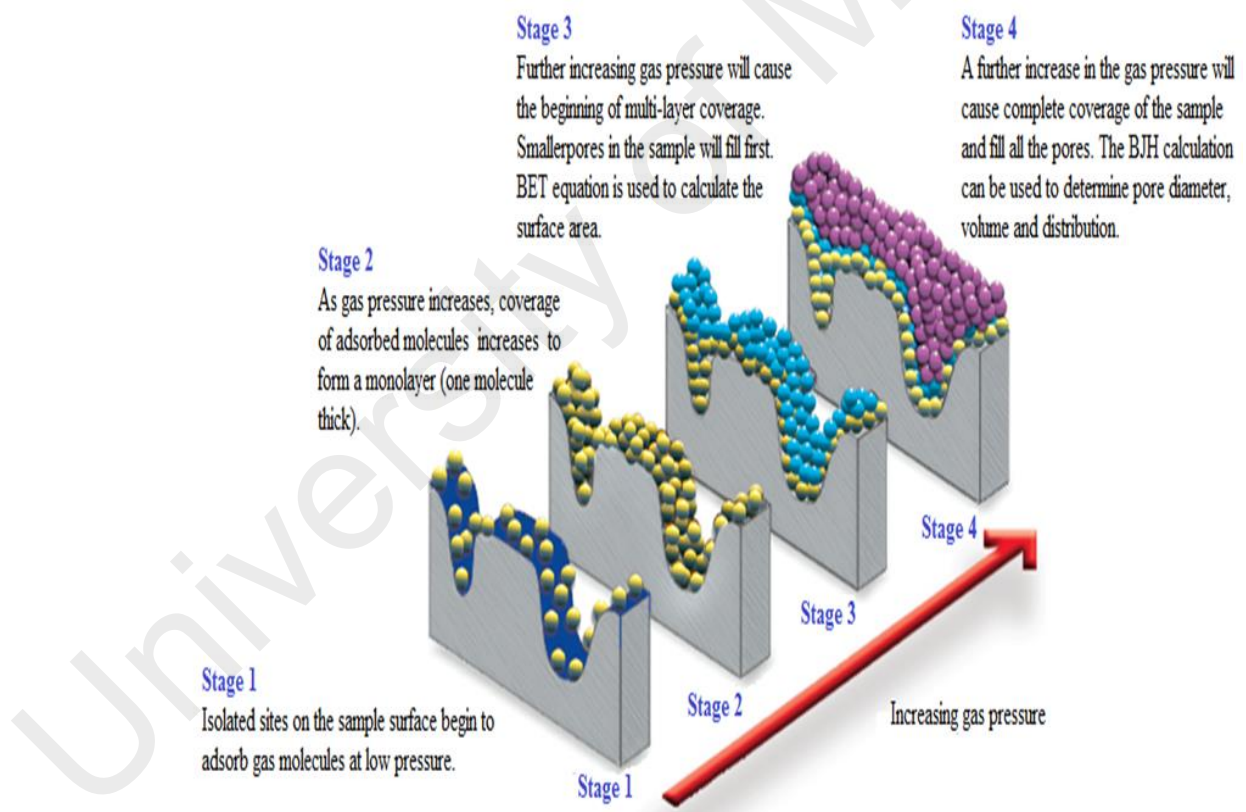


Figure 2.2: Gas adsorption and pore filling.

2.4 Factors affecting adsorption process

The amount adsorbed and the kinetics of adsorption of a particular adsorbate by the adsorbent depend on a number of factors. For a practical application, optimization of these factors is very important from economic and environmental point of view. These factors can broadly be classified into two namely; adsorbent-based factors and solution-based factors. The adsorbent-based factors are those that relate to the surface area of the adsorbent and the nature of the surface functional groups. Whereas, the solution-based factors are those due to the pH of the aqueous solution, temperature, presence of inorganic salts, initial adsorbate concentration, contact time and nature of solvent. These factors are briefly discussed in the following sections.

2.4.1 Solution pH

A major factor influencing sorption capacity of different sorbents is solution pH. Different adsorbents have different behaviours in solution media and therefore, their efficiency in removing adsorbate from such solutions (Yaqub et al., 2014). A change in the pH of a solution affects not only the degree of protonation but also the metal chemistry such as speciation and precipitation and the surface properties (charge and functional groups) of the sorbents (Nandi et al., 2009; Zhang et al., 1998). This depends in part on the electrical charge possesses by the adsorbate relative to the charge on the surface of the adsorbent. But adsorbed species cannot pile up on the surface of the adsorbent very densely, due to the mutual electrical repulsion existing between the adsorbate species (Al-Nasri, 2013). For a neutral adsorbate, the possibility of increased adsorption is high due to the ability of the adsorbate to pack together on the sorbent surface. But this also depends on the physico-chemical properties of the adsorbent and the pH values of the solution.

Additionally, an important property of the adsorbent surface closely related to the solution pH is the point of zero charge (pH_{pzc}) and that describes the pH value at which a solid submerged in an electrolyte exhibits zero net electrical charge on the adsorbent surface (Olds & Xue, 2009). It determines the adsorption ability of the surface and the type of surface active centers. The value of pH_{pzc} is particularly used to describe only adsorption systems in which H^+/OH^- are the potential-determining ions. Adsorption of anion is favourable when the surface functional groups become positively charged and this happens at $\text{pH}_{\text{pzc}} > \text{pH}$, that is when the concentration of H^+ ion becomes increased in liquid-solid interface. On the other hand, at $\text{pH}_{\text{pzc}} < \text{pH}$ adsorption of cations (radioactive metal ions) is most favoured due to the negative adsorbent surface, leading to strong interactions of the cations towards the sorbent surface by electrostatics. The extent of this phenomenon defers largely on different metals, due to the speciation of each metal in solution as pH changes. For instance, cesium exists as Cs(I) ion in the solution over a wide range of at least $\text{pH} = 12$ but hydrated cadmium is formed at $\text{pH} > 9$, cerium and cobalt exist as Ce^{3+} and Co^{2+} ion at $\text{pH} \leq 8$ but form hydroxides at elevated pH (Park et al., 2010; Ahn et al., 2009). So, the chemical species of each radioactive metals with pH determine the true adsorbability of metal on the sorbent surface.

2.4.2 Temperature

Temperature is another important factor for adsorption studies, and it tells more about the mechanism involved in the sorption process. Basically, there are two major effects of temperature on adsorption process. When temperature is increased, the diffusion rate of the adsorbed molecules is increased across the external boundary layer and in the internal pores of the adsorbent particle, due to the decrease in the viscosity of the solution (Abd El-Rahman et al., 2006). In the same vein, variation in the temperature of the adsorption system results into variation in the equilibrium capacity of the adsorbent for a particular adsorbate (Wang et al., 2005).

Therefore, if the rate of adsorption is increased with temperature, the mechanism controlling the process is endothermic, but if the rate is decreased with temperature, it is exothermic. The spontaneity of the process depends on whether the change in entropy and the free energy of adsorption system is positive or negative (El-Naggar et al., 2012a). A positive change in entropy and negative change in free energy values indicate the solution interface is in random increase and spontaneous sorption process, but negative change in entropy and positive free energy change show that the solution interface is slow and hence non-spontaneous sorption process (Kamaraj & Vasudevan, 2015). So, it could be said that temperature is responsible for the behaviour/ nature of sorbate in solution and the availability of active sorption sites on the adsorbent surface as temperature varies (Yagub et al., 2014). This means that if the solution temperature increases, it weakens the electrostatic interactions of the ions in solution and hence, increases their mobility to be attracted to the sorbent surface and vice versa. Besides, if the sorption is governed by physical phenomenon, an increase in temperature will cause a reduction in sorption capacity. In other words, increase in sorption capacity with temperature is as a result of chemical process involved in the adsorption. For instance, the effect of temperature on sorption of Cs^+ , Eu^{3+} and Co^{2+} onto non-activated and activated-SiSb (1:2) from different acidic media was reported to involve chemisorption process and that the equilibrium sorption capacity of the metal ions was increased from 0.36 to 0.41 mg/g when temperature increased from 303 to 333 K (Ali, 2009). Nilchi et al., (2011a) and El-Naggar et al., (2012b) also reported similar results with solution temperature ranging from 298 to 338 K. The increase in adsorption coefficient with a rise in temperature was attributed to the faster migration of ions and stronger electrostatic interactions of adsorbate-adsorbent.

2.4.3 Initial adsorbate concentration

The initial concentration of the adsorbate is an important factor that determines the amount of adsorbate ion that is adsorbed on the sorbent surface. The percentage removal

of adsorbate from the bulk and the sorption capacity of every adsorbent depend strongly on the possible existing relation between the adsorbate and the adsorbent. This in turn depends on the initial concentration of the adsorbate in solution and the available sites or the sorption pores in the adsorbent surface (Yagub et al., 2014). When the initial concentration increases, sorption capacity of the adsorbent is increased, which may be due to the high driving force provided to overcome the mass transfer resistance between the solution and the sorbent surface. On the other hand, the percentage removal is decreased with increasing initial concentration, which can be attributed to the saturation of the sorbent surface.

2.4.4 Contact time

Adsorption time is an important factor that determines if an appropriate technology has been designed. If the treatment technologies implemented for separation of any adsorbates from their solutions are appropriate and considered economically viable then, optimum equilibrium and adsorption time must be short with higher adsorption rate (Sheha & El-Khouly, 2013). However, the equilibration time for adsorption of adsorbate ions onto different adsorbents may also depend on a number of factors, such as: the electrostatic attraction of adsorbate-adsorbent, complexation reaction on the outside surfaces of adsorbents, distribution of pores on adsorbents, availability of sorption sites or pores or composition of the adsorbents, inter particle diffusion of adsorbate on the pores of the adsorbents and other environmental conditions (Long et al., 2013; Kim et al., 2014).

2.4.5 Presence of interfering ions

Adsorption of radioactive metal ions from solution onto sorbents could be greatly influenced by the presence of competing ions for the binding sites on adsorbent surfaces. The selectivity of sorbents depends largely on the behaviours of the target metal ions and

other ions in solution. Depending on the source of aqueous solutions, both cations and anions can be contained in the solution to be treated and that may impede or hinder adsorption of the target substances. Cations such as K^+ , Na^+ , Ca^{2+} , Mg^{2+} and Rb^+ are common in both natural waters and waste solution due to their solubility and ease of migration within the aqueous media and they are much responsible for negative influence on adsorption (Saber et al., 2010; Park et al., 2010).

2.4.6 Adsorbent dosage

Adsorbent dosage determines the capacity of an adsorbent for a given amount of adsorbent at the operating conditions. From the economical point of view, high capacity is expected for a smallest amount of adsorbent to make it practical at industrial-scale level. As a result, effective contact of the adsorbent and the adsorbate solution must be ensured to limit possible overlapping of the active sorption sites, due to overcrowding of the adsorbent particles (Tumin et al., 2008). Generally, increase in adsorbent dosage leads to increase in percentage removal of the adsorbate due to the increase in active sorption sites of the sorbent surface, until a roll-up or overcrowding of sorbent particles set in. However, this depends on the availability of the adsorbate ions in the solution.

2.4.7 Adsorbent surface area and pore size

Apart from the properties of the adsorbates and solution, the intrinsic nature of adsorbents plays an important role in adsorption (Chen & Wang, 2008). Since adsorption is a surface phenomenon, the study of surface characteristics of a preferred sorbent is very essential. From various studies, the size of particles of adsorbents has been found to affect the sorption capacity of the sorbent (Olatunji et al., 2015). This is because the bigger the particle size, the smaller the sorbent surface area and vice versa (Leusch et al., 1996). An excellent sorbent for sorption must have larger surface area, i.e., more sorption sites or higher pore volume and reduced effective density to accommodate the adsorbate. Both

the surface area and pore size are obtained from nitrogen adsorption tests at temperature of which nitrogen changes from liquid to gas, if the atmospheric pressure were equal to exactly 1 atm.

2.5 Categories of adsorbent materials

As a major characteristic that makes its relevant in wastewater treatment, adsorption has involved several adsorbents in recent time. The adsorbents used for wastewater treatment come from various sources, they are either from natural origins or as a result of industrial production and/ or due to activation process of some materials (Worch, 2012). In developing a suitable adsorbent for radioactive element removal, the physical or chemical properties of the adsorbent, surface morphology and the surface functional groups of the adsorbent are important parameters that must be considered. A good adsorbent for radioactive elements should also possess high mechanical and radiation stability as well as stable to chemicals either in acidic or basic environment. Most importantly, such adsorbents and/ or their precursors must be readily available in the environment, must also be cost effective to procure and operate, must be easy to regenerate and be reusable for a number of cycles.

For the purpose of classifications, adsorbents that have been investigated as feasible in radioactive waste-effluent treatment are put in the following categories:

- ❖ Inorganic materials
- ❖ Agricultural wastes
- ❖ Biological wastes
- ❖ Industrial wastes
- ❖ Polymeric adsorbents
- ❖ Polymer composite materials

2.5.1 Inorganic materials

Several inorganic materials have been discovered as suitable for adsorption of contaminants from aqueous solution. They range from metal oxides, phosphate, hexacyanoferrates and ferrocyanides of transition metals, natural clay minerals, siliceous materials, zeolites and activated carbons. Each of these materials is briefly reviewed below:

2.5.1.1 Metal oxides

Nanostructured metal oxides with high surface area, high surface-to-bulk ratio and surface functional groups that can interact favourably have been synthesized and investigated for metal ions removal in recent time (Vermeer et al., 1999; Hu et al., 2008; Kumar et al., 2013). For example, a well-aged hematite was synthesized by Vermeer et al. and they reported mean particle size of 50 nm, BET surface area of 43 m²/g and the point of zero charge (pzc) of 8.9 (Vermeer et al., 1999). Mishra and his colleagues reported the ion-exchange capacity of hydrous titanium oxide for radioactive cesium removal (Mishra, Dubey & Tiwari, 2004). It was observed that the adsorption was favourable by increasing the metal ion concentration from 10⁻⁸ to 10⁻² mol/L, temperature from 298 to 328 K and pH from 2.50 to 10.20. The adsorption process followed Freundlich isotherm and kinetic data was fitted by pseudo first-order kinetic.

Similar observation was reported when hydrous ferric oxide was synthesized and used for radioactive cerium adsorption (Dubey & Rao, 2011). Tin oxide particles have also been synthesized and used for the adsorption of uranium and thorium from aqueous solution (Nilchi et al., 2013). The adsorbent particle was measured to have 30 nm average size and surface area of 27.5 m²/g. By different methods, graphene oxide, reduced graphene oxide nanosheets and composites incorporated with metal oxides have been prepared and investigated for the removal of radioactive uranium and others (Gao et al.,

2011; Sreepasad et al., 2011; Li et al., 2012). It was revealed that apart from the excellent surface area (which is higher than 2600 m²/g), the presence of oxygen-containing functional groups played vital roles in the adsorption process. Other material of high capacity for metal ions is tungstate oxide.

2.5.1.2 Clay minerals

The clay minerals can be synthesized or taken from natural deposits. Generally, they are characterized with less than 2 micrometers in size. Natural clay minerals form the colloidal fraction of soils, sediments, rock and water and may be a mixture of fine-grained clay minerals and clay-sized crystals of other minerals such as quartz, carbonate and metal oxides (Yagup et al., 2014). Among the inorganic adsorbents that have enjoyed extensive applications in wastewater are clay minerals, owing to their superior qualities such as natural abundance, large specific surface area, relative chemical and mechanical strength, relative cost effectiveness, layered structures, proven high sorption properties and ion exchange ability for the adsorbate ions. Depending on the layered structures, clay minerals are classified into different groups such as illite (mainly micas), kaolin (kaolinite, dickite, nicrite, etc), smectites (saponite, montmorillonite), serpentine, chlorite, vermiculite, sepiolite or attapulgite.

Up till date, several clay minerals such as sericite, bentonite, kaolinite, laterite, smectite and diatomite, attapulgite and the Fuller's earth/ activated natural montmorillonite have been investigated for adsorbing a range of polar and non-polar molecules. In general, strong affinity of clays for cations happened mainly due to the proton-bearing surface functional groups such as silanols and aluminols via covalent binding (Hizal & Apak, 2006). Adsorption of metal ions by clay minerals is mainly by ion-exchange mechanism.

2.5.1.3 Zeolites

Zeolites are porous crystalline aluminosilicates which comprise arrays of SiO_4 and AlO_4 . They occur naturally in nature but are also manufactured industrially in large scale. Large variety of zeolite types are known and more than 40 natural types have been identified and they are present in many countries across the globe. The synthetic zeolites are produced commercially by crystallization under hydrothermal conditions followed by calcinations (Thomas & Barry, 1997). The structures of zeolites consist of infinite three-dimensional frameworks of $[\text{SiO}_4]^{4-}$ and $[\text{AlO}_4]^{5-}$ tetrahedral linked together by sharing all the oxygen atoms. Within the zeolite structures are cavities and channels that made up of about 50 % of its total volume and the weight is 10 – 12 % of water. The adsorbate cations and water molecules are held within the zeolite frameworks easily by these cavities and channels. Although, cations mainly Na^+ , K^+ , Ca^{2+} and Mg^{2+} are also present in the zeolite structure, but are loosely bound and due to their high solubility, can easily exchange with other cations from the solution. In addition, zeolite structure is characterized with uniform pore sizes of very small diameters in comparison to silica beads and activated carbon (Al-Nasri, 2013). This often makes zeolite adsorbents to be referred to as molecular sieves due to its difference adsorption strength for molecules based on the size, shape and polarity of the adsorbate (Changkun, 2009).

Among other qualities, zeolites are low-cost adsorbents, relatively high specific surface areas and high ion-exchange capacity. Just like other inorganic adsorbents, zeolites like clinoptilolite are limitedly used alone but in combination with other adsorptive materials to improve on their ion-exchange capacity and make easy their separation from the solution (Huang et al., 2017).

2.5.1.4 Siliceous materials

Siliceous based materials have also been discovered as good adsorbents in wastewater due to their natural abundance, low cost and good sorption affinity for metal ions. These naturally occurring materials include perlite, dolomite, silica beads and alunite. Perlite is a dense glassy volcanic rock known to special features of interest in environmental remediation such as high mechanical and thermal stability, non-toxicity, high resistant to organic solvents, silica-rich content, availability and cost effectiveness. In addition, its original volume can be increased under high temperature making it interesting for adsorption, and both its natural and expanded form have been used for the removal of variety of metal ions including cobalt, cadmium and mercury (Ghassabzadeh et al., 2010). Dolomite is both mineral and a rock, consisting of mainly calcium and magnesium carbonate compound and it has previously demonstrated a high sorption capacity for strontium and barium (Ghaemi et al., 2011). The adsorption mechanism was by ion-exchange and complexation reactions of surface groups with the target ions in wastewater. In the case of alunite, its use as adsorbent for heavy metal ions is not common, except for color removal, however, it is an inexpensive and abundant natural material that has demonstrated good adsorption capacity for dye and various colours in solution.

Silica beads on the other hand seem to attract much interest in environmental remediation, owing to its chemical reactivity associated with its hydrophilic surface, porous texture, high surface area, large uniform pores and mechanical stability. Primarily, they are effectively used for dehydrating gas and solid substances. The hydrophilic surface contains silanol groups which can adsorb material containing- NH_2 or OH groups. At low temperatures, adsorption capacity of silica beads is more than that of alumina or zeolite and more importantly, easily regenerated compared to other siliceous materials.

2.5.1.5 Miscellaneous inorganic materials

In adsorption technique, some inorganic materials are good adsorbents with high sorption efficiency while a good number of others exhibit extremely low ion-exchange efficiency for target metal ions. In addition to this, most inorganic materials are faced with certain management problems, which often limit their extensive use. The inorganic materials are very fine particulates and therefore, make separation difficult after treatment, result in complex process of recovery of the adsorbed metal, regeneration of fine particulates for reuse is challenging and as a result, can lead to possible release of the contaminant-bearing compounds into the solution. Many other problems of inorganic materials in adsorption have been reviewed in the literature (Vincent, Vincent & Guibal, 2015). One effort to solve these problems is by immobilization of these fine materials on appropriate supports to control their shapes and morphologies for easy applications in batch and column operations as well as to improve their ion-exchange efficiency. Some of the materials that have frequently been immobilized on supports are hexacyanoferrate, ferrocyanides and hydroxide of transition metals. The resulted adsorbents as reported in the literature have better adsorption capacity compared to the individual materials or the precursors if used alone as adsorbents.

Sangvanich et al. (2010) and Lin et al. (2001) synthesized and characterized copper ferrocyanide functionalized mesoporous silica and found to have an excellent porous structure with 900 m²/g and ~1000 m²/g, respectively for surface area, 3.5 nm pore size and ligand loading capacity of 3.6 – 4.9 silane/nm² elemental and 3.7 silane/nm² gravimetric. The composite material was reported to have higher stability in both acidic and alkaline wastes and better sorption capacity compared to insoluble Prussian blue. Meanwhile, the stability and ease of separation of Prussian blue were enhanced when coated with magnetic nanoparticle (MNP), providing longer contact time with adsorbate in wastewater and better sorption capacity (Thammawong et al., 2013). Sol-gel

encapsulated cobalt hexacyanoferrate has also been synthesized and characterized for radioactive metal removal (Ca & Cox, 2004). The characterization of the sorbent material shows that increase in pore size does not cause a corresponding increase in sorption capacity. The pore volume and surface area were increased after modification by controlling the amount of hexacyanoferrate ions in the silica sol-gel solid sorbent. The surface area was increased from 408 to 457 m²/g while the pore volume was 0.194 to 0.217 cm³/g.

Silico-antimonate materials are also good sorbents which can be used for radioactive metal ions adsorption. However, the surface groups need to be activated for active sorption. Phosphoric acid has been used to activate silico-antimonate crystals and the surface was reported to contain hydroxyl and phosphate groups, which may enhance the ion exchange affinity for metal ions, because an increasing amount of water content increases the porosity of sorbent material and localization of protons (Ali, 2009). Zirconium vanadate (Roy et al., 2004), and magnetic graphene oxide nanocomposite (Deng et al., 2013), have also been synthesized and investigated for adsorption studies.

2.5.1.6 Activated carbons (AC)

The earliest understanding of adsorptive properties of carbonaceous materials can be traced to hundreds of years when they were being used only for the removal of colours, tastes and odours from water. Previously, the ancient Egyptians used charcoal for water purification, the Japanese used coal to purify well water and the Europeans have also used coal products for beet sugar refining process (Al-Nasri, 2013). Now, with the increasing understanding of its surface characteristics and interaction of surface functional groups with different contaminants, activated carbon has become a very important and common adsorbent used in many industrial processes to remove pollutants including solvent recovery, volatile organic compound control, hydrogen purification and wastewater

treatment. But in its natural form, activated carbon has low capacity for most of the pollutants except gases. Activated carbon can be produced from carbon-rich raw materials through different activation processes including physical, chemical, thermal or gas activation (Kobyra et al., 2005). The various activation processes help to increase its surface area and porosity greatly, which allows its optimization for different applications. Certain factors are crucial in the selection of raw materials for the manufacturing of activated carbons and these includes cost, carbon content and low organic content of the material. A good material must have high carbon (low ash), high-density structure such that it can withstand various treatment processes and must be cost effective. As a result, some of the raw materials that have been found in these categories are wood charcoal, wood, peat, lignin, refinery residues, coconut shell, poultry litters, plastic residues or sawdust. Generally, the abundant sources for generating activated carbon made its considerably less expensive, available and of interest for radioactive metal ion adsorption.

Although, it has low sorption capacity for radioactive metal ions, but by incorporation with appropriate media that can enhance its carboxylic/ basic functional groups, activated carbon can adsorb metal ions greatly. Several additives such as acid, surfactant, polymers and a host of others have been included to enhance its surface suitability for adsorption of metal ions (Yang et al., 2007; Fu & Wang, 2011). Today, there are many activated carbon-based adsorbents in use. Its main problem is regeneration difficulty.

The current study has investigated the use of polymer material impregnated in activated carbon to eliminate many of its aforementioned limitations.

2.5.1.7 Carbon nanotubes (CNT) adsorbents

As a relatively new adsorbent discovered in the last two decades, carbon nanotubes have enjoyed worldwide use for the removal of metal ions owing to its excellent

properties (Fu & Wang, 2011). There are two classes of CNT: (1) single-walled CNTs (SWCNTs) and (2) multi-walled CNTs (MWCNTs). Some complex reactions involving electrostatic attraction, sorption-precipitation and chemical interaction between the metal ions and the CNTs surface functional groups are attributed to the sorption mechanisms of metal ions by the CNTs. Because of their low sorption capacity for metal ions, CNTs are usually functionalized with various agents such as HNO_3 and KMnO_4 to increase its carboxylic acid groups for adsorption. CNTs based adsorbents could be more efficient than the widely applied ordinary activated carbons in wastewater treatment. Previous investigations revealed both functionalized and non-functionalized MWCNTs proven to have higher sorption capacity for metal ions than AC (Pillay et al., 2009).

2.5.2 Agricultural wastes and by-products

When it comes to selection of adsorbent materials in wastewater treatment, agricultural products and byproducts have a significant position due to their special features. They are abundant around the world, freely available, non-hazardous and possess many desirable functional groups of interests for pollutants removal among others. In addition, they are cost-inexpensive, because most of the materials require little or no cost to process and they possess good stability and minimize disposable sludge volume or chemical to be disposed of. There are many waste materials and agricultural solid wastes such as sawdust, wood bark, hazelnut shell, pecan shell, walnut shell, coconut shell, rice husk, arca shell, palm shell, jackfruit, maize cob, pine cone, orange peel and many others (Barakat, 2011; Ding et al., 2013; Ofomoja et al., 2013; Yagub et al., 2014). In most cases, common processing such as removing dirt particles, washing with water to clean the surface and drying to remove water molecules are sometimes sufficient to treat agricultural wastes and byproducts before they are used as adsorbents. Further processing such as chemical modification or conversion by heating to activated carbon are also common treatment processes to improve on their stabilities and sorption capacities.

Polymers or inorganic materials of both natural and synthetic origins can also be incorporated with agricultural wastes to enhance its performance in adsorption of radioactive and other heavy metal ions from aqueous solution.

2.5.3 Biological wastes

As a relatively new process, the use of biological wastes has been discovered and advocated as alternative adsorbent materials in addition to the agricultural byproducts to replace the high cost inorganic materials. Extensive research studies are still being focused to utilize the advantage they offer. Besides their inexpensive and abundant in nature, they have good stability, minimize disposable sludge volume, large porosity, good surface area, natural capacity to accumulate heavy- and radioactive metals and degrade organic compounds, and hence, increase their usage for environmental pollution remediation.

They have been reported to contain diverse functional groups such as carboxyl, amino groups, hydroxyl and sulphate groups, which are active sites for heavy metal ions. Until now, some of the biological materials that have been investigated include (1) non-living biomass lignin, shrimp, squid, krill etc; (2) marine alga biomass; (3) microbial biomass such as bacteria, yeast and fungi (Barakat, 2011). The major setbacks with bio-adsorbents are low sorption capacity, high chemical and biological oxygen demand due to dissolution of organic compounds contained in the plant materials and the weakening of active surface functional groups under extreme environmental conditions. To use biological/agricultural waste materials, it demands chemical pre-treatment or modification. Review on the advantages and disadvantages of untreated and chemically treated biomass as bio-sorbents has been reported (Ingole & Patil, 2013). Biomass materials can also be incorporated into the polymer matrix to enhance its sorption capacity and mechanical strength.

2.5.4 Industrial wastes

Industrial byproducts have also included in the search for more adsorbent materials for radioactive and non-radioactive heavy metal ion removal. Some of these industrial byproducts are metal hydroxides sludge, fly ash, waste biogas residual slurry, red mud, blast furnace sludge and many others. These industrial byproducts are available in large quantities and are inexpensive because they are generated as waste products from different industries, and are often constitute disposal problems to the industries. The use of these materials forms another pathway of saving the natural environment from long term effects of disposing these materials. Many great review works have been conducted on various industrial byproducts for heavy metal ions and other pollutants such as dyes by different researchers can be found in the literature (Ahmaruzzaman, 2011; Yagub et al., 2014).

2.5.5 Polymeric adsorbents

The discovery of polymers in materials science represents a great breakthrough to many scientific problems. Today, there are many emerging areas where polymers have found fundamental significance and potentials for myriad of product applications. They find applications in biosensors, environmentally sensitive membranes, artificial muscles, actuators, corrosion protection, electronic shielding, visual displays, solar materials and components in high-energy batteries (Finkenstadt, 2005). With the better understanding of the intrinsic nature and surface properties of polymers in recent time, they are now being identified as future consideration for water and wastewater treatment, for the recovery of precious metals from hydrometallurgical liquids and the removal of toxic contaminants from waste effluents before disposal. Polymers are generally described in terms of their structural units which are linked together covalently through the bonding sites to form polymer chains. The constituent monomers and the microstructure or the arrangement of the monomers within the polymer chains play vital roles in determining

the physical and chemical properties of each polymer. The bulk physical properties provide information on the interaction of the polymer with other chemicals or solvents, while the chemical properties describe how the polymer chains interact through various physical forces (Saad, 2013).

The interaction of polymer chains may range from ionic to hydrogen bonding, depending on the structural units or groups within the chains. Polymers having amide or carbonyl groups can form hydrogen bonds between the adjacent chains, whereas, the partially positively charged hydrogen atoms in N-H groups of one chain can be attracted to the partially negative charged of oxygen atoms in C=O groups in the other chain and thereby, producing strong interaction that can result into higher tensile strength and crystalline melting point of polymers. As adsorbents in wastewater treatment, polymers help to reduce secondary wastes arising after treatment due to large sludge production from the spent adsorbent, particularly when inorganic materials are used.

In addition, polymers themselves are good adsorbents due to the presence of reactive functional groups though fewer, but when used with other materials, they tend to yield enhanced sorption capacity (Bai et al., 2015). Apart from this, for safe disposal of spent adsorbents, polymers are suitable for this purpose (Valsala et al., 2009). Today, polymeric materials appear to assume leading position in most of the environmental management and wastewater treatment applications. There are naturally occurring and as well as several synthetic polymers that can be used in water and wastewater treatment, and they are generally abundant and cost effective.

2.5.5.1 Natural polymeric adsorbents

Chitin, lignin, starch and cellulose are some of the naturally occurring polymers that have been involved in wastewater treatment. They are usually referred to as natural biopolymers, due to their biological origins (commonly found in the exoskeleton of

crustaceans). They contain mechanically tough amino polysaccharides. Among them, cellulose, chitin and chitosan seem to have enjoyed much research interest due to the abundant functional groups, which often not present in synthetic polymers and their biological inactivity nature, making them safe for natural environment. Cellulose is the most abundant natural biopolymer which is available in the agricultural and byproducts of natural sources. It is a carbohydrate homopolymer containing many glucose units which are oriented with $-CH_2OH$ groups alternating below and above the plane of rings to produce long and un-branched chains, unlike the lignin which is a branched, three-dimensional natural polymer with aliphatic and aromatic constituents.

Chitin exists abundantly in the crustacean skeletons particularly the skeletons of the crabs. From chitin, chitosan is produced by partial deacetylation with strong alkaline. Both chitin and chitosan contain high contents of functional groups such as amino, acetamido and hydroxyl which are the active sites involved in the adsorption of contaminants. The main challenge with natural polymers as sorbents is that they dissolve in both organic and inorganic acids to become viscous and except other separation processes are combined, such as the use of membrane like ultra-filtration, natural polymers are not suitable to use alone in metal ion removal (Wang et al. 2009). Functionalization with different cross-linking agents has been the only way to enhance their resistance to chemicals and this also has contributed to the enhanced mechanical and as well as the adsorption properties of natural polymers for radioactive and non-radioactive metal ions (Humelnicu et al., 2011; Wang & Chen, 2014; Wojnárovits et al., 2010). Natural polymers have the advantages of biocompatibility, cheap, renewable, abundant and ready biodegradation.

2.5.5.2 Synthetic polymeric adsorbents

The discovery of synthetic polymers was a great breakthrough in human endeavours, particularly in the field of science and engineering. Starting with polyaniline (formerly known as aniline black for any product produced by oxidation of aniline) which could be dated back to 1885 and subsequent synthesis of polyacetylene in 1970s, numerous polymers have been discovered upon doping of appropriate reagents/ substrates. For instance, polypyrrole was discovered in 1977 and by 1979, its electrical conductivity has been improved upon by doping. Generally, serious research studies have been devoted for conducting polymers and in 2000, a Nobel Prize in Chemistry was given to Alan Heeger, Alan MacDiarmid and Hideki Shirakawa for the discovery and development of conducting polymers.

Today, there are many synthetic polymers in existence that have been used in various purposes (Huang et al., 2014). Unlike the natural polymers, synthetic polymers are not biodegradable but are quite stable in both acidic solutions and hence, can be used alone for adsorption of various contaminants. The polymeric adsorbents have a number of advantages over the conventional adsorbents. Their shapes can be controlled during preparation into beads, membranes and fibers, depending on the purpose in which it is intended. Methods such as brush formation, ligand immobilization, molecular imprinting, gamma-irradiation polymerization and/ or graft copolymerization are commonly used in polymer surface modification and that depends also on the solute to be adsorbed. Usually, functionalization of the substrate with appropriate ligands increases selectivity of polymers for target ions (Changkun, 2009; Wojnárovits et al., 2010). With the current demand for new materials with good selectivity for specific compounds both in environmental science and biomedical/ tissue engineering, synthetic polymers appear to be promising candidates for developing new such required materials with good selectivity.

2.5.6 Polymer composite adsorbents

In a bid to improve on the adsorbent capacity, selectivity towards a target solute and easy separation process after adsorption, surface modification of polymers with functional groups that have affinity for radioactive and non-radioactive metal ions have been examined. This has brought about the development of new adsorbents based on polymers such as polymer-to-polymer/inorganic materials/agricultural waste products as composites. Generally, polymer composite adsorbents have more improved physico-chemical properties for adsorption over pure polymers owing to the synergistic effect of individual components. However, a good understanding of the conditions of interaction and chemistry of the polymer intended to be used with the guest-host material is very important to yield homogeneous dispersion. The most commonly researched among these polymers and their composites are briefly reviewed below:

2.5.6.1 Polyethyleneimine-based (PEI) composites

PEI finds applications in adsorption of different pollutants, owing to the presence of high amine density and accessible primary amine sites on the chain ends. In PEI, one end of the polymer chain contains methyl and the other end is made up of hydroxyl. PEI is a cationic water-soluble polyamine which could be divided into two types namely: linear and branched PEIs. The linear PEI (LPEI) contains all secondary amine and exists as solid at room temperature while the branched PEI (BPEI) contains primary, secondary and tertiary amino groups and are liquids at all molecular weight. In addition, BPEI has a high concentration of polar groups containing nitrogen atoms with a molar ratio of primary to secondary to tertiary amine reported as 25:50:25 (Tang et al., 2013). As a result, the BPEI possesses strong metal chelating ability compared to LPEI. Because of its solubility in hot and cold water as well as in ethanol and methanol, it is limited in use as an adsorbent for the removal of contaminants except it is simultaneously employed with membrane or ultrafiltration process. However, to effectively use PEI as an adsorbent, it has to be

immobilized in porous matrix that will enable separation possible and increase sorption capacity. PEI with nanoporous carbon (Tang et al., 2013), protonated titanate nanotubes (Liu et al., 2012), mesoporous silica (Heydari-Gorji et al., 2011; Mészáros et al., 2002), polymeric support (Sehaqui et al., 2015), cellulose-grafted-PGMA-PEI (Tang et al., 2013), PEI/ polyvinylidene fluoride nanofibers (Ma et al., 2016), PEI/metal oxide nanocomposite (Wang et al., 2015) and many others have been synthesized and investigated for the removal of various pollutants (Unsal et al., 2000).

2.5.6.2 Polyacrylonitrile-based (PAN-based) composites

Polyacrylonitrile (PAN) is one of the favorable binders that have been studied in adsorption techniques based on its chemical stability, easy pelletizing and strong binding force (Aly et al., 2014). PAN is an inexpensive commercial product with porous beads that have ability to accommodate very high loadings of ion-exchange materials into the PAN matrix. The beads porosity is advantageous over the granular adsorbents owing to better kinetics and easy modifications of the physical and chemical properties such as surface area, hydrophilicity, porosity and mechanical strength (Saber et al., 2010). These advantages have been utilized in synthesizing PAN-based composites such as PAN-based sodium titanate (STS-PAN) composite (Saber et al., 2010), PAN-ammonium molybdophosphate granules (PAN-AMP) composite (Nilchi et al., 2011b), copper hexacyanoferrate-PAN (CHCF-PAN) composite (Nilchi et al., 2011a), aminated polyacrylonitrile nanofiber mats (Kampalanonwat & Supaphol, 2014), thermally treated and untreated PAN beads (Aly et al., 2014), PAN-bentonite and PAN-zeolite (Şimşek & Ulusoy, 2012), polyantimonic acid-PAN (PAA-PAN) composite beads (Ma et al., 2016). However, PAN polymer can only be prepared in organic solvents and in most cases, small amount of other vinyl comonomers are used along with acrylonitrile (AN).

2.5.6.3 Conducting polymer-based composites

Among various polymers in environmental remediation, conducting polymers have significant research interest. Unlike the other polymers discussed above, conducting polymers are not soluble in either hot or cold waters and generally, have limited solubility in most solvents. The main conducting polymers in research environment are polyaniline (PANI), polyphenylenes (PP), polythiophene (PTh), poly(3,4-ethylenedioxythiophene) (PEDOT) and polypyrrole (PPy). They are conjugated polymers with π -electron in the polymer backbone and also exhibit the unique properties of conventional polymers, such as ease of synthesis and flexibility in processing, mainly by dispersion. Their accessible redox states, controllable properties and facile chemistry make them ideal candidates for electrical and optical devices, similar to those of metals or semiconductors. In particular, their easy coordination with metal ions and different molecules, due to the presence of reactive functional groups, makes them attractive for environmental applications (Seid et al., 2014).

In the case of polyaniline conducting polymer as the most earliest known, it did not capture any research interest until in late 80s, following the rediscovery of its high electrical conductivity. Today, it has gained many research interest for various applications and particularly, in water and wastewater treatment as a result of the presence of a number of functional groups such as amine and imine groups. It exhibits chelating properties with metal ions as well as adsorb anionic species through electrostatic or hydrogen bonding. PANI has a good mechanical flexibility, high conductivity, and exists in three oxidation states with different colours (emeraldine, leucoemeraldine and pernigraniline) (Huang et al., 2014). The polymerization of aniline monomer can only be done in acids because it does not dissolve in water, which makes it costlier than the polypyrrole conducting polymer. PANI has adsorption affinity for both organic compounds and inorganic ions but the adsorption capacity is very low, due to the lower

surface area of the pure PANI. The low surface area arises from the aggregation of the particles following their strong inter- and intra-molecular interactions. To improve the surface area and modify the surface morphology, PANI has been synthesized on various substrates, ranging from organic to inorganic materials or by copolymerization with another polymer. The resulted composite materials can remove pollutants with higher sorption efficiency under equilibrium conditions better than the pure PANI. So far, PANI/PPy copolymers (Bhaumik et al., 2012), PANI/ silica composite (Belaib et al., 2012), PANI/hexagonal ordered silica nanocomposite (Gholivand & Abolghasemi, 2012), PANI/ attapulgite composite (Cui et al., 2012), magnetic PANI/Fe₃O₄ nanocomposite (Katal et al., 2013), PANI/CoFe₂O₄ (Xiong et al., 2012), PANI/sawdust (Ansari, 2006; Liu & Sun, 2012; Liu et al., 2010), PANI/hexagonal mesoporous silica (Javadian et al., 2013), flake-like PANI/montmorillonite (Chen et al., 2013), PANI doped with different inorganic salts (Özdemir et al., 2011), PANI/reduced graphene oxide nanocomposite (Li et al., 2013; Shao et al., 2014; Sun et al., 2013), PANI/CNT doped with or without surfactant (Kumar et al., 2013) and a few others have been investigated for the removal of heavy metal ions or other pollutants (Lü et al., 2007; Yang et al., 2007; Zhang et al., 2010).

Unlike the other conducting polymers, polypyrrole conducting polymer is the most research conducting polymer ever since its discovery in 1970s. Subsequent to the understanding of its possible increased electrical conductivity upon doping, its applications have increased tremendously towards development of many electrical devices. Today, polypyrrole is used in polymeric batteries, wire, micro-actuators, electronic devices, functional membranes, bio- and gas-sensors etc. (Chougule et al., 2011). Its facile use in various fields is borne out of the fact that it is easily synthesized via chemical and electrochemical polymerization methods in aqueous (including water) or non-aqueous media. Other interesting properties of polypyrrole conducting polymer

are the excellent reversible redox doping/ de-doping chemistry, non-toxicity, high conductivity and good affinity towards metal ions and organic compounds (Seid et al., 2014). In environmental remediation, its ion-exchange properties and the presence of nitrogen heteroatom in the structure coupled with easy doping chemistry are the main attractions. In addition, polypyrrole does not pose separation difficulty after use, making it useful in enhancing easy separation of fine particulate inorganic materials from solution. However, the main issue with the polypyrrole as an adsorbent is concerned with the polymerization conditions which significantly affect its sorption capacity. The type and size of the counterions involved in the process, ageing and thickness of the polymer are some of the parameters that determine the adsorption behaviour of polypyrrole as an anion or as a cation exchanger during adsorption (Weidlich et al., 2001). In addition, polypyrrole as adsorbent is confronted with its poor mechanical strength and low processability. Hence, to use polypyrrole for radioactive heavy metals removal, the choice of the precursors/ dopants, synthesis method and formation period have their significant roles. Up till date, complete removal of contaminants is still yet to be reported using only polypyrrole as adsorbent (Bai et al., 2015). As a result, different approaches varied from chemical/ physical treatments, copolymerization to surface modifications are employed to fabricate composites of polypyrrole with enhance sorption capacity compared to the pure polypyrrole particles.

Generally, to prepare polypyrrole composites one common method is to mix the oxidant with the substrate surface and exposes it to pyrrole or by soaking the substrate in pyrrole monomer and this is then immersed in oxidant solution. Polypyrrole can also be deposited directly on the substrate by placing the substrate on the solution containing the pyrrole monomer and the oxidant (Saville, 2005). Large dopants such as cationic and anionic surfactants are also used to control growth and stability of the polypyrrole

particles as well to aid the uniform dispersion of polypyrrole throughout the substrate, this has been proven to influence its sorption efficiency (Hasani & Eisazadeh, 2013).

A survey of the literature revealed that polypyrrole has been polymerized on different organic and inorganic materials to produce polymer composites of much better surface morphology and surface area for adsorption of pollutants. Some of these are PPy/montmorillonite clay nanocomposite (Setshedi et al., 2013), PPy/ Al_2O_3 composite (Hasani & Eisazadeh, 2013), PPy/ Fe_3O_4 nanoclusters (Yao et al., 2011), PPy/ magnetic Fe_3O_4 composite (Bhaumik et al., 2011), PPy/SD composite (Ansari & Fahim, 2007; Omraei et al., 2011), ATP/PPy/SDS composite (Chen et al., 2016), PPy-RGO (Chandra & Kim, 2011; Li et al., 2012; Zhao et al., 2012a & 2012b), Fe_3O_4 @PPy/RGO composite (Bai et al., 2015), PPy/PANI nanofibers and composites (Bhaumik et al., 2012; Ghorbani et al., 2010; Javadian, 2014), PPy-impregnated porous carbon (Choi & Jang, 2008), PPy/cellulose fiber composite (Lei et al., 2012), PPy/CNT composite (Ghorbani & Eisazadeh, 2013a), PPy/melanine or PPy/poly (styrene-sulfate) (Hepel et al., 1997), PPy/nylon 6, 6 granules (Zhang & Bai, 2002) and PPy/rice husk (Ghorbani & Eisazadeh, 2012 & 2013b).

Summarily, the high sorption capacities of these conducting polymer composite materials are attributed mainly to the strong binding affinities of oxygen and nitrogen-containing functional groups, complexation of the metal ions with nitrogen surface groups following the deprotonation of N-H groups. So, to enhance the nitrogen groups and/ or the oxygen-containing functional groups of the pure conducting polymers, other materials with rich oxygen-groups or nitrogen groups are necessary such that the resulting polymer composites would yield excellent sorption capacity for the metal cations. This is the main aim of the present study, to enhance the surface functional groups of polypyrrole conducting polymer for radioactive metal ions removal, which is still less studied.

2.6 Desorption and reusability of spent-adsorbent

As much as different adsorbent materials are still being advocated for in the water and wastewater purification, one important factor of consideration for selecting adsorbent materials is on the longevity and possibility of reuse in a number of cycles. There are special cases that discarding the adsorbent will be the most economical choice after use but that depends on the nature and the concentration of the adsorbates. A very low-cost adsorbent might be favorable to dispose after use and in a situation whereby the desorption of the loaded adsorbent is difficult or requires complex process to regenerate the adsorbent (this is often the situation with adsorption process involving chemical bond formation) and also when the non-adsorbed products of the adsorptive separation are of very high value (Thomas & Barry, 1997).

Generally, if an adsorbent cannot be regenerated and reused, such materials are not considered as feasible and cost effective from the economic point of view for all industries. This is to ensure the whole cost of adsorption process is reasonably low for all industries. Apart from this, desorption and regeneration of adsorbents ensure that the limited essential elements are recovered from the spent adsorbents, also helps to dispose solid wastes in a proper and safe way and most importantly, limits the cost involvement of disposing wastes and limit the environmental impacts of waste disposal.

Practical desorption and regeneration methods include one or a combination of the following (Thomas & Barry, 1997):

- ❖ Increase in temperature
- ❖ Reduction in concentration
- ❖ Reduction in partial pressure
- ❖ Change of chemical conditions e.g. pH
- ❖ Purging with an inert fluid

- ❖ Displacement with a more strongly adsorbing species

The final choice of any particular method of desorption and regeneration should be governed by the technical and economic considerations.

2.7 Adsorption isotherms

The interaction of adsorbate with the adsorbent material depends largely on the affinity that exists between the adsorbate and the adsorbent surface. Once the adsorbate and adsorbent are in contact, adsorption process begins until the equilibrium is reached between the adsorbate on the adsorbent surface and the adsorbate remaining in the aqueous solution. At this stage, the amount of adsorbate leaving the adsorbent surface will be equal to the amount being adsorbed to the adsorbent surface. The phenomenon that describes the adsorption mechanisms between the adsorbate on adsorbent surface (that is adsorption amount, q_e in mol g^{-1} or mg g^{-1}) and the adsorbate in aqueous phase (equilibrium concentration, C_e in mol L^{-1} or mg L^{-1}) is referred to as “adsorption isotherm”. The amount of adsorbate ions per unit mass of the adsorbent (q_e) and the equilibrium concentration of the adsorbate remaining in the aqueous phase (C_e) can be obtained over a wide range by changing the amount of adsorbent (m , g), the initial concentration of solute (element) and the volume of liquid (V in L or ml) (Crittenden et al., 2005).

Isotherm models are used to fit the adsorption equilibrium data by plotting q_e against C_e . Once the isotherm data are fitted by the models, the adsorption properties such as maximum adsorption amount, affinity constant, thermodynamic parameters and the mechanism of the adsorption can be obtained for the adsorption process. Such information allows the evaluation or prediction of performance of the adsorption process and is useful to optimize the use of the adsorbent in its intended applications. There are many

adsorption isotherm models that have been proposed and investigated in adsorption process. A few of these models are briefly reviewed in the following sections.

2.7.1 Langmuir isotherm model

In 1918, the isotherm model which describes and quantifies the adsorption of adsorbate on localized adsorption sites was proposed by Langmuir (Langmuir, 1918). As an empirical isotherm, it can be used to describe both the physical and chemical adsorption, but is only valid for monolayer adsorption of adsorbate by the surface containing uniform, finite number of homogenous adsorption sites. It is based on the supposition that no adsorbate/adsorbate interactions exist and that the energy of adsorption is constant during the adsorption process. The model is based on the assumption that: (1) the adsorption of the adsorbate onto the surface sites is independent of the occupational status of the neighboring sites; (2) the adsorbate behaves as an ideal gas; (3) no such thing as adsorbate/adsorbate interactions and; (4) a monolayer adsorption of the adsorbates occurs only on the adsorbent surface sites that have equal adsorption energy and enthalpy (Changkun, 2009; Al-Nasri, 2013). The equation of Langmuir adsorption isotherm can be expressed in non-linear form as follows:

$$q_e = \frac{b q_m C_e}{1 + b C_e} \quad 2.1$$

The linearized form of the equation is given as:

$$\frac{C_e}{q_e} = \frac{1}{b q_m} + \frac{C_e}{q_m} \quad 2.2$$

where C_e is the equilibrium concentration of the adsorbate remaining in the aqueous solution (mgL^{-1}), q_e is the adsorbed amount of adsorbate per unit mass of adsorbent (mgg^{-1}), q_m is the maximum adsorption capacity required for complete monolayer coverage

(mgg^{-1}) and b (Lmg^{-1}) is the adsorption equilibrium constant commonly called Langmuir constant and it relates to the adsorption rate.

The essential features of the Langmuir isotherm can be represented in terms of a dimensionless constant called separation factor, R_L . It is expressed as (Huang et al., 2014):

$$R_L = \frac{1}{1+bC_o} \quad 2.3$$

where C_o is the initial concentration of the adsorbate (mg/L), R_L indicates the type of isotherm, which can be favorable ($0 < R_L < 1$), unfavorable ($R_L > 1$), linear ($R_L = 1$) or irreversible ($R_L = 0$).

2.7.2 Freundlich isotherm model

Another empirical model that describes the adsorption isotherm was proposed in 1907 by Freundlich, known as Freundlich isotherm (Freundlich, 1907). The Freundlich isotherm can be applied to non-ideal and multi-layer adsorption on the heterogeneous surfaces and it assumes that the enthalpy of adsorption is independent of the amount adsorbed. Based on the model, increase in the adsorbed amount of the adsorbate is subsequent to the increase in the concentration of the adsorbate in the solution. The model has the non-linear form of Equation 2.4 (Huang et al., 2014):

$$q_e = K_F C_e^{1/n} \quad 2.4$$

By linearization, the equation becomes:

$$\log(q_e) = \log(K_F) + \frac{1}{n} \log(C_e) \quad 2.5$$

where K_F ($\text{mgg}^{-1}/\text{L}^{1/n}$, $\text{mg}^{1/n}$) is the Freundlich constants related to the adsorption capacity when the adsorbate equilibrium concentration is unity and n is the adsorption intensity. Other parameters retain their usual meaning as defined previously.

2.7.3 Dubinin-Radushkevich (D-R) isotherm model

The nature of the adsorption process in terms of whether chemisorption or physisorption is more easily determined by Dubinin-Radushkevich (D-R) isotherm (Kadam et al., 2016). The fact that it is not restricted by the surface heterogeneity and the adsorption constant, adsorption potential assumption makes the model more applicable than the Freundlich isotherm (Huang et al., 2014). The D-R isotherm is generally expressed in non-linear form as follows:

$$q_e = q_m \exp(-\beta \varepsilon^2) \quad 2.6$$

After transformation, it is expressed in linear form as:

$$\ln(q_e) = \ln(q_m) - \beta \varepsilon^2 \quad 2.7$$

where β relates to the mean adsorption energy constant ($\text{mg}^2\text{kJ}^{-2}$) which describes the energy requires to activate the process and the energy relationship is given as:

$$E = \frac{1}{(2\beta)^{1/2}} \quad 2.8$$

and ε is the Polanyi potential which is dependent on the temperature of the system and it is given as below:

$$\varepsilon = RT \ln\left(1 + \frac{1}{c_e}\right) \quad 2.9$$

R is the universal gas constant ($R = 8.314 \text{ Jmol/K}$) and T represents the absolute temperature of the adsorption system.

2.7.4 Temkin isotherm model

The model describes the effects of some indirect interactions between the adsorbent and the adsorbate on adsorption isotherms, with the assumption that the heat of adsorption

of all the molecules would decrease linearly rather than logarithmic as coverage proceeds (Temkin, 1941). The general form of the model is expressed as follows:

$$q_e = \frac{RT}{b} \ln(AC_e) \quad 2.10$$

It is given in linear form as:

$$q_e = B \ln(A) + B \ln(C_e) \quad 2.11$$

where $B = \frac{RT}{b}$ and A are constants related to the heat of the adsorption process and the maximum binding energy at equilibrium.

2.7.5 Sips isotherm model

Sips also proposed another isotherm model that comprises of both Langmuir and Freundlich isotherms and was called Sips or Langmuir-Freundlich isotherm model (Sips, 1948). It is a three-parameter fitting equation for predicting the heterogeneous adsorption systems and for solving the limitation of rising adsorbate concentration associated with the Freundlich isotherm model (Foo & Hameed, 2010). As shown in non-linear equation 2.12, and linear-form in Equation 2.13, the model resembles Langmuir isotherm but modified to conform to the Freundlich isotherm, in order to satisfy the Henry's law behavior at the equilibrium adsorption of the adsorbate (Changkun, 2009).

$$q_e = \frac{K_s C_e^\alpha}{1 + b_s C_e^\alpha} \quad 2.12$$

$$\ln(C_e) = -\ln\left(\frac{K_s}{q_e}\right) + \ln(b_s) \quad 2.13$$

where K_s ($\text{mg}^{1-1/\alpha} \text{L}^{1/\alpha} \text{g}^{-1}$) and b_s (Lmg^{-1}) ^{α} are the Sips constants, α is the heterogeneity coefficient while both q_e and C_e retain their usual meanings.

However, the model clearly shows that if the adsorbate concentration is low, the model reduces to conform with Freundlich isotherm while at higher concentrations, the model will become Langmuir isotherm. So, it can be seen that Sips is more advantageous in that it does not only consider the heterogeneity of the surface but as well as the monolayer adsorption capacity (q_m).

2.7.6 Redlich-Peterson (R-P) isotherm model

Redlich-Peterson (R-P) isotherm is a hybrid isotherm that combines both Langmuir and Freundlich isotherms (Redlich & Peterson, 1959). The model relates three adjustable parameters together in an empirical expression to reach a compromise between the two isotherms as shown in Equation 2.14.

$$q_e = \frac{K_R C_e}{1 + b_R C_e^\beta} \quad 2.14$$

After linearization, the model is expressed as follows:

$$\ln\left(K_R \frac{C_e}{q_e} - 1\right) = \beta \ln(C_e) + \ln(b_R) \quad 2.15$$

where K_R and b_R are the R-P constants while β is the heterogeneity coefficient. The model reduces to Langmuir isotherm when the value of β becomes unity but as the value of $b_R C_e^\beta$ increases higher than unity, the model becomes the Freundlich isotherm. The ratio of $K_R/b_R C_e^\beta$ indicates the adsorption capacity (Belhachemi & Addoun, 2011).

It is sufficed to mention here that before any isotherm can be chosen to describe the adsorption for a particular adsorbate/adsorbent interaction, isotherm experiments must be conducted to generate sufficient experimental data and the data are then analyzed by plotting each model. The suitable model should be characterized with highest regression constants and lowest statistical errors (such as root mean square error, standard deviation,

standard error or chi-square) for the concerned system. In addition, an isotherm which fits a particular adsorption system may not be suitable for another system, it depends on the mechanism of the interaction of the adsorbate to the adsorbent surface sites. However, among the various isotherms that have been developed and investigated, Langmuir and Freundlich isotherm models are the most commonly used in water and wastewater treatment.

In this study, the two most commonly used isotherm models (Langmuir and Freundlich) will be used to understand the interactions of the adsorbate onto the adsorbent.

2.8 Adsorption kinetic models

The rate of adsorption or adsorption kinetics is an important factor for designing adsorption system. This is because, predicting the mechanisms and characteristics of the adsorption, the performance of the adsorbent and most importantly, planning future facilities for a large-scale adsorption, whether in batch or column operation all depend on the understanding the adsorption kinetics. Adsorption kinetic models are used in similar way as isotherm models to fit the adsorption kinetic data. But adsorption process is governed by three steps, that is; external mass transferred of the adsorbate from the bulk solution to the external surface of the adsorbent, the internal diffusion of the adsorbate to the sorption sites and the sorption itself (Largitte & Pasquier, 2016). In adsorption process, some models are based on the fact that sorption is the rate limiting step while some based on the diffusion of the adsorbate as the rate limiting step. So, to understand the adsorption mechanism during the adsorption process, the fitting of the experimental kinetic data by the kinetic models is very important. Some of the adsorption kinetic models that have been proposed and found applications in water and wastewater treatment are reviewed in the following sections.

2.8.1 Lagergren First-order/ Pseudo First-order model

In 1898, Lagergren suggested the first kinetic equation for describing liquid-solid adsorption systems and was initially known as Lagergren first-order model. But, as more kinetic models were being discovered, Ho and McKay deemed it fit to rename the model as pseudo first-order (PFO) in 1999 (Tseng, Wu & Juang, 2010). Since then, several research studies have investigated this model to explain the mechanism of adsorption process for different solutes and commented to be suitable. The non-linear form of the PFO model is defined as below:

$$q_t = q_e(1 - e^{-k_1 t}) \quad 2.16$$

In linear-form, the equation becomes:

$$\log(q_e - q_t) = \log q_e - \frac{k_1 t}{2.303} \quad 2.17$$

where q_e and q_t (both in mgg^{-1}) are expressed as amounts of solute adsorbed by the adsorbent at equilibrium and at any time 't', and k_1 (min^{-1}) is the rate constant of adsorption.

2.8.2 Pseudo Second-order model

The pseudo second-order kinetic model was developed consequent to the pseudo first-order and it is based on the assumption that the rate-limiting step may be chemical sorption or chemisorption, involving valence forces through sharing or exchange of electrons between the adsorbate and the adsorbent (Ho & McKay, 1999). The non-linear form of the model is expressed as in Equation 2.18:

$$q_t = \frac{k_2 q_e^2 t}{1 + k_2 q_e t} \quad 2.18$$

After transformation, the model can be written as:

$$\frac{t}{q_t} = \frac{1}{k_2 q_e^2} + \frac{1}{q_e} t \quad 2.19$$

where k_2 (g/mg min) is the rate constant of pseudo second-order adsorption and other parameters retain their usual definitions as defined earlier.

2.8.3 Intra-particle diffusion model

It is a linear equation expressed as follows:

$$q_t = k_p t^{1/2} + C \quad 2.20$$

where k_p (mg g⁻¹ min^{-1/2}) is the intra-particle diffusion rate constant and C is the constant which indicates the thickness of the boundary layer and the larger the value of C , the greater the boundary layer effect. These parameters can be calculated from the slope and intercept of the plot of q_t against $t^{1/2}$. The IPD model often involves two or more stages and any can be responding for the rate controlling step for the adsorption process (Huang et al., 2014).

2.8.4 Elovich model

The model is represented in the form below (Ho, 2006):

$$q_t = \frac{1}{\beta} [\log(\alpha\beta) + \ln(t)] \quad 2.21$$

where α and β are the two constants.

In a similar manner, to validate the adsorption kinetic model for any adsorption process requires that the non-linear or the linear expression of the model be plotted. The suitable model will be identified by the higher linear regression constants or by the least error when the predicted value is compared with the experimental data.

So far, pseudo first-order (PFO) and pseudo second-order (PSO) models are the most commonly investigated adsorption kinetic models reported in the literature. In this study, the two models will be used to study the adsorption process.

2.9 Adsorption thermodynamics

Since a change in temperature of an adsorption system has effects on the adsorption rate and the equilibrium capacity of the adsorbent for a particular adsorbate, thermodynamic investigation can also give some useful information about the nature of the adsorption process. The parameters that are used to describe the feasibility and spontaneity of the adsorption process are enthalpy change (ΔH), entropy change (ΔS) and Gibb's free energy change (ΔG). So, to determine the thermodynamic parameters, isotherm experiments must be conducted at different temperatures and the different equilibrium constants (K_d) known as distribution coefficient, which defines the degree of the adsorption affinity of the adsorbate to the adsorbent must be determined. The following Equations 2.22–2.24 relate K_d and the thermodynamic parameters together (Huang et al., 2014):

$$K_d = \frac{C_e}{C_{e,o}} \quad 2.22$$

$$\ln K_d = \frac{\Delta S^0}{R} - \frac{\Delta H^0}{RT} \quad 2.23$$

$$\Delta G^0 = -RT \ln K_d \quad 2.24$$

Where C_e and $C_{e,o}$ (mgL^{-1}) are the equilibrium concentration adsorbed on the adsorbent and the equilibrium concentration remaining in the solution, respectively. R is the universal gas constant (8.314 JmolK^{-1}) and T is the temperature (K). By plotting the linear relation of $\ln K_d$ against $1/T$, all the thermodynamic parameters can be calculated from the slope and intercept.

2.10 Adsorbent characterization methods

Several methods are used in adsorption studies to understand the nature of the adsorbent, identify the surface functional groups of the adsorbent and the surface morphology of the adsorbent materials. Characterization helps to understand the mechanism of adsorption, the role of each functional group and possible changes in the adsorbent surface after adsorption. A few of these characterization methods are briefly discussed below:

2.10.1 Fourier Transform Infra-Red (FTIR)

The molecular structure of the adsorbent sample is studied by passing the infrared radiation through the sample. When IR radiation is passed through a sample, the radiation having same frequency as one of its vibrations will be absorbed while other is transmitted through the sample. This results into the stretching and bending of the molecular bonds. The amount of absorbed energy dictates the amplitude of the vibration but the vibration frequency is usually unchanged. Also, the amount of energy absorbed varies from one material to the other, depending on the molecular structure and the interaction of the IR radiation with the molecule of each material. The IR spectrum produced by one material is a unique characteristic of that material and no two materials have similar IR spectrum. The size of the peaks in the spectrum indicates the amount of material present. And once the wavenumbers of the absorbed energy are determined (through software algorithms), the kind of bond of each stretching and bending vibration of the molecule can be determined based on their characteristic frequency. With FTIR spectrometer, unknown material can easily be identified, the quality of a given sample or the number of components in a mixture can be determined. Besides, it has the advantage of being very sensitive making simultaneous measurement of frequencies of vibrations of the bond possible unlike the dispersive or filter methods of infrared spectral analysis, which scans through the frequencies.

2.10.2 Scanning Electron Microscopy (SEM)

To understand the surface morphology of sample of a material, SEM is a useful instrument for that purpose. A scanning electron microscope (SEM) is a type of electron microscope used to produce the image of a sample by passing a focused beam of electrons to the sample for scanning through it. Usually when the electron is passed to interact with the atoms in the sample, various signals containing information about the surface topography and composition of the sample are produced. Although, the signals produced include secondary electrons (SE), back-scattered electrons (BSE), characteristic X-rays, specimen current and transmitted electrons, but the most common standard SEM mode is detection of SE emitted by the excited atoms when the electron beam is passed. With SEM, it is possible to achieve high-resolution revealing details less than 1 nanometer. SEM micrographs produce three-dimensional appearance due to its large depth of field, making it easier to understand the structure of the material. This is made possible as a result of the very narrow electron beam. However, FESEM has more intensive and monochromatic electron beam with unlimited depth of field making its micrographs clearer, less electrostatically distorted and spatial resolution down to $\frac{1}{2}$ nanometers.

2.10.3 Field Emission Scanning Electron Microscopy (FESEM)

Just like SEM, FESEM is used to provide the surface topography, composition and other properties of the sample such as electrical conductivity at wider range of magnifications. Unlike SEM, it has unlimited depth of field with clearer and less electrostatically distorted images and spatial resolution down to $\frac{1}{2}$ nanometers. In addition, FESEM has more intensive and monochromatic electron beam which is responsible for the better image obtained compared to SEM. The electrons are liberated from a field emission source and accelerated in a high electrical field gradient (acceleration voltage of the order of magnitude of 0.5 to 30 kV). Within the high vacuum column ($\sim 10^{-7}$ Pa), the generated electrons are controlled to produce a narrow scan beam

that bombards the sample. This results into the emission of the secondary electrons from the sample, which is related to the surface structure of the material. A detector receives the secondary electrons and transforms that electrical signal which can be amplified or transduced to a video scan-image that can be obtained on the display unit connected to the instrument or as a digital image that can be saved and processed further.

To observe material under both SEM and FESEM techniques, the object must first be made suitable to high vacuum and should not alter the vacuum. However, it depends on the material to be scanned, some materials may need to be coated with gold, titanium or palladium while adsorbent materials like polymer and its composites can be scanned directly if they are in dried and fine powdered form.

2.10.4 Energy-dispersive X-ray Spectroscopy (EDX/EDS)

Energy-dispersive X-ray spectroscopy (EDX/EDS) is an analytical but powerful technique used to identify elemental composition of materials. The equipment is coupled with SEM/FESEM to allow for elemental information to be gathered about the material under investigation. The working of EDS is based on the detection of characteristic X-ray that is produced when a high-energy beam of electrons is focused on the sample. The electron beam causes excitation of the atoms contained in the sample which subsequently results into X-ray production in order to discharge the excess energy. The energy of X-rays is the characteristic of the atoms that produced them, forming peaks in the spectrum. However, a particular element may have more than one peak associated with it and in some cases, peaks of different elements may overlap. The analysis can be taken by selecting a specific point in the sample or a particle and can as well be done by mapping out a selected area of the sample to identify the elemental composition in that region.

2.10.5 Transmission Electron Microscopy (TEM)

Sometimes, SEM/FESEM images might not give detailed information about a specimen due to its low resolution. In a bid for much better analysis technique which helps to understand well the surface morphology and to give a high-magnification images of thin specimen, Transmission electron microscopy (TEM) was discovered in 1931 by Max Knoll and Ernst Ruska. TEM is a microscopy technique that makes use of electron beam (> 100 keV) as a source of high-energy instead of light to interact with the specimen. The use of electrons as energy source was due to the limitations of light, related to its longer wavelength as compared to electron which exhibits much shorter wavelength as result of its wave-particle duality (Juilong, 2014). Thus, making electron to produce high resolution images of several hundred better than the use of light waves. With these qualities of high resolution and magnifications of TEM technique, it has increased its applications in different fields such as in natural sciences, medical or tissue engineering for measuring the elemental compositions, crystallography and surface morphology of different specimens. Figure 2.3 shows the TEM diagram with all its components. When the electric field is set up, electrons are accelerated from the electron source at the top of the microscope and travel through the vacuum column. The wavelength of the accelerated electrons is given by the de Broglie equation given as equation 2.25 below (Juilong, 2014). Meanwhile, the electromagnetic lenses focused the electron beam to the specimen and since TEM operates in transmission, the sample must be thin to avoid multiple scattering of electrons due to thick sample or sample with large atomic number. The transmitted electrons from the sample then passes to the fluorescent screen where they are collected as a shadow image of the sample.

$$\lambda = \frac{h}{m_0 v \sqrt{(1-v^2/c^2)}} = \frac{h}{\sqrt{2m_0 eV - \left(1 + \frac{eV}{2m_0 c^2}\right)}} \quad 2.25$$

where h is called Planck's constant and it is given as 6.626×10^{-34} Js, m_o is the rest mass of the electron (9.109×10^{-31} kg), v is the velocity of the electron, c is the speed of light (2.998×10^8 m/s) and V is the accelerated electron beam voltage.

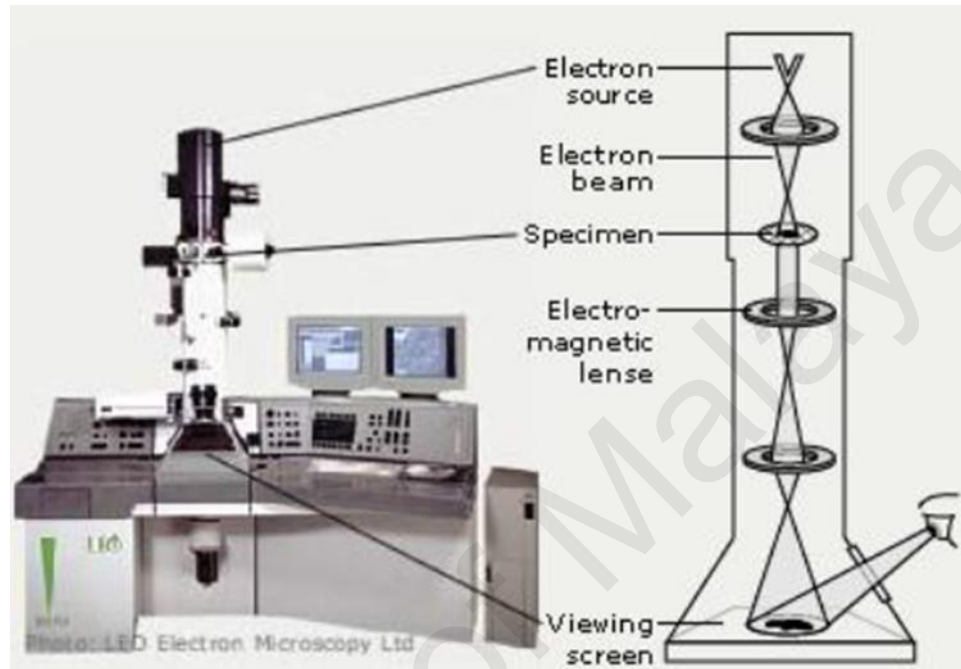


Figure 2.3: Operating mode of TEM with all its component parts (Al-Nasri, 2013).

2.10.6 X-ray diffraction (XRD)

X-ray diffraction (XRD) is a rapid and nondestructive technique for phase identification of crystalline materials and can provide information on unit cell dimension. The X-ray diffraction instrumentation consists of three main parts namely: The X-ray source, a sample holder and an X-ray detector.

A continuous beam of X-rays generated by the X-ray source is filtered to produce monochromatic X-rays required for diffraction and collimated to be focused on the sample under investigation. The interaction of the incident rays with the crystal material produces constructive interference (and diffracted rays). The wavelength of the radiation is given according to the Bragg's law as $n\lambda = 2d\sin\theta$ (where d is the lattice spacing in a

crystal sample, n is an integer and the θ is the angle of diffraction). The patterns of the diffracted radiation from the material are detected, processed and converted to count rate by the detector which is output to a device such as monitor or printer. By scanning the sample through a range of 2θ angles, all possible diffraction directions of the lattice should be attained due to the random orientation of the powdered material.

By converting the diffraction peaks to d -spacing, identification of minerals can be made possible since each mineral has its unique d -spacing if compared with standard reference patterns.

2.10.7 Thermogravimetric (TG) and Differential thermogravimetry (DTG) analysis

The temperature-dependence of adsorbent material is usually studied to know the changes in the material physical and chemical properties as a function of increasing temperature, as temperature changes or as a function of time. This will help to optimize the use of the adsorbent material when applied to remove adsorbate in solution of different temperatures. Different materials behave differently under varying temperature, a change in the temperature may increase or decrease the mass of the sample of adsorbent material. To do this, Thermogravimetric analysis (TGA) is a powerful technique which finds applications in monitoring thermal behaviors of materials under temperature.

TGA is specifically used to measure changes caused by mass loss or gain due to thermal decomposition, degradation mechanisms and decay kinetics, moisture content and volatility of materials, the composition and approximate lifetime of materials (Al-Nasri, 2013). To do this, the material is first measured in inert gas such as N_2 or Ar to reduce the oxidation or prevent undesired reactions and then under controlled atmosphere.

The main requirements of TGA are a precision balance with a pan loaded with sample and the furnace. The TGA features and the sample pan located inside the furnace are shown in Figure 2.4. However, in using TGA technique, calibrations are very important steps to ensure correct working of the instrument and to ensure the accuracy of obtained results. The first calibration is temperature calibration which is considered the heart of the TG analyzer and must be done periodically to ensure the thermos balance. Others are the precision balance calibration which supports the sample pan and the furnace calibration, which can be programmed for a constant heating rate or heating to acquire a constant mass loss with time. These are responsible for the measurement of the sample mass as a function of temperature and time.

Differential thermogravimetric (DTG) on the other hand is also a technique for thermal analysis for measuring the temperature difference between a sample and an inert reference material as a function of temperature or time, when the two materials are subjected to same temperature regimes in an environment heated or cooled at a constant rate. The inert reference helps to understand whether the change in the studied material is exothermic or endothermic. Thus, information such as structural changes, glass transitions, crystallization, melting and sublimation of a material can be gathered from DTG. In addition to the features of TGA, the DTG consists of two thermocouples which are connected to a voltmeter. One thermocouple is placed in an inert reference material and the other is placed in the material under investigation so that the differential temperature can easily be recorded.

However, modern technology has incorporated the two techniques together such that both TG-DTG analysis can be performed at the same time. This has helped the material analysis for mass loss and thermal information to be done simultaneously.

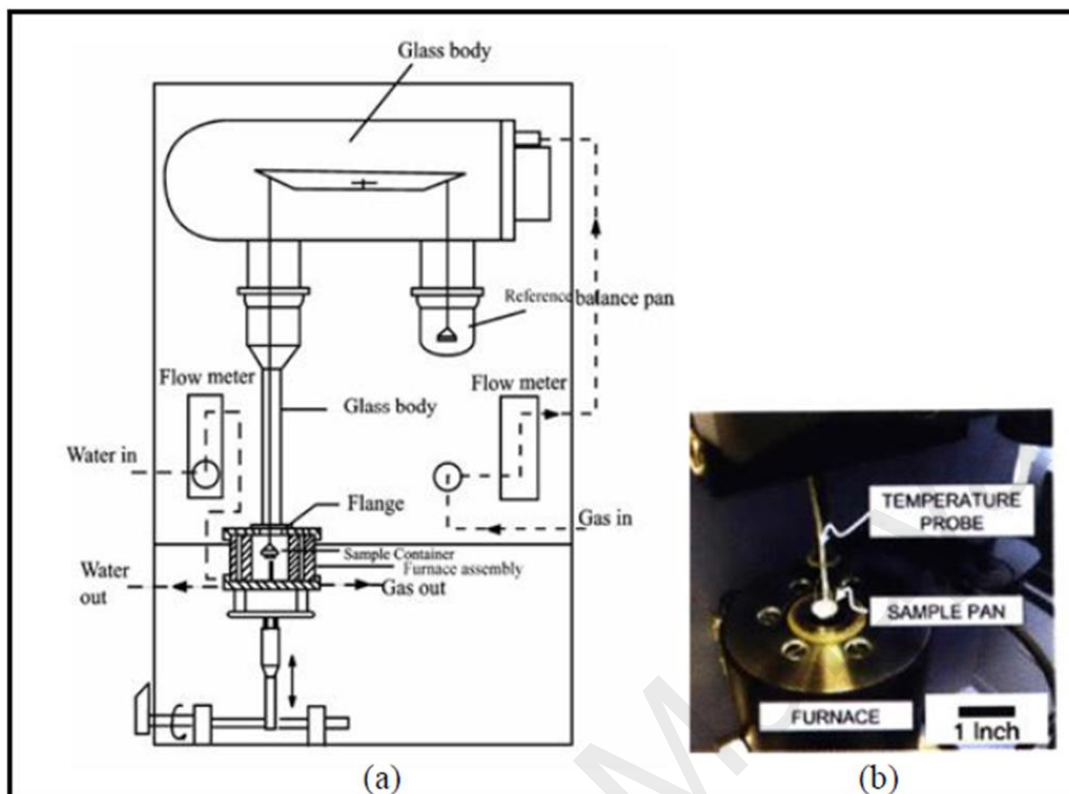


Figure 2.4: Schematic diagram of TGA (a) and top view of sample pan being loaded into furnace (b) (AL-Nasri, 2013).

2.11 Review of adsorption of radioactive materials

Several research studies have been conducted over the years but only the recent literature is reviewed in this study. In addition, attention is focused on the polymer adsorbents since the present study concerns the applications of polymer materials for radioactive materials removal. Meanwhile, many works could be found in the literature to address adsorption of radioactive and non-radioactive heavy metals in both single-solute and multi-solute systems, only cesium (Cs), cobalt (Co), cadmium (Cd) and their radioactive forms are considered.

2.11.1 Multi-solute adsorption

Seid et al., (2014) studied the removal of Cd(II) and Co(II) ions from aqueous solutions using polypyrrole particles. The adsorbent was synthesized in acetonitrile by oxidative polymerization of pyrrole in the presence of polyethylene oxide as stabilizing agent using

potassium peroxydisulfate dissolved in sulphuric acid as oxidant. According to their findings, the equilibrium data were best fitted with the Langmuir isotherm and the kinetics data were in accordance with the pseudo first-order kinetic model. The as-prepared adsorbent could remove Cd and Co with maximum capacity of 71.4 and 70.04 mg/g, respectively, with equilibrium time being reached within 12 min. Adsorption rate was found to increase as temperature increased from 25 to 45 °C, confirming the spontaneous and endothermic nature of the adsorption process.

Chitosan benzoyl thiourea derivative (CTU) was synthesized and the adsorptive characteristics of the material was investigated for ^{60}Co and $^{152+154}\text{Eu}$ radionuclides (Metwally et al., 2009). Adsorptivity of the radionuclides was studied in terms of change in time, pH, ion concentration and equilibrium concentration. They reported that 1 and 4 h contact time is sufficient for ^{60}Co and $^{152+154}\text{Eu}$ to reach equilibration at pH 3.5 and 8.0, respectively. The equilibrium concentration was reached at 5×10^{-3} and 7×10^{-3} M for both ^{60}Co and $^{152+154}\text{Eu}$, respectively. Langmuir and Freundlich were successfully fitted to the experimental data and likewise, the kinetic data were fitted by pseudo first-order and Morris-Weber kinetic models.

Park et al., (2010) studied the adsorption of cobalt, strontium and cesium from radioactive laundry wastewater by using ammonium molybdophosphate-polyacrylonitrile (AMP-PAN) composites. The adsorbent was characterized with video microscope, EDS and FTIR techniques. Based on their findings, the adsorbent removed the radioactive materials from the nuclear waste effluent by both physical adsorption due to the weak Van der Waals forces and ion exchange of inorganic component of the adsorbent. The adsorptive characteristics of the adsorbent for single-solute adsorption of Co^{2+} , Sr^{2+} and Cs^{+} ions were investigated in the presence of different co-existing metal ions, surfactants and solution pH while temperature and contact time were kept at 20 °C

and 24 h, respectively. The presence of Na^+ was found to reduce the adsorption of Cs^+ and, Co^{2+} was inhibited by the presence of Ca^{2+} . Both cationic (OTMA and HDTMA) and anionic (SDBS and SOBS) surfactants also inhibited the radionuclides adsorption, while non-ionic surfactants (Tween 80 and Triton X-100) did not influence the adsorption. The adsorption data were fitted well with Langmuir and Freundlich models but showed that the D-R model could not be used. The maximum sorption capacity was reported as 0.16, 0.18 and 0.61 mmol g^{-1} for Co^{2+} , Sr^{2+} and Cs^+ , respectively. Bi-solute adsorption of competing metal ions was fitted with competitive Langmuir model (CLM) and the results showed that the presence of one metal ion suppressed the adsorption of another, except for the Cs^+ that was promoted. Similarly, Transition metal ions hexacyanoferrate-PAN composite adsorbent was used to remove cesium and cobalt from radioactive waste solution (Nilchi et al., 2007). XRD, FTIR and TGA-DTG analysis were performed to identify the successful formation of the composite material. The polymer adsorbent dissolved in concentrated solutions of ZrCl_2 , LiBr , NaSCN and CaCl_2 salts and in strong mineral acids due to the chemical instability of polyacrylonitrile but demonstrated radiation stability to gamma irradiation of 100 kGy. They reported Cs adsorption was higher than that of Co but adsorption was not affected by the increase in temperature.

A cross-linked poly (graphene oxide-aminopropyl) copolymer material (poly (GO-APP)) was synthesized via esterification reaction and in situ polymerization by Qin et al., (2014). The as-prepared composite material was characterized by different techniques including FTIR, XPS, SEM, TGA-DTG and Raman spectroscopy which confirmed the successful formation of the polymer on the GO surface. The material was studied for its swelling and adsorptive characteristics for various metal ions including Cd^{2+} , Cu^{2+} , Ni^{2+} and Pb^{2+} . The authors reported higher adsorption capacity of the cross-linked copolymer for the metal ions compared to GO and this was attributed to the higher oxygen-containing

and amino functional groups of the copolymer chain. Similarly, Graphene oxide-supported polyaniline (PANI/GO) was synthesized by chemical oxidation and used to enrich some radionuclides such as U(VI), Eu(III), Sr(II) and Cs(I) from aqueous solution (Sun et al., 2013). Raman, SEM, potentiometric titrations, FT-IR spectroscopy, TGA and XPS measurements have been used to characterize the adsorbent material. The maximum sorption capacities of the radionuclides at pH 3.0 and 298 K were calculated from the Langmuir model to be 1.03, 1.65, 1.68 and 1.39 mmol g⁻¹ for U(VI), Eu(III), Sr(II) and Cs(I), respectively. The adsorbent was reported to have strong affinity for the studied radionuclides due to its oxygen and nitrogen functional groups, but the affinity was much stronger for nitrogen groups than for the oxygen functional groups.

Cesium and strontium were separated from the acidic radioactive waste stimulants by microporous tungstate/ polyacrylonitrile composite adsorbent (Griffith et al., 2005). The composite demonstrated high dynamic cation exchange capacity for the investigated radioactive metal ions in fixed-bed column. Polymer matrixes were also used for simultaneous removal of Cd and Zn and it was reported that the Cd removal yielded 40 % removal higher than that of Zn (Pires et al., 2011). ZrPs nanoparticles impregnated within polystyrenesulfone cation-exchanger was used to remove various heavy metals including Cd. The material analysis by TEM revealed that the amorphous nanoparticles of size 10 nm were dispersed in the inner surface of the polymer (Zhang et al., 2008). Sorption mechanism was described based on the results of FT-IR, Raman and NMR analysis to be due to the presence of non-diffusible sulfonate and thiol groups in the adsorbent materials. Regeneration of the adsorbent was carried out using 6 M HCl and reuse was more than 84 % even after five cycles. Other chemically modified and chelating polymer adsorbents, particularly polystyrene based adsorbents for multi-solute adsorption of radioactive heavy metals removal such as Cs, Co, Hg, U(VI), La(III) and their sorption

capacities under various equilibrium conditions are contained in the review work of (Pan et al., 2009).

2.11.2 Single-solute adsorption

Cesium

Vincent et al., (2014) immobilized inorganic ion-exchanger into biopolymer foams and used for the adsorption of cesium from the aqueous solution. The adsorbent was characterized by SEM-EDX, XRD and wet mineralization for surface morphology and material constituents. According to their findings, the immobilization increases the binding affinity of the biopolymer foams and the maximum sorption capacity was calculated by Langmuir model, which was consistent with the value obtained by using Clark model for breakthrough curves in the column studies. The adsorption kinetic data fitted well to the pseudo-second order kinetic model. It was reported that Cs(I) was readily exchanged with K(I) during the adsorption process. Cellulose triacetate plasticized polymer inclusion membrane containing crown ethers was investigated for the removal of cesium from nuclear waste solutions by Mohapatra et al., (2009). The material was reported to have high selectivity or efficiency for cesium compared to most other membranes.

Manganese dioxide-polyacrylonitrile (MnO₂-PAN) was chemically synthesized and investigated for the removal of radiocesium from aqueous solution (Nilchi et al., 2012). The FTIR, XRD, CHN elemental analysis, SEM, BET and TGA-DSC techniques were used for physico-chemical characterizations of the composite adsorbent. The surface area of the adsorbent is 53.03 m²/g and was found to be stable in different solvents including water, dilute acidic and alkaline solutions and ethanol, but decomposes in high acidic solution. The radiation stability test confirmed that the adsorbent is resistant to gamma-ray irradiation of up to 200 kGy. Using a radiotracer technique, the batch adsorption

experiments were investigated as a function of contact time, interfering coexisting ions and initial pH. It was reported that cesium could be efficiently removed in the $\text{pH} > 4.0$ and at 35 min equilibration time but was affected by the presence of alkaline and alkaline earth metal ions. Freundlich model was found suitable to describe cesium sorption by the composite adsorbent. The thermodynamic studies revealed the endothermic and spontaneous nature of the adsorption process. Desorption was carried out on the loaded-composite adsorbent which revealed the adsorption is irreversible due to the difficulty in eluting cesium from the adsorbent. AMP-PAN was also investigated for the cesium removal from high concentrated acidic tank wastes by batch and column operations (Todd et al., 2002). The TGA of the adsorbent revealed it is stable to $400\text{ }^\circ\text{C}$, the loss in mass was attributed to loss of hydrated water. The equilibrium isotherm data fitted well by Langmuir isotherm model and the dynamic sorption capacities for cesium were calculated as 22.5 , 19.8 and 19.6 mgg^{-1} for 5, 10 and 20 bed volume per hour flows in column operation. Potassium inhibited selectivity of cesium onto the polymer adsorbent.

Saberi et al., (2010) used sodium titanate-polyacrylonitrile (STS-PAN) composite to remove radioactive cesium from the solution. Their adsorbent was characterized by FTIR, XRD, thermogravimetry-differential scanning calorimetry (TG-DSC), BET, XRF and CHN elemental analysis. Their thermal and gamma irradiation stability tests confirmed that the adsorbent is stable to temperature of $270\text{ }^\circ\text{C}$ and 200 kGy radiation, respectively, while the surface area was determined to be $96.66\text{ m}^2/\text{g}$. The adsorption studies investigated the effects of pH, contact time, temperature and competing cations in the aqueous solution. Adsorption equilibrium was obtained at pH 6.0, 130 min and the equilibrium data were fitted well by Langmuir model. The process was endothermic in nature as adsorption increased with temperature and the desorption studies showed that 0.1 molL^{-1} HCl at $25\text{ }^\circ\text{C}$ was capable of eluting the sorbed cesium from the adsorbent.

Polyaniline titanotungstate composite ion exchanger synthesized by oxidative coupling was investigated for the removal of cesium ion from aqueous solution including aqueous milk samples by batch and column experiments (El-Naggar et al., 2012b). The adsorbent material was characterized by FTIR and X-ray fluorescence (XRF). Equilibrium data were fitted by Freundlich isotherm with maximum uptake capacity being 217 mg g^{-1} . The column experiments showed that half breakthrough time increases proportionally with increasing bed depths. The composite adsorbent demonstrated that cesium can be removed from the aqueous solution of high acid concentration with high affinity and selectivity for cesium in the presence of different metal ions.

Cobalt

Polyvinyl alcohol (PVA)/ chitosan magnetic composite adsorbent was synthesized and applied for cobalt removal from the radioactive wastewater (Zhu et al., 2014). FTIR and SEM-EDAX analysis were performed to identify the functional groups and surface morphology of the composite material, which revealed that $-\text{NH}_2$ and $-\text{OH}$ groups were responsible for Co adsorption onto the adsorbent. Polymer (polyethyleneimine) enhanced ultrafiltration was used to remove Co ion from the aqueous solution using experimental design (Cojocaru et al., 2009). The influence of initial concentration of cobalt in feed solution, polymer/metal ratio, and pH of the feed solution were studied on the rejection efficiency and binding capacity of the polymer. They reported 96.65 % rejection efficiency at the optimum conditions of 65 mgL^{-1} initial concentration, polymer/metal ratio of 5.88 and the pH 6.84.

Poly(N,N-dimethylaminopropyl methacrylamide/ itaconic acid) copolymers obtained by gamma-radiation polymerization were used as Co removal from aqueous solution (Baş et al., 2014). The gelation percentage for the adsorbent sample was maximum with 25 kGy dose of irradiation, and that was used for the adsorption and swelling experiments.

The structural and morphological characteristics of the adsorbent materials were assessed by FTIR, SEM and EDS. They reported that the presence of COOH and NH groups were responsible for the polymer-metal interactions. Adsorption reached maximum at pH 5 with capacity of 220 to 245 mgg^{-1} of dry sorbent and desorption was done with 0.1 M ethylenediaminetetraacetic acid (EDTA) within 5 days.

Also, polyaniline/polypyrrole copolymer nanofibers were synthesized and investigated as an adsorbent for the removal of Co ions from solution (Javadian, 2014). The adsorbent was characterized using FTIR, FESEM, TEM, TGA, DSC and BET surface area. The surface area was measured as 72 m^2/g . Under the common adsorption conditions, the optimum adsorption of 99.68 % was found to be obtained with 0.11 g sorbent dosage, pH 7.0, 11 min contact time and 100 mgL^{-1} . The adsorption isotherm data were fitted by Langmuir, Freundlich, D-R and Temkin models, while the estimated thermodynamic parameters revealed the endothermic and spontaneity of the adsorption process. Desorption was successfully carried out with 0.1 M H_2SO_4 at pH 2.0 and the recycled adsorbent was further used for adsorption with more than 90 % efficiency after third cycle.

Study on the coating of polyethyleneimine on Fe nanoparticles (PEI-coated Fe_3O_4) and its applications for the removal of trace levels of cobalt ions has been conducted (Saad, 2013). It was reported that increasing the amount of the nanoparticles over the PEI enhances the performance of the polymer adsorbent.

Cadmium

Polyaniline was coated on sawdust particles and then used for cadmium adsorption from aqueous solution (Mansour et al., 2011). In their studies, the effects of pH, initial metal ion concentration, adsorbent dosage and equilibrium contact time were

investigated. Optimum adsorption was obtained at pH 6.0, 40 min contact time and concentration range of 10 – 40 mgL⁻¹. The isotherm data were best fitted by Freundlich isotherm model and pseudo second-order kinetic model was found appropriate for the kinetic data.

No doubts, polymer adsorbents are potential candidates for heavy metal removal from aqueous solutions and from the foregoing, various investigations have been conducted and shown high removal efficiency by different polymers composites. However, general review of literature as highlighted above still shows a paucity of data in the use of polypyrrole-based adsorbents for radioactive metals removal, which have been categorized as one of the cheapest polymers to synthesize.

In the current study, polypyrrole adsorbents were synthesized and investigated for the removal of radioactive Cd, Cs and Co from aqueous solutions. The composites of polypyrrole were also synthesized on various templates via different routes and used as adsorbents to study the sorption performance under various adsorption conditions, in order to optimize the use of polypyrrole adsorbents (details can be seen in Chapter 3).

CHAPTER 3: RESEARCH METHODOLOGY

3.1 Chemicals and Materials

All chemicals used were of analytical and reagent grades. Nitrate salts of cesium, cadmium, sodium, rubidium, calcium, magnesium and potassium, and cobalt chloride hexahydrate ($\text{CoCl}_2 \cdot 6\text{H}_2\text{O}$) were obtained from R & M Chemicals. Ferric chloride hexahydrate ($\text{FeCl}_3 \cdot 6\text{H}_2\text{O}$) was purchased from Merck AG (Germany) and pyrrole (98%) from Acros. Sodium hydroxide (NaOH), hydrochloric acid (HCl) and sodium dodecylbenzenesulfonate (SDBS) were purchased from Sigma-Aldrich. All chemicals and materials were used as obtained from the suppliers without further purification except for the pyrrole, which was first distilled for high purity and stored in the refrigerator in the absence of light prior to use.

The ^{137}Cs , ^{60}Co and ^{109}Cd radiotracers (each has activity of $3 \mu\text{Ci} = 111 \text{ kBq}$, traceable in 10 ml of 4 M HCl solution) was supplied in flame sealed vials and commercial granulated activated carbon (AC) were both purchased from Eckert and Ziegler Analytics. The AC was made from coconut shell. Deionized water was used all through the experiments.

The sawdust sample (*Dryobalanops aromatic*) used for surface modification of polypyrrole was kindly provided by the wood section of the Mechanical workshop of the Department of physics, University of Malaya. The *Dryobalanops aromatic* tree, also known as camphor tree, is a very heavy hardwood and probably the tallest tree found in the Malaysian forest, and it is commonly used as a building material in Southeastern Asia. The solid materials on the collected sawdust sample were hand-picked before washing with water to remove dust-related impurities from the surface. The clean sawdust (SD) was dried at 50°C for 48 h in an oven. The dried sample was sieved to fine particle sizes

(0.125 – 0.212 mm) using US standard stainless steel sieve series (A.S.T.M. E-11 Specifications, Dual Mfg. Co.).

3.2 Synthesis of polymeric materials

The polypyrrole adsorbents used in this study were prepared by in situ chemical polymerization of pyrrole using $\text{FeCl}_3 \cdot 6\text{H}_2\text{O}$ as oxidant. Here, polypyrrole was first prepared with different ratios of pyrrole to oxidant and the product was subsequently tested for adsorption performance. The pyrrole to oxidant ratio of as-prepared polypyrrole that yielded better adsorption performance was doped with SDBS surfactant. The choice of using a surfactant is to enhance its stability for environmental usage, since polypyrrole alone lacks long-term stability and mechanical properties (Chen et al., 2016). So, large size dopant and surfactant such as SDBS, SDS, etc are usually found suitable to enhance the polymer stability and also its surface morphology. In addition, pure PPy has low sorption capacity for metal ions due to the problem of easy aggregation in water. As a result, anionic surfactants were used to increase PPy water dispersion so as to increase the chances of adsorbate/adsorbent interactions, which could result into better adsorption. Apart from this, anionic surfactant was also envisaged to play additional role in increasing the fewer surface sites of the polypyrrole, which may lead to better adsorption performance over the pure polypyrrole. Previous works can be found where anionic surfactants have been used as additive materials to increase the sorption performance of adsorbent materials for contaminants (Aydiner et al., 2006; Rafatullah et al., 2011).

In a typical preparation, solutions of pyrrole and $\text{FeCl}_3 \cdot 6\text{H}_2\text{O}$ oxidant were prepared separately in a ratio of 1:1, 1:2 and 1:3, respectively. In each case, the oxidant solution was added in a slowly and continuously drop-wise steps to the pyrrole under agitation at 300 rpm on a platform shaker. After a few drops of the oxidant, it was noticed that the colourless solution of pyrrole changed to black solution, which was continued with more drops of the oxidant for 4 h until the pyrrole was completely oxidized. The black

polypyrrole product precipitated in the solution was separated by filtration and subsequently washed with deionized water until it was colourless. The PPy produced was then dried in an oven at 50 °C for 48 h and grinded in a mortar before use.

Commencing with the preliminary investigation of the adsorption tests using the as-prepared PPy, another synthesis was made with the anionic surfactant as mentioned earlier. Firstly, pyrrole was dissolved in the deionized water and 6.854 mM of SDBS was added and the solution was sonicated for 15 min until a uniform white pyrrole/surfactant solution was formed. After then, the already prepared oxidant solution was added in drop-wise as before and the mixture was monitored under agitation for 4 h until the surfactant-doped polypyrrole was fully formed. The fast growth of the PPy in SDBS resulted to high mass yield of the black product, which was separated, washed and dried as explained previously. All preparation was done at a room temperature (20 °C). The concentration of SDBS was varied from 1.714 to 27.416 mM for different products of surfactant-doped polypyrrole, which was investigated for adsorption performance and the best product with higher adsorption was latter modified with either sawdust or activated carbon. In each case, the SDBS-doped polypyrrole was named PPy/SDBS.

3.3 Composites of polypyrrole

One of the best ways to enhance sorption capacity of polymer adsorbent for different adsorbates is by modification with other functional materials. In this study, PPy was modified with sawdust and coconut-shell based commercial granulated activated carbon. Sawdust has been studied much for adsorption of various pollutants as well as activated carbon, particularly for the removal of organic compounds from aqueous solution. Although, these materials alone sometimes displayed low sorption capacity for heavy metal ions (Hong et al., 2014). The effects of these materials on the surface morphology and subsequent adsorption characteristics of PPy adsorbent were investigated in this

study. Pyrrole monomers were polymerized on the sawdust and granulated activated carbon as follows:

For the polypyrrole-sawdust and polypyrrole-activated carbon composites, a requisite amount of 1- 2.0 g of the sawdust or activated carbon (0.125 – 0.212 mm) was soaked in the pyrrole solution with or without SDBS for 12 h for uniform adsorption of the pyrrole into the pores of the sawdust or activated carbon under mechanical stirring at 500 rpm. For the preparation with SDBS, SDBS was initially dissolved in the pyrrole solution by sonication for 15 min before addition of sawdust or activated carbon. After the reaction period in each case, the already soaked sawdust/activated carbon was separated from the solution and dispersed into the solution of oxidant and further stirred for 4 h for complete polymerization. The composite adsorbent was separated from the solution, washed and dried as before. The as-prepared sample was named as PPy/SD, PPy/SDBS/SD, PPy/AC and PPy/SDBS/AC composites. Figure 3.1 shows the block diagrams for the polymerization of pyrrole and its composites as explained above.

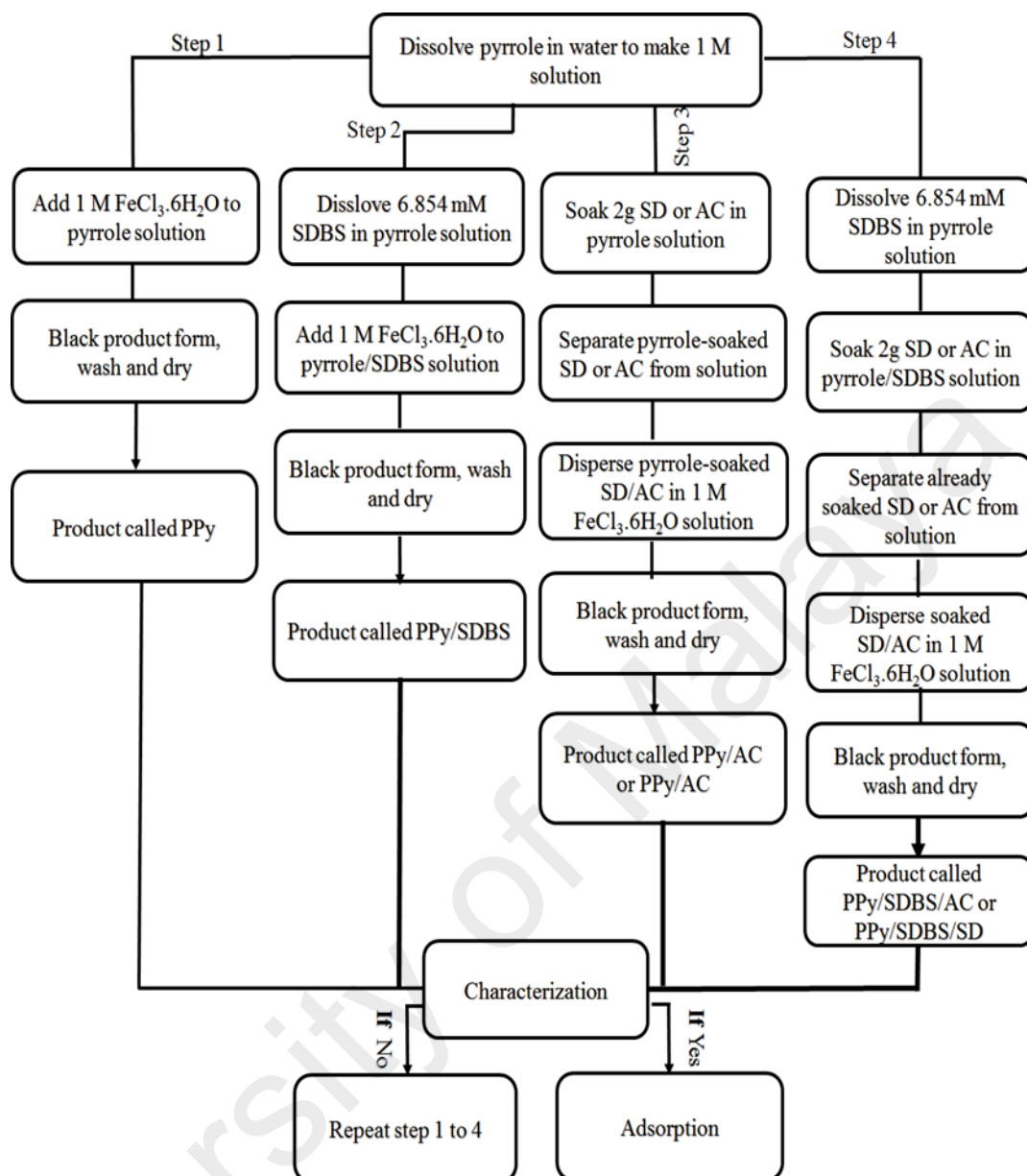


Figure 3.1: Block diagrams for the chemical synthesis of polypyrrole and its composites used in this study.

3.4 Characterization of polymeric adsorbent materials

The as-synthesized polypyrrole-based materials have been analyzed by different techniques to understand the physico-chemical properties, surface morphologies, surface functional groups, thermal stability and other adsorptive properties.

3.4.1 Surface characterization and thermal stability

In this study, BET surface analysis, FESEM, HR-TEM, FTIR, TG-DTG, and XRD techniques were employed for the prepared polymer-based adsorbents.

The BET surface area and porosity were measured from the N₂ gas-adsorption/desorption isotherm at 77.4 K using Micromeritics (ASAP 2020 and Tritar II 3020 Kr). The adsorbent samples were first degassed at 300 °C for 4 h before measurement to remove unwanted vapours and gasses. The minimum mass of the adsorbent sample required (about 181.5 mg) was placed in a glass cell. A glass rod was put inside the glass cell containing the sample to minimize the dead space in the glass cell. After the degassing process, the sample was transferred to the analysis port and cooled down using liquid N₂ dewar to maintain a constant low temperature for a good interaction between the adsorbate gas and the adsorbent sample. The dead volume of the sample was used to calibrate the cell prior to measurement and after the measurement using argon gas because it does not interact with the sample.

The surface morphology was conducted by Field emission scanning electron microscopy (FESEM, SU8220, Hitachi) at 2 kV accelerating voltage and at 11.3A emission current. The finely grounded powder sample was placed evenly on the carbon film and placed on the holder before it is put in the instrument for measurement. The morphology and particle size were further investigated by the HR-TEM analysis. A JEM 2100-F HR-TEM operated at 200 kV was used in this work. About 10 mg of the finely grounded adsorbent sample was suspended in 15 ml of dimethylformamide and the suspension was sonicated for 30 min. Then, the suspension was dropped onto a carbon-coated copper grid and dried at room temperature for 1 day. The copper grid containing sample was gently placed on the sample holder and put in HR-TEM instrument for measurement.

The analysis by FTIR spectroscopy was done using a Perkin-Elmer Spectrum (Wavenumber: 450-4000 cm^{-1}) on KBr pellets by press technique under uniform pressure.

The X-ray diffraction (XRD) data (on powders) were collected using PANalytical EMPYREAN diffractometer system in a 2θ configuration employing the $\text{Cu } \alpha$ radiation ($\lambda = 1.54 \text{ \AA}$) consisting of soller slits (0.04 rad), a fixed divergence slit (0.5°), a fixed anti-scatter slit (1°) and a rotating sample stage (rotating time of 8 s). The sample was scanned between $2\theta = 10^\circ$ and 70° with the PIXcel-3D detector.

Thermal decomposition was studied by thermogravimetric (TG) and derivative thermogravimetric (DTG) analysis to know the amount loss and the rate of change in the mass of the sample as a function of temperature using a Perkin Elmer TGA 4000 thermogravimetric analyzer with a computer interface. The analysis was done using approximately 0.825 mg of the adsorbent sample which was loaded in a ceramic crucible and, was spread evenly over the bottom of the ceramic to increase the surface area of the sample. The sample was then heated at a heating rate of $10 \text{ }^\circ\text{C min}^{-1}$ under nitrogen atmosphere ($25 \text{ cm}^3 \text{ min}^{-1}$) and temperature range of 20 – 900 $^\circ\text{C}$.

Finally, radiation stability of the as-prepared adsorbent sample was investigated by gamma irradiation at a dose rate of 2.42 Gy/min up to a total dose of 200 kGy using ^{60}Co γ -source (Gamma Cell 220, Product of Atomic Energy of Canada). The irradiated samples were further observed under FTIR for any structural changes and was subsequently used for adsorption studies.

3.4.2 Surface charge identification

Functional groups on the surface of AC are subjected to a wide variety of inter- and intra-molecular interactions. These interactions alter the surface chemistry of AC to be different from its parent material. As a result, the surface acid functional group

distribution for the AC and PPy/SDBS/AC composite was determined following Boehm titration scheme (Boehm et al., 1964). To do this, 0.20 g of either AC or PPy/SDBS/AC sample was added to 20 ml of each of the following 0.05 M solutions: sodium hydroxide (NaOH), sodium bicarbonate (Na_2CO_3), sodium carbonate (NaHCO_3) and hydrochloric acid (HCl). The mixtures were shaken for 72 h and then filtered (Whatman 42 filter paper) to remove particles. The filtrates were taken for titration of the excess of the base or acid using 0.1 M NaOH or HCl, respectively. The endpoint was determined using a phenolphthalein color indicator.

Hence, the total surface acidity was calculated as moles neutralized by NaOH, the lactonic group fraction was determined as moles neutralized by Na_2CO_3 , the carboxylic group fraction was calculated as moles neutralized by NaHCO_3 , the difference between the moles neutralized by NaOH and Na_2CO_3 was assumed as the phenolic groups content and the basic group fraction was calculated as moles neutralized by HCl following Mukherjee et al., (2011).

3.5 Preparation of radioactive solutions

The stock solution containing each of stable metal (cesium, cadmium, cobalt and cerium) was prepared by dissolving appropriate mass of the nitrate or chloride salts of the metal ions in the deionized water to make 1000 mg/L. From the stock solution, the required solutions were prepared and were spiked with the corresponding radiotracer solution for radioactivity monitoring by the HPGe detector. Assuming that both active and stable metal were equally sorbed on the adsorbent, the counting of active metal allowed determining of the residual traces of the corresponding stable metal (Vincent et al., 2014). For the working solutions, the initial radioactivities of the active metals were maintained at constant values (308.57 Bq/L for ^{109}Cd , 294.29 Bq/L for ^{137}Cs and 286.98 Bq/L for ^{60}Co in each 50 ml of radioactive solution) for easy subsequent calculations and

better understanding of the adsorption characteristics of the adsorbent for each radionuclide. The initial pH of the working solution was controlled by using 0.1 M NaOH and HCl solutions to the required pH value. The pH-meter (Orion, Model 720, Thermo Electron Corp., USA) was standardized prior to use by standard buffer solutions (pH values 4.0, 7.0 and 10.0).

3.6 Adsorption experiments

All the adsorption experiments were carried out in batch mode at room temperature. Preliminary investigations were first conducted to optimize adsorbent performance from various adsorbent preparation. To do this, 0.15 g of PPy (prepared from different pyrrole to oxidant ratio but without surfactant) was added to 50 ml each of 20 mg/L metal concentration spiked with respective radiotracer solution in a 250-ml polyethylene flask and agitated on an Environmental shaker-incubator (ES-20/60, Biosan) for 6 h at 150 rpm. The filtrate was separated using Whatman filter paper. Both the initial and filtrate solutions were analyzed for radioactivity by the HPGe gamma-ray detector. The mole ratio of pyrrole to oxidant (1:1) was used to prepare other polymer adsorbent materials as explained earlier and these were subsequently tested for adsorption performance. The preparation condition of PPy/SDBS showing highest adsorption was also used in the preparation of polypyrrole composite involving sawdust or activated carbon (details available in Chapters 4 and 5).

For the batch adsorption studies of single-solute of either ^{109}Cd , ^{137}Cs or ^{60}Co , adsorption was conducted with the prepared adsorbents. Firstly, the mass of the adsorbent was varied between 0.05 to 0.4 g with 50 ml solution containing 20 mg/L of stable metal, traced with the appropriate radiotracer solution. The pH of the solution was adjusted but was not increased beyond pH 9.0 (for ^{109}Cd), pH 10 (for ^{137}Cs) and pH 8.0 (^{60}Co) (this is to avoid metal oxides precipitation at higher pH in the case of cadmium and cobalt). The

contact time also was conducted at 30 min interval and did not go beyond 6 h, which was sufficient for equilibrium adsorption attainment. The temperature effect studies were conducted by varying the temperature from 20 to 50 °C. The Environmental shaker-incubator allowed easy switching of temperature of the solution. The effect of the initial stable metal concentration was studied by varying the concentration from 20 to 100 mg/L and in each case, the solution was agitated with the adsorbent for required contact time. The effect of metal ions on the adsorption of studied radionuclides was studied using the nitrate salts of common metals (such as sodium, potassium, rubidium, magnesium and calcium) found in the natural mineral waters.

The irradiated samples of the polypyrrole materials were investigated for adsorption of each radionuclide, following the conditions for adsorption by non-irradiated samples.

The isotherm, kinetics and thermodynamic parameters were investigated from the obtained experimental data to understand the nature of the adsorption process. The adsorption isotherms for the multi-solute adsorption of the studied radionuclides were conducted and the effect of preferential adsorption of one radionuclide over another was observed.

In each case, the initial and final radioactivities of the radionuclides contained in the solution were measured by the HPGe detector to determine the adsorption efficiency (AE, %) and adsorption capacity (q).

3.7 Gamma-ray spectroscopy system

Gamma spectrometry system is purposely used to detect the emitted gamma rays by the radioactive source, classified them according to their energies from which the activities of the rays are calculated in Becquerel (Bq). Each radionuclides ^{109}Cd , ^{137}Cs and ^{60}Co emits intense gamma rays that are measurable by the gamma-ray spectrometry system. The system consists of

- i. a high purity germanium crystal detector which converts the energy absorbed in the crystal into electrical pulses with height proportional to the incident photon energy
- ii. electrical, electronic and other transducers that can be used to determine the magnitude of the pulses.

A block diagram of the detector system used in this study is shown in Figure 3.2. The set up consists of

- i. a preamplifier for the amplification of the voltage pulse (signal) produced by the detector (or by the photomultiplier tube in the detector)
- ii. a linear amplifier for further amplification of the signal to obtain clean and strong signals
- iii. a low voltage power supply for the preamplifier
- iv. a high voltage power supply for the detector
- v. a multichannel analyzer which converts analog signals to digital signals with the aid of ADC
- vi. a PC unit for visual display of the spectrum and perform spectrum analysis

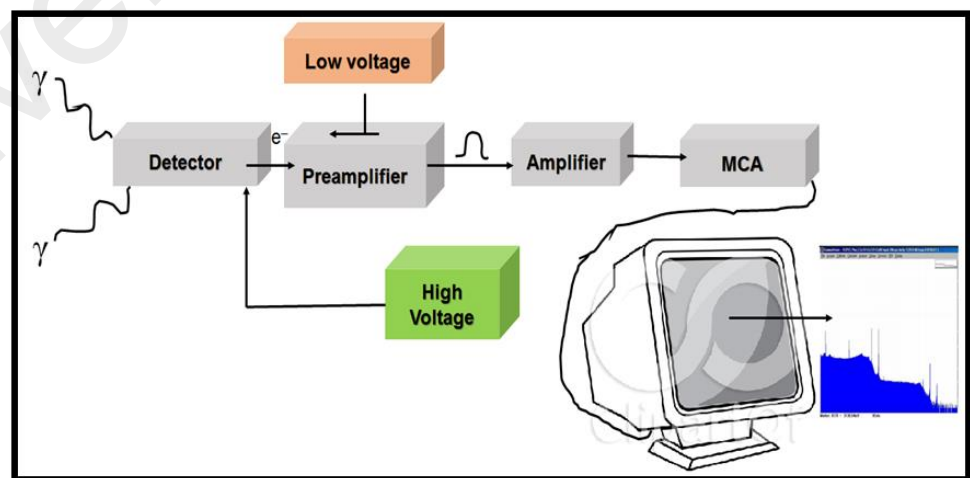


Figure 3.2: A block diagram of a basic gamma-ray spectroscopy.

3.7.1 Functions of the gamma-ray spectrometer components

The high energy-sensitive radiation detector coupled to a photomultiplier tube produces small voltage pulses (signals). The magnitude of these electrical pulses is proportional to the energy of the primary ionizing particles resulting from the gamma-ray interactions (the photoelectrons, Compton electrons, and positron-electron pairs).

The preamplifier receives the small voltage pulses (signals) from the detector and amplifies it. In addition, the preamplifier serves to provide a match between the high impedance of the detector and the low impedance of the coaxial cables to the amplifier. The main linear amplifier collects the amplified analog signals from the preamplifier and shapes, expands or magnifies the magnitude of the voltage pulses into easily and accurately measurable ranges. The amplifier filters the shape of the pulses to improve the signal-to-noise ratio and also prevents overlapping. The amplifier must amplify equally well at high count rates as it does at low count rates to prevent overloading.

The high voltage power supply gives stabilized high voltage for the operation of the detector. It is necessary that the voltage supply should be stable against fluctuations in temperature, line voltage and load. During the measurement, the high voltage supply was maintained at 2880 V.

The pulse sorter called Multichannel Analyzer (MCA) has an analog-to-digital converter (ADC). The signal from the linear amplifier is shaped into the Gaussian or Trapezoidal shape and converts that signal into a digital signal. The analog-to-digital converter (ADC) also sorts the pulses by height spectrum. The digitized signal is stored in an appropriate memory channel. Analog-to-digital conversion is made possible by charging a capacitor to the peak voltage of the pulse to be analyzed and then discharging it. The time for this discharge is a direct measure of the pulse voltage and is determined by counting the number of pulses generated by a high-frequency of the oscillator. The

data is stored in the memory channel whose number (address) has a storage capacity of 10^5 to 10^6 counts each per channel.

3.7.2 Shielding

The radiation detector is shielded in order to reduce the amount of radiation from background sources getting to the detector due to radioactive nuclides within the surrounding. The shielding is done in a way that it reduces backscattering.

Lead shield is usually used because it reduces the number of gamma-rays being scattered considerably. Other shielding materials like iron are as well being used but Compton-scattered in these is usually higher. However, the use of the lead ensures that fewer gamma-rays penetrate the shielding from outside and fewer backscattered gamma-rays from within the shield. The detector used for this work meets the optimum conventional detector shielding of 100 mm thickness of lead, 3 mm of cadmium or tin and 0.7 mm of copper.

Figure 3.3 shows the detector's absorber with the interactions that occur when gamma-rays are being detected from radioactive sources.

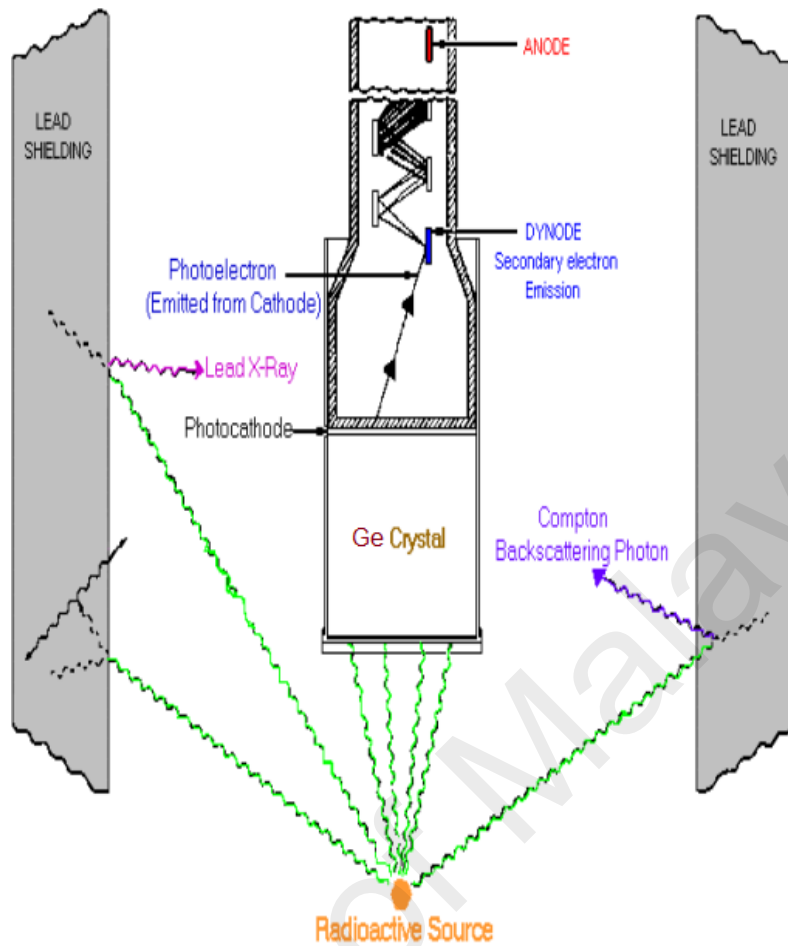


Figure 3.3: Radiation detector showing lead shielding and interaction that occur from radioactive source.

3.7.3 Detection system calibration

If a gamma spectrometer is to be used for identifying samples of unknown composition, its energy must be calibrated. The calibration is very crucial if accurate results of the gamma-ray spectra are to be achieved in terms of energy and specific activity. According to IAEA (1989), calibration is defined as the quantitative determination, under a controlled set of standard conditions, of the indication given by a radiation measuring instrument as a function of the value of the quantity the instrument is intended to measure.

The spectrometer calibration is done in processes which are:

- i. Energy calibration
- ii. Detection efficiency calibration

3.7.3.1 Energy calibration

The purpose of energy calibration is to ensure that a relationship exists between the peak position in the spectrum and the corresponding gamma-ray energy. Normally, calibration is achieved by measuring the spectrum of a source emitting gamma-rays of known energy and comparing the same with the measured peak position. It is advisable that for any source, the calibration energies should cover the entire energy range over which the spectrometer is to be used. The calibration process involved marking the peaks to be used and their correct energy, and then the energy/ channel relationship is deduced.

For the purpose of this work, the energy calibration of the spectrometer was performed using different gamma sources of known energies from Isotope Products Laboratories by Eckert & Ziegler Company, containing ^{241}Am , ^{109}Cd , ^{57}Co , ^{203}Hg , ^{113}Sn , ^{85}Sr , ^{137}Cs , ^{88}Y , and ^{60}Co emitting γ -rays (see Appendix A).

3.7.3.2 Efficiency calibration

The efficiency calibration was used to calculate the detection efficiency of the HPGe detector system as a function of energy. Efficiency calibration ensures that the calibration standard reference sample represents the samples to be counted. The calibration ensures the detector has maximum efficiency.

The equation that relates the efficiency, count C under the photopeak and the radioactivity, A , of the radionuclide is given as:

$$A = \frac{C}{\epsilon_{\gamma} \times T \times I_{\gamma} \times V} \quad 3.1$$

Where ε_γ is the detection efficiency for each radionuclide, T is the counting time in seconds, I_γ is the gamma yield (a fraction of the gamma rays of the particular energy per disintegration) and V is the volume of radioactive solution (see Appendix B for radioactivity calculations).

For the purpose of this work, the radionuclides used to fit the detection efficiency for the activity determination of both initial and supernatant radionuclide solutions are seen in Table 3.1 and the fitting of energy with efficiency is shown in Figure 3.4.

Table 3.1: Energy of the radionuclides with corresponding efficiency.

Nuclides	Energy (keV)	Intensity (%)	Efficiency (%)
^{57}Co	122.1	85.6	2.922769
$^{123\text{m}}\text{Te}$	159.0	84.0	2.836454
^{113}Sn	391.7	64.9	1.836565
^{85}Sr	514.0	98.4	1.229094
^{137}Cs	661.7	85.1	1.157831
^{88}Y	898.0	94.0	0.936829
^{60}Co	1173.2	99.86	0.87022
^{60}Co	1332.5	99.98	0.812756
^{88}Y	1836.1	99.4	0.665708

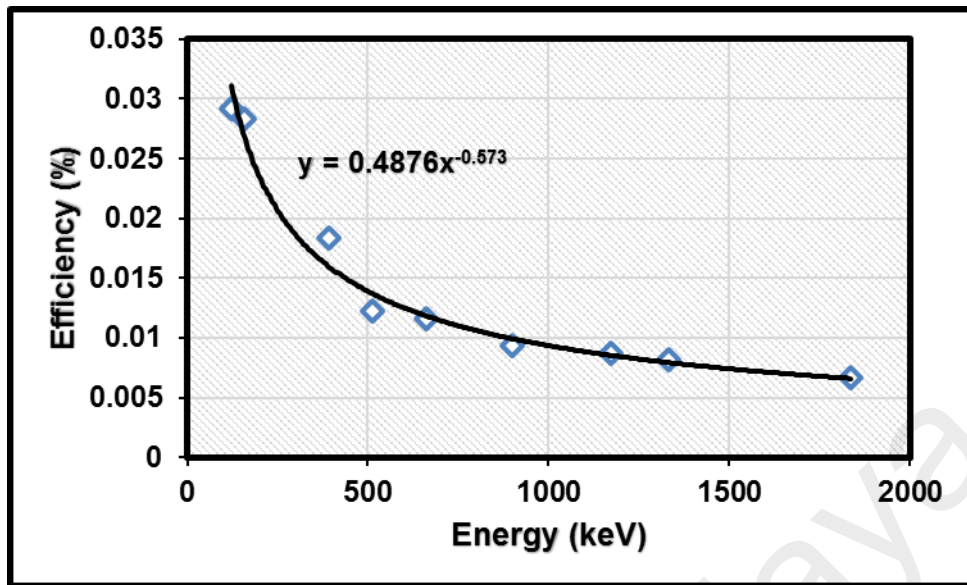


Figure 3.4: Energy of adsorption parameters.

3.8 Evaluation of adsorption parameters

To estimate the adsorption efficiency of each radionuclide under study, the radioactivity of each radionuclide before and after adsorption was measured. The adsorption efficiency was estimated using the relation below:

$$\text{Adsorption Efficiency (\%)} = \frac{A_o - A_e}{A_o} \times 100 \quad 3.2$$

where A_o and A_e represent the initial and supernatant radioactivity of the radionuclide.

Since the adsorbate solution contains both active and stable metal and both were equally sorbed on the adsorbent, the counting of active metal allowed determination of the residual traces of the corresponding stable metal (Vincent et al., 2014). As a result, to estimate the amount of the stable metal ion sorbed (q_e) by the adsorbent, the equation below was used:

$$q_e = \frac{C_o V_o - C_e V_e}{m} \quad 3.3$$

where C_o and C_e are the initial and supernatant concentrations of the stable metal ions, V_o and V_e are the corresponding initial and supernatant volumes of the aqueous solution, m is the mass of the adsorbent used (see Appendix C for examples on adsorption efficiency and sorption capacity calculations).

The statistical analysis as well as the fitting of the kinetic data by the Pseudo First-order (PFO) and Pseudo Second-order (PSO) models and the fitting of isotherm data by the Langmuir and Freundlich models were performed by the OriginPro 8.5. The non-linear forms of these models were applied in this work and the estimated correlation coefficient (R^2) from the non-linear regression analysis of each model was used to justify the good fit of the experimental data to each model.

The non-linearized PFO is given as:

$$q_t = q_e(1 - e^{-k_1 t}) \quad 3.4$$

The non-linearized PSO is given as:

$$q_t = \frac{k_2 q_e^2 t}{1 + k_2 q_e t} \quad 3.5$$

The non-linearized Langmuir isotherm model is given as:

$$q_e = \frac{b q_m C_e}{1 + b C_e} \quad 3.6$$

The essential feature of Langmuir isotherm model called the separation factor, R_L , was estimated using the equation below:

$$R_L = \frac{1}{1 + b C_o} \quad 3.7$$

The non-linearized Freundlich isotherm model is given as:

$$q_e = K_F C_e^{1/n} \quad 3.8$$

where the kinetics and isotherm models' parameters retain their usual meanings as defined in Chapter 2.

The thermodynamics parameters were estimated from the following equations:

$$\ln K_d = \frac{\Delta S^0}{R} - \frac{\Delta H^0}{RT} \quad 3.9$$

$$K_d(\text{ml/g}) = \frac{A_0 - A_e}{A_e} * \frac{V}{m} \quad 3.10$$

$$\Delta G^0 = \Delta H^0 - T\Delta S^0 \quad 3.11$$

The unknown parameters have been defined in Chapter 2.

In addition, chi-square analysis (χ^2) was also applied to estimate the degree of difference between the experimental data and the predicted isotherm data. The expressions that define this statistical parameter is given as:

$$\chi^2 = \sum \frac{(\text{Predicted value} - \text{Experimental})^2}{\text{Experimental value}} \quad 3.12$$

For the bi-solute adsorption system, bi-solute competitive adsorption behaviour of the radionuclides was analyzed by using competitive Langmuir model (CLM) (Park et al., 2010). The CLM was first developed by Butler and Ockrent in 1930 to describe the sorption equilibrium in multicomponent systems (Ho and McKay, 1999). It is an extended form of Langmuir model which allows the prediction of amount of a solute adsorbed per unit weight of an adsorbent in the presence of other solutes.

For the presence of two solutes (that is, $^{109}\text{Cd}/^{137}\text{Cs}$, $^{109}\text{Cd}/^{60}\text{Co}$ or $^{137}\text{Cs}/^{60}\text{Co}$) in the adsorption system, the competitive Langmuir isotherm models used in this study are given as (Ho and McKay, 1999):

$$q_1 = \frac{q_{m,1}b_1C_{e,1}}{1+b_1C_{e,1}+b_2C_{e,2}} \quad 3.13$$

$$q_2 = \frac{q_{m,2}b_2C_{e,2}}{1+b_1C_{e,1}+b_2C_{e,2}} \quad 3.14$$

where q_1 and q_2 are the amounts of solutes 1 and 2 sorbed per unit weight of sorbent at equilibrium concentrations $C_{e,1}$ and $C_{e,2}$, respectively. $q_{m,1}$ and $q_{m,2}$ are the maximum sorption capacities of solute 1 and solute 2, respectively. The constants b_1 and b_2 are the parameters obtained by fitting the Langmuir model to the single-solute adsorption data of either solute 1 or 2.

CHAPTER 4: ADSORBENT CHARACTERIZATION

4.1 Nitrogen physisorption measurements

Nitrogen adsorption-desorption measurements for each as-prepared adsorbent was done to know the pore volume distribution and BET surface area as well as the nature of adsorption-desorption isotherm.

4.1.1 BET surface area and pore volume

Table 4.1 shows the pore volume distributions and BET surface areas of the various adsorbents as measured by N₂ physisorption at 77.4 K using Micromeritics (ASAP 2020 and Tritar II 3020 Kr). For the pure polypyrrole prepared with different pyrrole to oxidant ratio (1:1, 1:2 and 1:3), it is clearly revealed that the higher the molar concentration of the oxidant with respect to the concentration of the pyrrole, the lower the BET surface areas and the corresponding pore volumes. Meanwhile, it is important to state here that higher pyrrole to oxidant molarity ratio (greater than 1:3) was avoided in the preparation to prevent possible incomplete polymerization of monomers and reduction in the amount of the polypyrrole product formed. Previous authors have also reported negative influence of higher pyrrole molarity on physico-chemical properties and adsorption performance for pollutant (Hong et al., 2014). Based on the results of preliminary adsorption tests (see detail in Chapter 5), the synthesis of the polypyrrole composites were based on the pyrrole to oxidant ratio (1:1) with higher BET surface area and pore volume.

The pore volume distribution and BET surface area of the PPy/SD composite showed a reduction in values compared to the pure PPy (1:1). The decrease could be attributed to the successful adsorption of the polypyrrole throughout the sawdust (SD) pore matrix and catalytic effect of the oxidant (FeCl₃.6H₂O) in the polymerization of the polypyrrole throughout this pore matrix. Contrarily, the effect of the incorporation of large size dopant

(SDBS) in the polypyrrole was clearly shown in the results of pore volume and BET surface area of the PPy/SDBS. This confirmed the fact that the choice of dopant used in the polypyrrole preparation can greatly affect its diameter as well as its morphology (Pan et al., 2010). Regarding adsorption of pollutants, the presence of anionic surfactant such as SDBS in the polypyrrole products could enhance its sorption capacity for the target pollutant due to the high immobility of sulfonate anion in the polymer matrix as well as easy of water dispersion, making surface interaction with the pollutant easier (Chen et al., 2016). Besides, the yield (%) of the polymer product was significantly increased with a rise in the concentration of the SDBS used.

When the pyrrole was polymerized in the presence of SD with and without SDBS, the BET surface area and the pore volume decreased significantly from 7.06 m²/g and 0.0171 cm³/g (in the case of PPy/SD) to 3.98 m²/g and 0.0052 cm³/g (in the case of PPy/SDBS/SD), respectively. Finally, the PPy/SDBS and PPy/SDBS/AC composites showed a clear-cut difference in the pore volume and BET surface area measurements from the other products under study. As shown, there is no doubt that the AC plays a major role for the higher pore volume and BET surface area and this, shows that the polypyrrole was successfully sorbed throughout the AC pore matrix and that the oxidant also polymerized the pyrrole throughout this pore matrix. In addition, the difference in the pore volume and BET surface area measurements of the PPy/AC and PPy/SDBS/AC composites compared with the original AC is an indication of the structural heterogeneity of the materials and that means, other adsorbent precursors have influenced the original structure and the physico-chemical properties of the parent AC, confirming the successful polymerization of PPy within the AC pore matrix and outside its surface. The obtained result of the PPy/SDBS/AC composite is comparable to the reports of other authors on polypyrrole-grafted and metal-impregnated granular activated carbon (Hong et al., 2014; Yürüm et al., 2014; Maroto-Valer et al., 2004).

Table 4.1: Preparation of polypyrrole and composites, pore volume distribution and surface area measurements.

Adsorbent Name	Pyrrole : Oxidant	SDBS (mM)	^a BET Surface Area (m ² /g)	^b Total Pore volume (cm ³ /g)	Pore size (Å)	Yield (%)
PPy	1:1	0	10.57	0.02102	79.53	12
PPy	1:2	0	8.90	0.01876	82.36	18.3
PPy	1:3	0	7.87	0.0161	82.28	17.8
PPy/SDBS (1)	1:1	1.714	11.34	0.0264	93.00	31.4
PPy/SDBS (2)	1:1	3.427	11.73	0.0276	94.22	33.7
PPy/SDBS (3)	1:1	6.854	11.28	0.0292	103.72	37.9
PPy/SDBS (4)	1:1	13.708	10.78	0.0294	108.97	43.5
PPy/SDBS (5)	1:1	27.416	14.62	0.0435	119.15	49.3
PPy/SD	1:1	0	7.06	0.0171	96.82	60
PPy/SDBS/SD	1:1	6.854	3.98	0.0052	52.76	70.1
PPy/AC	1:1	0	872.13	0.366	16.80	57.2
PPy/SDBS/AC	1:1	6.854	793.38	0.339	17.09	65.4

Pyrrole and oxidant as FeCl₃.6H₂O amount were 1.342 g (0.1 mol/L) and 5.406 g (0.1 mol/L) in 200 ml reaction volume for PPy (1:1). ^aBET surface area calculated in the relative pressure (P/P^o) = 0.20, ^bTotal pore volume measured at P/P^o = 0.995. Yield (%) = (g of polymer product/g of oxidant) × 100, where g of polymer product and oxidant represents weights of synthesized polymer adsorbent and FeCl₃.6H₂O.

4.1.2 Nitrogen adsorption/desorption curves

Based on the BET surface area measurements of the as-prepared polymer-based adsorbents, the N₂ adsorption/desorption isotherm curves with pore size distribution (inset) have been obtained to compare the variation in the adsorption and desorption of adsorbate by various materials (PPy, PPy/SDBS, PPy/SD and PPy/SDBS/AC composites). As shown in Figure 4.1–Figure 4.3, the adsorption/desorption isotherm curves for PPy, PPy/SD and PPy/SDBS are typical of Type II (IUPAC classifications) showing a very low adsorption and desorption in low relative pressure region. Moreover, there is a steep monolayer adsorption above the partial pressure of 0.8, which suggests the existence of mesopores and macropores on the polymer samples, which is also confirmed by the pore size distribution curve (Xin et al., 2015). On the other hand, the adsorption isotherm curve for PPy/SDBS/AC sample reveals a Type I isotherm, which has a sharp adsorption uptake almost immediately at partial pressure of zero (Figure 4.4).

This indicates that the PPy/SDBS/AC composite is more microporous than the other polymer-based adsorbents, which is due to the effect of the highly microporous activated carbon in the polymer composite. Meanwhile, there is an explicit hysteresis in the desorption as seen in the desorption isotherm curves for all of the adsorbents, which further indicates the existence of mesopores in the polymer composites (Maroto-Valer et al., 2004). The pore size distributions of the adsorbents are equally shown as inset in the figures. Again, the pore size distribution for the PPy/SDBS/AC composite shows a distinct difference from others, which can also be attributed to the oxidative polymerization of pyrrole in the activated carbon (Yürüm et al., 2014). In all, the pore diameters are fixed between 17 and 2170 Å (average pore diameters are shown in Table 4.1). These pores might be as a result of the interstitial spaces among the polymer matrix and that of the individual components. Such pore structure is advantageous for applications that require rapid mass transport and effective adsorption/desorption of adsorbate molecules.

In summary, the obtained results of N₂ physisorption measurements indicated that the metal-adsorbents interactions could be somewhat varied for the pure PPy, PPy/SD and PPy/SDBS composites compared to that of PPy/SDBS/AC composites.

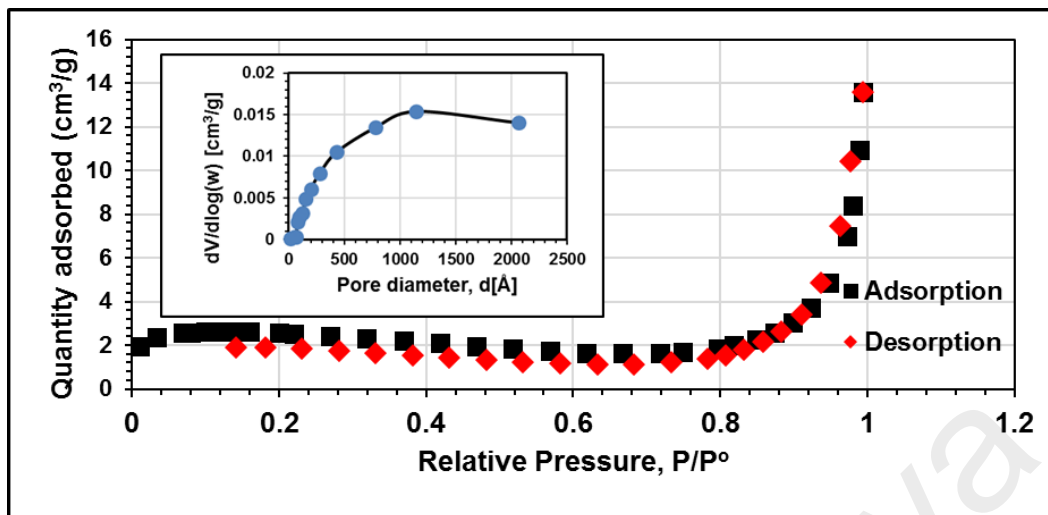


Figure 4.1: N_2 adsorption/desorption isotherms and pore size distribution (inset) of PPy.

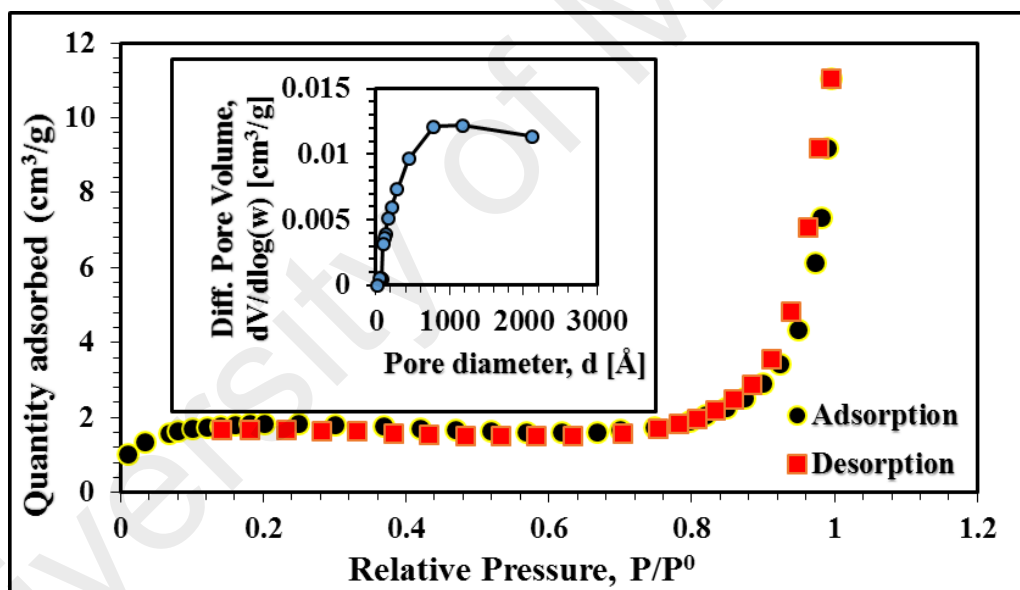


Figure 4.2: N_2 adsorption/desorption isotherms and pore size distribution (inset) of PPy/SD composite.

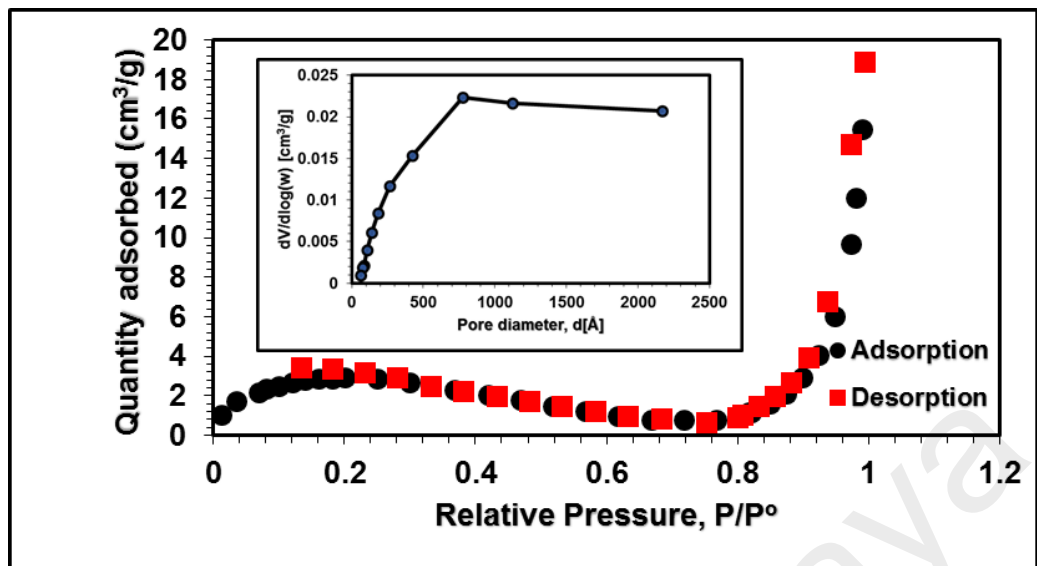


Figure 4.3: N₂ adsorption/desorption isotherms and pore size distribution (inset) of PPy/SDBS.

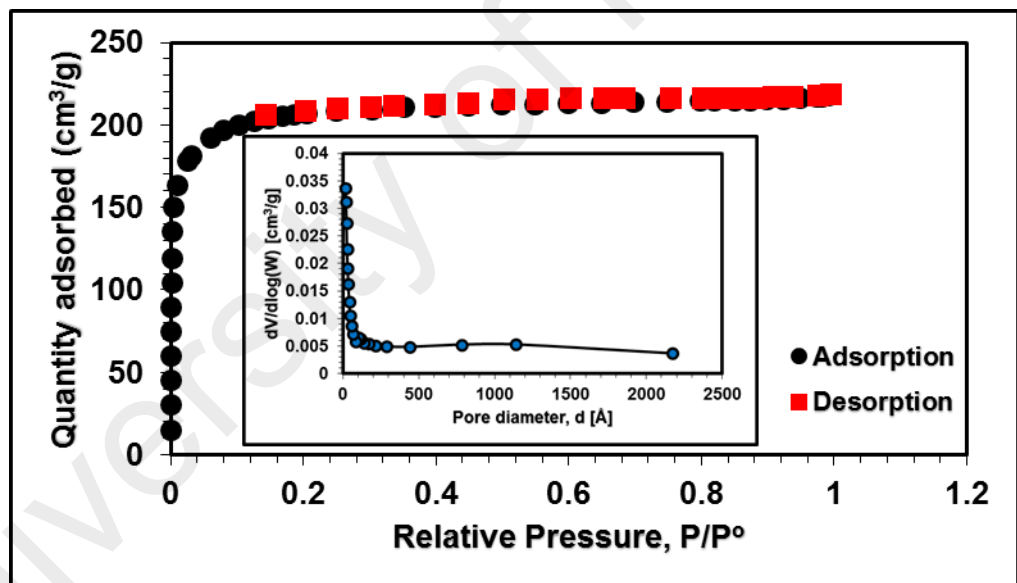


Figure 4.4: N₂ adsorption/desorption isotherms and pore size distribution (inset) of PPy/SDBS/AC composite.

4.2 Surface morphology by FESEM and HR-TEM

4.2.1 FESEM analysis

Figure 4.5 represents FESEM image of the as-prepared PPy. The FESEM image revealed that the pure polypyrrole has been successfully synthesized, with its characteristic cauli-like flower or tumor-like structure.

When the pyrrole was polymerized in the presence of sawdust, the polymer product (PPy/SD) formed shows a unique structure with bubble-like globules of PPy formed on the surface of the polypyrrole composite (Figure 4.6). This indicates that the polypyrrole was distributed on the surface of sawdust matrix.

Figure 4.7 and Figure 4.8 portray the FESEM images of both PPy/SDBS and PPy/SDBS/AC composites. In Figure 4.7, it can be seen that the uniform globular or cauli-flower structure of PPy has been formed. Here, the presence of SDBS has great effect on the size and homogeneity of the particles (Zoleikani et al., 2015). It can be seen that the SDBS provides the space factor for pyrrole orderly growth, resulting in globular or sphere-like morphology of PPy. Obviously, the physical and chemical properties of the adsorbent are determined by the surface-active agents but depends largely on the amount of the additive adsorbed during polymerization. The amount of the SDBS involved was sufficient to modify the surface properties of the pure PPy (as already discussed in Table 4.1). In addition, the dopant surfactant has been reported to produce effect on the PPy that can enhance the conductivity of the PPy (Hoshina et al., 2012).

For the PPy/SDBS/AC composite (Figure 4.8), the FESEM image shows that polypyrrole was successfully adsorbed into the pore matrix of the activated carbon and little or no physically observable PPy was found to have been formed on the surface of the PPy/SDBS/AC composite unlike what is observed on the surface of the PPy/SD composite, in which the PPy formation was found to aggregate on the surface. The easy

aggregation tendency of PPy in an irregular morphology via π - π stacking and poor water dispersion are major factors that are responsible for low sorption capacity of polypyrrole for metal ions (Bai et al., 2015) and that is why it is good to synthesize polypyrrole on another material to make good adsorbents. Here, the presence of SDBS seemed to have aided the uniform dispersion of PPy through the AC. The synergy effect of the individual components on PPy/SDBS/AC is expected to be favourable for mass diffusion of guest molecules.

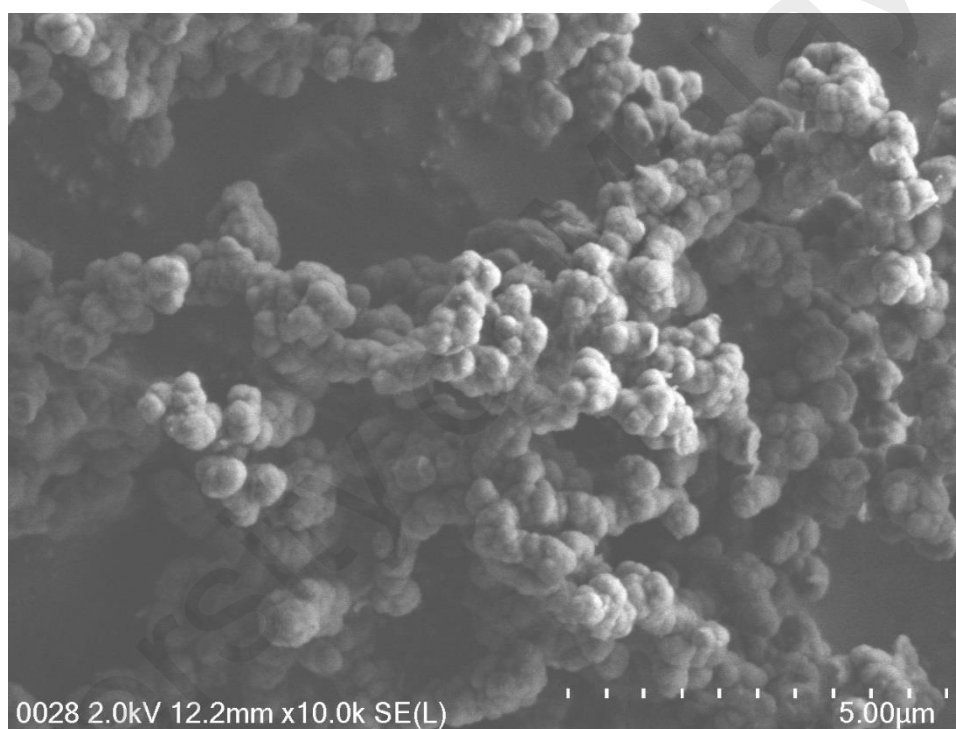


Figure 4.5: FESEM image of pure polypyrrole (PPy) adsorbent.

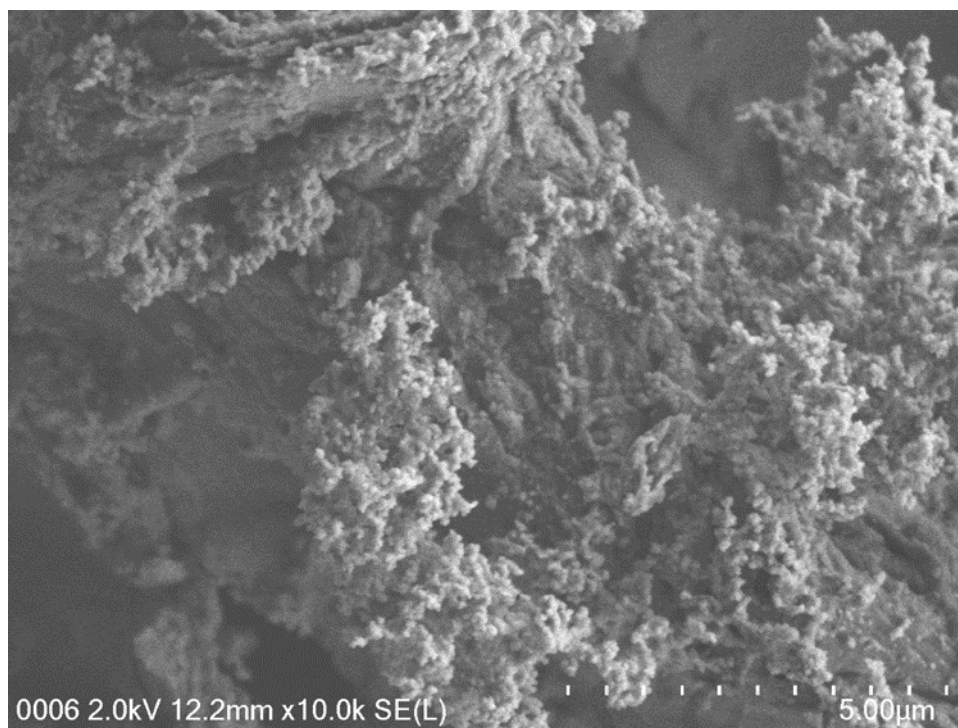


Figure 4.6: FESEM image of polypyrrole/sawdust (PPy/SD) composite.

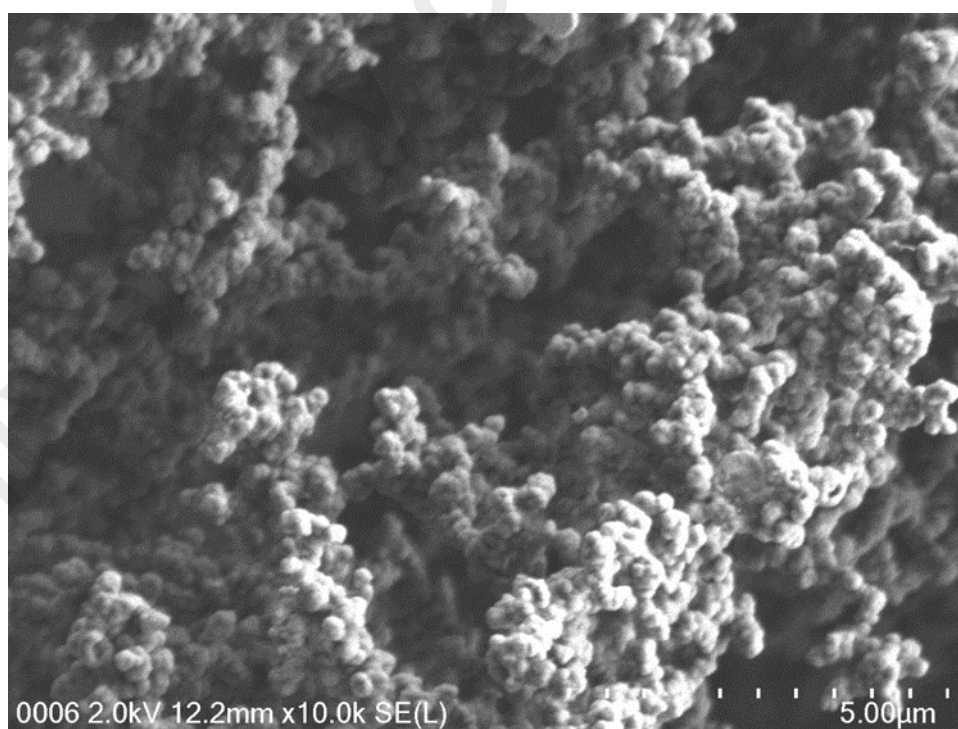


Figure 4.7: FESEM image of SDBS-doped polypyrrole (PPy/SDBS).



Figure 4.8: FESEM image of SDBS-doped polypyrrole/activated carbon (PPy/SDBS/AC) composite.

4.2.2 HR-TEM analysis

To deeply investigate the surface morphology, high-resolution TEM images of the adsorbents were taken. As seen in Figure 4.9 (a) and (b), the contrast between PPy and PPy/SDBS can be easily discerned, where PPy/SDBS appeared to have rough surface which could be responsible to increase surface area obtained compared to the pure PPy and hence, that could also result into more active adsorption sites which would be favourable for the removal of the radionuclides. The average particle size is in the range of 68.37 to 116.26 nm for PPy/SDBS, which is much less than that of PPy which is between 80 and 130 nm.

Figure 4.9 (c) represents the HR-TEM image of PPy/SD composite which again shows the surface of the sawdust is covered by the polypyrrole. The smooth surface of the particle explains why PPy/SD composite has low surface area compare to other polymer materials.

Similarly, the image of PPy/SDBS/AC composite in Figure 4.9 (d) shows that there is a nonexistence of individual components that make up the polymer composite (only a partial covering of PPy is noticed by the dense small-globules on the carbon grains), which is a proof of adsorption of PPy into the activated carbon matrix. Similar observations have been reported on the TEM analysis by different authors (Kumar et al., 2014).

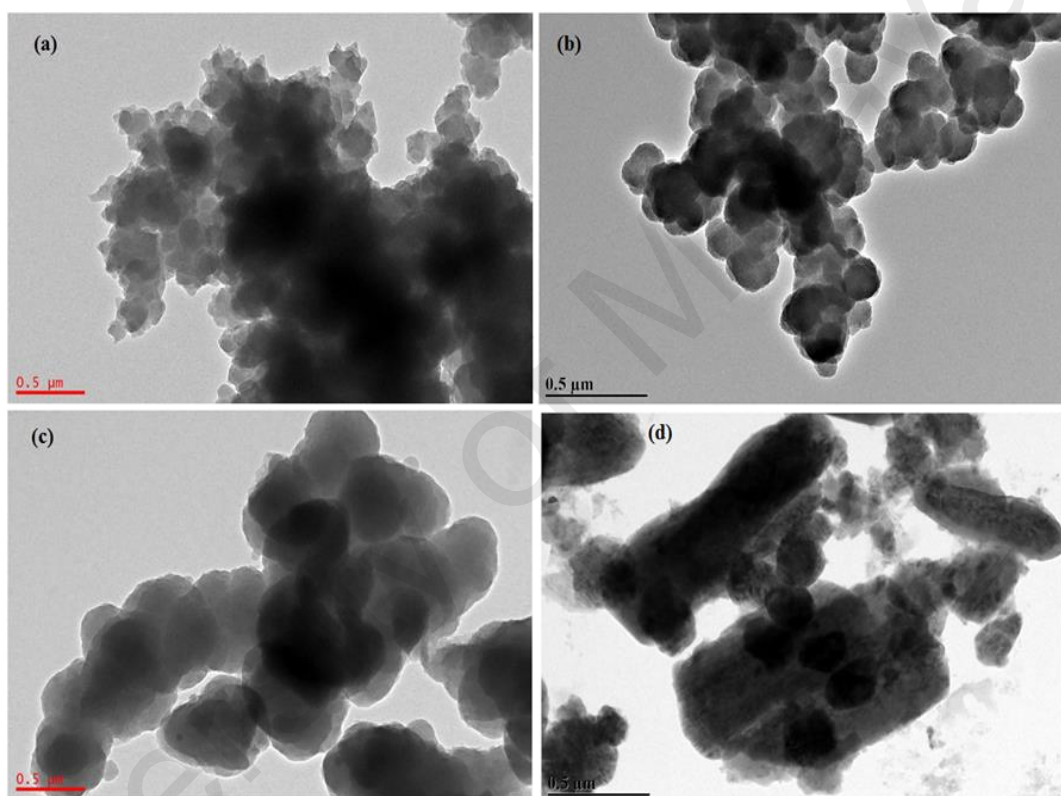


Figure 4.9: HR-TEM images of (a) PPy, (b) PPy/SDBS, (c) PPy/SD and (d) PPy/SDBS/AC composite.

4.3 X-ray diffraction (XRD) analysis

The X-ray diffraction patterns of as-prepared polymer powders have been observed to understand the nature of the polymer materials (Figure 4.10). The amorphous nature of the pure PPy is clearly shown via the broad peak centered at $2\theta = 26.12^\circ$. The peak is as a result of the scattering from polymer chains at the inter-planar spacing. The corresponding inter-planar spacing was found to be at $d = 3.41 \text{ \AA}$. The average chain

separation has been found to be 4.35 Å. In the case of PPy/SD and PPy/SDBS/SD composites, the broad peak observed in PPy has been shifted backward to around $2\theta = 15.5^\circ$ in both cases while a new sharp peak has appeared at $2\theta = 22.7^\circ$ with an inter-planar spacing $d = 3.91$ Å, which is the characteristic crystalline structure of the sawdust. The average crystallite size has been found by Scherrer's formula ($D = \frac{K\lambda}{\beta \cos\theta}$) to be 18.5 nm. Other than the transformation of the amorphous structure of PPy to crystalline structure in the presence of sawdust, introduction of SDBS in the PPy/SDBS/SD composite did not result into any further changes in the structure of the polymer material. This shows that the pyrrole monomers were successfully synthesized on sawdust in the presence of SDBS.

In the case of PPy/SDBS without SD or AC, the XRD patterns for the different concentrations of SDBS used in the synthesis were taken to check if there are any observable changes in the XRD patterns. As shown, there was no significant change in the amorphous structure of the PPy adsorbent except for the backward shift in the position of the characteristic broad peak of the PPy. However, the broad peak became narrower and increased in intensity with SDBS concentration. The highest broad peak position was found to have diffraction maxima at $2\theta = 18.52^\circ$ with an inter-planar spacing $d = 4.79$ Å for PPy/SDBS(5). When AC was introduced in the polymerization of pyrrole with and without SDBS, the products (that is, PPy/AC and PPy/SDBS/AC composites) show a highly amorphous characteristic broad peak being maximum at $2\theta = 24.0^\circ$ and the inter-planar spacing $d = 3.71$ Å (in both cases). Another weak but broad peak was found at $2\theta = 44.11^\circ$ with inter-planar spacing $d = 2.05$ Å, which is as a result of the addition of carbon into the polymer. The X-ray diffraction patterns observed here are similar to the previously reported diffraction patterns for polypyrrole and its composites (Li et al., 2012; Scienza & Thompson, 2001).

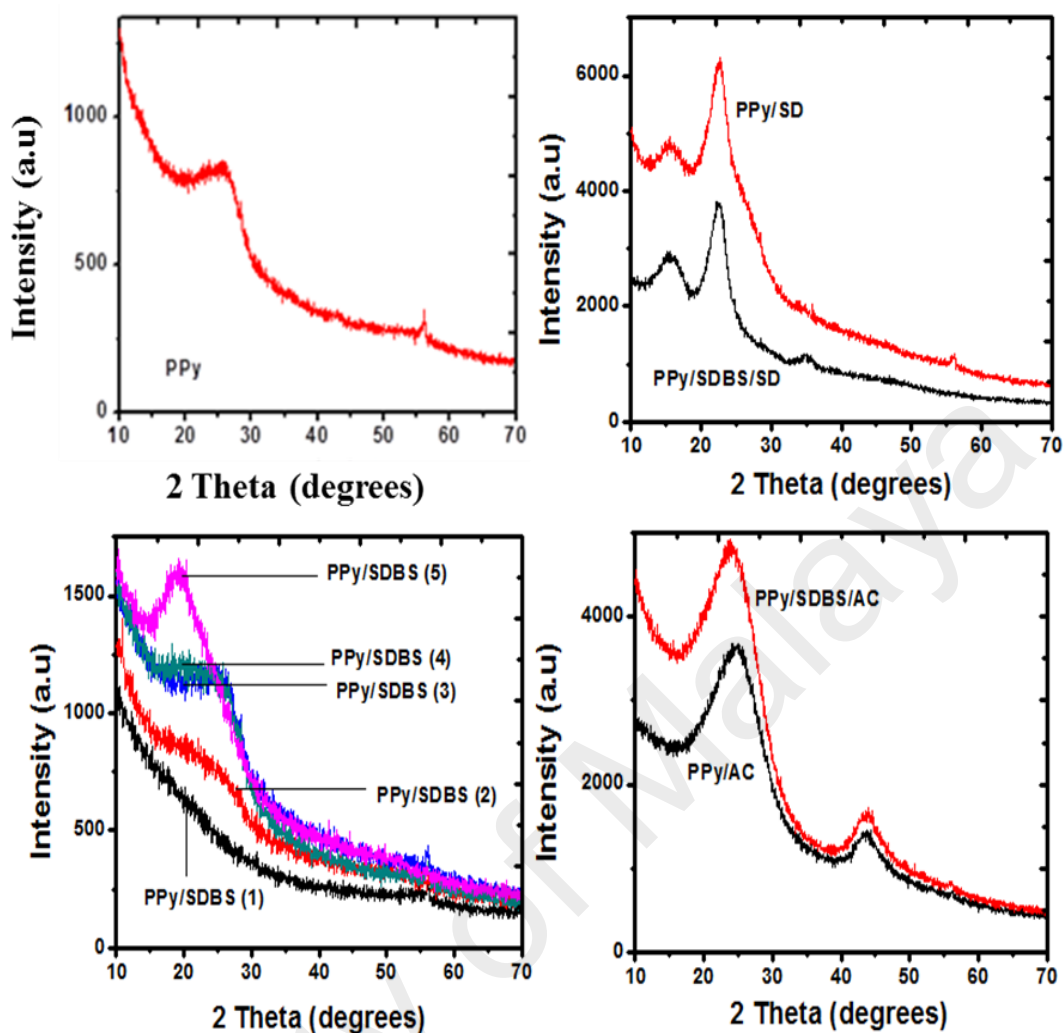


Figure 4.10: XRD patterns of different polypyrrole-based materials.

4.4 FTIR analysis

4.4.1 PPy

The FTIR spectra of as-prepared PPy adsorbent for different pyrrole to oxidant ratio were analyzed to identify various functional groups present in polypyrrole. As shown in Figure 4.11, several peaks were observed in the spectra of the PPy. The generally notable peaks are those found at 2924 and 2855 cm^{-1} , which are related to the C-H asymmetric and symmetric stretching vibration of the alkyl chain attached to benzene ring of the pyrrole monomers, respectively, the peak at 2099 cm^{-1} is assigned to the C-H out-of-plane deformations in aromatics. The peaks at 1533 and 1447 cm^{-1} are due to the C=C stretching vibrations of quinoid and benzenoid rings of PPy, the peak at 1280 cm^{-1} is due to the C-

N stretching vibration. Other peaks at 1023, 961, 879, 769, 658 and 592 cm^{-1} are related to the C-H and N-H in-plane deformation vibrations as well as the C-H outer bending vibrations. However, some changes were observed in the PPy's when the reactant ratios were varied. For instance, it could be seen that the peak at 1747 cm^{-1} in PPy (1:1) had disappeared when the oxidant concentration increased in the case of PPy (1:2) and PPy (1:3). The reduction in the functional groups of PPy (1:2 and 1:3) may affect adsorption of metal ions, due to the result of fewer sorption sites compared to the PPy (1:1). Again, it was noticed that the peak at 1145 cm^{-1} in the PPy (1:1) due to in-plane bending of the C-H bond had a blue shift to 1138 cm^{-1} in the PPy (1:3) and to 1128 cm^{-1} in the PPy (1:2). The observed absorption peaks are similar to those previously reported by other authors (Qin et al., 2014; Scienza and Thompson, 2001; Seid et al., 2014).

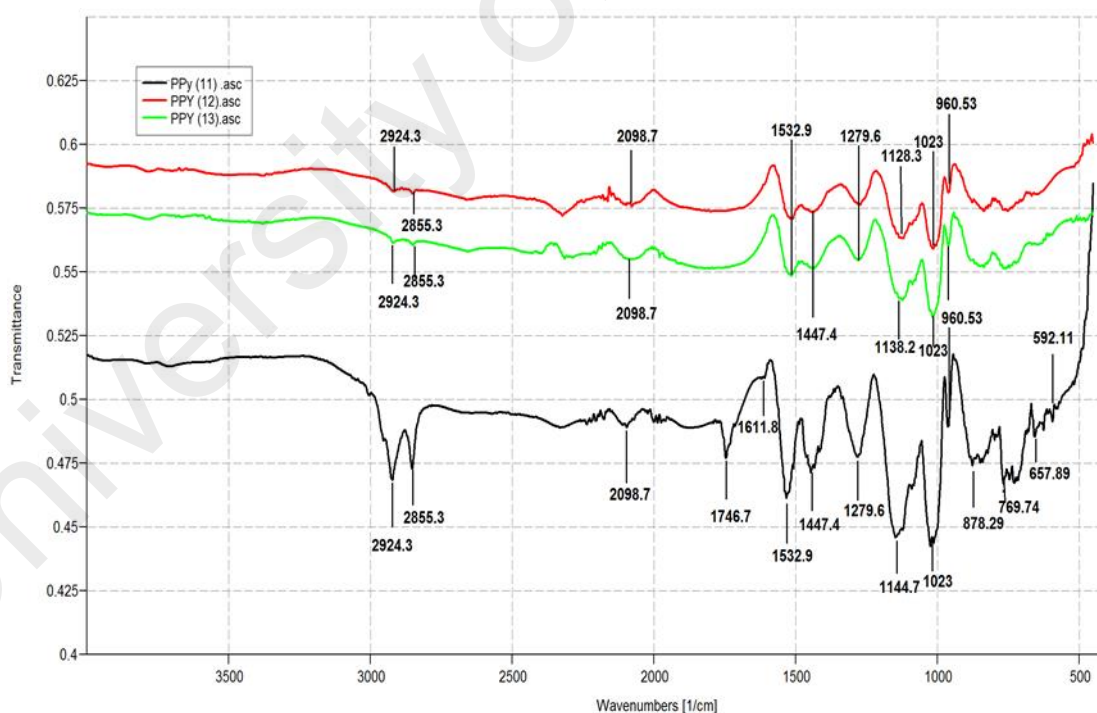


Figure 4.11: FTIR spectra of PPy for different ratios.

4.4.2 PPy/SD composite

To identify the functional groups in the PPy/SD composite and also the changes between the pure PPy and its composite when pyrrole was polymerized in sawdust particles, the FTIR spectrum of the as-prepared PPy/SD composite was taken as shown in Figure 4.12. The pyrrole to oxidant ratio of 1:1 was involved in the composite preparation and so, it can be compared with pure PPy (Figure 4.11). It can be seen that the peaks at 2924 and 2855 cm^{-1} , which represent the C-H asymmetric and symmetric stretching vibrations of the alkyl chain attached to benzene ring of the pyrrole monomers were observed also in the PPy/SD as in the PPy above. The peaks at 2322 and 2099 cm^{-1} are assigned to C-H out-of-plane deformations in aromatics. The peak at 1747 cm^{-1} in the pure PPy (1:1) due to C-O stretching vibration was missing in the PPy/SD composite while the peak at 1612 cm^{-1} , which indicates bending vibration of -COO in this case has been shifted to a higher wavenumber at 1684 cm^{-1} . The peaks at 1533 and 1447 cm^{-1} in the PPy (1:1) due to the C=C stretching vibrations of quinoid and benzenoid rings or carboxylic acids vibration have been shifted to 1546 and 1470 cm^{-1} , respectively, in the PPy/SD composite. Other peaks at 1280, 1145, 1023, 961, 879, 769 and 592 cm^{-1} , which are due to C-N stretching vibrations, C-H and N-H in-plane deformation vibrations as well as the C-H outer bending vibrations, respectively, have all been shifted to higher wavenumbers at 1303, 1171, 1095, 964, 891, 789 and 605 cm^{-1} , respectively. The red shifts in the spectrum of the PPy/SD composite when compared to the pure PPy (1:1) is an indication of the successful polymerization of the pyrrole within and outside the surfaces of sawdust as initially confirmed by the FESEM analysis.

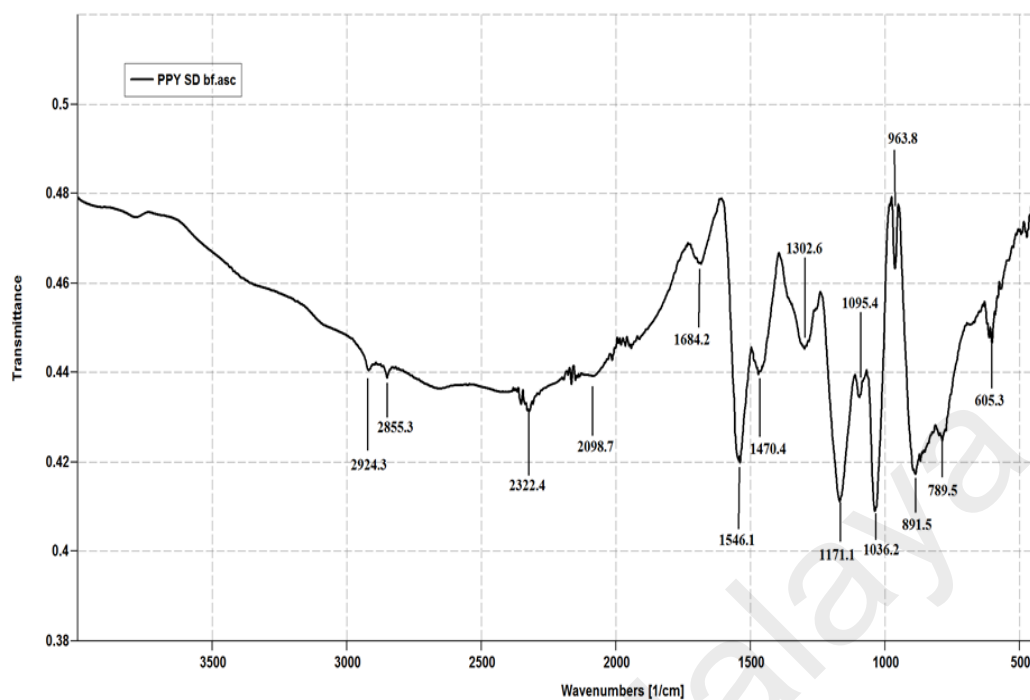


Figure 4.12: FTIR spectrum of PPy/SD composite.

4.4.3 PPy/AC composite

Figure 4.13 represents the FTIR spectrum of the PPy/AC composite prepared with 2 g of AC and pyrrole to oxidant ratio of 1:1 as in the case of PPy/SD composite above. Here, the absorption peaks at 2924 and 2855 cm^{-1} in the pure PPy (1:1), which represent the C-H asymmetric and symmetric stretching vibrations of the alkyl chain attached to benzene ring of the pyrrole monomers were noticed to have become weak and shifted to lower wavenumbers at 2921 and 2852 cm^{-1} , respectively, in the PPy/AC composite. The peaks between 2326 to 1951 cm^{-1} are due to C-H out-of-plane deformations, the peak at 1612 cm^{-1} in the PPy has been shifted to a higher wavenumber at 1691 cm^{-1} in PPy/AC while the peak at 1533 cm^{-1} due to C=C stretching vibrations of quinoid rings of PPy is now located at 1573 cm^{-1} . Other peaks found in the PPy (1:1) have equally been shifted to lower wavenumbers in most cases in the PPy/AC composite, and are now found at 1217, 1109, 1049, 934, 796, 694 and 605 cm^{-1} . In addition, new peaks are observed at 3191 and 1329 cm^{-1} , which can be assigned to the N-H and C-O vibrations. These are indications

of the increase in the hydroxyl (from the phenol groups) and carbon-oxygen groups (from the carboxylic COOH) in the PPy/AC composite, following the oxidation reaction of pyrrole within and outside the AC. The respective shifts in the peaks as well as the introduction of new peaks suggest the successful formation of pyrrole in the activated carbon.

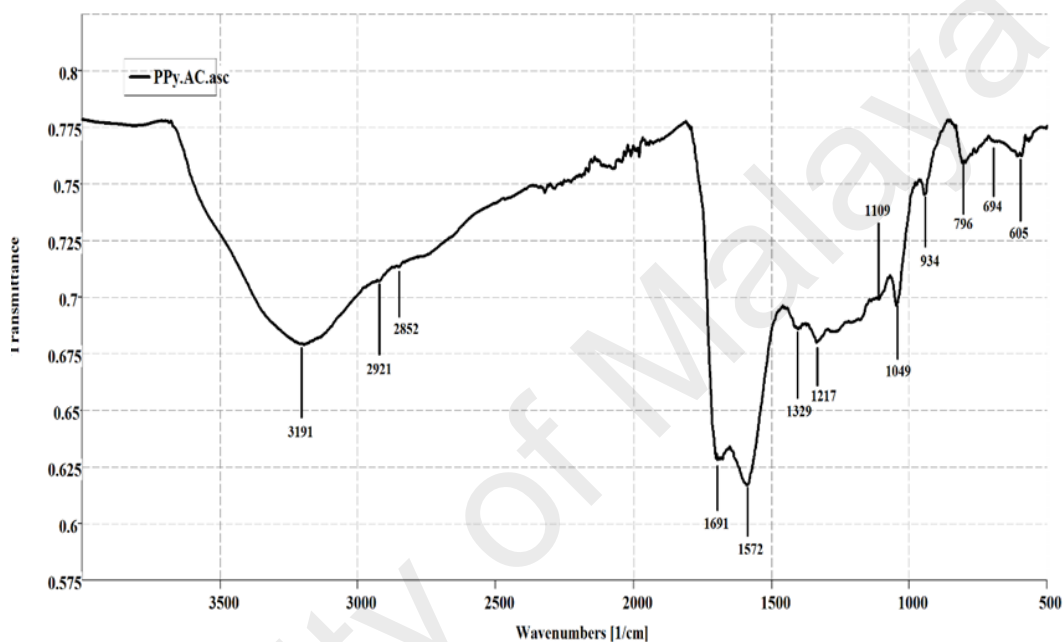


Figure 4.13: FTIR spectrum of PPy/AC composite.

4.4.4 PPy/SDBS

Following the doping of pure polypyrrole particles with different concentrations of SDBS surfactant, the FTIR spectra were compared for any changes with the undoped PPy and within the various concentration of SDBS. As shown in Figure 4.14, all the absorption peaks observed in the pure PPy (see Figure 4.11) are present in the PPy/SDBS, except that they have been shifted in most cases to higher wavenumbers. For instance, the peaks at 1612, 1533 and 1280 cm^{-1} in the pure PPy (1:1) have been shifted to 1615, 1520 and 1283 cm^{-1} , respectively, when compared to PPy/SDBS(1). In addition to this, two more peaks have been added to the spectra at 3796 and 3701 cm^{-1} , which have been attributed to the physically adsorbed water molecule (Seid et al., 2014; Chen et al., 2016), and these

peaks could also represent formation of pyrrolidinone rings in the polymer chain due to the effect of large size dopant (Saville, 2005). Beside this, the peaks at 1283, 1118 and 1000 cm^{-1} show the clear evidence that the sulfonate groups from the SDBS are dispersed in the polymer backbone. These peaks can be ascribed to the SO_3^- group (O=S=O and S-O stretching vibration) and to aliphatic $-\text{CH}_3$ and $-\text{CH}_2$ from the alky chain attached to the benzene ring of dodecylbenzene sulfonate anion, respectively. However, when the concentration of SDBS was increased in the PPy particles, some changes were observed in the spectra. The peak at 1615 cm^{-1} due to aromatic C=C stretching vibrations disappeared with a rise in the SDBS concentration. Other peaks such as 1520, 961, 836 and 727 cm^{-1} and those due to the sulfonate groups mentioned above have all been shifted to higher absorption peaks at 1543, 1306, 1168, 1043, 970, 898 and 793 cm^{-1} , respectively, as SDBS concentration increases (Figure 4.14). Also, it was noticed that increase in SDBS corresponds to the increase in the intensity of the peak that defines the presence of $-\text{OH}$ groups in the as-synthesized polymer (peak at 3701 cm^{-1} in the spectra). This indicates that the amount of hydroxyl groups increases with concentration of SDBS. Previous studies have also revealed similar observations as noticed in this study (Hoshina et al., 2012; Kumar, Ansari & Barakat, 2013; Saville, 2005; Scienza & Thompson, 2001).

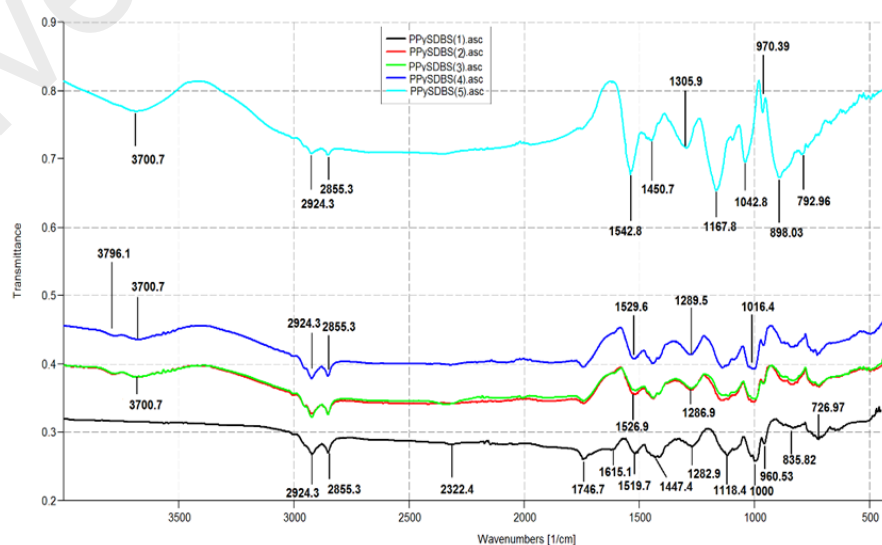


Figure 4.14: FTIR spectra of PPy/SDBS prepared with different concentration of SDBS as in Table 4.1.

4.4.5 PPy/SDBS/SD and PPy/SDBS/AC composites

Figure 4.15 shows the FTIR spectrum of PPy/SDBS/SD composite. Here, a new absorption peak which was not present in PPy/SD (without SDBS) has been introduced at 3326 cm^{-1} , which shows the presence of -OH groups possibly from SDBS. Also, the peaks at 2924 and 2855 cm^{-1} (due to C-H asymmetric and symmetric stretching vibrations of the alkyl chain attached to benzene ring of the pyrrole monomers) have been shifted to 2928 and 2859 cm^{-1} , respectively, after SDBS was introduced. Besides, several other peaks have been found in addition to the mentioned peaks for PPy, PPy/SD and PPy/SDBS. These peaks are found at 1734 cm^{-1} (due to C=O stretching vibrations of -COOH), 1595 cm^{-1} (due to NH-C=O stretching vibrations), 1507 cm^{-1} (due to C-C stretching), 1368 cm^{-1} (due to O-C-O stretching of carboxylic groups). All these show that SDBS was successfully incorporated into the composite of PPy/SD.

Similarly, the FTIR spectrum of PPy/SDBS/AC composite shows also that the polypyrrole was successfully synthesized with AC in the presence of SDBS (Figure 4.16). Comparing the spectra of PPy, PPy/AC and PPy/SDBS with the spectrum of PPy/SDBS/AC composite, shows that the peaks that represent hydroxyl groups have been shifted to new positions at 3750 and 3612 cm^{-1} and other peaks due to the C-H out-of-plane deformations in aromatic have been shifted to between 2217 and 1993 cm^{-1} . In particular, the peak due to the sulfonate groups (O=S=O and S-O stretching vibrations) have been shifted to 1168 cm^{-1} . All these peaks have been reported by the previous authors (Kumar et al., 2013; Scienza and Thompson, 2001).

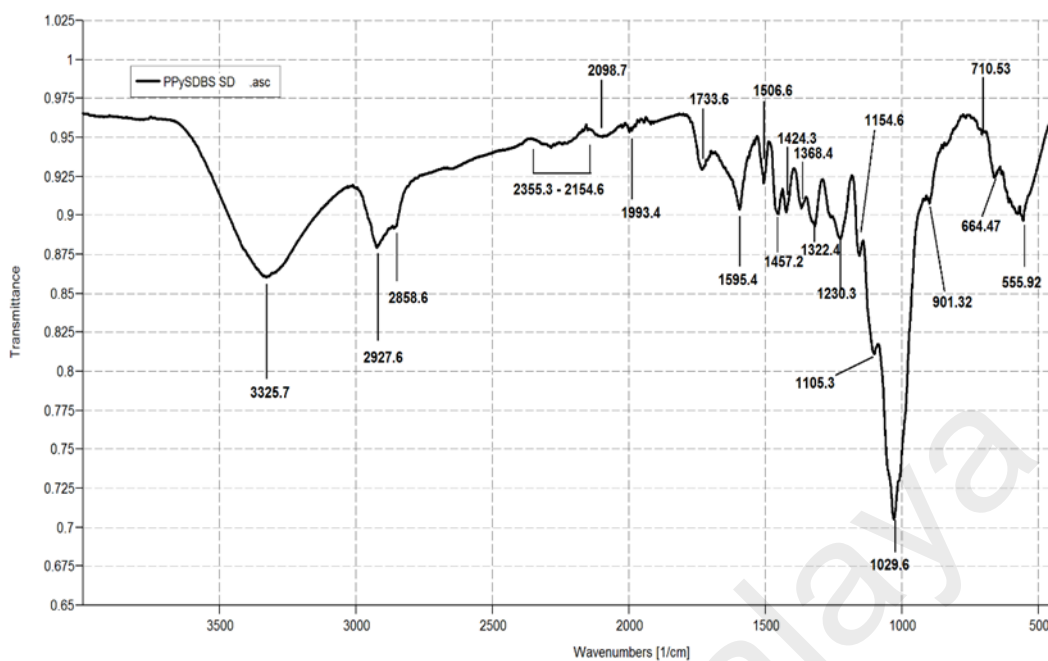


Figure 4.15: FTIR spectrum of PPy/SDBS/SD composite.

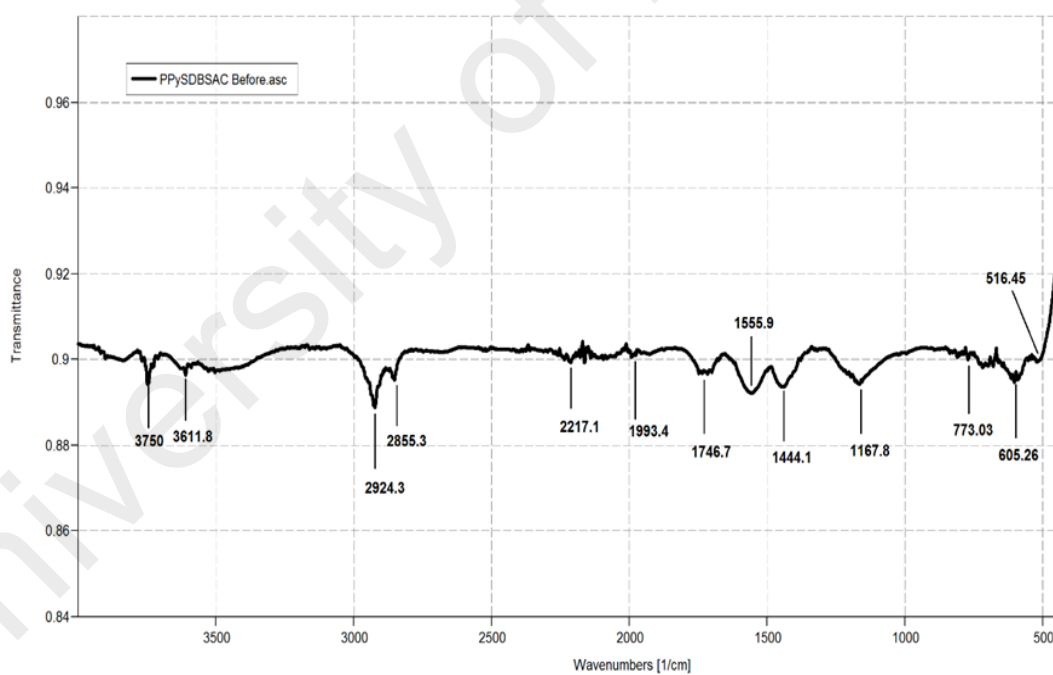


Figure 4.16: FTIR spectrum of PPy/SDBS/AC composite.

4.4.6 FTIR of irradiated polypyrrole-based materials

Exposure of organic materials such as polymers and their composites to energetic radiations (such as ^{60}Co gamma-source) may cause a change in chemical composition and

their physico-chemical properties (Banhart, 1999; Brostow et al., 2009; Vincent et al., 2015). Previous studies have shown that gamma irradiation can change the molecular weight of polymers due to radical production and/ or induce crosslinking at higher doses (Shahabi et al., 2014; Saito et al., 1999). This means that gamma-irradiation can sometimes induce positive or negative effect on the surface functional groups of polymer materials. Also, studies on the irradiation of activated carbons have been reported to cause surface erosion and loss of surface functional groups from the activated carbons (Erçin et al., 2005). The implication is that exposure of polymer materials or carbon-containing materials to high energetic radiations may not only affect the adsorption affinity of the polymer and its composites, but also the long-term stability after it has been used for environmental remediation of pollutants. As a result, the effect of ^{60}Co -source gamma irradiation on the surface functional groups of some of the polypyrrole materials was evaluated by irradiating the samples with 100 and 200 kGy doses.

The FTIR spectra of the irradiated PPy (1:1) are shown in Figure 4.17. A close look at the FTIR spectra of the PPy shows that the peak at 1747 cm^{-1} has disappeared after irradiation, but one new peak was also introduced at 2336 cm^{-1} (which can be assigned to C-H out-of- plane deformations) only for 200 kGy dose gamma irradiation. Other than these, there were no observable changes in the FTIR spectra of the PPy before and after irradiation.

Similarly, Figure 4.18 represents the FTIR spectra of irradiated PPy/SD composite, which shows largely that no observable change in the composite material, except for the weak peak at 2336 cm^{-1} in unirradiated PPy/SD composite, which became strong peak when gamma dose of 200 kGy was applied. In the same vein, Figure 4.19 shows the FTIR spectra of the irradiated PPy/AC composite. Comparing the spectra before and after irradiation reveals the introduction of new peak at 2336 cm^{-1} , only at dose of 200 kGy.

There is a different observation with the irradiated PPy/SDBS/AC composite compare to what is generally observed with other samples. As shown in Figure 4.20, the FTIR spectra of irradiated PPy/SDBS/AC composites show an increase in the number of peaks due to different functionalities and in addition, the peaks are more stronger compare to those of unirradiated samples. Apart from this, the observed peaks in unirradiated sample have shifted to higher wavenumbers in the irradiated samples. For instance, the peaks at 1747, 1556, 1444, 1168, 605 and 516 cm^{-1} have been shifted to new positions at 1769, 1600, 1464, 1191, 641 and 555 cm^{-1} after irradiation with 100 kGy and 200 kGy doses of gamma source, respectively. Some of the newly formed peaks are found at 1505, 1412, 1366, 1225, 1162, 1081, 1015, 952, 889 and 831 cm^{-1} , respectively. The observed changes further confirm in part the successful modification of polypyrrole/activated composite by the anionic surfactant, which is obvious by the formation of new structures or inducement of new surface functionalities after irradiation with 100 and 200 kGy doses of gamma source, unlike what is observed when the polypyrrole/activated carbon was not modified with anionic surfactant. Since the adsorbent is intended for liquid radioactive waste treatment, the irradiated sample needs to be subjected to adsorption studies in order to understand whether the newly formed surface functionalities can be added advantage for the adsorption of radionuclides or not.

In general, gamma irradiation up to 200 kGy dose shows no significant change in the surface structures of PPy, PPy/SD and PPy/AC materials, but lead to new and self-organized structure formation in the PPy/SDBS/AC composite at least within 200 kGy dose of gamma irradiation. The different changes observed in the various samples after irradiation are indication that adsorption of studied radionuclides from radioactive wastewater would be somewhat different.

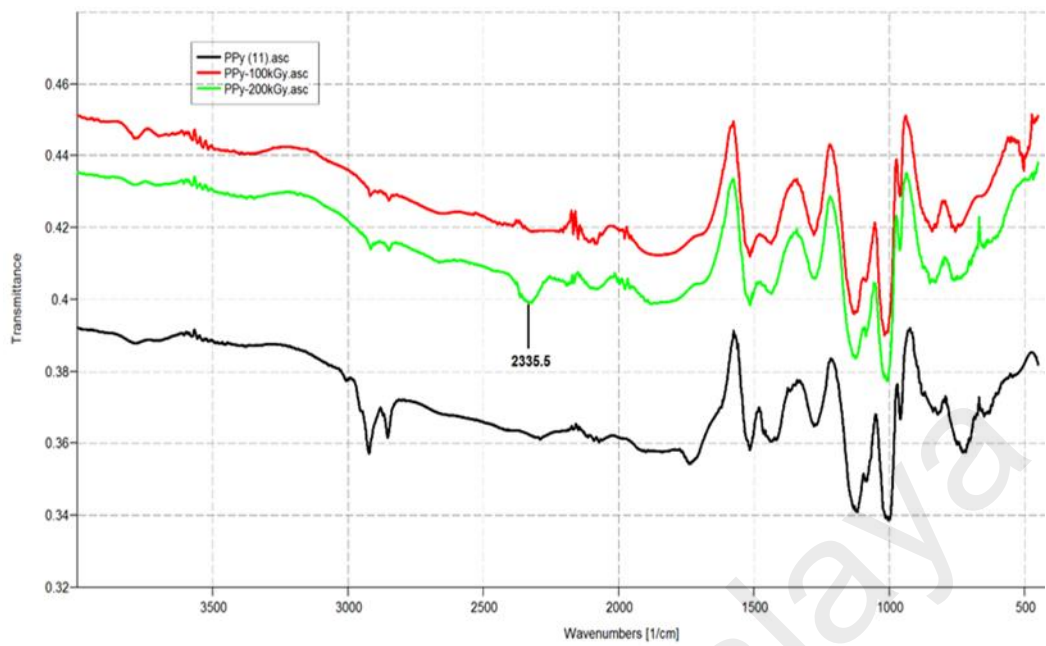


Figure 4.17: FTIR spectra of irradiated PPy at different gamma doses.

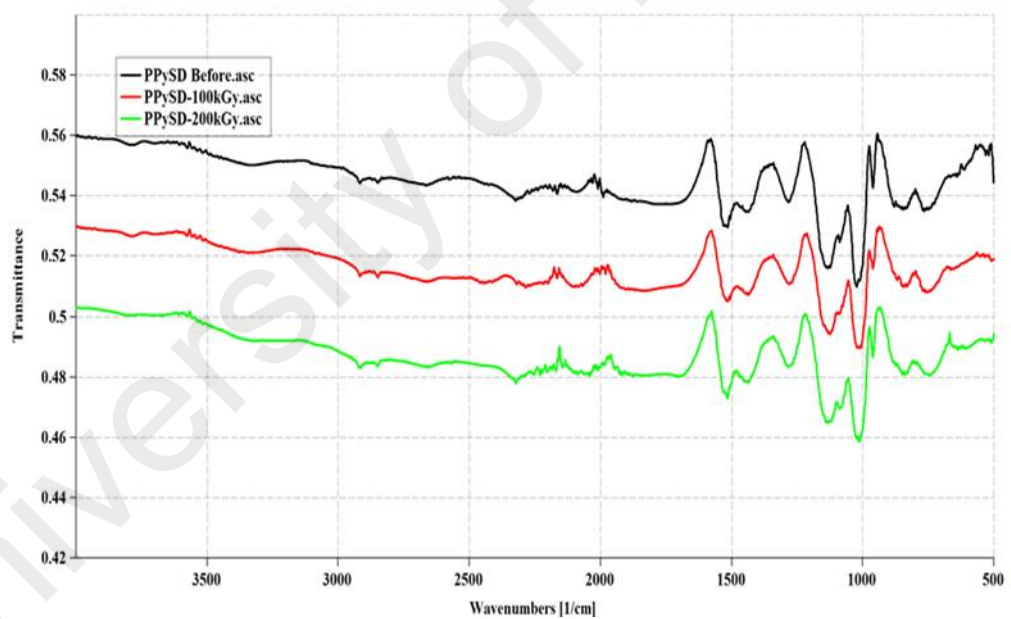


Figure 4.18: FTIR spectra of irradiated PPY/SD composite at different gamma doses.

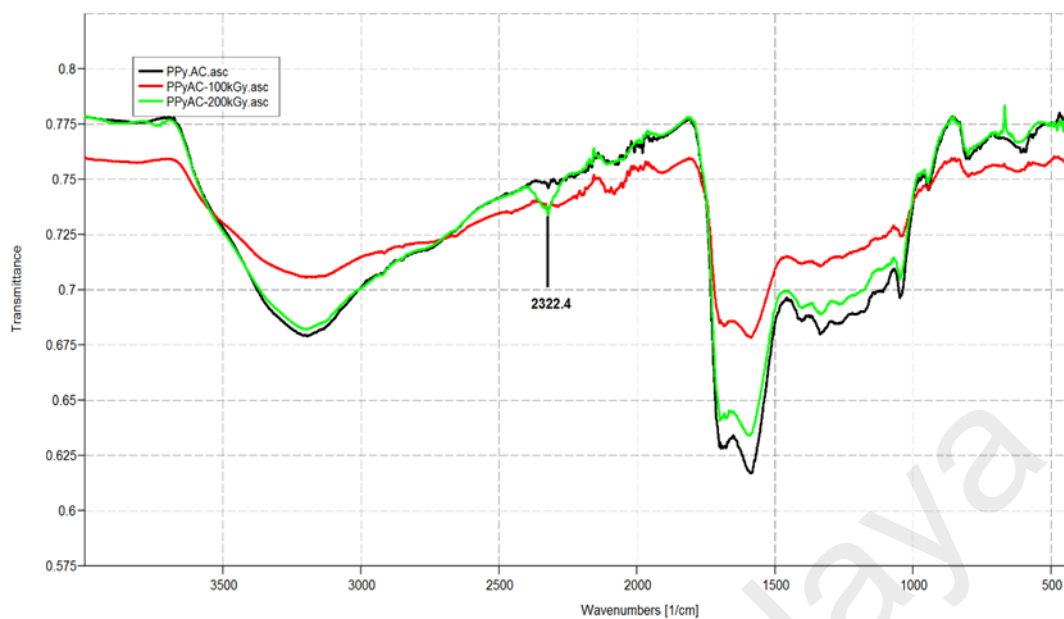


Figure 4.19: FTIR spectra of irradiated PPy/AC composite at different gamma doses.

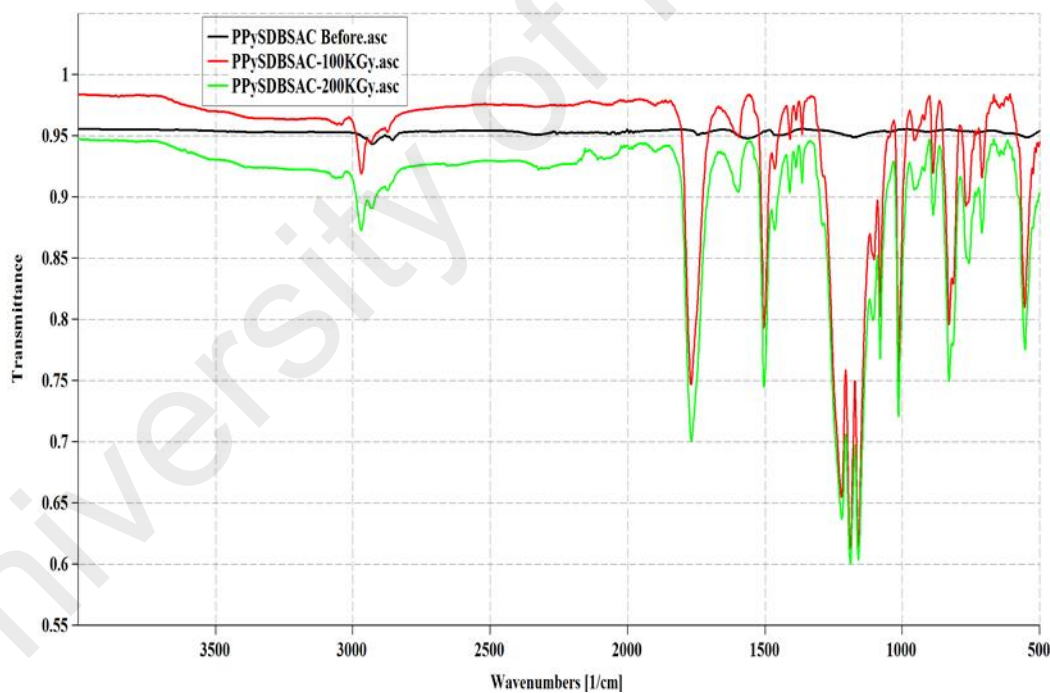


Figure 4.20: FTIR spectra of irradiated PPy/SDBS/AC composite at different gamma doses.

4.5 Thermogravimetric analysis

The thermal behavior of the polymer adsorbents has been determined by TG and DTG analysis and is shown in Figure 4.21. Generally, the TG curves reveal that there are

several stages of weight loss upon heating of the samples in a nitrogen atmosphere at a heating rate of $10\text{ }^{\circ}\text{C min}^{-1}$. The initial weight loss in the samples started at about $50\text{ }^{\circ}\text{C}$ and continued until $200\text{ }^{\circ}\text{C}$, which results in the loss of 17.96 % in PPy, 5.86 % in PPy/SD, 10.08 % in PPy/SDBS and 10.97 % in PPy/SDBS/AC. This initial weight loss can be attributed to the moisture evaporation or the removal of volatile contents from the polymer matrix. In the temperature range of $200\text{--}420\text{ }^{\circ}\text{C}$, there was a loss of 44.94 % in PPy, 24.14 % in PPy/SD, 6.58 % in PPy/SDBS and 3.56 % in PPy/SDBS/AC, respectively. The weight loss at this stage is due to the thermal degradation of oligometric or unsaturated groups in the polymer and can also be attributed to the decomposition of hemicelluloses in the polymer composite containing sawdust (thermal decomposition of hemicelluloses ranged from $225\text{--}350\text{ }^{\circ}\text{C}$).

There was a progressive loss in weight from $400\text{ }^{\circ}\text{C}$ until the temperature of about $800\text{ }^{\circ}\text{C}$ but the weight loss was more intensive for the pure PPy up to $600\text{ }^{\circ}\text{C}$ after which no significant change was observed. The intensive thermal degradation in PPy in the final stage is due to oxidation process, leaving behind 5.513 % residual weight of the original polymer sample and that also suggests that thermal decomposition of PPy occurs at about $600\text{ }^{\circ}\text{C}$. The loss in weight in the composites is due to decomposition of cellulose and lignin in PPy/SD and, the decomposition of complex dopant (SDBS) and the oxidation of carbon particles in PPy/SDBS and PPy/SDBS/AC, respectively. The presence of other component materials in the polymer composites is noticed to produce a synergy effect on the thermal stability unlike in the pure PPy. The residual weight after thermal degradation of the PPy/SD is 37.03 % and for both PPy/SDBS and PPy/SDBS/AC, the residual weights are 48.35 % and $> 82\%$, respectively, showing the positive impact of the large size dopant of SDBS as a good stabilizer for polymer materials. The concentration of the dopant is also important in determining the thermal stability of polypyrrole, which has

been reported to increase the thermal stability of the polypyrrole as concentration of dopant increases.

However, the observed maximum weight losses on the DTG curve around 400 °C and 575 °C in pure PPy confirms the decomposition of polymer chains as stated above. In the DTG curve for PPy/SD, the maximum weight loss at 373 °C is due to the decomposition of the complexes at the surface of the sawdust. The sharp peaks in DTG curves at about 100 and 115 °C in PPy/SDBS and PPy/SDBS/AC, respectively may be due to the decomposition of alkylbenzene groups in the surfactant (Jakab et al., 2007) and thermodesorption of physically adsorbed materials such as hydrocarbons or residual oxidizing agent (Maroto-Valer et al., 2004), while the peak at 578 °C observed in the PPy/SDBS is due to the degradation of the polymer chains. Many reports can be found in the literature to be similar to the above observations on the thermal stability test (Biniak et al., 1997; Castagno et al., 2011; Gao et al., 2013; Javadian, 2014; Kumar et al., 2014).

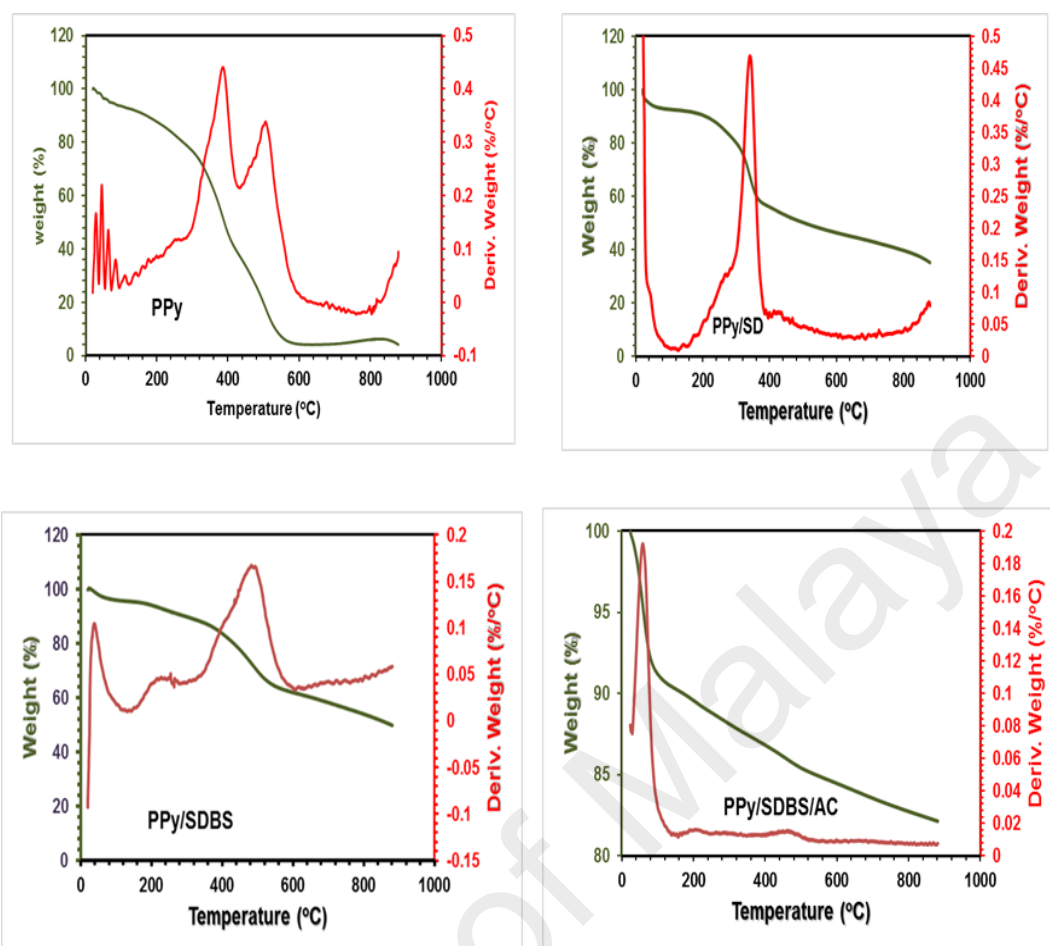


Figure 4.21: TG (green) and DTG (red) results for thermal decomposition of as-prepared polypyrrole-based materials as a function of temperature.

4.6 Surface charge titration

Acid-base titration was used to further determine and quantify the surface functional groups in terms of acidity and basicity present on the activated carbons and composite with polypyrrole using Boehm titration approach.

The obtained results of the titration of the prepared samples after reaction with the AC and PPy/SDBS/AC composite are shown in Table 4.2. The graphical presentation of the titration and surface functional groups calculations which helps to determine the quantity of each reagent adsorbed by the AC and polymer composite are found in Appendix D. Unfortunately, the curves due to sodium carbonate (Na_2CO_3) depict two equivalent volumes for the HCl acid involved in the titration. One equivalent volume was found at

approximately 8.53 ml and the other at 18.48 ml for the AC and, approximately 8.5 ml and 17.68 ml for the PPy/SDBS/AC composite. The same results were obtained for the two tests conducted.

For the other titrations, the equivalent volumes were easily obtained from the curves. Despite the lack of data from titration of Na_2CO_3 treated samples with HCl, the obtained results revealed that there is difference in the quantity of surface functional groups of the polymer composite and that of virgin AC. The virgin AC reveals that it contains more basicity but less surface acidity when compare with the polymer composite. As shown, incorporation of polypyrrole in the activated carbon in the presence of anionic surfactant reduces the base sites and increases the surface acid sites largely in the form of carboxylic sites in the polymer composite.

The sulfonic acid sites in the polymer composite should erroneously be reported as carboxylic in Boehm titration. Alternatively, the negatively charged sulfate group of the SDBS-doped PPy sorbed onto activated carbon provides more active sites capable of binding metal ions. Generally, the oxygen-containing groups and the structures containing nitro groups has considerably increased in the polymer composite. The quantity of acidic functional groups corresponds to the capacity of the polymer composite to adsorb metallic compounds. Thus, PPy/SDBS/AC composite should have more active sorption sites for metal ions. Similar observations were reported by the other authors who modified the activated carbons with anionic surfactants (Ahn et al., 2009; Wu et al., 2007). In particular, Yang et al., (2007) modified activated carbon with polyaniline and explained the difference in the surface charge density to be due to protonation and deprotonation of functional groups at the carbon-liquid interface. It was affirmed that the surface functional groups can be easily protonated in acidic solution, while deprotonation of functional groups occurs in basic solution. The additional surface acidity groups in the

PPy/SDBS/AC are likely to come from the aromatic ring structures, nitrogen-containing functional groups and sulfonate acid groups (which should erroneously be reported as carboxylic in Boehm titration). These groups are electron rich with high proton affinity, hence, it indicates that the PPy/SDBS/AC composite has a larger proton capture capacity. This implies also that PPy/SDBS/AC would have a higher affinity for radioactive cations by electrostatic attractive interactions to the negatively charged sites. The presence of these functional groups is consistent with the results of FTIR analysis.

Table 4.2: The acidity and basicity of surface functional groups on AC and PPy/SDBS/AC composite.

Sample	Surface acidity (mmol)			Basicity (mmol)
	Carboxylic groups	Lactonic and phenolic groups	Total surface acidity	
AC	0.02	0.02	0.04	0.445
PPy/SDBS/AC	0.158	0.112	0.27	0.356

CHAPTER 5: APPLICATION OF POLYPYRROLE-BASED ADSORBENTS IN ADSORPTION STUDIES

5.0 Introduction

The main aim of wastewater treatment process by adsorption was carried out to study the role of polypyrrole conducting polymer and its composite as adsorbents in removing the undesirable radioactive materials from the synthetic wastewater.

In the tests, ^{109}Cd , ^{137}Cs and ^{60}Co radionuclides were selected as a model in order to study the removal of all radioactive materials from the aqueous media by polymer-based adsorbents. The influence of several parameters such as adsorbent dosage, contact time, solution pH, rotation speed, temperature and initial radioactive metal ion concentrations were studied in order to understand the behavior of the polymer materials during the adsorption process.

The sorption kinetics data were analyzed by pseudo first-order and pseudo second-order kinetic models in order to evaluate the rate of adsorption and possibly to identify the mechanism of adsorption of the radioactive materials by the polymer adsorbents. The sorption isotherm data were analyzed by Langmuir and Freundlich isotherm models to investigate the possibility of fitting the experimental data by the isotherm models. However, selection of preparation conditions plays a vital role in the adsorption performance of polypyrrole-based adsorbents. As a result, preliminary tests were conducted for different adsorbent preparation conditions to select suitable preparation conditions for the adsorbents used in the study.

5.1 Preliminary investigation

To optimize the production conditions of polypyrrole and polypyrrole-composites used in the study, different preliminary adsorption experiments were performed based on different conditions for the adsorbents preparation and the performance of the polymer products in radionuclide removal.

5.1.1 Pyrrole to oxidant mole ratios

Since the mole ratio of pyrrole to oxidant can influence the adsorption properties of polypyrrole (Weidlich et al., 2001), different mole ratios were used to produce polypyrrole adsorbents for the removal of radionuclides. In a separate batch operation, 50 ml of each radionuclide-spiked solution (containing 20 mg/L of ^{109}Cd , ^{137}Cs and ^{60}Co radionuclides) at a pH of 5, 0.15 g of each PPy, contact time of 6 h was shaken at 200 rpm.

Table 5.1 presents the results obtained after the equilibration time for different PPy products. As shown, the performance of PPy varied for different ratio of the pyrrole and oxidant involved during polymerization. Although, the oxidant controls the polymerization of pyrrole monomers and the yield of the PPy product, it appears also that the adsorption performance of the PPy depends on the oxidant molarity. It can be clearly observed from the results that higher oxidant to pyrrole molarity reduces the removal efficiency for all the studied radionuclides. This could be explained by the decrease of pore volume and surface area as shown in Table 4.1. Consequent to the obtained results, the polypyrrole was synthesized in the presence of large size dopant (anionic surfactant) using pyrrole to oxidant ratio of 1:1.

Table 5.1: Adsorption performance of PPy prepared with different ratios of pyrrole to oxidant.

Pyrrole:oxidant	¹⁰⁹Cd (%)	¹³⁷Cs (%)	⁶⁰Co (%)
1:1	60	43	54
1:2	53	29	25
1:3	23	2	11

5.1.2 Selection of SDBS concentration for PPy/SDBS

The roles of surfactants have been well-stressed in synthesizing polypyrrole with high water dispersion, high thermal and chemical stability (Iqbal et al., 2013; Saville, 2005). In regard to adsorption, previous authors have reported that large size dopants (such as sulfonate ions) can enhance cation exchange capacity of pure polypyrrole, which would be good for adsorption of metal ions (Bai et al., 2015; Chen et al., 2016). The reason is that these ions are immobile in the polymer matrix, thereby, contributing additional sites for adsorption of metal ions. (Johanson et al., 2005). Hence, PPy was synthesized on SDBS with various concentration ratios and the products were used for adsorption of radioactive metal ions.

Table 5.2 represents the results of the effect of SDBS concentration on the removal of ¹⁰⁹Cd, ¹³⁷Cs and ⁶⁰Co radionuclides. As shown, adsorption performance of SDBS-doped PPy is improved for all the radionuclides, except for ⁶⁰Co radionuclide which shows low effect. As previously reported, better performance of SDBS-doped PPy over pure PPy can be attributed to the added sorption sites contributed by sulfonate ions and the ease of interaction of the adsorbate ions with SDBS-doped PPy when compared with the pure PPy, which agglomerates in solution (Bai et al., 2015; Chen et al., 2016). However, higher concentration of SDBS (> 13.708 mM) does not contribute to more adsorption in most cases. This may be that excess surfactant blocks the surface sites for adsorption of radionuclide metal ions. This supports previous authors that free surfactant aggregates resulted in the blockage of the surfactant-enhanced membrane pores (Aydiner et al.,

2006), which may also be the case here. For subsequent investigation, concentration of SDBS was reduced to 6.854 mM.

Table 5.2: Effect of SDBS concentration on % removal of ^{109}Cd , ^{137}Cs and ^{60}Co radionuclides by PPy/SDBS.

Adsorbent	SDBS amount (mM)	^{109}Cd (%)	^{137}Cs (%)	^{60}Co (%)
PPy/SDBS (1)	1.71	37	19	36
PPy/SDBS (2)	3.43	58	44	37
PPy/SDBS (3)	6.85	85	70	44
PPy/SDBS (4)	13.7	73	80	48
PPy/SDBS (5)	27.4	44	25	58

5.1.3 Effect of SD/AC mass on adsorption performance of polypyrrole composites

To further study the influence of other components in the sorption performance of polypyrrole particles, pyrrole monomers were polymerized in the presence of sawdust/activated carbon. Both sawdust and activated carbon as well as polypyrrole/sawdust composites have been widely used in adsorption studies (Ahn et al., 2009; Božić et al. 2009; Stanković et al., 2009), but fewer studies are available on polypyrrole/activated carbon composites. The earliest work on polypyrrole/carbon black was conducted to study its electronic conductivity by Wampler et al., (1995) but in recent years, only Hong et al., (2014) have explored the possibility of using polypyrrole-impregnated in activated carbon for sulfate removal from acid mine drainage. In the current study, both polypyrrole/sawdust and polypyrrole/activated carbon were synthesized with and without anionic surfactant (SDBS) and the products were investigated for adsorption of radioactive metal ions.

Table 5.3 represents the results of the adsorption of ^{109}Cd , ^{137}Cs and ^{60}Co radionuclides from aqueous solution using 0.15 g of each adsorbent. Generally, polypyrrole composites show improved adsorption performance over the pure PPy. When 1 g of either SD or AC was involved in the polymer composites, the performance of the adsorbents was 48 % (PPy/SD-1) and 48 % (PPy/AC-1) for ^{109}Cd , 33 % (PPy/SD-1) and 54 % (PPy/AC-1) for ^{137}Cs , and 38 % (PPy/SD-1) and 59 % (PPy/AC-1) for ^{60}Co , respectively. But, as the amount of SD or AC increased to 2 g, the adsorption performance was found to increase and was maximum with 77 % (^{109}Cd) in case of PPy/SD-2 and 70 % (^{137}Cs) in case of PPy/AC-2. The reason for this observation is that, increase in the amount of either SD or AC in the polypyrrole composites corresponds to the increase of sorption sites for the radionuclides.

However, when the pyrrole monomers were polymerized in SDBS-impregnated SD, adsorption performance of PPy/SDBS/SD composite formed was poor compared with PPy/SD-2 (without SDBS). But when pyrrole was polymerized in SDBS-impregnated AC, the PPy/SDBS/AC composite formed showed a rise in adsorption performance from 59 to 95 % (^{109}Cd), 70 to 91 % (^{137}Cs) and 63 to 68 % (^{60}Co) when compared with PPy/AC-2. It could be that SDBS created more active sites for adsorption on PPy/SDBS/AC composite but in the case of PPy/SDBS/SD composite, it is more likely that SDBS blocked the sorption sites of SD or may be due to disruption of the functional surface sites occurred due to oxidation.

Table 5.3: Adsorption performance of polypyrrole composites prepared with SD, AC and SDBS.

Adsorbent name	SD/AC (g)	¹⁰⁹ Cd	¹³⁷ Cs	⁶⁰ Co
PPy/SD (1)	1	48	33	38
PPy/SD (2)	2	77	46	57
PPy/SDBS/SD	2	47	31	48
PPy/AC (1)	1	48	54	59
PPy/AC (2)	2	59	70	63
PPy/SDBS/AC	2	95	91	68

Summarily, based on the results of preliminary adsorption tests by different adsorbents prepared under various synthesis conditions, all adsorption studies to investigate the effect of environmental variables on the uptake of ¹⁰⁹Cd, ¹³⁷Cs and ⁶⁰Co radionuclides were carried out by using SDBS-doped PPy (simply named PPy/SDBS) and PPy/SDBS/AC composites and the results were compared with the performance of pure PPy. In addition, pure PPy though has low sorption performance, has been selected to make comparison of the adsorption results with that of PPy/SDBS and PPy/SDBS/AC composites. The conditions of synthesis of the selected polypyrrole-based adsorbents, which are considered as optimal for adsorption of the radionuclides under study are represented in Table 5.4.

Table 5.4: Optimized adsorbents production conditions for higher adsorption performance.

Adsorbent	Pyrrole:oxidant ratio	SDBS concentration (mM)	AC (g)	Reaction time (h)
PPy	1:1	0	0	4
PPy/SDBS	1:1	6.854	0	4
PPy/SDBS/AC	1:1	6.854	2	16

5.2 Single-solute adsorption of ^{109}Cd , ^{137}Cs and ^{60}Co radionuclides by PPy, PPy/SDBS and PPy/SDBS/AC composites

Adsorption of ^{109}Cd , ^{137}Cs and ^{60}Co radionuclides was conducted separately at temperature of 20 °C. In batch mode, the adsorbent dosage was varied for each of the adsorbent types while other parameters such as temperature, solution volume, stirring time, rotating speed and initial concentration of each solution remained constant. As shown in Figures 5.1 (a), (b) and (c), the results of the experiments carried out for 0.05 to 0.40 g adsorbent dosage show that the adsorbate concentration in the solution decreased significantly as adsorbent dosage increased from 0.05 to 0.2 g. This can be explained in the sense that when the adsorbent dosage increases, more vacant sites were created for the adsorption of adsorbate ions, leading to more sorption or decrease in sorbate concentration in the solution. But at higher doses (above 0.2 g), there was no significant reduction in the concentration of the adsorbate ions in the solution although, more sorption sites were created. This is due to possible roll-up (aggregation) of the adsorbent particles at higher doses thereby, preventing a good contact between the adsorbate ions and the available sorption sites. In addition, the decrease in the concentration varied significantly with pure PPy showing the least adsorption while PPy/SDBS and PPy/SDBS/AC composites show high adsorption.

Comparing adsorption performance by PPy/SDBS and PPy/SDBS/AC composites, shows that the latter has higher sorption performance than the former. Specifically, when 0.2 g of pure PPy adsorbent was used, 55 % of the initial concentration was removed by PPy and that was not increased beyond 63 % when the dosage increased to 0.4 g for ^{109}Cd , 42 % was removed for ^{137}Cs at the same dosage and was not more than 53 % when the dosage increased to 0.4 g, and 52 % in case of ^{60}Co and was not increased beyond 58 % at 0.4 g of the pure PPy adsorbent. For the PPy/SDBS composite, 82 % was removed at 0.2 g while 99 % removal was obtained when the dosage increased to 0.4 g for ^{109}Cd

whereas, 84 to 86 % removal was obtained as dosage increased from 0.2 to 0.4 g in case of ^{137}Cs and 73 to 77 % removal was obtained for ^{60}Co within the same dosage range. Similarly, 100 % removal was easily achieved at 0.2 g for ^{109}Cd and 96 to 97 % for ^{137}Cs when dosage increased from 0.2 to 0.4 g, while 82 to 88 % for ^{60}Co was obtained at the same dosage increase for PPy/SBS/AC composite.

In all cases, higher removal efficiency was achieved for ^{109}Cd using PPy/SDBS/AC composite followed by PPy/SBS composite and the least is pure PPy. It is known that although pure polypyrrole contains reactive functional groups, but due to the ease of aggregation in aqueous media limits its sorption capacity for metal ions (Bai et al., 2015). As a result, it is customary to synthesis polypyrrole with other materials if higher adsorption is to be envisaged. For subsequent experiments, 0.2 g of each of the adsorbent materials was used.

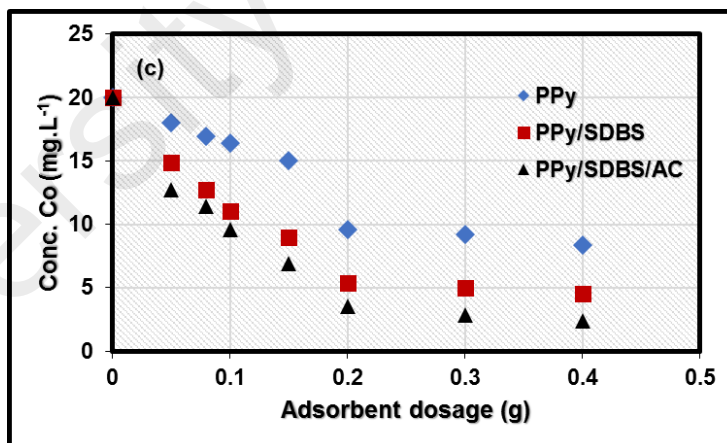
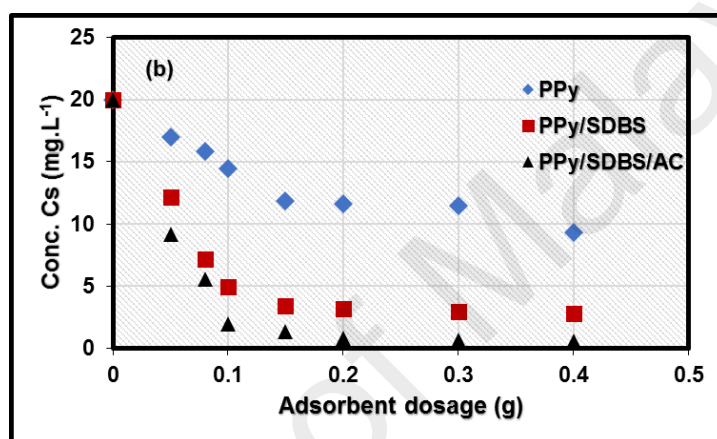
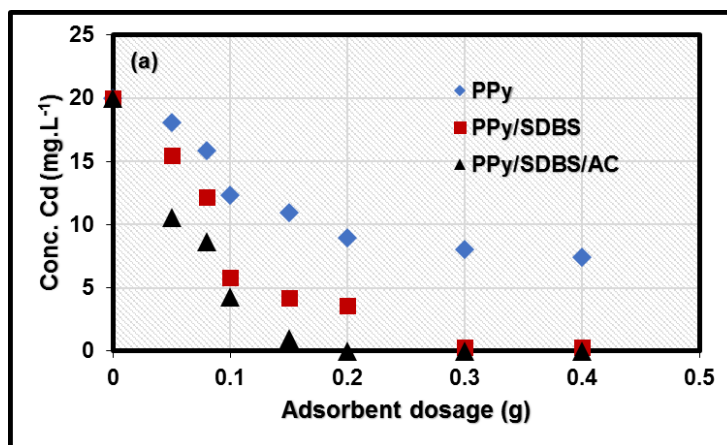


Figure 5.1: Effect of adsorbent dosage on concentration of (a) ^{109}Cd , (b) ^{137}Cs and (c) ^{60}Co radionuclides.

5.2.1 Results on effects of pH and contact time

The effect of pH on the sorption of ^{109}Cd , ^{137}Cs and ^{60}Co radionuclides by the as-prepared polypyrrole-based adsorbents was investigated. Before experiments, the speciation of each radionuclide metal ions in the aqueous solutions was conducted using the program of Visual MINTEQ version 3.0 for Windows (Environmental Research Software, USA), assuming equilibrium with the atmosphere in the pH range of 1-14, 0.001 M ionic strength and 20 °C temperature. This is to ensure that the studied radioactive materials are present in the solution as metal ions within the pH range. Figure 5.2 (a, b and c) shows that cadmium is predominantly present in the solution as metal ions up to $\text{pH} \leq 9.0$ (speciation percent more than 92.9 %) while cesium remains as metal ions in all pH range of 1-14 (speciation percent > 99 %), but hydrated cobalt ions only predominated in the pH 1-8 (with speciation percent of 95.9 %). Beyond the pH mentioned, hydroxides of these metals predominated in the solution, except for the cesium that remains as metal ions in all the pH range. As a result, the effect of pH from pH 1.4 to 9 for ^{109}Cd , pH 1.4 to 10 for ^{137}Cs and pH 1.4 to 8 for ^{60}Co was investigated.

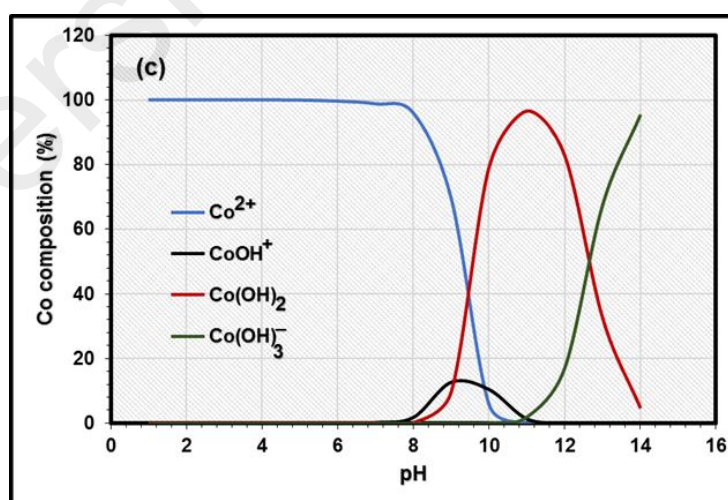
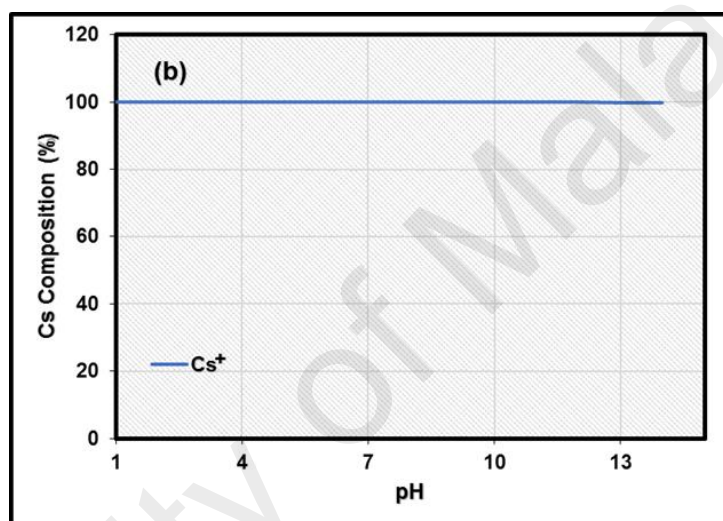
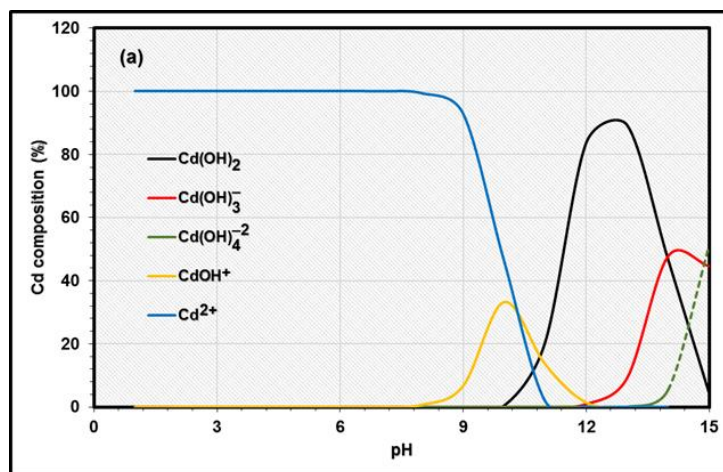


Figure 5.2: Speciation diagrams for radioactive metal ions (a) cadmium, (b) cesium and (c) cobalt distribution in the solution as a function of pH.

Figure 5.3 – Figure 5.5 represent the results of pH effect on the adsorption of ^{109}Cd , ^{137}Cs and ^{60}Co radionuclides. As shown, the uptake of the radionuclides was positively correlated with the solution pH values. Specifically, sorption of the radioactive metal ions increases with an increase in pH level of the solution, which may be explained in terms of the surface properties of the materials and the protonation state of the functional groups present at the sorbent surface.

In the case of pure PPy and PPy/SDBS which are dominantly contained amine functional groups, can be greatly influenced by solution pH. At low pH range ($\text{pH} \leq 4.5$), there is higher concentration of hydrogen ions in the liquid phase competing for sorption sites with the radionuclide, that can induce slight protonation of the lone pair of electrons on nitrogen. The protonation can lead to less electrostatic interactions between the polymer surface and adsorbate ions, resulting in the reduction of sorption capacity of the adsorbents for the radionuclides under study. At higher pH above pH 4.5 (low concentration of hydrogen ions), less hydrogen ions would be available for protonation. In this case, neutral nitrogen of amine groups can easily bind with metal ions to form complexation through sharing of electron pair (Chandra & Kim, 2011; Baş et al., 2014).

More complex situation could be expected in the case of PPy/SDBS/AC composite, which contains unsaturated $>\text{C}=\text{C}$ bonds from the activated carbon that form various functional groups already discussed in Chapter 4, in addition with amine groups from PPy. To start with, the low sorption capacity of activated carbon for metal ions arises from the fact that the acidic surface groups become easily ionized when placed in water, leading to the production of hydrogen ions which are released to the liquid phase and then the adsorbent surface becomes negatively charged (Bansal & Goyal, 2005). As a result, the negatively charged sites creates a competition between the hydrogen ions and the metal ions towards the adsorbent surface. Now, at low pH ($\text{pH} \leq 4$), the protonation of

lone pair of nitrogen as discussed earlier and ionization of carboxylic acid groups to form -COO^- would take precedence, due to higher concentration of hydrogen ions present in the solution, leading to less available sites for the metal ions. But, as pH increased further towards neutral and to alkaline range (pH 4-8), the hydrogen ion concentration decreased significantly at the surface of the adsorbent, thereby creating active sites for the adsorption of these radioactive metal ions which is the result of higher sorption observed. At pH 6, the maximum capacity of PPy was $2.98 \text{ mgCd. g}^{-1}$, $2.40 \text{ mgCs. g}^{-1}$ and $2.84 \text{ mgCo. g}^{-1}$, respectively, whereas, PPy/SDBS has $4.19 \text{ mgCd. g}^{-1}$, $4.28 \text{ mgCs. g}^{-1}$ and $3.79 \text{ mgCo. g}^{-1}$, respectively, and 5.0 mgCd. g^{-1} , $4.82 \text{ mgCs. g}^{-1}$ and $4.05 \text{ mgCo. g}^{-1}$, was achieved by PPy/SDBS/AC composite.

It is apparent that cadmium and cesium ions show higher affinity towards the polypyrrole-based materials than cobalt ions. This may be related to a number of factors such as different molecular mass, ion charges, ionic radius, hydrated ionic radius and hydrated energy of the metal ions. Nassar (2012), proposed a model to explain the surface-ionic interactions that lead to higher sorption capacity of cadmium and cesium ions by the adsorbents as follows; metal ions with larger ionic radius have smaller hydrated radius and hence, smaller hydrated energy. Metal ions with lower hydrated radius will have higher binding affinity towards the adsorbent than the higher ones. Considering the ionic radii of the studied radionuclides ($\text{Cd} = 109 \text{ pm}$, $\text{Cs} = 181 \text{ pm}$ and $\text{Co} = 88 \text{ pm}$), one would expect cadmium and cesium ions to have higher uptake by the adsorbents than cobalt ions due to their ionic radii, which is the case in this study. Likewise, Al-Nasri (2013) in his work on the adsorption of radioactive strontium and cobalt by different zeolite composite adsorbents, described the higher uptake of strontium over cobalt to be related to the larger ionic size of the former, which helps in the reduction of amount of repulsive forces that can hinder its transport across the bulk of the solution onto the surface of the adsorbent. Similar observations were also reported by others who

used chitosan and its composites to sorb cesium from natural and simulated wastewaters (Yang et al., 2015), Park et al. (2010) investigated adsorption of cobalt, cesium and strontium from radioactive laundry wastewater by ammonium molybdophosphate-polyacrylonitrile (AMP-PAN).

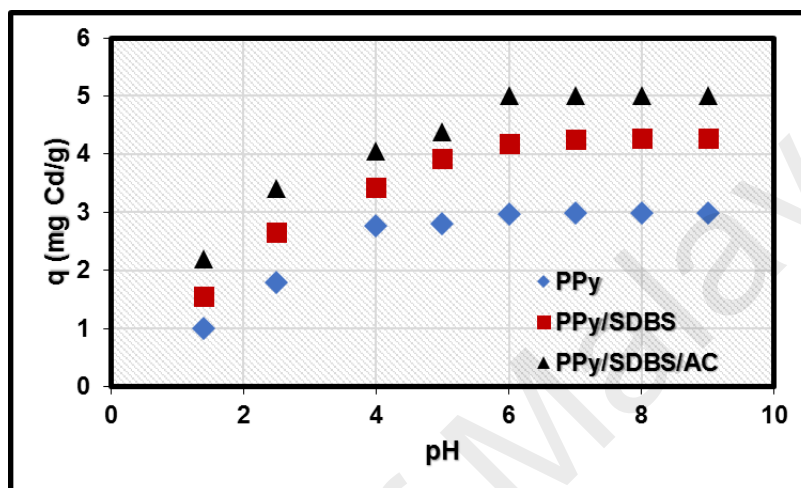


Figure 5.3: Effect of pH on adsorption capacity of ^{109}Cd .

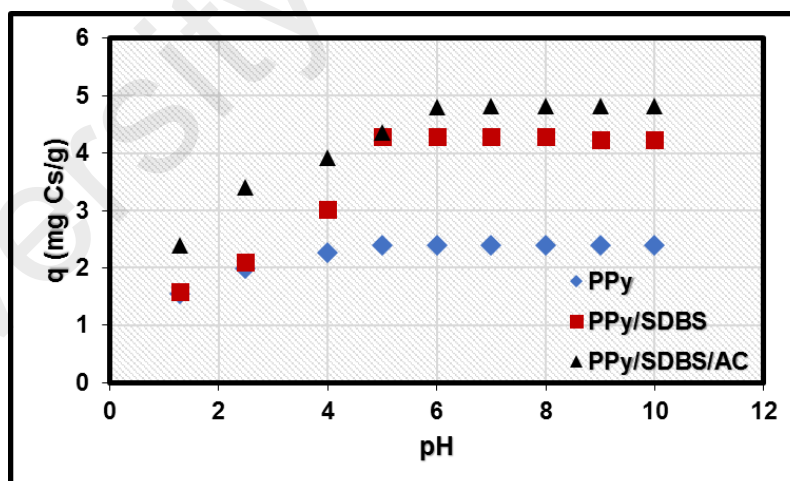


Figure 5.4: Effect of pH on adsorption capacity of ^{137}Cs .

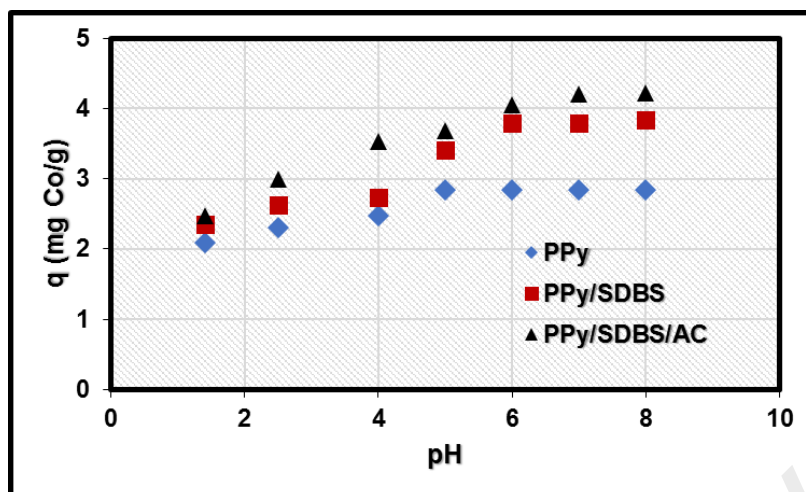


Figure 5.5: Effect of pH on adsorption capacity of ^{60}Co .

Figure 5.6 – Figure 5.8 illustrate the results of interaction time of the adsorbate ions and adsorbents. It is shown that fast adsorption of radionuclides was possible within 180 min, which then slowly reached equilibrium in 240 min. Contact time was extended to 360 min to ensure equilibrium. Rapid adsorption at the initial period can be related to available vacant sites for adsorption of the radionuclides. As the surface sites are nearly occupied by the adsorbate ions with increase in contact time, adsorption was expected to proceed by diffusion of remaining adsorbate ions into the bulk of the adsorbent. In addition, as adsorbate concentration reduced to infinite dilution with a rise in time, the sorption capacity of the adsorbent also increased to its maximum.

The sorption capacities of pure PPy ranged between $2.40 \text{ mgCs. g}^{-1}$ and $3.02 \text{ mgCd. g}^{-1}$ while PPy/SDBS has its highest capacity of $4.33 \text{ mgCs. g}^{-1}$ and the least is $3.79 \text{ mgCo. g}^{-1}$, and PPy/SDBS/AC composite has the highest sorption capacity of 5.0 mgCd. g^{-1} and the least is $4.23 \text{ mgCo. g}^{-1}$. The sorption capacities for the composite adsorbent materials would have been higher if the concentration were to be increased because before contact time of 240 min, adsorbate concentration has reduced to infinite dilution in the case of PPy/SDBS/AC composite. Similar contact time was reported in removing different radionuclides including cesium and cobalt from solutions by inorganic and ligand

conjugate adsorbents and by activated silico-antimonate crystals (Ali, 2009; Awual et al., 2014), but much shorter time was reported when latex particle functionalized with transition metals ferrocyanides were used to sorb cesium from aqueous solution (Avramenko et al., 2011).

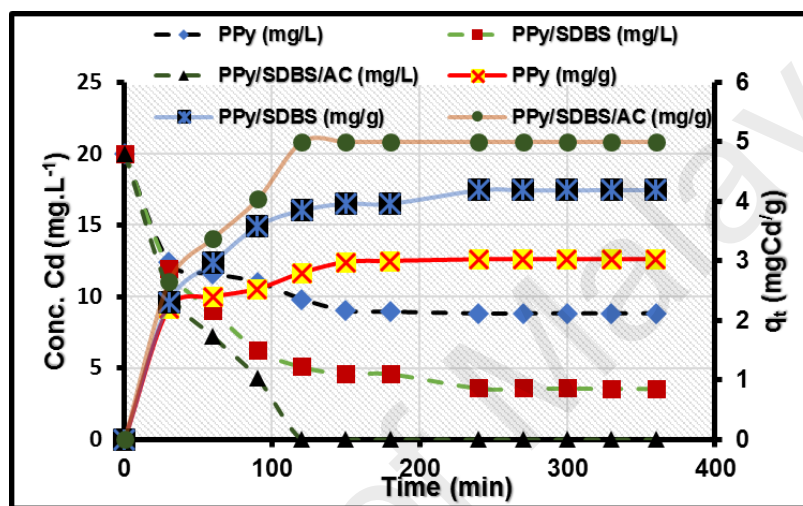


Figure 5.6: Effect of contact time on amount of ¹⁰⁹Cd adsorbed.

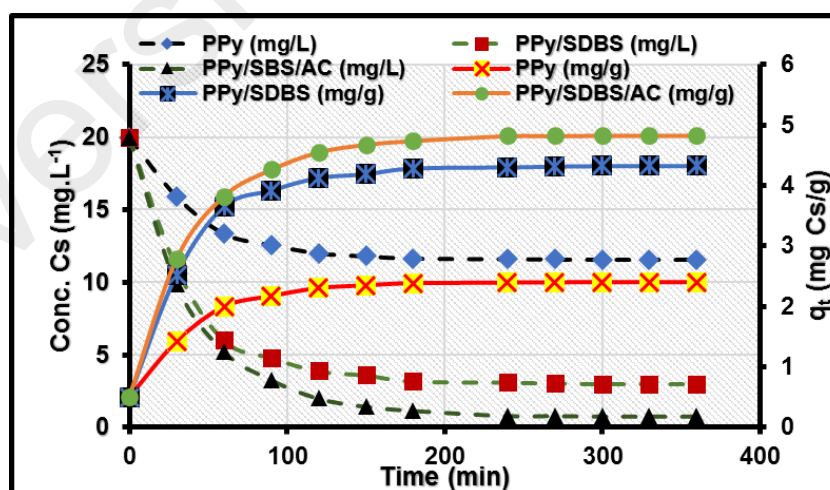


Figure 5.7: Effect of contact time on amount of ¹³⁷Cs adsorbed.

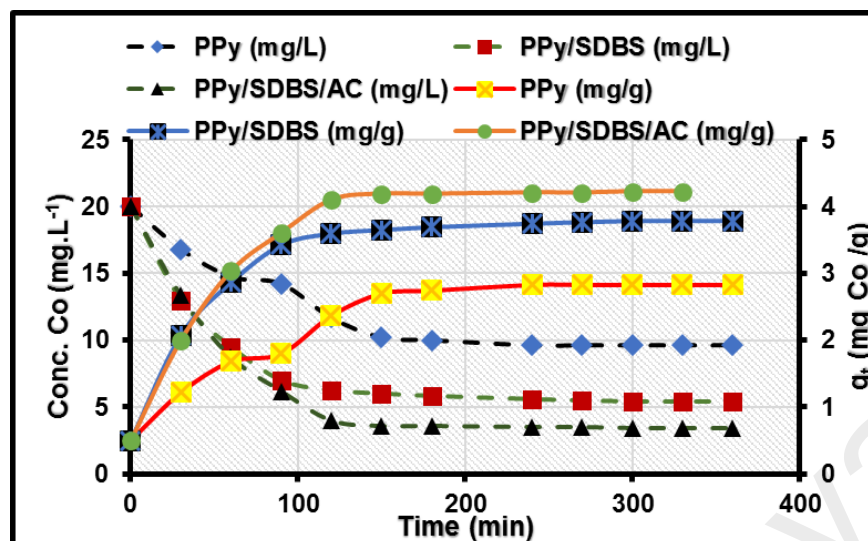


Figure 5.8: Effect of contact time on amount of ^{60}Co adsorbed.

5.2.2 Results on effects of initial concentration, temperature and interfering metal ions

To investigate the possibility of higher sorption capacities with a rise in initial concentration of radionuclide ions, the effect of increasing initial ions concentration on sorption capacity was performed. Figure 5.9 – Figure 5.11 represent the results obtained for different initial concentrations that ranged from 20 to 100 mgL^{-1} for each radionuclide. As shown, increasing the initial concentration of radioactive metal ions corresponded to higher sorption capacity for all the adsorbents. This can be related to the metal ions concentration gradient between aqueous solution and the adsorbents, leading to increasing collision of ions onto the adsorbents. In addition, increasing initial concentration may possibly increase the driving force to overcome the resistance to mass transfer of activity of radionuclide from the aqueous phase to the solid phase, which can lead to high adsorption as obtained. In all experiments, PPy/SDBS/AC composite showed superiority in adsorption of the radionuclides as initial concentration increases, which may be due to complex surface functionality compared to other adsorbents.

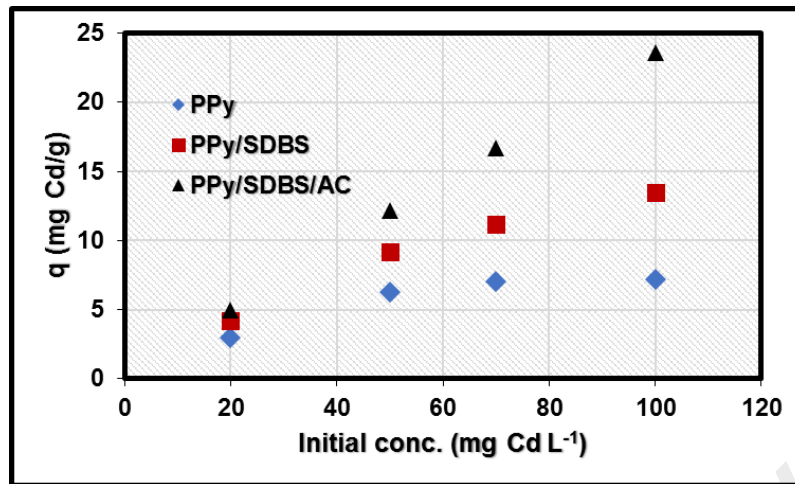


Figure 5.9: Effect of initial concentration on amount of ^{109}Cd adsorbed.

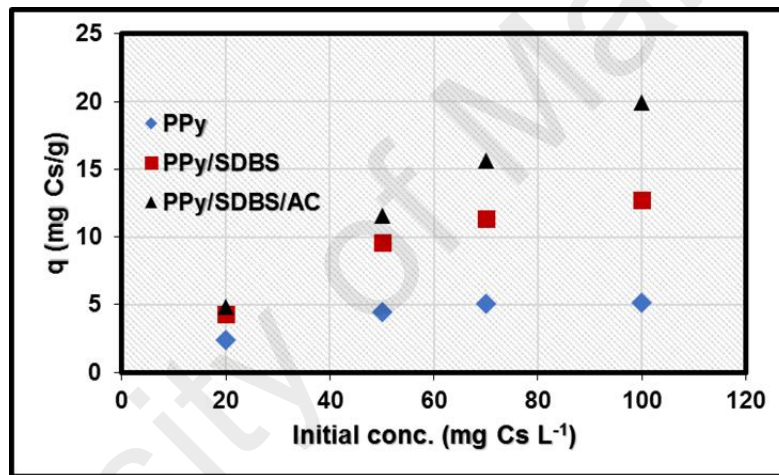


Figure 5.10: Effect of initial concentration on amount of ^{137}Cs adsorbed.

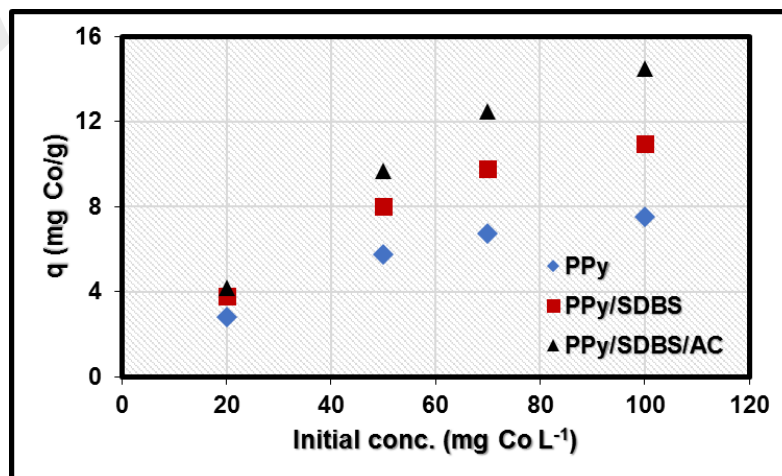


Figure 5.11: Effect of initial concentration on amount of ^{60}Co adsorbed.

Variation in temperature of adsorbate solutions can significantly influence the adsorption process in different ways. Firstly, it can increase the rates of diffusion of molecules across the external boundary layer and the internal pores of the adsorbent particles, due to the reduction in the viscosity of the adsorbate solution (Seid et al., 2014). Increase in temperature can also increase the mobility of metal ions from aqueous to solid phase and also, produces a swelling effect in the internal pores of adsorbents for easy adsorption of adsorbate ions. To illustrate the effect of temperature on the adsorption of cadmium, cesium and cobalt radionuclides from aqueous solution, all experiments were performed through the applications of four different temperatures: 20, 30, 40 and 50 °C.

Figure 5.12 – Figure 5.14, respectively, show that the uptake of ^{109}Cd radionuclide was slightly reduced as temperature was raised from 20 to 50 °C, but increased in the case of ^{137}Cs and ^{60}Co . Since increasing adsorption temperature should favour diffusion of ions through the adsorbents, it must be that diffusion of cadmium ions through the adsorbents was not controlled by a rise in temperature in this study. This suggests that the bond between Cd ions and the active sites of the adsorbents is weak and that also may lead to reduction in the adsorption rates (Benguella & Benaissa, 2002). Hence, the behaviour of cadmium adsorption with temperature indicates that cadmium adsorption by polymer composite materials is an exothermic process and that maximum adsorption can only be achieved at a lower temperature. In the case of ^{137}Cs and ^{60}Co radionuclides, a rise in temperature favours higher adsorption, which is an indication that the adsorption of both radionuclides follows endothermic process. As temperature rises, the rate of adsorption was increased due to the increase in diffusion of ions through the adsorbents. Similar results of effect of temperature have been previously reported for radioactive cesium and cobalt by other authors (Ali, 2009; Kamaraj & Vasudevan, 2015).

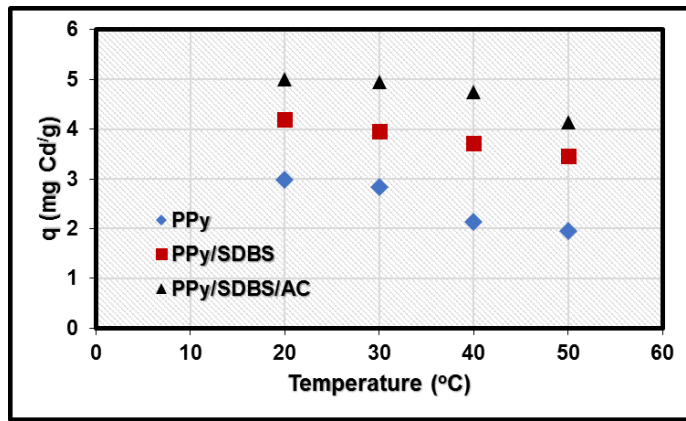


Figure 5.12: Effect of temperature on amount of ^{109}Cd adsorbed.

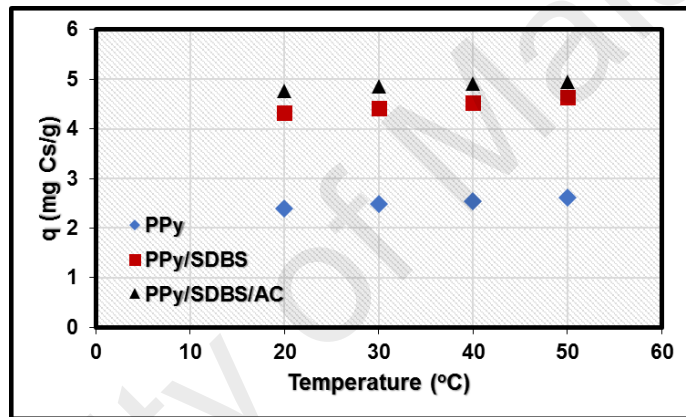


Figure 5.13: Effect of temperature on amount of ^{137}Cs adsorbed.

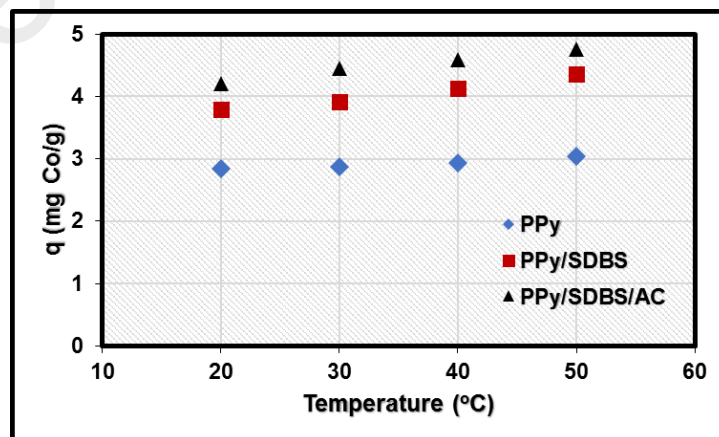


Figure 5.14: Effect of temperature on amount of ^{60}Co adsorbed.

Adsorption of target species by adsorbent can be greatly influenced by the presence of other metal ions in the aqueous solutions (Sangvanich et al., 2010). The effect of common metal ions found in the wastewater such as Na^+ (100 mg/L), K^+ (20 mg/L), Ca^{2+} (30 mg/L), Mg^{2+} (70 mg/L) and Rb^+ (20 mg/L) was investigated using 20 mg/L of initial concentration of each radionuclide, spiked with respective radiotracer solution (that is, ^{109}Cd , ^{137}Cs and ^{60}Co). Figure 5.15 to Figure 5.17 represent the results of effect of interfering ions in the solution. Within the metal ions concentration considered, it is generally shown that adsorption of all radionuclides was decreased in the presence of all metal ions, but the presence of Na^+ has negligible effect on the removal of ^{137}Cs and ^{60}Co radionuclides.

In all experiments, only the presence of K^+ and Rb^+ ions show somewhat reduction in the Cd adsorption, while only K^+ , Rb^+ , Ca^{2+} and Mg^{2+} ions have significant negative effect on both Cs and Co adsorption. As shown, the influence of these interfering ions varied in magnitude and that can be attributed to their different hydrated radii, hydration energies, chemical reactivity and strong complexation towards solid surfaces compared with radionuclides under study. Some authors have also reported similar observations of these metal ions on adsorption of these radionuclide by various adsorbents including polymer-based materials (Ararem et al., 2011; Bondar et al., 2014; Faghihian et al., 2013; Saberi et al., 2010; Yang et al., 2015). Despite the influence of these ions, selectivity of the studied radionuclides is still high, showing that the polymer adsorbents can adsorb these radionuclides in the presence of different interfering ions.

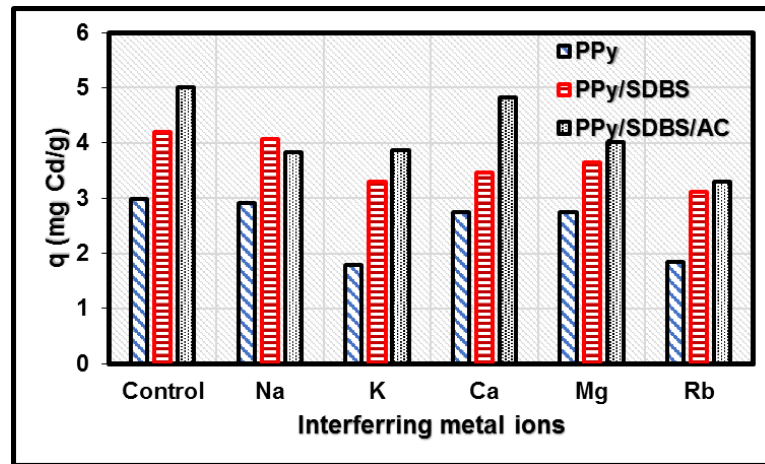


Figure 5.15: Effect of interfering metal ions on amount of ¹⁰⁹Cd adsorbed.

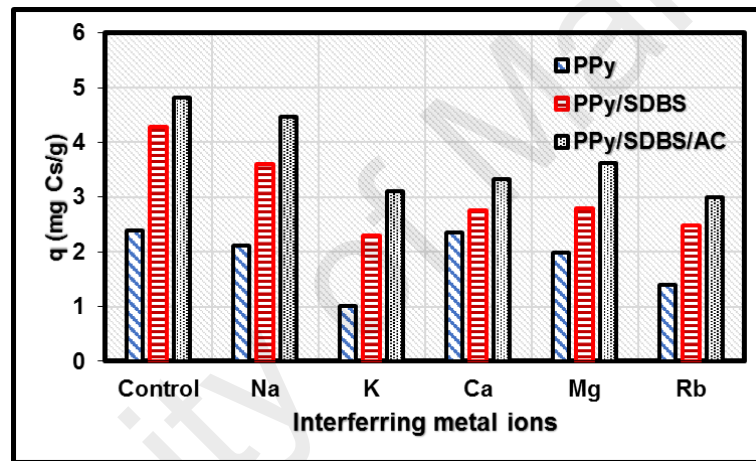


Figure 5.16: Effect of interfering metal ions on amount of ¹³⁷Cs adsorbed.

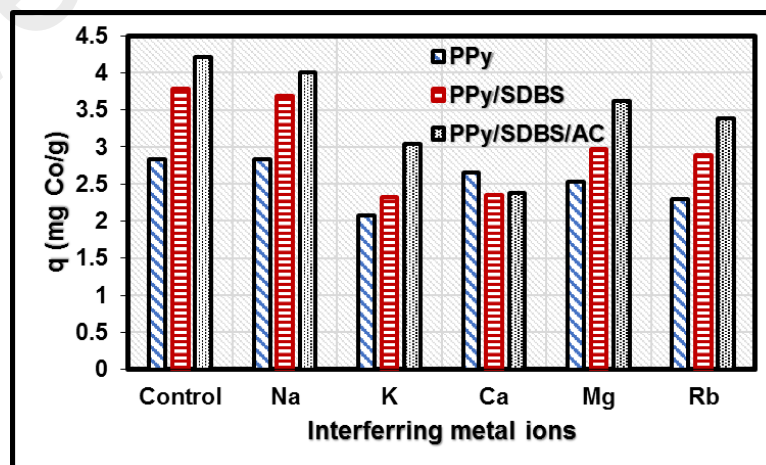


Figure 5.17: Effect of interfering metal ions on amount of ⁶⁰Co adsorbed.

5.2.3 Results on adsorption kinetic model analysis

Depending on the heterogeneity of reactive sites and physico-chemical conditions under which adsorption takes place, adsorbate can be adsorbed onto the adsorbent surface by different mechanisms. The knowledge of adsorption mechanism is not only important in describing the efficiency but also important in designing future feasibility of the adsorption in large scale. In the current study, the two commonly used kinetic models namely; pseudo first-order and pseudo second-order kinetic models were used to predict the adsorption mechanism and the rate controlling steps during the adsorption process. For this purpose, non-linear regression analysis by OriginPro 8.5 program was adopted to calculate the model parameters and correlation coefficient (R^2) which determines the best-fitting model to the kinetic data. The plots of these models and results are presented in Figure 5.18 to Figure 5.20 and Table 5.5 to Table 5.7, respectively.

In all cases, the two models yield good correlations to the kinetic data with strong correlation coefficients ($R^2 \sim 0.9$). For comparison purpose, higher correlation coefficients (R^2) and lower χ^2 (which defines the degree of difference between the experimental data and theoretical data) are obtainable with pseudo first-order kinetic model when compared with pseudo second-order kinetic model in most cases. This suggests that the rate limiting of the adsorption process might be physisorption. It is an indication that the adsorption process is initiated by the weak intermolecular forces (such as Van der Waals interactions, π - π stacking interactions etc.). Since the process involves weak forces, it further suggests that the adsorbate can be recovered by a reverse process called desorption (Pignatello, 2011). However, due to the complex nature of polymer adsorbents, chemisorption involving transferring or sharing of valence electrons between the adsorbate and adsorbent surface, and pore filling could also involve in the adsorption process.

Table 5.5: Adsorption kinetic model parameters for ^{109}Cd radionuclide.

Parameters	PPy	PPy/SDBS	PPy/SDBS/AC
Pseudo First-Order for ^{109}Cd			
q_e (mg/g)	2.95±0.06	4.17±0.04	5.03±0.08
k_1 (min^{-1})	0.04±0.005	0.02±0.001	0.02±0.001
R^2	0.967	0.994	0.985
χ^2	0.025	0.009	0.034
Pseudo Second-Order for ^{109}Cd			
q_e (mg/g)	3.18±0.05	4.66±0.07	5.71±0.15
k_2 (g/mgmin)	0.02±0.003	0.01±6.72E-4	0.01±7.2E-4
R^2	0.989	0.994	0.983
χ^2	0.008	0.009	0.039

Table 5.6: Adsorption kinetic model parameters for ^{137}Cs radionuclide.

Parameters	PPy	PPy/SDBS	PPy/SDBS/AC
Pseudo First-Order for ^{137}Cs			
q_e (mg/g)	2.39±0.06	4.30±0.06	4.79±0.06
k_1 (min^{-1})	0.03±0.004	0.03±0.003	0.03±0.002
R^2	0.924	0.979	0.983
χ^2	0.03	0.03	0.03
Pseudo Second-Order for ^{137}Cs			
q_e (mg/g)	2.61±0.10	4.69±0.12	5.27±0.12
k_2 (g/mgmin)	0.02±0.006	0.01±0.002	0.01±0.001
R^2	0.912	0.969	0.979
χ^2	0.03	0.04	0.04

Table 5.7: Adsorption kinetic model parameters for ^{60}Co radionuclide.

Parameters	PPy	PPy/SDBS	PPy/SDBS/AC
Pseudo First-Order for ^{60}Co			
q_e (mg/g)	2.89±0.10	3.76±0.06	4.26±0.07
k_1 (min^{-1})	0.02±0.002	0.03±0.002	0.02±0.002
R^2	0.933	0.973	0.979
χ^2	0.04	0.03	0.03
Pseudo Second-Order for ^{60}Co			
q_e (mg/g)	3.43±0.21	4.17±0.13	4.81±0.18
k_2 (g/mgmin)	0.01±0.001	0.01±0.002	0.006±0.001
R^2	0.928	0.962	0.957
χ^2	0.05	0.04	0.06

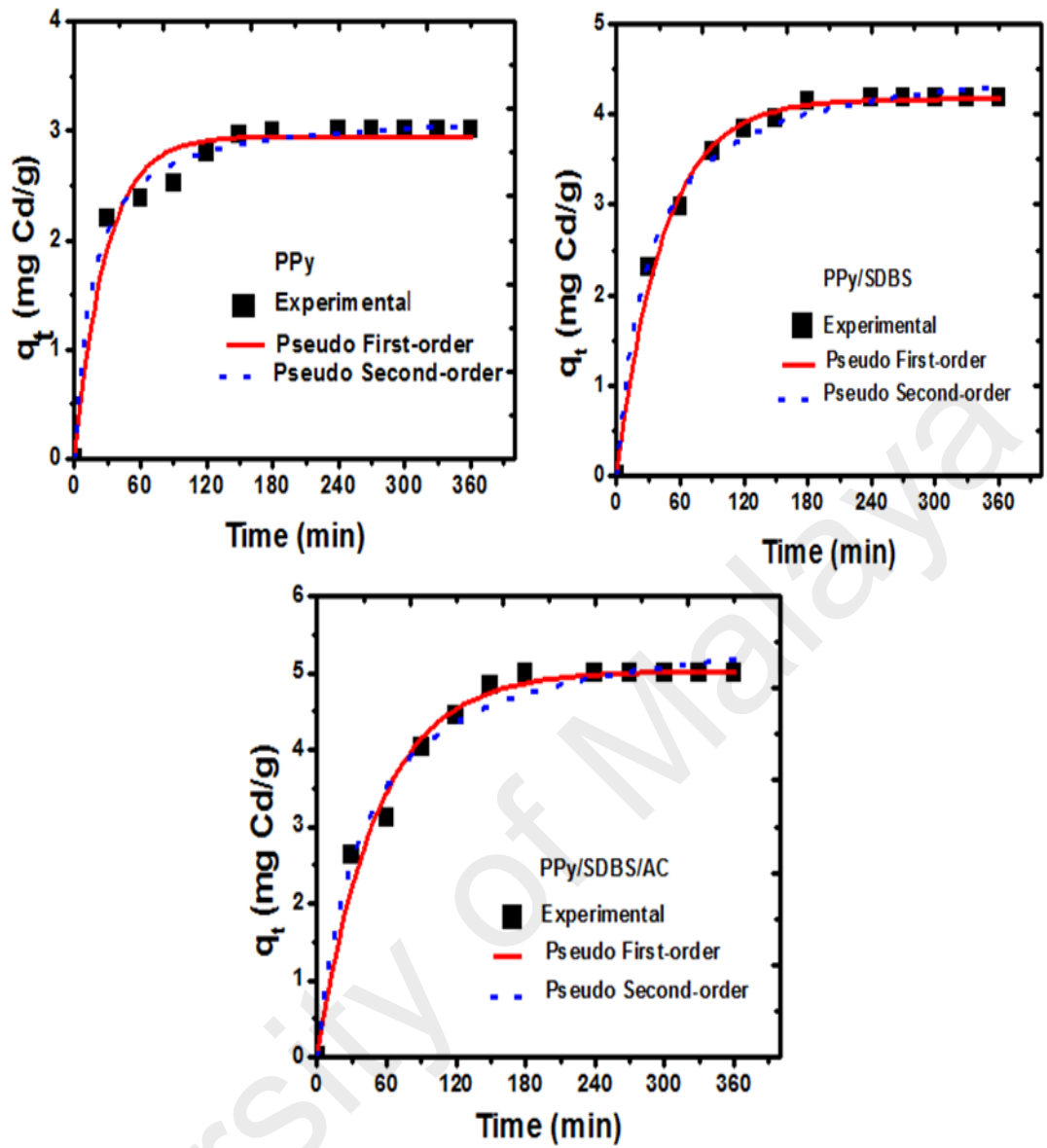


Figure 5.18: Plots of adsorption kinetics for ^{109}Cd . The solid and dotted lines show the fitting of theoretical and experimental data.

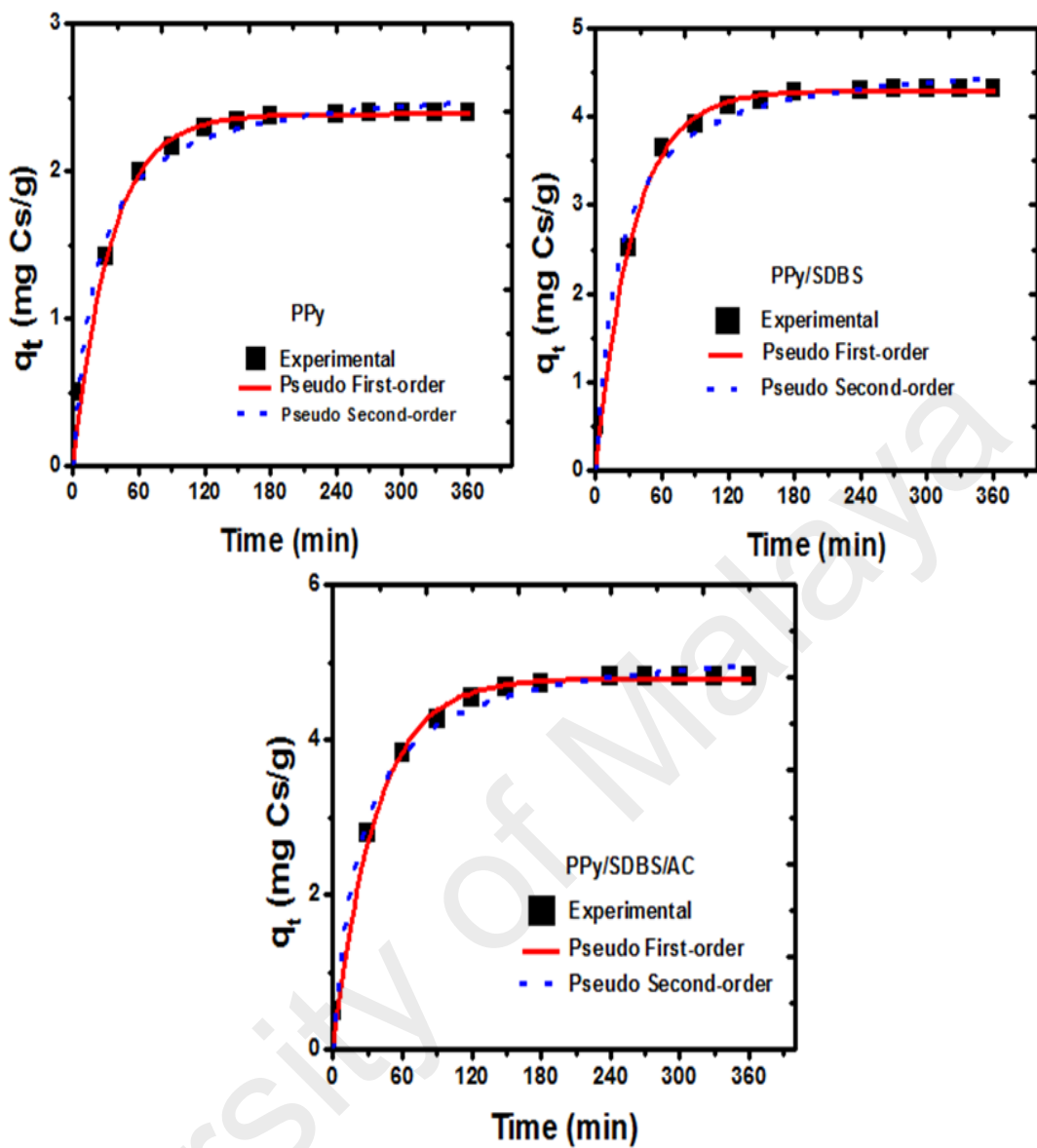


Figure 5.19: Plots of adsorption kinetics for ^{137}Cs . The solid and dotted lines show the fitting of theoretical and experimental data.

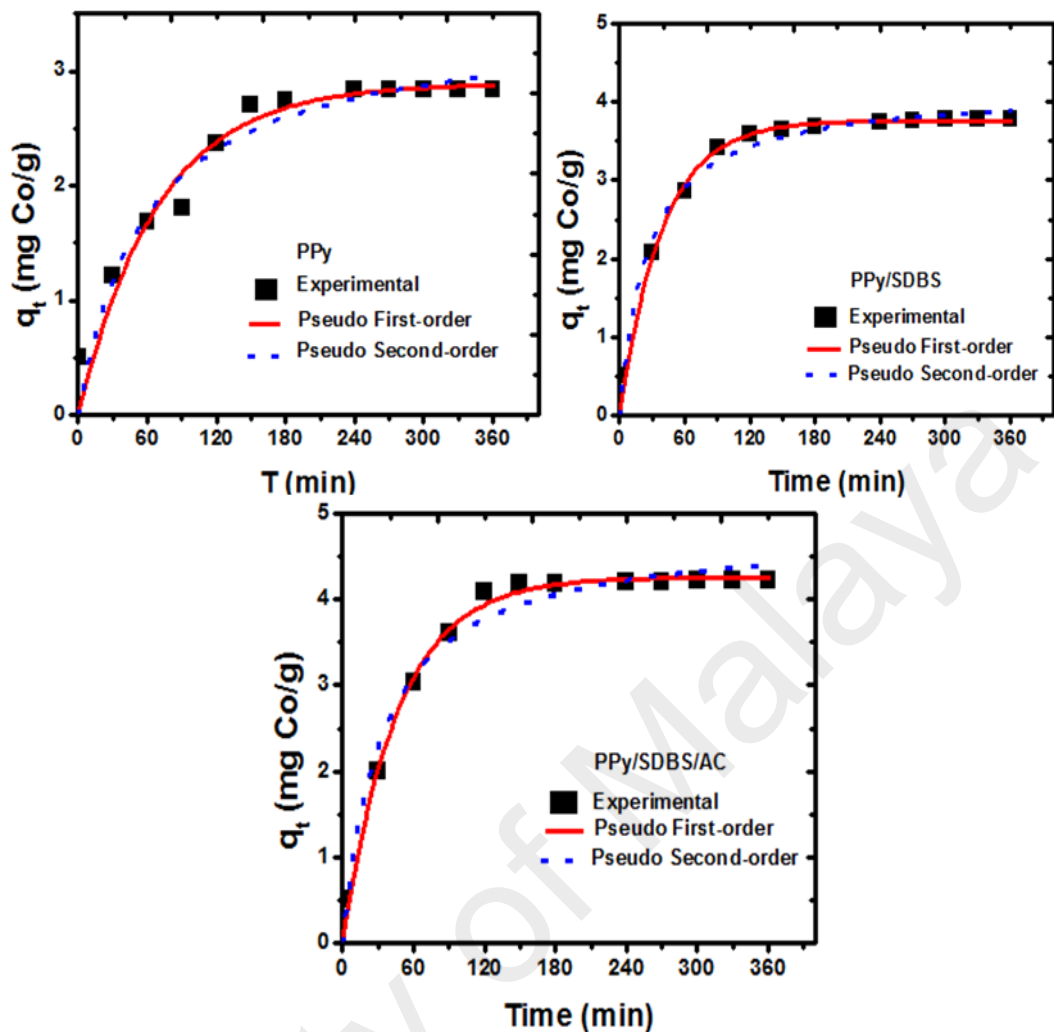


Figure 5.20: Plots of adsorption kinetics for ^{60}Co . The solid and dotted lines show the fitting of theoretical and experimental data.

5.2.4 Results on adsorption isotherm model analysis

The relationship existing between the adsorbate ions in the liquid and solid phase at equilibrium is very essential in order to optimize the use of adsorbent material for a particular radionuclide. To do this, the studies of isotherm were carried out. The isotherm data are analyzed using Langmuir and Freundlich isotherm models. These models are used to reconcile the theoretical data with the experimental data for each adsorbent. A non-linear approach was adopted to calculate the model parameters and statistical parameters (coefficient of correlation, R^2) and the chi-square, χ^2) that describe the

adsorption process using OriginPro 8.5 program. The plots of these models and the Tables of obtained results are presented in order in the subsequent sections.

5.2.4.1 The plots and results of isotherm models for adsorption of ^{109}Cd radionuclide

The plots which show the isotherm model analysis and the obtained theoretical data for ^{109}Cd adsorption are presented in Figure 5.21 and Table 5.8, respectively. The non-linear regression coefficients (R^2) and the chi-square (χ^2) obtained show the two models can be used to fit the experimental data. This suggests that the adsorbents can be used for the adsorption of cadmium radionuclide.

For Langmuir model, the trend of R^2 is $\text{PPy/SDBS} > \text{PPy} > \text{PPy/SDBS/AC}$, while the b value reveals that the energy of the adsorption increases in the order of $\text{PPy/SDBS/AC} > \text{PPy/SDBS} > \text{PPy}$. The q value which equals the trend in the sorption capacity, has the trend $\text{PPy/SDBS/AC} > \text{PPy/SDBS} > \text{PPy}$. This is the maximum sorption capacity which corresponds to complete monolayer coverage for each adsorbent as measured by the Langmuir model. The values of R_L (0.13 – 0.43) for PPy, R_L (0.10 – 0.35) for PPy/SDBS and R_L (0.03 – 0.14) for PPy/SDBS/AC obtained from the Langmuir model support that the adsorbents can be exploited in practical application for the adsorption of ^{109}Cd radionuclide.

With respect to the Freundlich model, the obtained correlation coefficients (R^2) is in order of $\text{PPy/SDBS} > \text{PPy/SDBS/AC} > \text{PPy}$. The n value which describes the intensity of adsorption has a trend of $\text{PPy} (2.99) > \text{PPy/SDBS} (2.55) > \text{PPy/SDBS/AC} (2.01)$ and that, shows that the adsorption of ^{109}Cd by the polymer adsorbents is favourable, as obtained values are within 1 to 10, which is the range of determining the favourable adsorption by Freundlich constant n . The trend of K_F value which is a measure of adsorption capacity of the adsorbents is $\text{PPy/SDBS/AC} > \text{PPy/SDBS} > \text{PPy}$.

Table 5.8: Langmuir and Freundlich parameters for adsorption of ^{109}Cd radionuclide.

Parameters	PPy	PPy/SDBS	PPy/SDBS/AC
Langmuir isotherm for ^{109}Cd			
b (Lmg^{-1})	0.068 ± 0.02	0.093 ± 0.013	0.30 ± 0.32
q_m (mgg^{-1})	8.96 ± 0.85	16.0 ± 0.72	35.3 ± 16.9
R_L	$0.13-0.43$	$0.10-0.35$	$0.03-0.14$
R^2	0.934	0.990	0.770
χ^2	0.25	0.15	14.1
Freundlich isotherm for ^{109}Cd			
K_F ($\text{mgg}^{-1} \text{L}^{1/n} \text{mg}^{-1/n}$)	1.81 ± 0.84	2.95 ± 0.56	9.38 ± 3.44
n	2.99 ± 1.08	2.55 ± 0.36	2.01 ± 0.97
R^2	0.763	0.962	0.788
χ^2	0.909	0.59	13.0

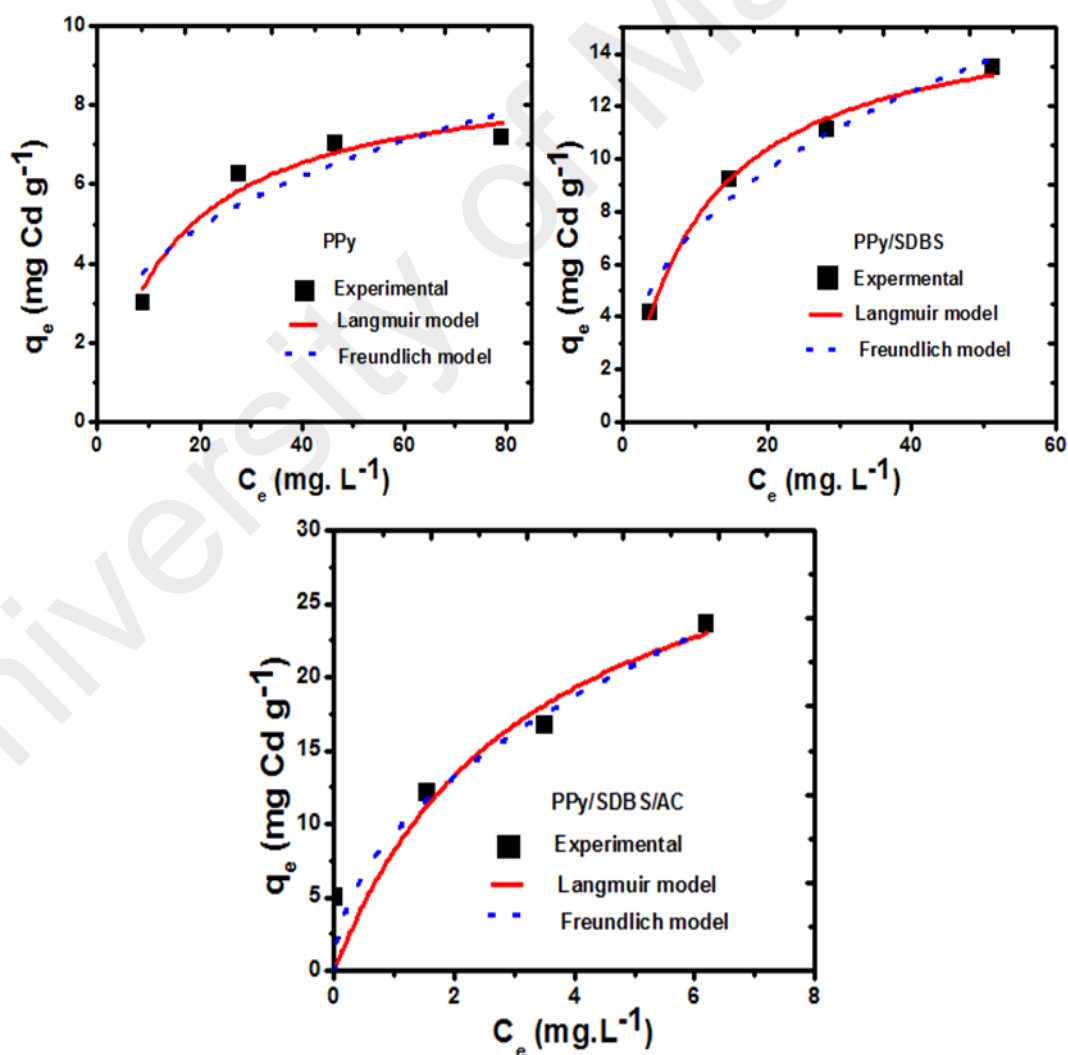


Figure 5.21: Plots of adsorption isotherms for ^{109}Cd . The solid and dotted lines show the fitting of theoretical and experimental data.

5.2.4.2 The plots and results of isotherm models for adsorption of ^{137}Cs radionuclide

The plots which show the isotherm model analysis and the obtained theoretical data are presented in Figure 5.22 and Table 5.9, respectively. From the obtained adsorption and statistical parameters, it is revealed that the experimental data can be fitted by both Langmuir and Freundlich models, with Langmuir model showing good data fit, as shown by higher correlation factors. Again, the higher correlation factors obtained suggests that all the adsorbents can be exploited in the adsorption of ^{137}Cs radionuclide.

Looking through the adsorption parameters obtained from Langmuir model, show that the R^2 has a trend order of PPy/SDBS > PPy/SDBS/AC > PPy, while the b value which defines the energy of adsorption of the radionuclide varies between 0.06 Lmg^{-1} (PPy) and 0.27 Lmg^{-1} (PPy/SDBS/AC). The maximum sorption capacity of the Langmuir model, which describes the complete monolayer coverage of the adsorbents has a trend of PPy/SDBS/AC (23.0 mg. g^{-1}) > PPy/SDBS (14.2 mg. g^{-1}) > PPy (6.40 mg. g^{-1}). The obtained R_L values, which show the trend of PPy > PPy/SDBS > PPy/SDBS/AC supports that the polymer composite adsorbents have more favourability in practical application for the adsorption of cesium radionuclide than the pure PPy.

With regards to the Freundlich model, the parameter K_F , which also defines the adsorption capacity of each adsorbent shows the trend of PPy/SDBS/AC > PPy/SDBS > PPy, while the R^2 has the trend of PPy/SDBS/AC > PPy/SDBS > PPy. The results show that sorption capacity of the polymer composites is higher for cesium than the pure PPy adsorbent. For the Freundlich constant n , which can be used to measure the favourability of the adsorption process if the value lies within 1-10, revealed that the adsorption process is favourable with values lying between 2.75 and 3.21.

Table 5.9: Langmuir and Freundlich parameters for adsorption of ^{137}Cs radionuclide.

Parameters	PPy	PPy/SDBS	PPy/SDBS/AC
Langmuir isotherm			
b (Lmg^{-1})	0.06 ± 0.02	0.15 ± 0.01	0.27 ± 0.04
q_m (mgg^{-1})	6.40 ± 0.47	14.2 ± 0.26	23.0 ± 1.10
R_L	$0.15 - 0.47$	$0.06 - 0.25$	$0.04 - 0.16$
R^2	0.956	0.9971	0.990
χ^2	0.07	0.04	0.43
Freundlich isotherm			
K_F ($\text{mgg}^{-1} \text{L}^{1/n} \text{mg}^{-1/n}$)	1.23 ± 0.50	3.85 ± 1.0	6.67 ± 1.02
n	2.98 ± 0.92	3.21 ± 0.79	2.75 ± 0.45
R^2	0.818	0.886	0.948
χ^2	0.30	1.55	2.15

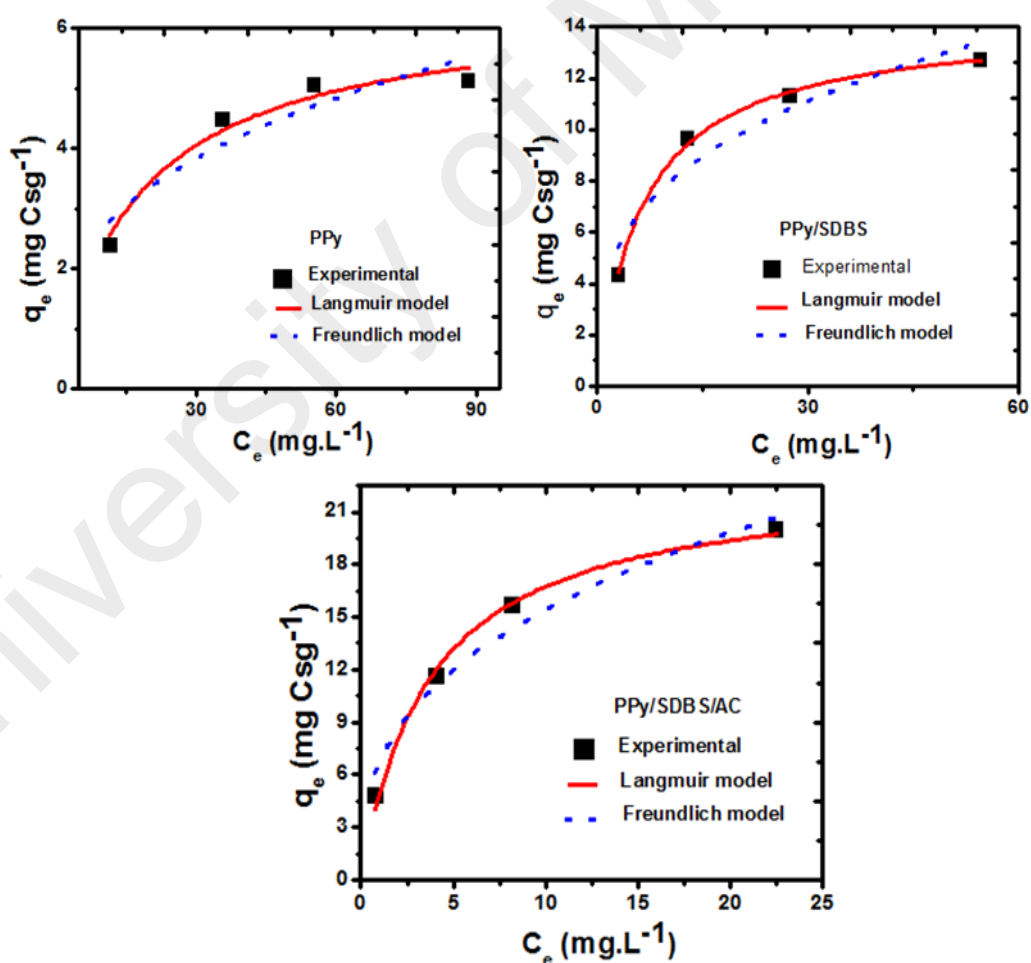


Figure 5.22: Plots of adsorption isotherms for ^{137}Cs . The solid and dotted lines show the fitting of theoretical and experimental data.

5.2.4.3 The plots and results of isotherm models for adsorption of ^{60}Co radionuclide

Figure 5.23 and Table 5.10 present the plots of the isotherm model analysis and obtained parameters for the cobalt radionuclide. Considering the non-linear correlation coefficients (R^2) obtained, it reveals that the Langmuir and Freundlich models can be used to fit the experimental data based on the strong correlation factors. This implies that the polymer materials can be used suitably for the sorption of ^{60}Co radionuclide. When the R^2 values are compared, it is noticed that the Langmuir model has the best fit to the experimental data than the Freundlich model. The R^2 value by the Langmuir model has a trend order of PPy/SDBS > PPy/SDBS/AC > PPy. The maximum sorption capacity that describes the complete monolayer coverage of the sorbent surface is of the order PPy/SDBS/AC > PPy/SDBS > PPy, which is the same order for the b value that measures the energy of adsorption. The separation factor R_L which is used to determine whether the adsorption process is suitable or otherwise, was calculated and the range of values has a trend PPy > PPy/SDBS > PPy/SDBS/AC, confirming that the adsorption of ^{60}Co radionuclide is favourable under the selected equilibrium conditions.

For the R^2 values estimated by the Freundlich model, the trend is PPy/SDBS > PPy > PPy/SDBS/AC. The K_F value, which is also a measure of sorption capacity of the polymer adsorbents has the order of PPy/SDBS/AC > PPy/SDBS > PPy but the n values, which determine the intensity of adsorption have a trend of PPy/SDBS > PPy/SDBS/AC > PPy. The results show that the adsorption of cobalt radionuclide by the adsorbent is favourable under the equilibrium conditions.

Table 5.10: Langmuir and Freundlich parameters for adsorption of ^{60}Co radionuclide.

Parameters	PPy	PPy/SDBS	PPy/SDBS/AC
Langmuir isotherm			
$b \text{ (Lmg}^{-1}\text{)}$	0.05 ± 0.005	0.07 ± 0.003	0.09 ± 0.01
$q_m \text{ (mgg}^{-1}\text{)}$	9.78 ± 0.36	13.5 ± 0.20	18.1 ± 0.61
R_L	$0.18 - 0.53$	$0.12 - 0.40$	$0.10 - 0.35$
R^2	0.994	0.9989	0.995
χ^2	0.02	0.01	0.09
Freundlich isotherm			
$K_F \text{ (mgg}^{-1} \text{ L}^{1/n} \text{ mg}^{-1/n}\text{)}$	1.29 ± 0.42	2.37 ± 0.65	3.30 ± 0.97
n	2.41 ± 0.49	2.61 ± 0.52	2.51 ± 0.56
R^2	0.921	0.923	0.904
χ^2	0.33	0.76	1.92

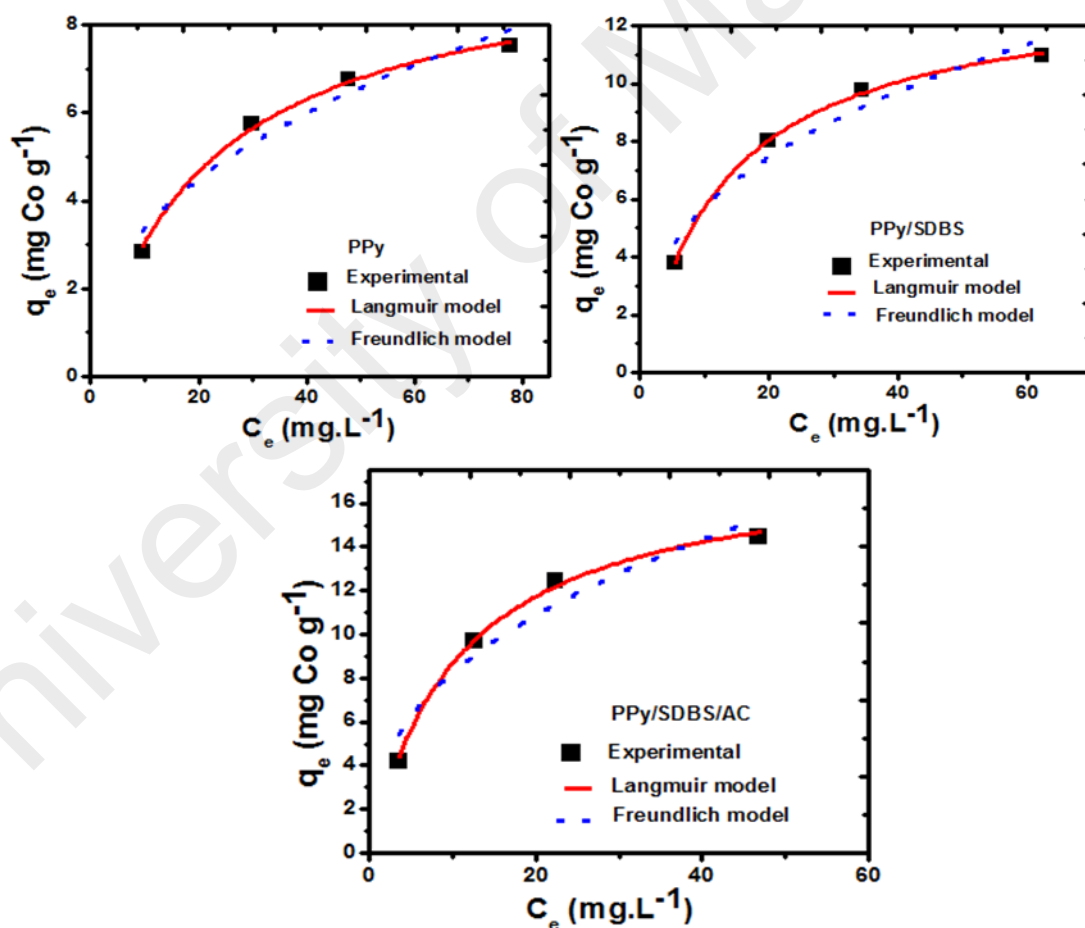


Figure 5.23: Plots of adsorption isotherms for ^{60}Co . The solid and dotted lines show the fitting of theoretical and experimental data.

Summarily, the isotherm models' investigation on the experimental data for the adsorption of ^{109}Cd , ^{137}Cs and ^{60}Co indicates that the experimental data are generally best fit to the Langmuir model than the Freundlich model, based on the correlation factors obtained. However, it must be noted that the difference in the correlation factors is not sufficient to assign mechanism for the adsorption of these radionuclides or other metal ions. It is just to investigate the possibility of exploring the polymer materials for the adsorption of the studied radionuclides. So, a good correlation factor shows that the adsorbent material can be used for the adsorption.

To describe the mechanism of adsorption on solid surfaces adequately, surface complexation models which involve the surface charging processes, the effect of electrostatics arising from surface charges, and formation of complexes between the metal ions species and the ionized surface sites must be considered (Yiacoumi & Tien, 1995). For one thing, adsorption onto organic system such as polymer-based material is a complex one and hence, other variables such as pH, ionic strength, type of electrolyte and electrostatic effect on the extent of adsorption are required to accurately understand the nature of metal-to-organic interactions before adsorption mechanism can be defined. Unfortunately, the isotherm equations obtained from data-fitting cannot predict the effect of these variables (Yiacoumi & Tien, 1995).

In addition, while Freundlich model can provide information on the distribution of active sorption sites and their energies, it cannot predict for saturation of the sorbent surface by the adsorbate, due to its failure to linearize as adsorbate concentration tends to infinite dilution, which is the case for adsorption (Javadian, 2014). Hence, it is considered inappropriate to describe adsorbate/adsorbent interactions by a particular mechanism predominantly on the basis of good data fit to a particular model (Pignatello, 2011). Despite these limitations, we can consider the application of these models for

mathematical representation of the sorption equilibrium for a given metal ion concentration range. Apart from this, these models still provide information on adsorption capacities and differences in uptake of adsorbate between various species (Benguella & Benaissa, 2002). To that effect, the estimated maximum sorption capacity by Langmuir model shows that PPy/SDBS/AC has a high adsorption capacity for each of the radionuclide, followed by PPy/SDBS and the least is pure PPy. The higher capacity of the polymer composites is related to the synergy effect of the individual component materials, resulting into more surface functional groups and higher adsorbate-adsorbent interactions compare to the pure PPy.

5.2.5 Thermodynamic parameters for adsorption

The thermodynamics parameters for the adsorption isotherms at various temperature were obtained in order to gain an insightful knowledge of the adsorption nature by the adsorbent materials. The results are presented in Figure 5.24 – Figure 5.26 and the parameters that describe the thermodynamic nature of the adsorption are in Table 5.11 to Table 5.13.

As estimated, the ΔH° for the adsorption of ^{109}Cd radionuclide are equal to -24.2 , -21.9 and -176 kJ mol^{-1} for PPy, PPy/SDBS and PPy/SDBS/AC adsorbents, respectively. The obtained negative values for ΔH° indicate that the nature of adsorption is exothermic within the temperature range of $20 - 50 \text{ }^\circ\text{C}$. This means that the diffusion of ions would not be favoured by a rise in temperature. The values of ΔS° were found to be -91.1 , -73.6 and $-548 \text{ Jmol}^{-1} \text{ K}$ for ^{109}Cd using PPy, PPy/SDBS and PPy/SDBS/AC, respectively. Again, the obtained negative values indicate a decrease in the randomness at solid/liquid interface during the adsorption of the radionuclides by the adsorbents (Ghassabzadeh et al., 2010). The ΔG° values obtained show that adsorption of ^{109}Cd is thermodynamically feasible and spontaneous within the temperature range of $20 - 50 \text{ }^\circ\text{C}$ using

PPy/SDBS/AC, but it is only feasible at lower temperature using PPy/SDBS. However, the positive and weak values of ΔG^o obtained by using PPy indicates that the adsorption process is feasible but not spontaneous. Generally, the ΔG^o values increased to a positive value by increasing the temperature, which confirms that the adsorption feasibility for ^{109}Cd is lower at higher temperature as explained previously.

For the ^{137}Cs radionuclide, the ΔH^o values are 4.46, 17.7 and 36.5 kJ mol^{-1} for PPy, PPy/SDBS and PPy/SDBS/AC adsorbents, respectively. The positive values obtained indicate the endothermic nature of adsorption in the temperature range of 20 – 50 °C. Because diffusion is endothermic in nature, it is expected that a rise in the temperature would increase the mobility of ions from the aqueous solution to the adsorbents. Similarly, the values of ΔS^o were found to be 2.11, 63.2 and 137 $\text{Jmol}^{-1} \text{K}$ for ^{137}Cs using PPy, PPy/SDBS and PPy/SDBS/AC, respectively. These values indicate increased randomness of the ions at liquid/ solid interface during the process, the higher values obtained for the polymer composites also explained why adsorption is higher for both PPy/SDBS and PPy/SDBS/AC compared with the pure PPy. The ΔG^o values obtained show that adsorption of ^{137}Cs is thermodynamically feasible and naturally spontaneous within the temperature range of 20 – 50 °C using PPy/SDBS and PPy/SDBS/AC composites whereas, adsorption shows to be thermodynamically feasible but not spontaneous by using pure PPy. Generally, the values of ΔG^o decrease to a negative value with temperature, which confirms that the adsorption is feasible at higher temperature for ^{137}Cs radionuclide.

On the other hand, the ΔH^o values for ^{60}Co radionuclide are 4.21, 20.3 and 32.2 kJmol^{-1} for PPy, PPy/SDBS and PPy/SDBS/AC adsorbent, respectively. These values show that the adsorption process is endothermic within the temperature range of 20 – 50 °C. As a result, diffusion of ions through the adsorbents would be favoured as temperature

increases. Similarly, the values of ΔS° were found to be 4.10, 65.8 and 111 Jmol⁻¹ K for ⁶⁰Co using PPy, PPy/SDBS and PPy/SDBS/AC, respectively. These values again indicate increased randomness of the ions at solid/liquid interface during the process. The estimated values of ΔG° indicate a decrease to a negative value, which shows that the adsorption is thermodynamically feasible and spontaneous within the temperature range of 20 – 50 °C.

Table 5.11: Estimated values of thermodynamic parameters for adsorption of radionuclides by PPy at different temperature.

Radionuclide	Temp. (K)	K _d (Lg ⁻¹)	ΔG° (kJmol ⁻¹)	ΔH° (kJmol ⁻¹)	ΔS° (Jmol ⁻¹ K)
¹⁰⁹ Cd	293	0.331	2.54	-24.2	-91.1
	303	0.296	3.45		
	313	0.168	4.36		
	323	0.143	5.27		
¹³⁷ Cs	293	0.206	3.84	4.46	2.11
	303	0.221	3.82		
	313	0.232	3.80		
	323	0.244	3.77		
⁶⁰ Co	293	0.295	3.01	4.21	4.10
	303	0.305	2.97		
	313	0.320	2.92		
	323	0.347	2.88		

Table 5.12: Estimated values of thermodynamic parameters for adsorption of radionuclides by PPy/SDBS at different temperature.

Radionuclide	Temp. (K)	K _d (Lg ⁻¹)	ΔG° (kJmol ⁻¹)	ΔH° (kJmol ⁻¹)	ΔS° (Jmol ⁻¹ K)
¹⁰⁹ Cd	293	1.16	-0.36	-21.9	-73.6
	303	0.87	0.38		
	313	0.65	1.11		
	323	0.50	1.85		
¹³⁷ Cs	293	1.44	-0.81	17.7	63.2
	303	1.71	-1.45		
	313	2.18	-2.08		
	323	2.82	-2.71		
⁶⁰ Co	293	0.70	1.02	20.3	65.8
	303	0.81	0.36		
	313	1.06	-0.29		
	323	1.52	-0.95		

Table 5.13: Estimated values of thermodynamic parameters for adsorption of radionuclides by PPy/SDBS/AC at different temperature.

Radionuclide	Temp. (K)	K _d (L/g)	ΔG° (kJ/mol)	ΔH° (kJ/mol)	ΔS° (J/mol K)
¹⁰⁹ Cd	293	1000	-15.5	-176	-548
	303	24.8	-10.0		
	313	4.40	-4.54		
	323	1.08	0.94		
¹³⁷ Cs	293	4.78	-3.76	36.5	137
	303	7.47	-5.13		
	313	12.3	-6.51		
	323	19.0	-7.88		
⁶⁰ Co	293	1.20	-0.39	32.2	111
	303	1.25	-1.50		
	313	1.34	-2.61		
	323	1.39	-3.73		

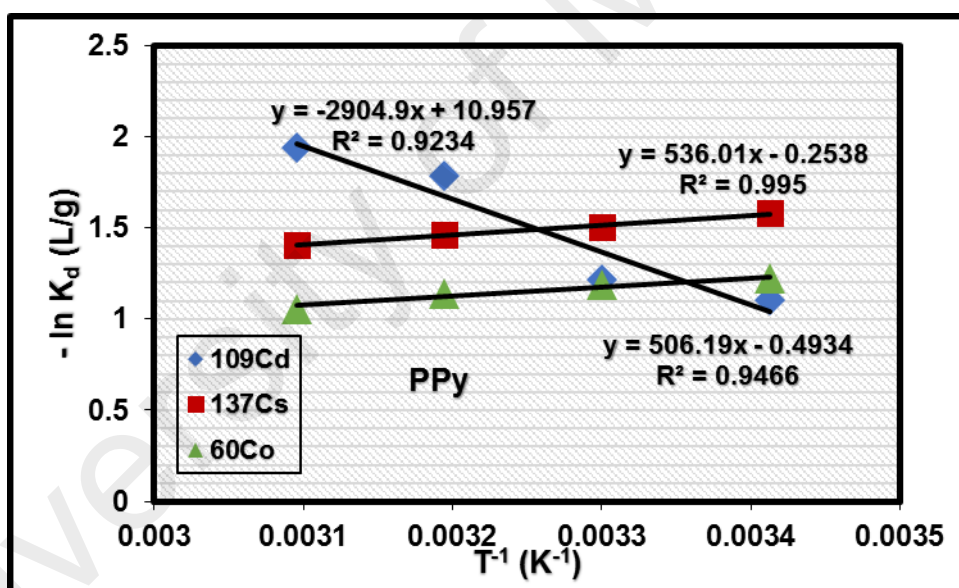


Figure 5.24: Plot of $\ln K_d$ against T^{-1} for adsorption of radionuclides by PPy.

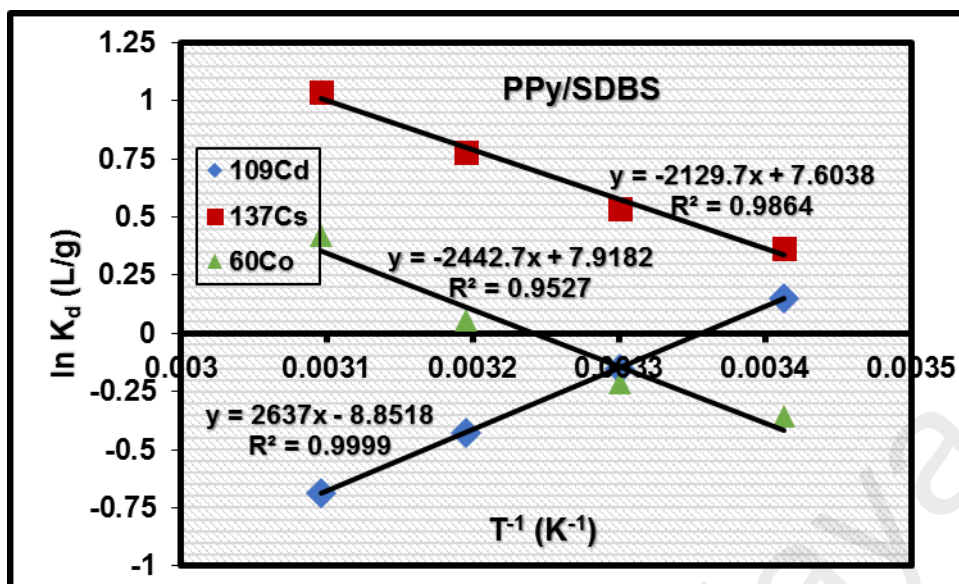


Figure 5.25: Plot of $\ln K_d$ against T^{-1} for adsorption of radionuclides by PPy/SDBS.

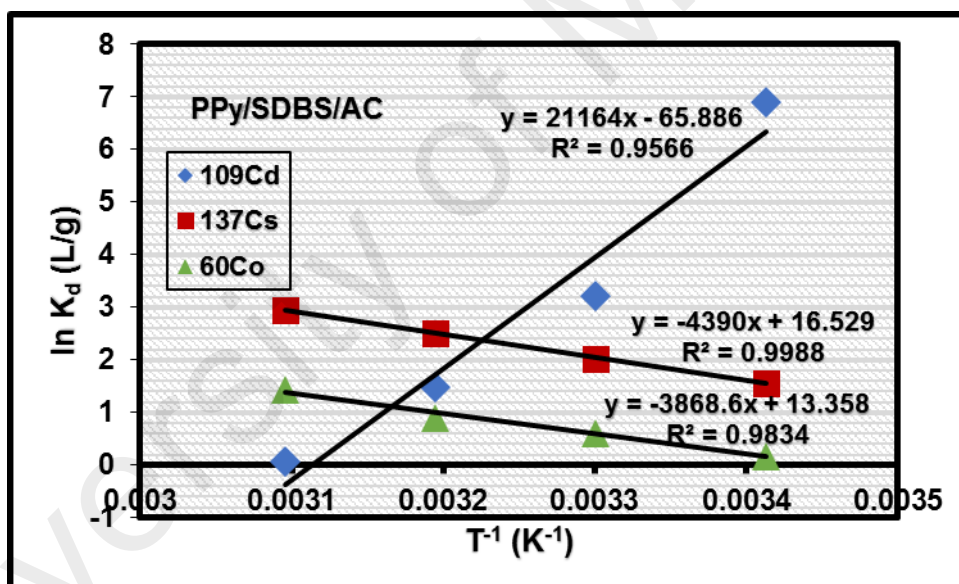


Figure 5.26: Plot of $\ln K_d$ against T^{-1} for adsorption of radionuclides by PPy/SDBS/AC.

In summary, the thermodynamic parameters reveal that the ^{109}Cd adsorption onto the polymer adsorbents is a physical process controlled totally by some weak intermolecular forces of attraction. In the case of ^{137}Cs and ^{60}Co adsorption onto the polymer adsorbents, the adsorption process is also somewhat controlled by physical process but enhanced partly by a chemical effect (possibly emanated from the extra sorption sites introduced

into the polymer surface by the component materials) (Nassar, 2012). This is also supported by the fact that $\Delta H^{\circ} < 40 \text{ kJmol}^{-1}$ in all cases, indicating a physical adsorption process (Nassar, 2012). The plots of ΔG° vs temperature can be seen in Appendix F. The results obtained in this study are similar to those reported in the literature by different authors ((Ding et al., 2013; Seid et al., 2014).

5.2.6 Results of desorption and reusability of spent adsorbents

5.2.6.1 Desorption

The desorption behaviour of the spent polymer adsorbents was studied using 25 ml each of deionized water, 0.1 M NaOH and 0.1 M HCl. It was generally revealed that deionized water and NaOH have low % desorption for the radionuclides from the spent polymer adsorbents compared to % desorption by HCl (Table 5.14). This is as a result of the fact that alkaline condition favours the adsorption of all the radionuclides as already discussed under the adsorption studies. Consequently, further investigation was conducted by increasing the concentration of HCl from 0.1 to 2 M and the results of desorption was found to increase for each rise in concentration. Also, using 1 M HCl, desorption was studied for different temperature from 20 to 50 °C.

The results of the effect of concentration of HCl and temperature are presented in Figure 5.27 to Figure 5.29. For ^{109}Cd , maximum % desorption was 82, 87.4 and 77.6 % from PPy, PPy/SDBS and PPy/SDBS/AC, respectively. For ^{137}Cs , maximum % desorption of 73, 88.9 and 72 % from PPy, PPy/SDBS and PPy/SDBS/AC, respectively. Whereas, 70.8, 85.6 and 76.5 % of ^{60}Co were desorbed from PPy, PPy/SDBS and PPy/SDBS/AC, respectively. The incomplete desorption of the radionuclides could be attributed to the electrostatic interaction as well as the complexation reaction existing between the radionuclides and surface functional groups of the adsorbents.

Table 5.14: Desorption results of ^{109}Cd , ^{137}Cs and ^{60}Co radionuclides from spent polypyrrole-based adsorbents.

Eluent	Concentration (M)	PPy	PPy/SDBS	PPy/SDBS/AC
% Desorption of ^{109}Cd				
Deionized water	–	17.9	8.67	18.8
NaOH	0.1	23	11.6	53.6
HCl	0.1	60.4	69	64
% Desorption of ^{137}Cs				
Deionized water	–	5	0	0
NaOH	0.1	28	22.6	42.9
HCl	0.1	48	72	38.9
% Desorption of ^{60}Co				
Deionized water	–	40	45.5	26.7
NaOH	0.1	35	40	40
HCl	0.1	46	72	56

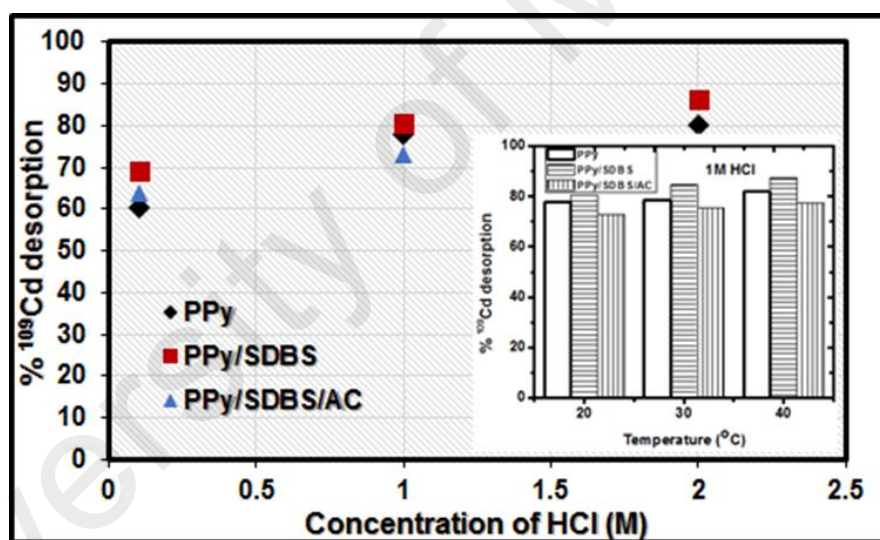


Figure 5.27: Effect of HCl concentration and temperature on the desorption of ^{109}Cd radionuclide.

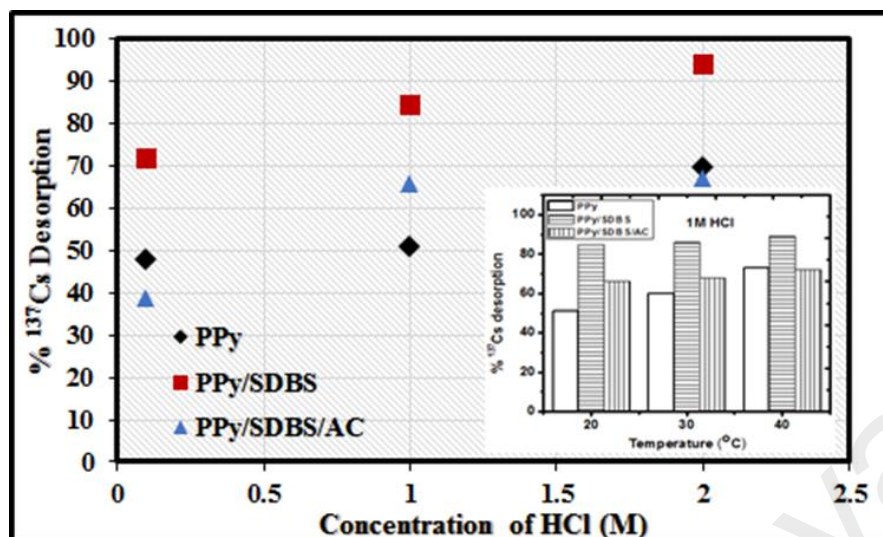


Figure 5.28: Effect of HCl concentration and temperature on the desorption of ¹³⁷Cs radionuclide.

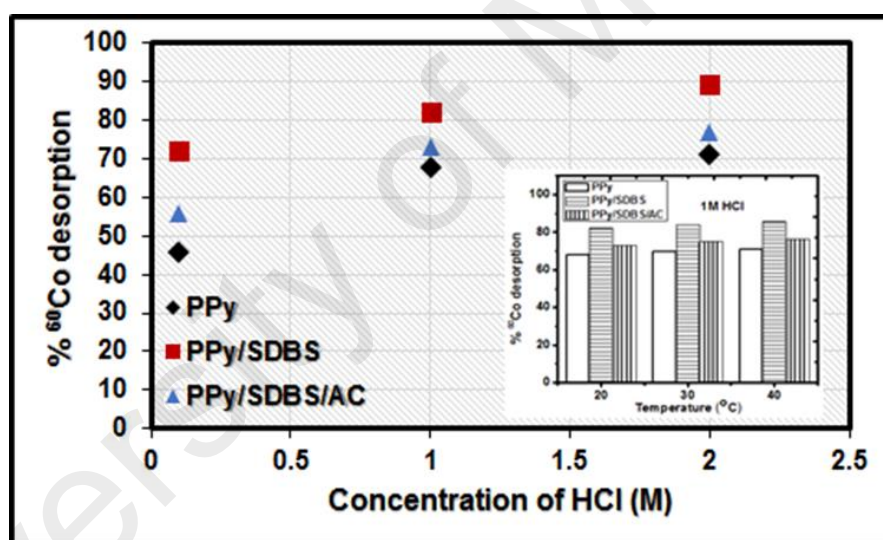


Figure 5.29: Effect of HCl concentration and temperature on the desorption of ⁶⁰Co radionuclide.

5.2.6.2 Reusability of recycled polypyrrole-based adsorbents

After desorption, the recycled adsorbents were washed with deionized water and then dried before reused for wastewater treatment. Following previous adsorption steps, each adsorbent was contacted for 240 min with 50 ml of 20 mg/L of each metal ions containing the respective radionuclide. After the contact period, the supernatant was separated and analyzed as before. The procedure was followed for five cycles.

The results of five cycles are represented in Figure 5.30 – Figure 5.32. As shown, % adsorption decreased progressively with the number of cycle for all the radionuclides. After the third cycle, % adsorption of the radionuclides decreased significantly from 55.4 to 33 % for ^{109}Cd , 42 to 29 % for ^{137}Cs , and from 52 to 29 % for ^{60}Co when the recycled PPy was used. For the recycled PPy/SDBS, the % adsorption decreased from 82 to 38 % for ^{109}Cd , 84 to 41 % for ^{137}Cs , and from 73 to 41 % for ^{60}Co . In the case of recycled PPy/SDBS/AC composite, the decrease in % adsorption after third cycle was from 100 to 56 % for ^{109}Cd , 96 to 56 % for ^{137}Cs , and from 82 to 52 % for ^{60}Co . In all, % adsorption was insignificant after the fourth cycle, especially for ^{137}Cs and ^{60}Co . Generally, the composite materials show to be promising for the real wastewater application.

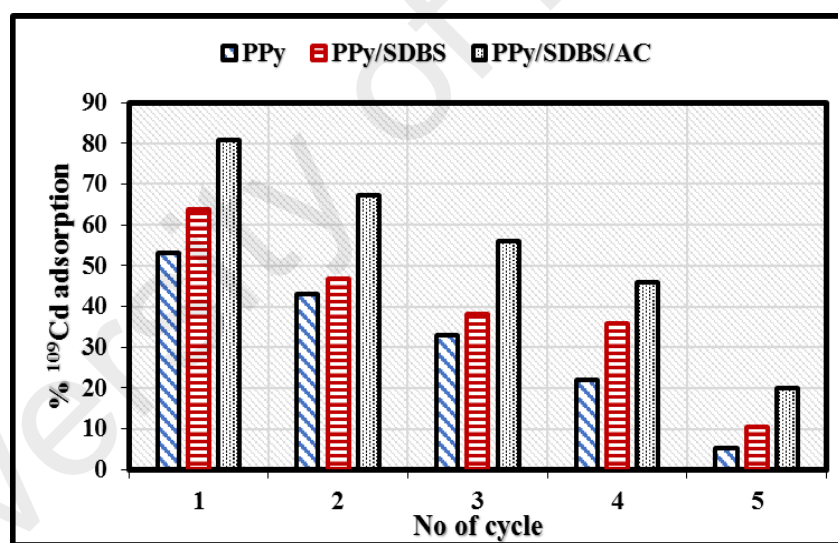


Figure 5.30: Effect of recyclability and reusability of the adsorbents on ^{109}Cd adsorption.

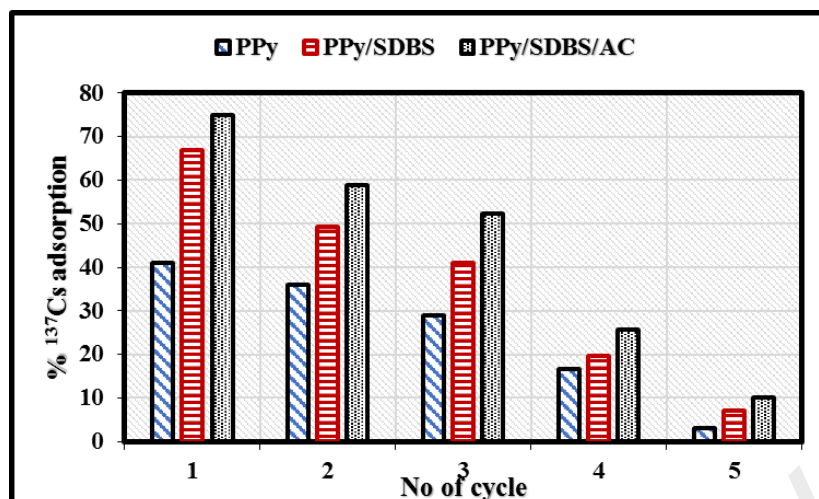


Figure 5.31: Effect of recyclability and reusability of the adsorbents on ¹³⁷Cs adsorption.

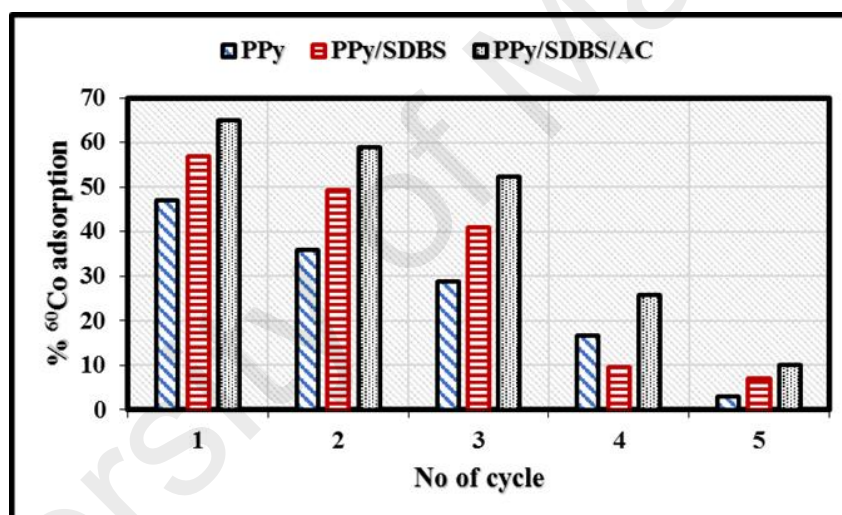


Figure 5.32: Effect of recyclability and reusability of the adsorbents on ⁶⁰Co adsorption.

5.2.7 Radiation hardness of polypyrrole-based materials

Since the as-prepared polymer materials are intended for the removal of radioactive materials from industrial/ nuclear waste solutions, it is important to determine the suitability of these polymer materials for adsorption after a prolonged exposure to radiation. Some authors have reported that gamma irradiation of polymers results into a change of molecular weight, due to radical production and/ or induce crosslinking at

higher doses (Shahabi et al., 2014). This may not only affect the adsorption affinity but also the long-term stability of radionuclide-loaded polymer adsorbent.

As a result, some of the polymer materials which were exposed to 100 and 200 kGy doses of gamma-source (^{60}Co) were evaluated for irradiation effect on the adsorption capacity by repeating the adsorption experiments with the irradiated samples. The results of adsorption are presented in Figure 5.33 - Figure 5.35. Within the dose of 200 kGy, irradiation shows practically no significant effect on the adsorption capacity of the polymer materials, except for irradiated PPy/SDBS/AC samples that showed some slight increase in adsorption capacity. The results obtained are similar to reported work by other authors on the effect of radiation exposure of polymer on sorption capacity (Gupta & Shankar, 2004). According to the previous authors, the slight decrease in adsorption capacity of irradiated polymer was due to the decrease in the surface area of the adsorbent and interference or sintering of the active sites on the surface of the polymer materials, due to high radiation exposure and, the new structural formation in the irradiated PPy/SDBS/AC samples (see detail in Chapter 4) could be responsible for the slight increase in adsorption capacity after irradiation. The general observation here partly explains why polymers are suitable for conditioning radioactive spent organic resin for safe disposal (Valsala et al., 2009).

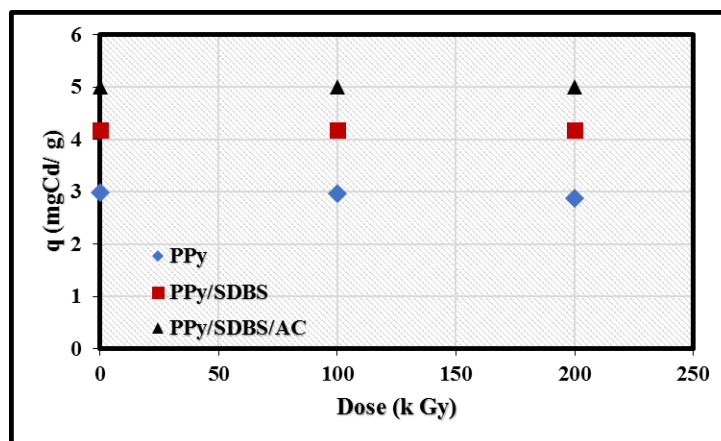


Figure 5.33: Effect of gamma-irradiation of polypyrrole-based adsorbents on ^{109}Cd adsorption.

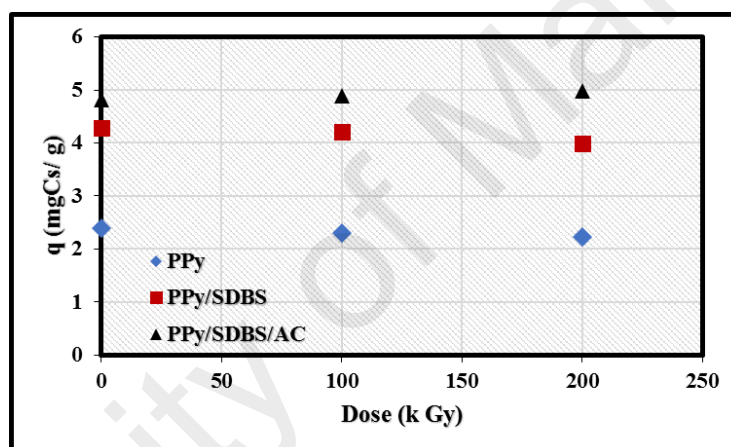


Figure 5.34: Effect of gamma-irradiation of polypyrrole-based adsorbents on ^{137}Cs adsorption.

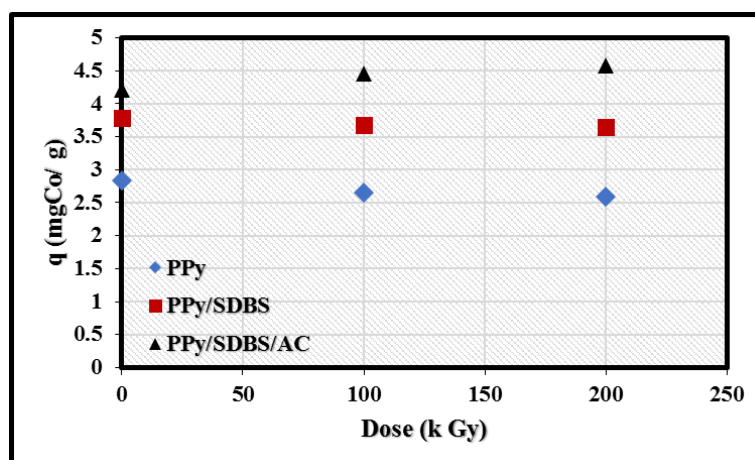


Figure 5.35: Effect of gamma-irradiation of polypyrrole-based adsorbents on ^{60}Co adsorption.

5.3 Bi-solute competitive adsorption of radionuclides by PPy/SDBS and PPy/SDBS/AC composites

Interactions between different adsorbates may mutually enhance or mutually inhibit sorption capacity (Ho & McKay, 1999). Basically, three possible types of behaviour may be exhibited when different adsorbates are mixed together in a reaction vessel. The three possible behaviours are usually referred to as antagonism, synergism and non-interaction (Srivastava et al., 2006). As a result, since the radionuclides under study are mostly present in single waste solution, emanating particularly from nuclear reactor or reprocessing of fuels, bi-solute adsorption of the radionuclides was investigated by mixing the radionuclides in the same concentration ratio. The competitive Langmuir model (CLM) was used to analyze multi-solute adsorption behaviours of the radionuclides (Park et al., 2010). In Chapter 3, the expression of this model and the assumptions underlining its application have been discussed in details.

Figure 5.36 and Figure 5.37 show the plots of bi-solute competitive adsorption of the studied radionuclides onto PPy/SDBS and PPy/SDBS/AC composites, respectively. The estimated parameters by the Langmuir model which explain the bi-solute adsorption are presented in Table 5.15. The effect of simultaneous existence of competing radionuclide on adsorption was evaluated by the ratio of adsorption capacity of the radionuclide in single-solute (q_i) and bi-solute (q^*_i) competitive adsorptions (i represents the radionuclide). If the ratio of adsorption capacity in the bi-solute system to that of single-solute system is greater than 1, it means that adsorption is accelerated in the bi-solute system. When the ratio is equal to 1, it means there is no influence of one radionuclide adsorption over the other. The ratio of less than 1 implies the presence of one radionuclide hinders or suppresses the adsorption of the other (Park et al., 2010).

Table 5.15: Langmuir model parameters for bi-solute competitive adsorption of ^{109}Cd , ^{137}Cs and ^{60}Co radionuclides.

Radionuclide	Solute	q^* (mgg^{-1})	b^* (Lmg^{-1})	R^2	χ^2
		PPy/SDBS adsorbent			
^{109}Cd	$^{109}\text{Cd}/^{137}\text{Cs}$	13.25 ± 0.31	0.11 ± 0.01	0.996	0.0044
	$^{109}\text{Cd}/^{60}\text{Co}$	15.80 ± 0.75	0.14 ± 0.03	0.985	0.25
^{137}Cs	$^{137}\text{Cs}/^{109}\text{Cd}$	13.81 ± 0.26	0.05 ± 0.003	0.999	0.011
	$^{137}\text{Cs}/^{60}\text{Co}$	28.9 ± 2.02	0.021 ± 0.003	0.998	0.054
^{60}Co	$^{60}\text{Co}/^{109}\text{Cd}$	8.49 ± 0.73	0.076 ± 0.02	0.935	0.22
	$^{60}\text{Co}/^{137}\text{Cs}$	8.67 ± 0.71	0.073 ± 0.02	0.945	0.20
		PPy/SDBS/AC adsorbent			
^{109}Cd	$^{109}\text{Cd}/^{137}\text{Cs}$	26.2 ± 1.34	0.097 ± 0.012	0.994	0.22
	$^{109}\text{Cd}/^{60}\text{Co}$	16.17 ± 0.54	1.43 ± 0.28	0.982	0.46
^{137}Cs	$^{137}\text{Cs}/^{109}\text{Cd}$	20.9 ± 0.83	0.11 ± 0.01	0.9977	0.064
	$^{137}\text{Cs}/^{60}\text{Co}$	33.7 ± 0.12	0.039 ± 0.0003	0.9999	0.0003
^{60}Co	$^{60}\text{Co}/^{109}\text{Cd}$	15.9 ± 0.63	0.077 ± 0.01	0.9936	0.093
	$^{60}\text{Co}/^{137}\text{Cs}$	14.6 ± 1.06	0.083 ± 0.02	0.9745	0.32

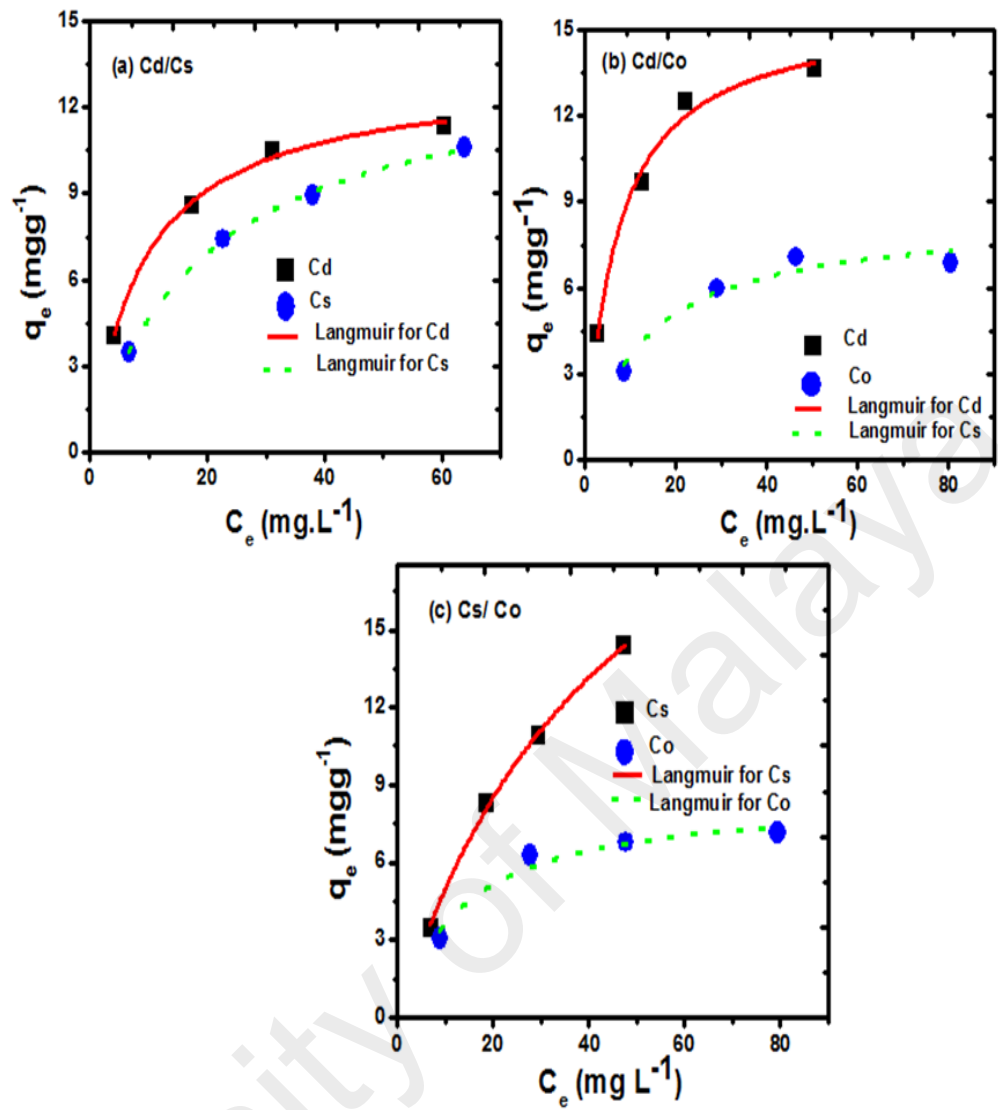


Figure 5.36: Plots of bi-solute competitive adsorption of (a) $^{109}\text{Cd}/^{137}\text{Cs}$, (b) $^{109}\text{Cd}/^{60}\text{Co}$ and (c) $^{137}\text{Cs}/^{60}\text{Co}$ by PPy/SDBS.

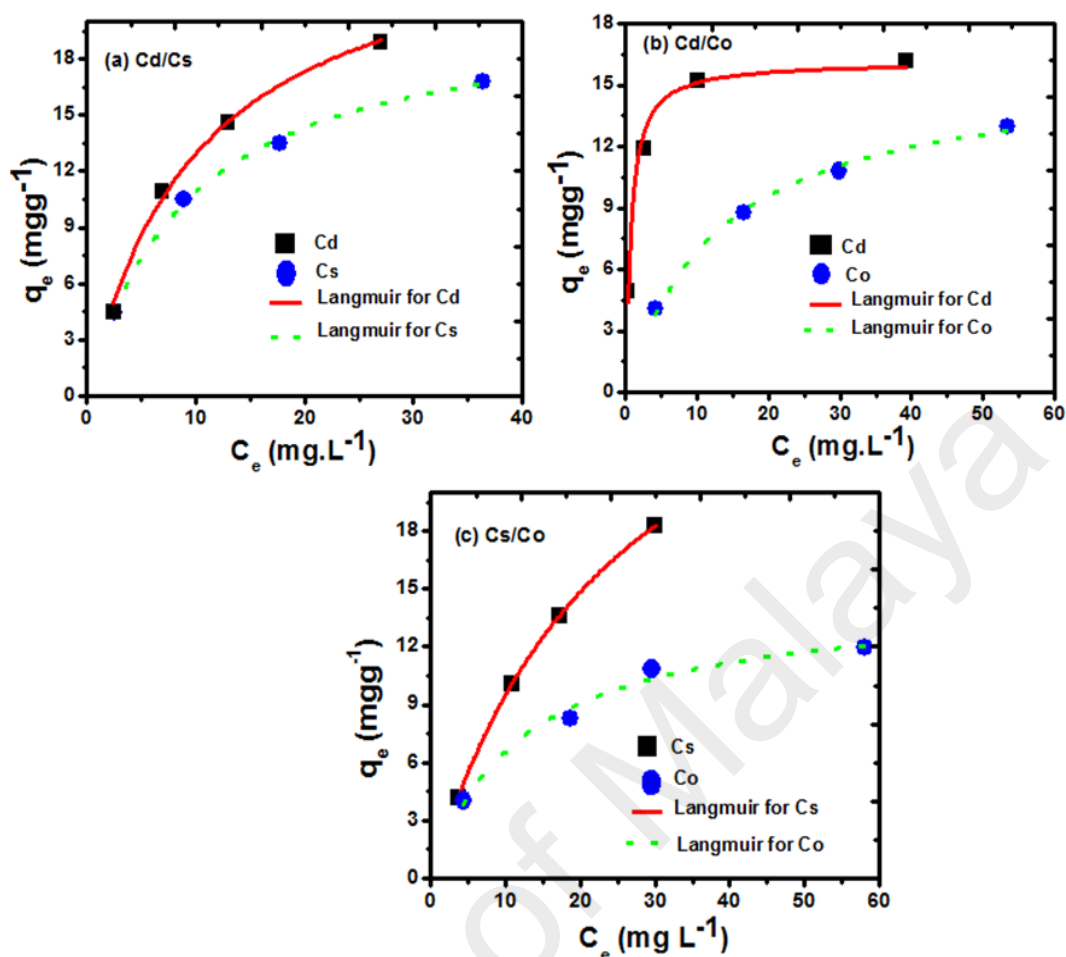


Figure 5.37: Plots of bi-solute competitive adsorption of (a) $^{109}\text{Cd}/^{137}\text{Cs}$, (b) $^{109}\text{Cd}/^{60}\text{Co}$ and (c) $^{137}\text{Cs}/^{60}\text{Co}$ by PPy/SDBS/AC.

Table 5.16 shows the comparison of single-solute and bi-solute adsorption of the radionuclides. As shown, when ^{137}Cs competed with ^{109}Cd radionuclide in the binary systems, the ratios of both $q^*_{^{137}\text{Cs}}/q_{^{137}\text{Cs}}$ and $q^*_{^{109}\text{Cd}}/q_{^{109}\text{Cd}}$ were less than 1 (when both PPy/SDBS and PPy/SDBS/AC composites were used). Similarly, when ^{109}Cd competed with ^{60}Co , the ratio of $q^*_{^{109}\text{Cd}}/q_{^{109}\text{Cd}}$ and $q^*_{^{60}\text{Co}}/q_{^{60}\text{Co}}$ is less than unity. In contrast, when ^{137}Cs competed with ^{60}Co radionuclide, the ratio of $q^*_{^{137}\text{Cs}}/q_{^{137}\text{Cs}}$ was greater than 1 but the ratio of $q^*_{^{60}\text{Co}}/q_{^{60}\text{Co}}$ was less than one. This indicates that adsorption of ^{137}Cs radionuclide was suppressed in the presence of ^{109}Cd but it was promoted in the presence of ^{60}Co . In addition, adsorption of either ^{109}Cd or ^{60}Co was suppressed when both were present in the binary system.

Table 5.16: Comparison of q and b values for single-solute and bi-solute competitive adsorption.

Binary system (1/2) ^x	(q ₁ /q ₂) ^y	(q* ₁ /q* ₂) ^z	(q* ₁ /q ₁)	(q* ₂ /q ₂)
PPy/SDBS adsorbent				
¹⁰⁹ Cd/ ¹³⁷ Cs	1.12	0.96	0.83	0.97
¹⁰⁹ Cd/ ⁶⁰ Co	1.19	1.86	0.99	0.63
¹³⁷ Cs/ ⁶⁰ Co	0.99	3.34	1.24	0.37
Binary system (1/2) ^x	(b ₁ /b ₂) ^y	(b* ₁ /b* ₂) ^z	(b* ₁ /b ₁)	(b* ₂ /b ₂)
¹⁰⁹ Cd/ ¹³⁷ Cs	0.61	2.20	1.19	0.33
¹⁰⁹ Cd/ ⁶⁰ Co	1.25	1.87	1.54	1.03
¹³⁷ Cs/ ⁶⁰ Co	2.05	0.29	0.25	1.82
PPy/SDBS/AC adsorbent				
¹⁰⁹ Cd/ ¹³⁷ Cs	1.53	1.25	0.74	0.91
¹⁰⁹ Cd/ ⁶⁰ Co	1.95	1.02	0.46	0.88
¹³⁷ Cs/ ⁶⁰ Co	1.00	2.32	1.08	0.47
Binary system (1/2) ^x	(b ₁ /b ₂) ^y	(b* ₁ /b* ₂) ^z	(b* ₁ /b ₁)	(b* ₂ /b ₂)
¹⁰⁹ Cd/ ¹³⁷ Cs	1.13	0.89	0.32	0.41
¹⁰⁹ Cd/ ⁶⁰ Co	3.27	18.6	4.76	0.84
¹³⁷ Cs/ ⁶⁰ Co	2.71	0.48	0.32	1.79

^xThe metal ions in binary system in the order of (1) and (2).

^yq and b represent Langmuir model parameters for single-solute adsorption.

^zq* and b* represent Langmuir model parameters for bi-solute adsorption.

In the binary systems, several factors ranging from the adsorbents to adsorbates or solution chemistry may determine the adsorption behaviour of adsorbate by the adsorbent. The characteristics of the adsorbent binding sites (such as surface properties, functional groups, structure, etc.), the properties of the adsorbates (such as concentration, ionic size, ionic weight, molecular structure, ionic nature or standard reduction potential, etc.) and solution chemistry (such as pH, ionic strength, etc.) have been described as major factors responsible for different behaviours of adsorbate-adsorbent interactions in the binary systems (Aksu & Akpınar, 2001). In the current study, any or combination of the aforementioned factors could be responsible for the adsorption behaviours of the radionuclides, particularly that of ¹³⁷Cs, but further investigations may be required to ascertain the results.

Meanwhile, the maximum adsorption capacity values in the bi-solute competitive adsorption (q^*) were somewhat lower (in some cases) than in the single-solute adsorption system (q). This has been related to the fact that competition for adsorption sites can suppress the retention of adsorbate ions on more specific sorption positions and the metal ions are adsorbed more weakly (Park et al., 2010). The binding affinity constant (b) of the polymer composite adsorbents for the radionuclides shows a relative trend order of b (^{137}Cs) $>$ b (^{109}Cd) $>$ b (^{60}Co) for PPy/SDBS and b (^{109}Cd) $>$ b (^{137}Cs) $>$ b (^{60}Co) for PPy/SDBS/AC in the single-solute adsorption and b^* (^{109}Cd) $>$ b^* (^{60}Co) \gg b^* (^{137}Cs) in the bi-solute adsorption using both adsorbents. The values of b^* in the bi-solute system are higher than the values of b in the single-solute system. The higher b^* values have been related to specifically adsorbed metals at high-energy surfaces with low dissociation constants and lower values related to the adsorption at low-energy surfaces with high dissociation constants (Adhikari & Singh, 2003; Serrano et al., 2005).

The relationship between the measured and the CLM predicted equilibrium sorption capacities for the competitive adsorptions of $^{109}\text{Cd}/^{137}\text{Cs}$, $^{109}\text{Cd}/^{60}\text{Co}$ and $^{137}\text{Cs}/^{60}\text{Co}$ radionuclides is shown in Figure 3.38. To compare the predictions with measured data, R^2 and χ^2 were used and the results are listed in Table 5.17. The results show that the predictions were successful in most of the adsorption with $R^2 \geq 0.79$ in both cases (with PPy/SDBS and PPy/SDBS/AC) except for ^{60}Co in $^{109}\text{Cd}/^{60}\text{Co}$ ($R^2 = -0.5$) using PPy/SDBS/AC.

Table 5.17: Statistical parameters for bi-solute competitive adsorption predictions for competitive Langmuir model (CLM) proposed by Butler-Ockrent.

Bi-solute system	Compound	R ²	χ ²
PPy/SDBS adsorbent			
¹⁰⁹ Cd/ ¹³⁷ Cs	¹⁰⁹ Cd	0.996	0.016
	¹³⁷ Cs	0.961	0.021
¹⁰⁹ Cd/ ⁶⁰ Co	¹⁰⁹ Cd	0.981	0.085
	⁶⁰ Co	0.839	0.047
¹³⁷ Cs/ ⁶⁰ Co	¹³⁷ Cs	0.999	0.0004
	⁶⁰ Co	0.988	0.026
PPy/SDBS/AC adsorbent			
¹⁰⁹ Cd/ ¹³⁷ Cs	¹⁰⁹ Cd	0.987	0.061
	¹³⁷ Cs	0.997	0.032
¹⁰⁹ Cd/ ⁶⁰ Co	¹⁰⁹ Cd	0.791	5.16
	⁶⁰ Co	-0.5	1.67
¹³⁷ Cs/ ⁶⁰ Co	¹³⁷ Cs	0.971	0.038
	⁶⁰ Co	0.983	0.14

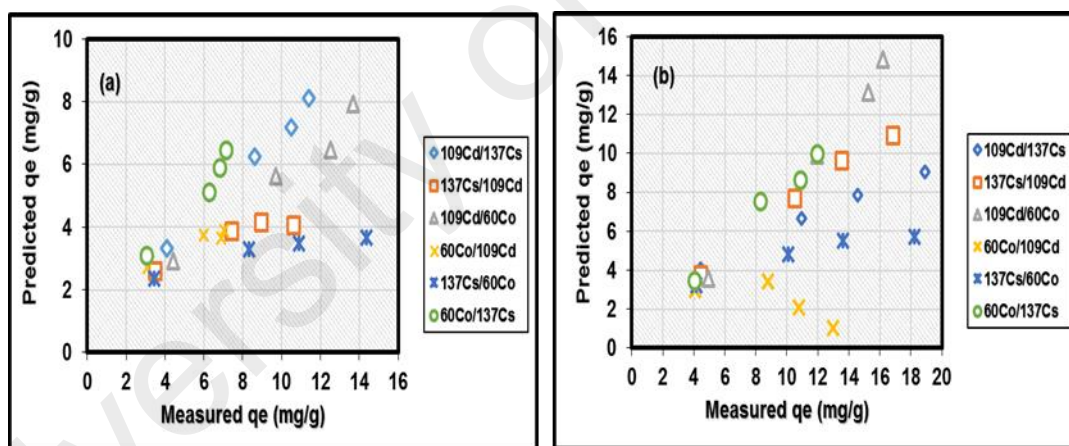


Figure 5.38: The relationship between measured and predicted equilibrium sorption capacities from competitive Langmuir models (a) PPy/SDBS and (b) PPy/SDBS/AC.

5.4 Evidence of adsorption of radionuclides by polypyrrole-based adsorbents

After adsorption of ¹⁰⁹Cd, ¹³⁷Cs and ⁶⁰Co radionuclides by the polymer adsorbents, the spent-adsorbents were analyzed to identify any possible change to the adsorbent materials using FTIR and XRD analysis.

5.4.1 FTIR analysis of polypyrrole-based adsorbents after adsorption

Figure 5.39 presents the FTIR spectra of PPy before and after adsorption of ^{109}Cd , ^{137}Cs and ^{60}Co radionuclides. By comparison, some notable changes were observed in the FTIR spectra after adsorption. The characteristic bands observed at 1533, 1280, 1145, 1023, 878 and 770 cm^{-1} in the PPy before adsorption have been shifted to higher frequencies in the case of PPy loaded with Cs and Co, while some backward shifts were noticed in PPy loaded with Cd. For PPy-loaded Cd, the shifted bands were located at 1520, 1273, 1122, 1000, 852 and 760 cm^{-1} . For PPy-loaded Cs, the shifted bands are observed at 1553, 1306, 1171, 1046, 908 and 789 cm^{-1} , while in the PPy-loaded Co, the shifted bands are found at 1546, 1296, 1165, 1033 and 891 cm^{-1} . Furthermore, appearance of new bands is observed in the PPy-loaded Cd at 1622 and 2040 cm^{-1} due to metal ion interaction and at 3000–3500 cm^{-1} due to stretching vibration of the O-H bond of water coordination. The shifts of all the bands in PPy spectrum confirmed the adsorption of the radionuclides and in particular, the shift in the band at 1023 cm^{-1} revealed the deprotonation of N-H groups, followed by the coordination of nitrogen to the metal ions.

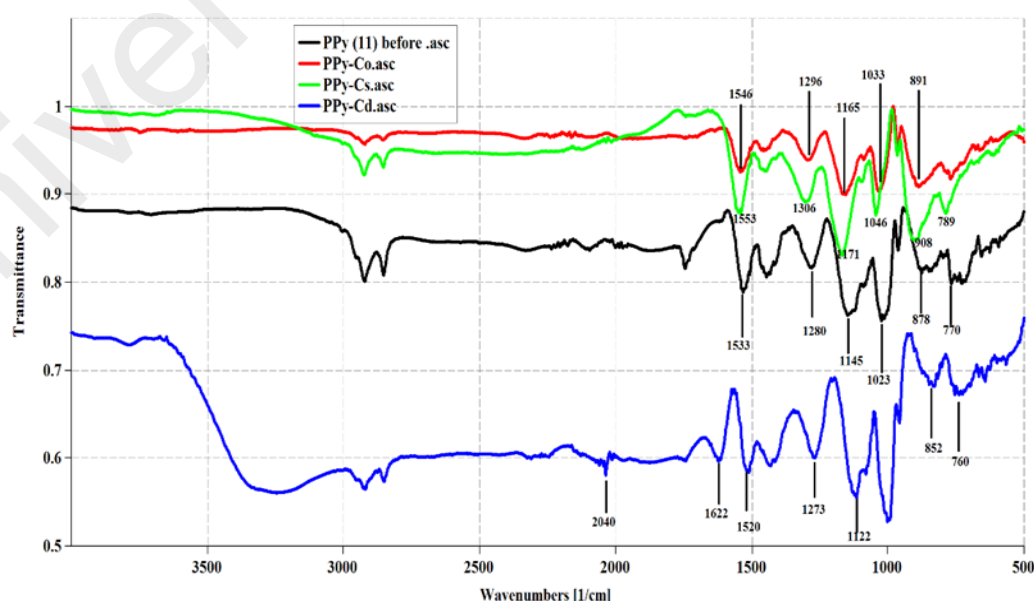


Figure 5.39: FTIR of PPy after adsorption.

Figure 5.40 represents the FTIR spectra of PPy/SDBS before and after adsorption of ^{109}Cd , ^{137}Cs and ^{60}Co radionuclides. Before adsorption, the PPy/SDBS spectrum shows some notable bands at 1527, 1444, 1287, 1125, 1000, 866 and 765 cm^{-1} . These bands have been well shifted to higher frequencies in case of PPy/SDBS-loaded Cs and PPy/SDBS-loaded Co, while PPy/SDBS-loaded Cd mostly shifted to lower frequencies after adsorption. For PPy/SDBS-loaded Cd, the shifted bands are located at 1525, 1438, 1271, 1116, 1004 cm^{-1} and new bands have also appeared at 1620 cm^{-1} and between 3000 and 3500 cm^{-1} . The blue shift in the bands and the appearance of new bands indicated the adsorption of cadmium ions by the material, particularly by coordination of nitrogen to the metal ions. In the case of PPy/SDBS-loaded Cs, the bands have been shifted to 1539, 1456, 1294, 1168, 1044, 897 cm^{-1} and a new band appeared at 2331 cm^{-1} . All the shifts and the new band confirmed the adsorption of Cs by the polymer material. For the PPy/SDBS-loaded Co, the shifted bands are found at 1542, 1447, 1289, 1171, 1027, 887 and 768 cm^{-1} , and new bands have also been formed at 1617 cm^{-1} and between 3000 and 3500 cm^{-1} . The red shift in the band and the appearance of new ones are indication for the metallic bond formation by the adsorbent.

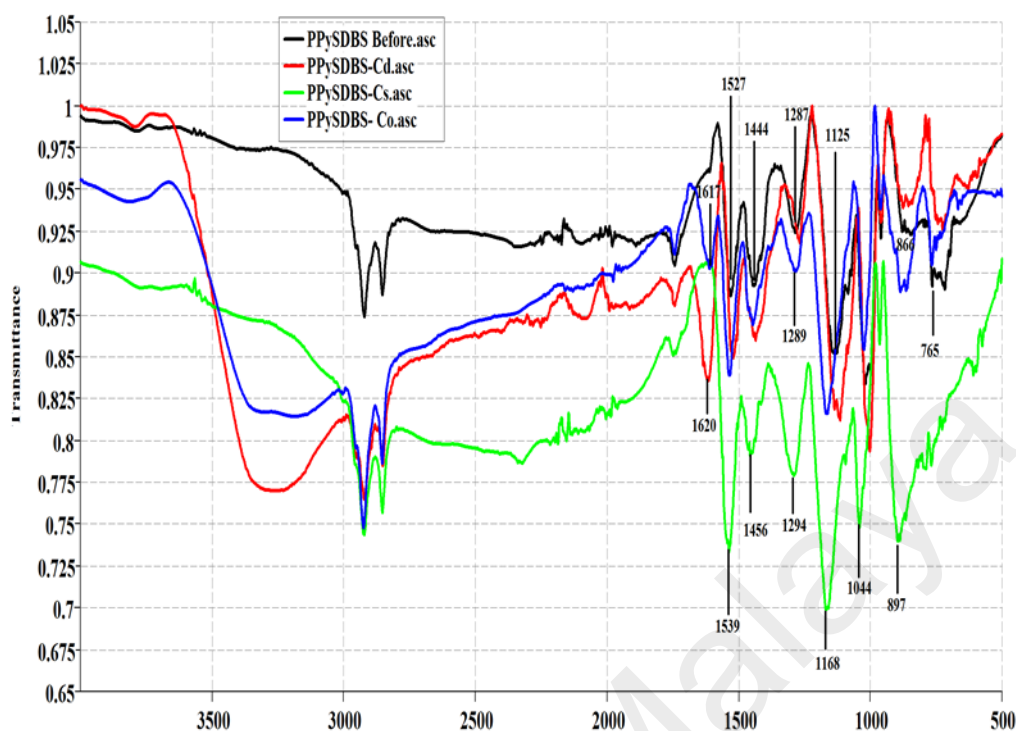


Figure 5.40: FTIR analysis of PPy/SDBS after adsorption.

Figure 5.41 represents the results of FTIR analysis of PPy/SDBS/AC composite before and after adsorption of ^{109}Cd , ^{137}Cs and ^{60}Co radionuclides. Before adsorption, clearly observable bands are found at 3750, 2924, 2855, 1747, 1556, 1444, 719 and 606 cm^{-1} . However, after adsorption of the radionuclides, the loaded PPy/SDBS/AC composite shows some changes in the spectra positions. For the adsorption of ^{109}Cd , the bands have been shifted to 2929, 2857, 1749, 1577, 1450, 727 and 624 cm^{-1} while a new band is observed at around 2183 and 2068 cm^{-1} . In the PPy/SDBS/AC-loaded Cs, the shifted bands are found at 2926, 2957, 1758, 1571, 1459 and 742 cm^{-1} , while some new bands have been formed at around 2000 – 2500 cm^{-1} . In the case of PPy/SDBS/AC-loaded Co, the original bands have been shifted to 2935, 2857, 1758, 1574, 1456 and 739 cm^{-1} and the appearance of new bands between 2000 and 2500 cm^{-1} were also observed in the spectra. The observed changes in the spectra of the adsorbent are indications of adsorption of radionuclide by the polymer composite.

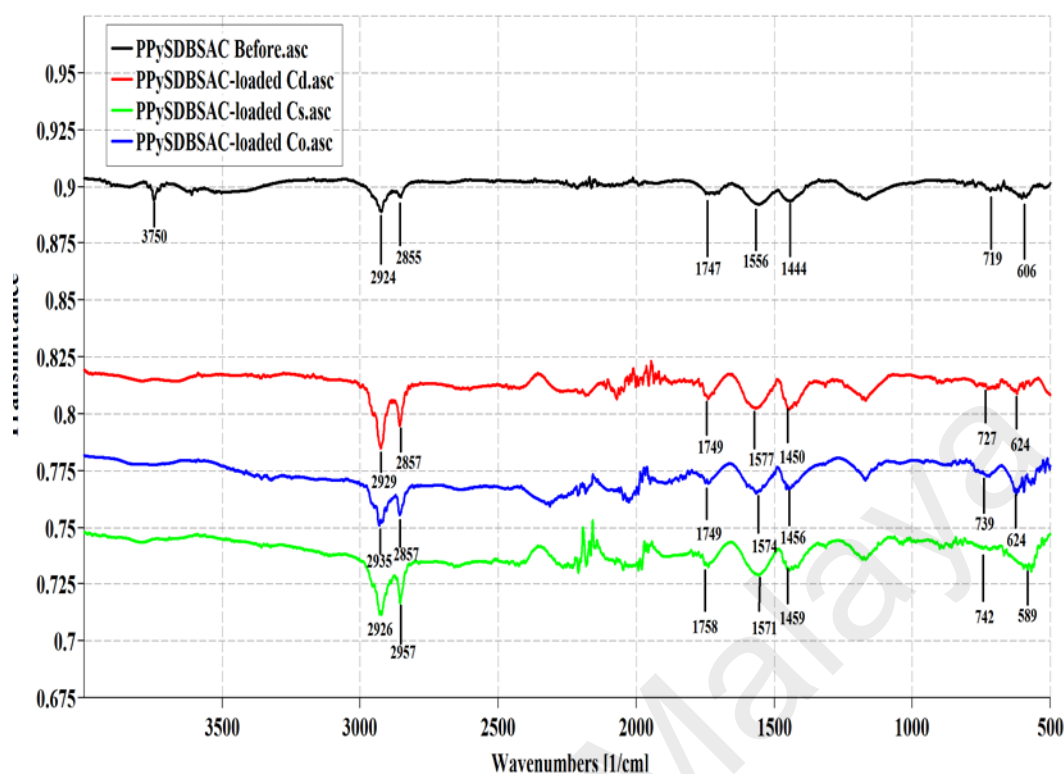


Figure 5.41: FTIR analysis of PPy/SDBS/AC after adsorption.

5.4.2 XRD analysis of polypyrrole-based adsorbents after adsorption

The X-ray diffraction pattern of each adsorbent was also observed for the influence of adsorbed radionuclides in the adsorbent materials. Figure 5.42 shows the XRD pattern of PPy after adsorption. Before adsorption, the PPy presents a broad peak centered at about $2\theta = 26.12^\circ$ (d -spacing of 3.41), which is ascribed mainly to the periodicity parallel to the polymer chain. When cadmium, cesium and cobalt ions were introduced into the PPy particles, the broad peak which was observed in the pure PPy became narrower and increased in intensity. The increase of background noise can be related to the introduction of the radionuclide metal ions in the polymer, because backscattering of X-ray radiation increases with increasing atomic number (Seid et al., 2014). In addition, the narrow peaks show a backward shift to a new position at $2\theta = 25.04^\circ$ with d -spacing of 3.55 for PPy-loaded Cd, $2\theta = 25.58^\circ$ with d -spacing of 3.48 for PPy-loaded Cs and $2\theta = 25.76^\circ$ with d -spacing of 3.46 for PPy-loaded Co, indicating adsorption of the studied radionuclides.

Because the peaks were not significantly crystalline in nature, it shows that the radionuclide metal ions were atomically bonded to the polymer.

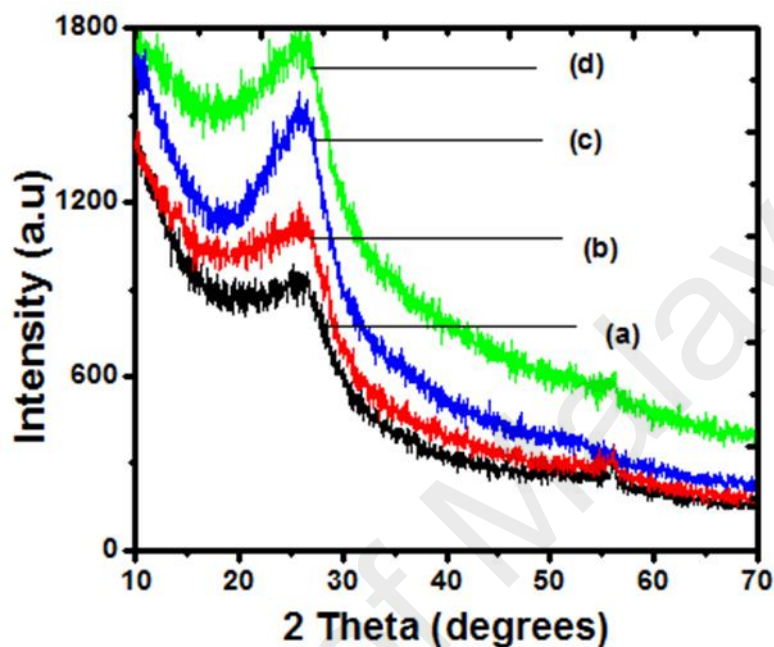


Figure 5.42: XRD patterns of PPy adsorbent (a) before adsorption, (b) after ^{109}Cd adsorption, (c) after ^{137}Cs adsorption and (d) after ^{60}Co adsorption.

Figure 5.43 presented the XRD patterns of PPy/SDBS after adsorption of the radionuclides. As shown, the characteristic broad peak initially observed at around $2\theta = 17.31$ to 29.00° has become crystalline with several sharp peaks formed at different locations after adsorption of cadmium and cesium ions. In the case of PPy/SDBS-loaded Co, the broad peak has shifted position and also increased in intensity, and the increase of background noise can be related to the introduction of cobalt ions in the polymer composite material. This is evident by the backward shift in the peak to a new position at around $2\theta = 15.69$ to 27.74° .

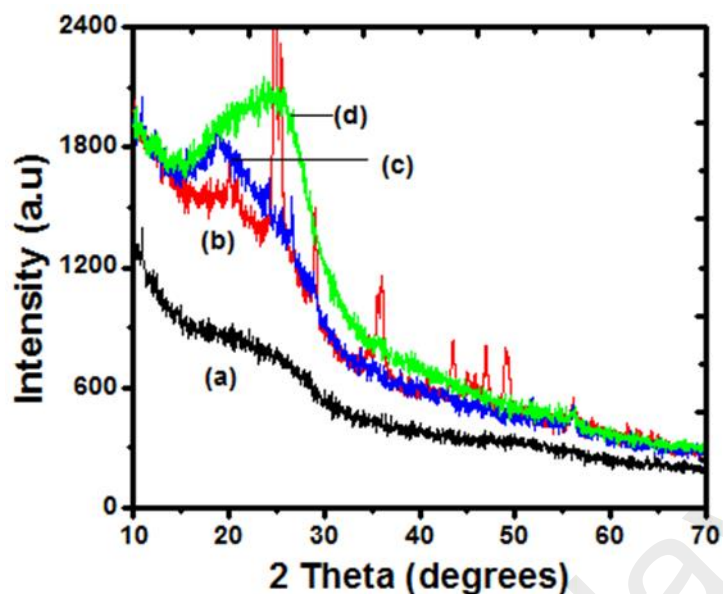


Figure 5.43: XRD patterns of PPy/SDBS (a) before adsorption, (b) after ^{109}Cd adsorption, (c) after ^{137}Cs adsorption and (d) after ^{60}Co adsorption.

Figure 5.44 shows the XRD patterns for PPy/SDBS/AC after adsorption. As shown, when cadmium, cesium and cobalt ions were introduced, the broad peak which was observed in the virgin PPy/SDBS/AC composite has assumed crystalline nature (but not well-defined) and increased in intensity. The increase of background noise is an evident for the adsorption of the radionuclide metal ions in the polymer composite because backscattering of X-ray radiation increases with increasing atomic number (Seid et al., 2014). However, since the observed peaks after adsorption were not clearly crystalline or significantly different from the peak before adsorption, it appears that the radionuclide metal ions were atomically bonded to the polymer composite adsorbent.

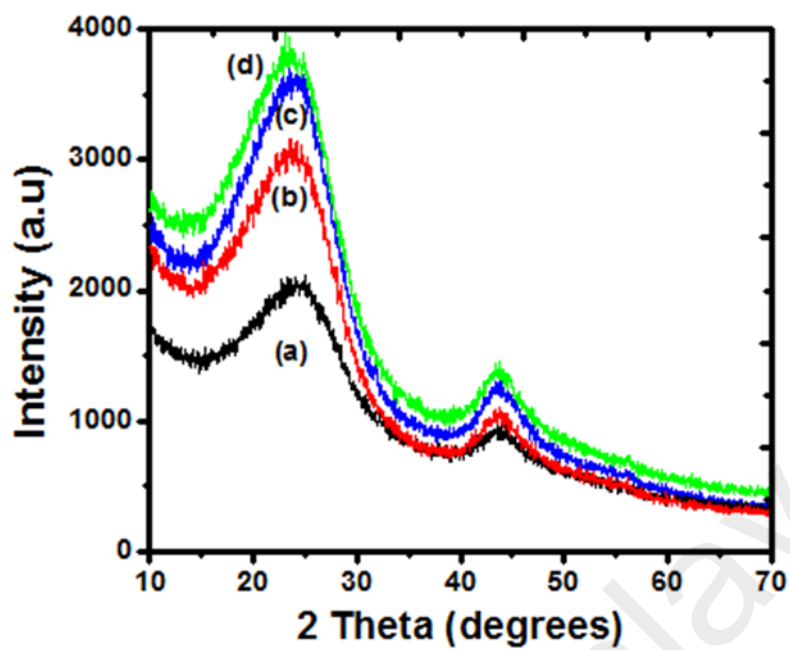


Figure 5.44: XRD patterns of PPy/SDBS/AC (a) before adsorption, (b) after ^{109}Cd , (c) after ^{137}Cs adsorption and (d) ^{60}Co adsorption.

CHAPTER 6: CONCLUSIONS AND SUGGESTIONS

6.1 Conclusion

In this study, polypyrrole was successfully synthesized with anionic surfactant (SDBS), sawdust, activated carbon and in combination of these materials to make polypyrrole composite adsorbents using ferric chloride hexahydrate as oxidant for the removal of radioactive materials from wastewater.

The formation of polypyrrole and its composites was confirmed by various techniques. The pore volume distributions and surface area measurements of the prepared polypyrrole-based adsorbents were examined by BET technique, while the surface morphologies and structures were performed using FESEM and XRD, respectively. The high thermal stability of the polypyrrole composite adsorbents over the pure polypyrrole adsorbent was confirmed by the TG-DTG technique. The various surface functional groups of the prepared adsorbents were identified by FTIR and Boehm titration methods. Modification of pure polypyrrole by different materials was found to be an easy and cheap route in enhancing the surface functional groups of pure polypyrrole adsorbent. No significant physico-chemical changes of the prepared polypyrrole-based adsorbents were observed, except for surfactant-doped polypyrrole/activated carbon composite which showed self-organized structure formation after irradiation by ^{60}Co source, suggesting that the prepared adsorbents were fully capable of adsorbing radioactive materials.

The prepared polypyrrole-based adsorbents were investigated for the removal of radioactive cadmium (^{109}Cd), cesium (^{137}Cs) and cobalt (^{60}Co) from aqueous solution. It was revealed that the polypyrrole composite adsorbents demonstrated higher adsorption performance over the pure polypyrrole adsorbent, but the SDBS-doped polypyrrole and SDBS-doped polypyrrole/activated carbon composites showed highest adsorption

efficiency for the studied radioactive materials compared to SDBS-doped polypyrrole/sawdust composite and undoped polypyrrole composite adsorbents. It is suggested that the presence of microporous activated carbon and the large size SDBS dopant improved the sorption performance of the polypyrrole composites.

The applicability of polypyrrole (PPy), SBDS-doped polypyrrole (PPy/SDBS) and SDBS-doped polypyrrole/activated carbon (PPy/SDBS/AC) composites for the removal of low-activity of radioactive cadmium, cesium and cobalt from wastewater suggested the good performance of the adsorbents at relatively high pH values and at low temperature range, if the concentrations of both monovalent and divalent interfering metal ions are moderately low in the radioactive-containing solutions. The fast kinetics, rapid equilibration and most importantly, the separation factor (R_L) which lies within 0 and 1, indicate the polypyrrole-based adsorbents are favourable for the adsorption of studied radionuclides. In all cases, the high sorption capacity of the SDBS-doped polypyrrole/activated carbon composite over other adsorbents indicate that the composite adsorbent can serve as a good adsorbent in large scale radioactive-water treatment for the removal of radioactive materials.

Adsorption thermodynamics process indicates that the adsorption is controlled by a physical process but partly enhanced by a chemical effect (possibly emanated from the sharing of lone-pair electron of the nitrogen atom between the radionuclide and the surface amine groups of the polypyrrole adsorbents or from the extra sorption sites introduced into the polymer surface by the composite materials). This is also supported by the fact that the $\Delta H^0 < 40$ kJ/mol, indicating a physical adsorption process. The decrease in the values of ΔG^0 confirms the spontaneity of the process for both ^{137}Cs and ^{60}Co . On the other hand, the increase in ΔG^0 value means the adsorption is feasible but not spontaneous in the case of ^{109}Cd radionuclide.

The prepared polypyrrole-based adsorbents demonstrated outstanding potential for re-use by regeneration through the use of low concentration of HCl as a desorbing agent, thus creating the possibility of recovery of desorbed radioactive metals for other application in nuclear industries. This is an additional consideration for the feasibility of the prepared polypyrrole-based adsorbents in adsorption, which should make the whole process cost effective if explored in practical application.

Summarily, the current study shows that polypyrrole composite adsorbents are more effective to treat wastewater to remove ^{109}Cd , ^{137}Cs and ^{60}Co than the pure polypyrrole adsorbent. The reason has been ascribed to the synergy effect of the individual component materials present in the polymer composite materials compared to the pure PPy. The study shows that the application of as-prepared polypyrrole-based adsorbents is a lot cheaper and can be employed by any industry to treat wastewater-containing radioactive contents and does not require large number of operators.

6.2 Suggestion for further work

In this study, adsorption of polypyrrole synthesized in the presence of few surface enhancing materials (anionic surfactant, sawdust and activated carbons) has been examined for the removal of ^{109}Cd , ^{137}Cs and ^{60}Co radionuclides from synthetic radioactive wastewater. Based on the obtained results, further works could be suggested which may include:

- ❖ applications of other adsorptive materials could be employed during the synthesis of polypyrrole to enhance its adsorption performance.
- ❖ further studies are required to study the effects of preparation conditions (such as time, temperature and pH) on the as-synthesized polypyrrole adsorbents and adsorption performance for the studied radionuclides.

- ❖ the composite materials used in the current study can be investigated for the adsorption of other challenging radioactive materials such as europium, uranium and strontium.
- ❖ since different matrices have different compositions which may impede selectivity of target radionuclides of interest, real wastewaters such as nuclear waste-effluents and other industrial wastewaters containing various radionuclides are advocated for future studies.
- ❖ by using the optimized parameters, a practical generator/ reactor could be designed (in future) for commercial use of wastewater treatment.

University of Malaya

REFERENCES

- Abd El-Rahman, K. M., El-Kamash, A. M., ElvSourougy, M. R., & Abdel-Moniem, N. M. (2006). Thermodynamic modeling for the removal of Cs^+ , Sr^{2+} , Ca^{2+} and Mg^{2+} ions from aqueous waste solutions using zeolite A. *Journal of Radioanalytical and Nuclear Chemistry*, 268(2), 221 – 230.
- Abdel-Rahman, R.O., Ibrahim H.A., & Hung Y. -T. (2011a). Liquid radioactive treatment: A review. *Water*, 3, 551 – 565.
- Abdel-Rahman, R. O., El-Kamash, A. M., Ali, H. F., & Hung, Y. T. (2011b). Overview on recent trends and development on radioactive liquid waste treatment part 1: Sorption/ Ion exchange technique. *International Journal of Environmental and Engineering Science*, 2, 1 – 16.
- Adhikari, T., & Singh, M. V. (2003). Sorption characteristics of lead and cadmium in some soil of India. *Geoderma*, 114, 81 – 92.
- Ahmaruzzaman, M. (2011). Industrial wastes as low-cost potential adsorbents for the treatment of wastewater laden with heavy metals. *Advances in Colloid and Interface Science*, 166(1-2), 36 – 59.
- Ahn, C., Kim, Y., Woo, S., & Park, J. (2009). Removal of cadmium using acid-treated activated carbon in the presence of nonionic and/or anionic surfactants. *Hydrometallurgy*, (99), 209 – 213.
- Aksu, Z., & Akpınar, D. (2001). Competitive biosorption of phenol and chromium (VI) from binary mixtures onto dried anaerobic activated sludge. *Biochemical Engineering Journal*, 7, 183 – 193.
- Al-Nasri, S. K. A. (2013). Treatment of wastewater containing cobalt (Co-59) and strontium (Sr-89) as a model to remove radioactive Co-60 and Sr-90 using hierarchical structures incorporating zeolites. *A Thesis Submitted to the University of Manchester for the Degree of Doctor of Philosophy in the Faculty of Engineering and Physical Sciences*. Retrieved March 3, 2015 from <https://www.escholar.manchester.ac.uk/uk-ac-man-scw:215892>
- Ali, I. M. (2009). Sorption studies of ^{134}Cs , ^{60}Co and $^{152+154}\text{Eu}$ on phosphoric acid activated silico-antimonate crystals in high acidic media. *Chemical Engineering Journal*, 155(3), 580 – 585.

- Aly, Z., Graulet, A., Scales, N., & Hanley, T. (2014). Removal of aluminium from aqueous solutions using PAN-based adsorbents: characterisation, kinetics, equilibrium and thermodynamic studies. *Environmental Science and Pollution Research*, 21(5), 3972 – 3986.
- Ansari, R. (2006). Application of polyaniline and its composites for adsorption/recovery of chromium (VI) from aqueous solutions. *Acta Chimica Slovenica*, 53(1), 88.
- Ansari, R., & Fahim, N. K. (2007). Application of polypyrrole coated on wood sawdust for removal of Cr (VI) ion from aqueous solutions. *Reactive and Functional Polymers*, 67(4), 367 – 374.
- Ararem, A., Bouras, O., & Arbaoui, F. (2011). Adsorption of caesium from aqueous solution on binary mixture of iron pillared layered montmorillonite and goethite. *Chemical Engineering Journal*, 172(1), 230 – 236.
- Avramenko, V., Bratskaya, S., Zheleznov, V., Sheveleva, I., Voitenko, O., & Sergienko, V. (2011). Colloid stable sorbents for cesium removal: Preparation and application of latex particles functionalized with transition metals ferrocyanides. *Journal of Hazardous Materials*, 186, 1343 – 1350.
- Awual, M. R., Suzuki, S., Taguchi, T., Shiwaku, H., Okamoto, Y., & Yaita, T. (2014). Radioactive cesium removal from nuclear wastewater by novel inorganic and conjugate adsorbents. *Chemical Engineering Journal*, 242, 127 – 135.
- Aydiner, C., Bayramoglu, M., Kara, S., Keskinler, B., & Ince, O. (2006). Nickel Removal from Waters Using Surfactant-Enhanced Hybrid PAC/MF Process. I. The Influence of System-Component Variables. *Industrial and Engineering Chemistry Research*, 45, 3926 – 3933.
- Bai, L., Li, Z., Zhang, Y., Wang, T., Lu, R., Zhou, W., . . . & Zhang, S. (2015). Synthesis of water-dispersible graphene-modified magnetic polypyrrole nanocomposite and its ability to efficiently adsorb methylene blue from aqueous solution. *Chemical Engineering Journal*, 279, 757 – 766.
- Banhart, F. (1999). Irradiation effects in carbon nanostructures. *Reports on Progress in Physics*, 62, 1181 – 1221.
- Bansal, R.C., & Goyal, M. (2005). *Activated carbon adsorption*. CRC Press, Taylor & Francis group.

- Barakat, M.A. (2011). New trends in removing heavy metals from industrial wastewater. *Arabian Journal of Chemistry*, 4, 361 – 377.
- Baş, N., Yakar, A., & Bayramgil, N. P. (2014). Removal of cobalt ions from aqueous solutions by using poly (N, N-dimethylaminopropyl methacrylamide/itaconic acid) hydrogels. *Journal of Applied Polymer Science*, 131(7), 39569.
- Belaib, F., Meniai, A., & Lehocine, M. B. (2012). Elimination of phenol by adsorption onto mineral/polyaniline composite solid support. *Energy Procedia*, 18, 1254 – 1260.
- Belhachemi, M., & Addoun, F. (2011). Comparative adsorption isotherms and modeling of methylene blue onto activated carbons. *Applied Water Science*, 1(3-4), 111 – 117.
- Benguella, B., & Benaissa, H. (2002). Cadmium removal from aqueous solutions by chitin: kinetic and equilibrium studies. *Water research*, 36(10), 2463 – 2474.
- Bhaumik, M., Maity, A., Srinivasu, V., & Onyango, M. S. (2011). Enhanced removal of Cr(VI) from aqueous solution using polypyrrole/Fe₃O₄ magnetic nanocomposite. *Journal of Hazardous Materials*, 190, 381 – 390.
- Bhaumik, M., Maity, A., Srinivasu, V., & Onyango, M. S. (2012). Removal of hexavalent chromium from aqueous solution using polypyrrole-polyaniline nanofiber. *Chemical Engineering Journal*, 181 – 182, 323 – 333.
- Biniak, S., Szymański, G., Siedlewski, J., & Świątkowski, A. (1997). The characterization of activated carbons with oxygen and nitrogen surface groups. *Carbon*, 35(12), 1799 – 1810.
- Boehm, H. P., Diehl, E., Heck, W., & Sappok, R. (1964). Surface oxides of carbon. *Angewandte Chemie International Edition in English*, 3(10), 669 – 677.
- Bondar, Y., Kuzenko, S., Han, D. -H., & Cho, H. -K. (2014). Development of novel nanocomposite adsorbent based on potassium nickel hexacyanoferrate-loaded polypropylene fabric. *Nanoscale Research Letters*, 9, 180.
- Božić, D., Stanković, V., Gorgievski, M., Bogdanović, G., & Kovačević, R. (2009). Adsorption of heavy metal ions by sawdust of deciduous trees. *Journal of Hazardous Materials*, 171(1), 684 – 692.

- Bratby, J. (2006). *Coagulation and Flocculation in water and wastewater treatment*. IWA Publishing, London, Seattle.
- Brostow, W., Deshpande, S., Fan, K., Mahendrakar, S., Pietkiewicz, D., & Wisner, S. R. (2009). Gamma-irradiation effects on polypropylene-based composites with and without an internal lubricant. *Polymer Engineering and Science*, 49(5), 1035.
- Ca, D. V., & Cox, J. A. (2004). Solid phase extraction of cesium from aqueous solution using sol-gel encapsulated cobalt hexacyanoferrate. *Microchimica Acta*, 147, 31 – 37.
- Castagno, K. R., Dalmoro, V., & Azambuja, D. S. (2011). Characterization and corrosion of polypyrrole/sodium dodecylbenzene sulfonate electropolymerised on aluminum alloy 1100. *Materials Chemistry and Physics*, 130(1), 721 – 726.
- Chandra, V., & Kim, K.S. (2011). Highly selective adsorption of Hg²⁺ by a polypyrrole-reduced graphene oxide composite. *Chemical Communications*, 47(13), 3942 – 3944.
- Changkun, L. (2009). Study of polyamines-functionalized PGMA beads as adsorbents for the removal of heavy metal ions from aqueous solution. *A Thesis submitted for the Degree of Doctor of Philosophy, Department of Chemical and Biomolecular Engineering, National University of Singapore*. Retrieved June 2, 2016 from scholarbank.nus.edu.sg/handle/10635/16352
- Chen, C., & Wang, J. (2008). Removal of Pb²⁺, Ag⁺, Cs⁺ and Sr²⁺ from aqueous solution by brewery's waste biomass. *Journal of Hazardous Material*, 151, 65 – 70.
- Chen, J., Hong, X., Zhao, Y., Xia, Y., Li, D., & Zhang, Q. (2013). Preparation of flake-like polyaniline/montmorillonite nanocomposites and their application for removal of Cr (VI) ions in aqueous solution. *Journal of Materials Science*, 48(21), 7708 – 7717.
- Chen, Y., Wang, S., Kang, L., & Kong, L. (2016). Enhanced adsorption of Ni(II) using ATP/PPy/SDS composite. *RSC Advances*, 6(14), 11735-11741.
- Choi, M., & Jang, J. (2008). Heavy metal ion adsorption onto polypyrrole-impregnated porous carbon. *Journal of Colloid and Interface Science*, 325, 287 – 289.
- Chougule, M. A., Pawar, S. G., Godse, P. R., Mulik, R. N., Sen S., & Patil, V. B. (2011). Synthesis and Characterization of polypyrrole (PPy) thin films. *Soft Nanoscale Letters*, 1, 6 – 10.

- Clifford, D. A. (1999). Ion exchange and inorganic adsorption. In: Letterman, R. D. (Ed.), *Water Quality and Treatment*, fifth ed. McGraw-Hill, New York.
- Cojocaru, C., Zakrzewska-Trznadel, G., & Jaworska, A. (2009). Removal of cobalt ions from aqueous solutions by polymer assisted ultrafiltration using experimental design approach. part 1: Optimization of complexation conditions. *Journal of Hazardous Materials*, 169(1), 599 – 609.
- Cui, H., Qian, Y., Li, Q., Zhang, Q., & Zhai, J. (2012). Adsorption of aqueous Hg(II) by a polyaniline/attapulgite composite. *Chemical Engineering Journal*, 211, 216 – 223.
- Deng, J. -H., Zhang, X. -R., Zeng, G. -M., Gong, J. -L., Niu, Q. -Y., & Liang, J. (2013). Simultaneous removal of Cd(II) and ionic dyes from aqueous solution using magnetic graphene oxide nanocomposite as an adsorbent. *Chemical Engineering Journal*, 226, 189 – 200.
- Ding, D., Zhao, Y., Yang, S., Shi, W., Zhang, Z., Lei, Z., & Yang, Y. (2013). Adsorption of cesium from aqueous solution using agricultural residue–walnut shell: Equilibrium, kinetic and thermodynamic modeling studies. *Water Research.*, 47(7), 2563 – 2571.
- Dubey, S.S., & Rao, B.S. (2011). Removal of cerium ions from aqueous solution by hydrous ferric oxide- A radiotracer study. *Journal of Hazardous Material*, 186, 1028 – 1032.
- Eroglu, H., Yapici, S., Nuhogu, C., & Varoglu, E. (2009). Biosorption of Ga-67 radionuclides from aqueous solutions onto waste pomace of an olive oil factory. *Journal of Hazardous Material*, 172, 729 – 738.
- Eisenbud, M., & Gesell, T. (1997). *Environmental radioactivity from natural, industrial and military sources*. Academic Press, London, pp 656.
- El-Naggar, I. M., Zakaria, E. S., Ali, I. M., Khalil, M., & El-Shahat, M. F. (2012a). Kinetic modelling analysis for the removal of cesium ions from aqueous solutions using polyaniline titanotungstate. *Arabian Journal of Chemistry*, 5, 109 – 119.
- El-Naggar, I. M., Zakaria, E. S., Ali, I. M., Khalil, M., & El-Shahat, M. F. (2012b). Chemical studies on polyaniline titanotungstate and its uses to reduction cesium from solutions and polluted milk. *Journal of Environmental Radioactivity*, 112, 108 – 117.

- Erçin, D., Eken, M., Aktas, Z., Çetinkaya, S., Sakintuna, B., & Yürüm, Y. (2005). Effect of γ -irradiation on the structure of activated carbons produced from Turkish Elbistan lignite. *Radiation Physics and Chemistry*, 73(5), 263 – 271.
- Faghihian, H., Iravani, M., Moayed, M., & Ghannadi-Maragheh, M. (2013). Preparation of a novel PAN–zeolite nanocomposite for removal of Cs^+ and Sr^{2+} from aqueous solutions: Kinetic, equilibrium, and thermodynamic studies. *Chemical Engineering Journal*, 222, 41 – 48.
- Finkenstadt, V. L. (2005). Natural polysaccharides as electroactive polymers. *Applied Microbiology and Biotechnology*, 67(6), 735 – 745.
- Foo, K., & Hameed, B. (2010). Insights into the modeling of adsorption isotherm systems. *Chemical Engineering Journal*, 156(1), 2 – 10.
- Freundlich, H. (1907). Über die adsorption in lösungen. *Journal of Physical Chemistry*, 57, 385 – 490.
- Fu, F., Wang, Q. (2011). Removal of heavy metal ions from wastewaters: a review. *Journal of Environmental Management*, 92, 407 – 418.
- Gao, N., Li, A., Quan, C., Du, L., & Duan, Y. (2013). TG-FTIR and Py-GC/MS analysis on pyrolysis and combustion of pine sawdust. *Journal of Analytical and Applied Pyrolysis*, 100, 26 – 32.
- Gao, W., Majumder, M., Alemany, L. B., Narayanan, T. N., Ibarra, M. A., Pradhan, B. K., & Ajayan, P. M. (2011). Engineered graphite oxide materials for application in water purification. *ACS Applied Materials and Interfaces*, 3(6), 1821 – 1826.
- Gebrekidan, M., & Samuel, Z. (2011). Concentration of heavy metals in drinking water from urban areas of Tigray region, Northern Ethiopia. *Momona Ethiopian Journal of Science*, 3(1), 105 – 121.
- Ghaemi, A., Torab-Mostaedi, M., & Ghannadi-Maragheh, M. (2011). Characterizations of strontium (II) and barium (II) adsorption from aqueous solutions using dolomite powder. *Journal of Hazardous Materials*, 190, 916 – 921.
- Ghassabzadeh, H., Mohadespour, A., Torab-Mostaedi, M., Zaheri, P., Maragheh, M. G., & Taheri, H. (2010). Adsorption of Ag, Cu and Hg from aqueous solutions using expanded perlite. *Journal of Hazardous Materials*, 177(1), 950 – 955.

- Gholivand, M. B., & Abolghasemi, M. M. (2012). Inside needle capillary adsorption trap device for headspace solid-phase dynamic extraction based on polyaniline/hexagonally ordered silica nanocomposite. *Journal of Separation Science*, 35, 695 – 701.
- Ghorbani, M., & Eisazadeh, H. (2012). Fixed bed column study for Zn, Cu, Fe and Mn removal from wastewater using nanometer size polypyrrole coated on rice husk ash. *Synthetic Metals*, 162(15), 1429 – 1433.
- Ghorbani, M., & Eisazadeh, H. (2013a). Fixed-bed column removal of chemical oxygen demand, anions, and heavy metals from paper mill wastewater by using polyaniline and polypyrrole nanocomposites on carbon nanotubes. *Journal of Vinyl and Additive Technology*, 19(3), 213 – 218.
- Ghorbani, M., & Eisazadeh, H. (2013b). Removal of COD, color, anions and heavy metals from cotton textile wastewater by using polyaniline and polypyrrole nanocomposites coated on rice husk ash. *Composites Part B: Engineering*, 45(1), 1 – 7.
- Ghorbani, M., Esfandian, H., Taghipour, N., & Katal, R. (2010). Application of polyaniline and polypyrrole composites for paper mill wastewater treatment. *Desalination*, 263, 279 – 284.
- Griffith, C. S., Luca, V., Šebesta, F., & Yee, P. (2005). Separation of cesium and strontium from acidic radioactive waste simulants using a microporous tungstate/polyacrylonitrile (PAN) composite adsorbent. *Separation Science and Technology*, 40(9), 1781 – 1796.
- Gupta, R., & Shankar, S. (2004). Toxic waste removal from aqueous solutions by polyaniline: a radiotracer study. *Adsorption Science and Technology*, 22(6), 485 – 496.
- Gupta, V.K., & Suhas. (2009). Application of low-cost adsorbents for dye removal - A review. *Journal of Environmental Management*, 90, 2313 – 2342.
- Hasani, T., & Eisazadeh, H. (2013). Removal of Cd(II) by using polypyrrole and its nanocomposites. *Synthetic Metals*, 175, 15 – 20.
- Hepel, M., Xingmin, Z., Stephenson, R., & Perkins, S. (1997). Use of electrochemical quartz crystal microbalance technique to track electrochemically assisted removal of heavy metals from aqueous solutions by cation-exchange composite polypyrrole-modified electrodes. *Microchemical Journal*, 56(1), 79 – 92.

- Heydari-Gorji, A., Belmabkhout, Y., & Sayari, A. (2011). Polyethylenimine-impregnated mesoporous silica: effect of amine loading and surface alkyl chains on CO₂ adsorption. *Langmuir*, 27(20), 12411 – 12416.
- Hizal, J., & Apak, R. (2006). Modelling of copper (II) and lead (II) adsorption on kaolinite-based clay minerals individually and in the presence of humic acid. *Journal of Colloid and Interface Science*, 295, 1 – 13.
- Ho, Y. -S. (2006). Second-order kinetic model for the sorption of cadmium onto tree fern: A comparison of linear and non-linear methods. *Water Research*, 40, 119 – 125.
- Ho, Y. -S., & McKay, G. (1999). Pseudo-second order model for sorption processes. *Process Biochemistry*, 34(5), 451 – 465.
- Ho, Y., & McKay, G. (1999). Competitive sorption of copper and nickel ions from aqueous solution using peat. *Adsorption*, 5(4), 409 – 417.
- Holleman, A. F., Wiberg, E., & Wiberg, N. (1985). Vergleichende Übersicht über die Gruppe der Alkalimetalle, Lehrbuch der Anorganischen Chemie (in German), 91-100 edn, Walter de Gruyter, ISBN 3-11-007511-3, pp 953 – 955.
- Hong, S., Cannon, F. S., Hou, P., Byrne, T., & Nieto-Delgado, C. (2014). Sulfate removal from acid mine drainage using polypyrrole-grafted granular activated carbon. *Carbon*, 73, 51 – 60.
- Hoshina, Y., Zaragoza-Contreras, E. A., Farnood, R., & Kobayashi, T. (2012). Nanosized polypyrrole affected by surfactant agitation for emulsion polymerization. *Polymer Bulletin*, 68(6), 1689 – 1705.
- Hu, B. J., Zhong, L. S., Song, W. G., & Wan, L. J. (2008). Synthesis of hierarchically structured metal oxides and their application in heavy metal ion removal. *Advanced Materials*, 20, 2977 – 2982.
- Hua, M., Zhang, S., Pan, B., Zhang, W., Lv Lu, & Zhang, Q. (2012.) Heavy metal removal from water/ wastewater by nanosized metal oxides: A review. *Journal of Hazardous Materials*, 211 – 212, 317 – 331.
- Huang, Y., Wang, W., Feng, Q., & Dong, F. (2017). Preparation of magnetic clinoptilolite/Co₂FeO₄ composites for removal of Sr²⁺ from aqueous solutions: Kinetic, equilibrium and thermodynamic studies. *Journal of Saudi Chemical Society*, 21, 58 – 66.

- Huang, Y., Li, J., Chen, X., & Wang, X. (2014). Applications of conjugated polymer based composites in wastewater purification. *RSC Advances*, 4(107), 62160 – 62178.
- Humelnicu, D., Dinu, M., & Dragan, E. (2011). Adsorption characteristics of (UO₂)²⁺ and Th⁴⁺ ions from simulated radioactive solutions onto chitosan/clinoptilolite sorbents. *Journal of Hazardous Materials*, 185, 447 – 455.
- IAEA. (1989). International Atomic Energy Agency: *Measurement of of Radionuclides in Food and the Environment A Guidebook*. Technical Reports series No. 295, IAEA, Vienna, Austria.
- IAEA. (1999). International Atomic Energy Agency: *Review of the factors affecting the selection and implementation of waste management technologies: IAEA-TECDOC-1096*, IAEA, Vienna, Austria.
- IAEA. (2003). International Atomic Energy Agency: *Combined methods for liquid radioactive waste treatment*. IAEA-TECDOC-1336. Final Report of a coordinated research project 1997 – 2001.
- Ingole, N. W., & Patil, V. N. (2013). Cadmium removal from aqueous solution by modified low cost adsorbent (s): A state of the art. *International Journal of Civil, Structural, Environmental and Infrastructure Engineering Research and Development*, 3(4), 17 – 26.
- Iqbal, N., Mobin, M., Rafiquee, M., & Al-Lohedan, H. A. (2013). Removal of Cu²⁺, Cd²⁺, Pb²⁺ and Hg²⁺ ions by the synthesized sodium dodecyl benzene sulphonate-based tin (IV) phosphate (SDBS-SnP) cation exchanger. *Desalination and Water Treatment*, 51(34-36), 6688 – 6697.
- Jakab, E., Mészáros, E., & Omastová, M. (2007). Thermal decomposition of polypyrroles. *Journal of Thermal Analysis and Calorimetry*, 88(2), 515 – 521.
- Javadian, H. (2014). Application of kinetic, isotherm and thermodynamic models for the adsorption of Co(II) ions on polyaniline/polypyrrole copolymer nanofibers from aqueous solution. *Journal of Industrial and Engineering Chemistry*, 20, 4233 – 4241.
- Javadian, H., Vahedian, P., & Toosi, M. (2013). Adsorption characteristics of Ni(II) from aqueous solution and industrial wastewater onto Polyaniline/HMS nanocomposite powder. *Applied Surface Science*, 284, 13 – 22.

- Johanson, U., Marandi, M., Tamm, T., & Tamm, J. (2005). Comparative study of the behavior of anions in polypyrrole films. *Electrochimica Acta*, 50(7), 1523 – 1528.
- Juilong, S. (2014). Development of Inorganic-organic hybrid materials for waste water treatment. *A Thesis submitted for the degree of Doctor of Philosophy of Science, Department of Chemistry, National University of Singapore*. Retrieved September 24, 2015 from scholarbank.nus.edu.sg/handle/10635/119803
- Kadam, A. A., Jang, J., & Lee, D. S. (2016). Facile synthesis of pectin-stabilized magnetic graphene oxide Prussian blue nanocomposites for selective cesium removal from aqueous solution. *Bioresource Technology*, 216, 391 – 398.
- Kalkan, E., Nadaroglu, H., Dikbaş, N., Taşgin, E., & Celebi, N. (2013). Bacteria-modified red mud for adsorption of cadmium ions from aqueous solutions. *Polish Journal of Environmental Studies*, 22(2), 417 – 429.
- Kamaraj, R., & Vasudevan, S. (2015). Evaluation of electrocoagulation process for the removal of strontium and cesium from aqueous solution. *Chemical Engineering Research and Design*, 93, 522 – 530.
- Kampalanonwat, P., & Supaphol, P. (2014). The Study of Competitive Adsorption of Heavy Metal Ions from Aqueous Solution by Aminated Polyacrylonitrile Nanofiber Mats. *Energy Procedia*, 56, 142 – 151.
- Katal, R., Pourkarimi, S., Bahmani, E., Dehkordi, H. A., Ghayyem, M. A., & Esfandian, H. (2013). Synthesis of Fe₃O₄/polyaniline nanocomposite and its application for nitrate removal from aqueous solutions. *Journal of Vinyl and Additive Technology*, 19(2), 147 – 156.
- Kim, J. O., Lee, S. M., & Jeon, C. (2014). Adsorption characteristics of sericite for cesium ions from an aqueous solution. *Chemical Engineering Research and Design*, 92, 368 – 374.
- Kobya, M., Demirbas, E., Senturk, E., & Ince, M. (2005). Adsorption of heavy metal ions from aqueous solutions by activated carbon prepared from apricot stone. *Bioresource Technology*, 96(13), 1518 – 1521.
- Kumar, A., Singh, R. K., Singh, H. K., Srivastava, P., & Singh, R. (2014). Enhanced capacitance and stability of p-toluenesulfonate doped polypyrrole/carbon composite for electrode application in electrochemical capacitors. *Journal of Power Sources*, 246, 800 – 807.

- Kumar, R., Ansari, M. O., & Barakat, M. (2013). DBSA doped polyaniline/multi-walled carbon nanotubes composite for high efficiency removal of Cr(VI) from aqueous solution. *Chemical Engineering Journal*, 228, 748 – 755.
- Kumar, K. Y., Muralidhara, H. B., Nayaka, Y. A., Balasubramanyam, J., & Hanumanthappa, H. (2013). Low-cost synthesis of metal oxide nanoparticles and their application in adsorption of commercial dye and heavy metal in aqueous solution. *Powder Technology*, 246, 125 – 136.
- Langmuir, I. (1918). The adsorption of gases on plane surfaces of glass, mica and platinum. *Journal of the American Chemical Society*, 40, 1361 – 1403.
- Largitte, L., & Pasquier, R. (2016). A review of the kinetics adsorption models and their application to the adsorption of lead by an activated carbon. *Chemical Engineering Research and Design*, 109, 495 – 504.
- Lauwerys, R., & Lison, D. (1994). Health risks associated with cobalt exposure. *Science of Total Environment*, 150(1 – 3), 1 – 6.
- Lei, Y., Qian, X., Shen, J., & An, X. (2012). Integrated reductive/adsorptive detoxification of Cr (VI)-contaminated water by polypyrrole/cellulose fiber composite. *Industrial and Engineering Chemistry Research*, 51(31), 10408 – 10415.
- Leusch, A., Holan, Z.R., & Volesky, B. (1996). Solution and particle effects on the biosorption of heavy metals by seaweed biomass. *Applied Biochemistry and Biotechnology*, 61, 231 – 249.
- LeVan, M. D., Carta, G., & Yon, C. M. (1997). In: R. H. Perry, D. W. Green, J. O. Maloney (Eds.), *Adsorption and Ion Exchange, seventh ed. Perry's chemical engineers' handbook*. McGraw-Hill, New York.
- Li, Z., Chen, F., Yuan, L., Liu, Y., Zhao, Y., Chai, Z., & Shin, W. (2012). Uranium(VI) adsorption on graphene oxide nanosheets from aqueous solution. *Chemical Engineering Journal*, 210, 539 – 546.
- Li, R., Liu, L., & Yang, F. (2013). Preparation of polyaniline/reduced graphene oxide nanocomposite and its application in adsorption of aqueous Hg(II). *Chemical Engineering Journal*, 229, 460 – 468.

- Li, S., Lu, X., Xue, Y., Lei, J., Zheng, T., & Wang, C. (2012). Fabrication of Polypyrrole/Graphene Oxide Composite Nanosheets and Their Applications for Cr(VI) Removal in Aqueous Solution. *PLOS ONE*, 7(8), 1–7.
- Lin, Y., Fryxell, G.E., Wu, H., & Engelhard, M. (2001). Sorption of cesium using self-assembled monolayers on mesoporous supports. *Environmental Science and Technology*, 35, 3962 – 3966.
- Liu, D., & Sun, D. (2012). Modeling adsorption of Cu(II) using polyaniline-coated sawdust in a Fixed-bed column. *Environmental Engineering Science*, 29(6), 461 – 465.
- Liu, D., Sun, D., & Li, Y. (2010). Removal of Cu(II) and Cd(II) from aqueous solutions by polyaniline on sawdust. *Separation Science and Technology*, 46(2), 321 – 329.
- Liu, J., Liu, Y., Wu, Z., Chen, X., Wang, H., & Weng, X. (2012). Polyethyleneimine functionalized protonated titanate nanotubes as superior carbon dioxide adsorbents. *Journal of Colloid and Interface Science*, 386(1), 392 – 397.
- Long, H., Wu, P., & Zhu, N. (2013). Evaluation of Cs⁺ removal from aqueous solution by adsorption on ethylamine-modified montmorillonite. *Chemical Engineering Journal*, 225, 237 – 244.
- Lü, Q. F., Huang, M. R., & Li, X. G. (2007). Synthesis and heavy-metal-ion sorption of pure sulfophenylenediamine copolymer nanoparticles with intrinsic conductivity and stability. *Chemistry—A European Journal*, 13(21), 6009 – 6018.
- Ma, F., Shi, W., Meng, H., Li, Z., Zhou, W., & Zhang, L. (2016). Preparation, characterization and ion-exchange behavior of polyantimonic acid-polyacrylonitrile (PAA-PAN) composite beads for strontium (II). *Journal of Radioanalytical and Nuclear Chemistry*, 308(1), 155 – 163.
- Ma, Y., Zhang, B., Ma, H., Yu, M., Li, L., & Li, J. (2016). Polyethylenimine nanofibrous adsorbent for highly effective removal of anionic dyes from aqueous solution. *Science China Materials*, 1(59), 38 – 50.
- Mansour, M., Ossman, M., & Farag, H. (2011). Removal of Cd (II) ion from waste water by adsorption onto polyaniline coated on sawdust. *Desalination*, 272(1), 301 – 305.

- Maroto-Valer, M. M., Dranca, I., Lupascu, T., & Nastas, R. (2004). Effect of adsorbate polarity on thermodesorption profiles from oxidized and metal-impregnated activated carbons. *Carbon*, 42(12), 2655 – 2659.
- Mészáros, R., Thompson, L., Bos, M., & De Groot, P. (2002). Adsorption and electrokinetic properties of polyethylenimine on silica surfaces. *Langmuir*, 18(16), 6164 – 6169.
- Metwally, E., Elkholy, S., Salem, H., & Elsabee, M. (2009). Sorption behavior of ^{60}Co and $^{152+154}\text{Eu}$ radionuclides onto chitosan derivatives. *Carbohydrate Polymers*, 76(4), 622 – 631.
- Mishra, S. P., Dubey, S. S., & Tiwari, D. (2004). Ion-exchangers in radioactive wastewater management Part XIV: Removal behavior of hydrous titanium oxide and sodium titanate for Cs(I). *Journal of Radioanalytical and Nuclear Chemistry*, 261(2), 457 – 463.
- Mohapatra, P., Lakshmi, D., Bhattacharyya, A., & Manchanda, V. (2009). Evaluation of polymer inclusion membranes containing crown ethers for selective cesium separation from nuclear waste solution. *Journal of Hazardous Materials*, 169(1), 472 – 479.
- Mukherjee, A., Zimmerman, A., & Harris, W. (2011). Surface chemistry variations among a series of laboratory-produced biochars. *Geoderma*, 163(3), 247 – 255.
- Nandi, B. K., Goswami, A., & Porkait, M. K. (2009). Adsorption characteristics of brilliant green dye on kaolin. *Journal of Hazardous Materials*, 161, 387 – 395.
- Nassar, N. N. (2012). Kinetics, equilibrium and thermodynamic studies on the adsorptive removal of nickel, cadmium and cobalt from wastewater by superparamagnetic iron oxide nanoadsorbents. *The Canadian Journal of Chemical Engineering*, 90(5), 1231 – 1238.
- Nilchi, A., Dehaghan, T. S., & Garmarodi, S. R. (2013). Kinetic, isotherm and thermodynamics for uranium and thorium ions adsorption from aqueous solutions by crystalline tin oxide particles. *Desalination*, 321, 67 – 71.
- Nilchi, A., Saberi, R., Garmarodi, S. R., & Bagheri, A. (2012). Evaluation of PAN-based manganese dioxide composite for the sorptive removal of cesium-137 from aqueous solutions. *Applied Radiation and Isotopes*, 70(2), 369 – 374.

- Nilchi, A., Saberi, R., Moradi, M., Azizpour, H., & Zarghami, R. (2011a). Adsorption of cesium on copper hexacyanoferrate-PAN composite ion exchanger from aqueous solution. *Chemical Engineering Journal*, 172, 572 – 580.
- Nilchi, A., Saberi, R., Moradi, M., Azizpour, H., & Zarghami, R. (2011b). Evaluation of AMP-PAN composite for adsorption of Cs⁺ ions from aqueous solution using batch and fixed bed operations. *Journal of Radioanalytical and Nuclear Chemistry*, 292(2), 609 – 617.
- Nilchi, A., Atashi, H., Javid, A., & Saberi, R. (2007). Preparations of PAN-based adsorbents for separation of cesium and cobalt from radioactive wastes. *Applied Radiation and Isotopes*, 65(5), 482 – 487.
- Ofomoja, A. E., Pholosi, A., & Naidoo, E. B. (2013). Kinetics and competitive modelling of cesium biosorption onto chemically modified pine cone powder. *Journal of Taiwan Institute of Chemical Engineers*, 44, 943 – 951.
- Olatunji, M. A., Khandaker, M.U., Amin, Y.M., & Mahmud, H. N. M. E. (2016). Cadmium-109 radioisotope adsorption onto polypyrrole coated sawdust of dryobalanops aromatic: Kinetics and adsorption isotherms modelling. *PLOS ONE*, 11(10). doi.org/10.1371/journal.pone.0164119
- Olatunji, M. A., Khandaker, M. U., Mahmud, H. N. M. E., & Amin, Y. M. (2015). Influence of adsorption parameters on cesium uptake from aqueous solutions- a brief review. *RSC Advances*, 5, 71658 – 71683.
- Olds, W., & Xue, Y. G. (2009). *Remediation of PHA contaminated soils and groundwater using activated carbon. ENNR 429: Final Report*. Retrieved from http://www.civil.canterbury.ac.nz/cochrane/NREProjects/2009/Project11_Olds_Xue.pdf (Retrieved March 30, 2016)
- Omraei, M., Esfandian, H., Katal, R., & Ghorbani, M. (2011). Study of the removal of Zn(II) from aqueous solution using polypyrrole nanocomposite. *Desalination*, 271, 248 – 256.
- Özdemir, U., Özbay, B., Veli, S., & Zor, S. (2011). Modeling adsorption of sodium dodecyl benzene sulfonate (SDBS) onto polyaniline (PANI) by using multi linear regression and artificial neural networks. *Chemical Engineering Journal*, 178, 183 – 190.
- Pan, B., Pan, B., Zhang, W., Lv, L., Zhang, Q., & Zheng, S. (2009). Development of polymeric and polymer-based hybrid adsorbents for pollutants removal from waters. *Chemical Engineering Journal*, 151(1), 19 – 29.

- Pan, L., Qiu, H., Dou, C., Li, Y., Pu, L., Xu, J., & Shi, Y. (2010). Conducting polymer nanostructures: template synthesis and applications in energy storage. *International Journal of Molecular Sciences*, 11(7), 2636 – 2657.
- Parab, H., Joshi, S., Sudersanan, M., Shenoy, N., Lali, A. & Sarma, U. (2010). Removal and recovery of cobalt from aqueous solutions by adsorption using low cost lignocellulosic biomass-coir pith. *Journal of Environmental Science and Health, Part A: Toxic/Hazardous Substances and Environmental Engineering*, 45(5), 603 – 611.
- Park, Y., Lee, Y.-C., Shin, W. S., & Choi, S.-J. (2010). Removal of cobalt, strontium and cesium from radioactive laundry wastewater by ammonium molybdophosphate-polyacrylonitrile (AMP-PAN). *Chemical Engineering Journal*, 162(2), 685 – 695.
- Pillay, K., Cukrowska, E. M., & Coville, N. J. (2009). Multi-walled carbon nanotubes as adsorbents for the removal of parts per billion levels of hexavalent chromium from aqueous solution. *Journal of Hazardous Materials*, 166, 1067 – 1075.
- Pignatello, J. J. (2011). Interactions of anthropogenic organic chemicals with natural organic matter and black carbon in environmental particles. In: Xing, B., Senesis, N., Huang, P.M., editors. *Biophysico-chemical processes of anthropogenic organic compounds in environmental systems*. John Wiley & Sons, Inc., pp 1 – 50. doi:10.1002/9780470944479.ch1
- Pires, C., Marques, A. P., Guerreiro, A., Magan, N., & Castro, P. M. (2011). Removal of heavy metals using different polymer matrixes as support for bacterial immobilisation. *Journal of Hazardous Materials*, 191(1), 277 – 286.
- Qin, H., Gong, T., Cho, Y., Lee, C., & Kim, T. (2014). A conductive copolymer of graphene oxide/poly (1-(3-aminopropyl) pyrrole) and the adsorption of metal ions. *Polymer Chemistry*, 5, 4466 – 4473.
- Rafatullah, M., Sulaiman, O., Hashim, R., & Amini, M.H.M. (2011). Adsorption of copper (II) ions onto surfactant-modified oil palm leaf powder. *Journal of Dispersion Science and Technology*, 32, 1641 – 1648.
- Raut, D., Mohapatra, P., Choudhary, M., & Nayak, S. (2013). Evaluation of two calix-crown-6 ligands for the recovery of radio cesium from nuclear waste solutions: Solvent extraction and liquid membrane studies. *Journal of Membrane Science*, 429, 197 – 205.
- Real, A., Sundell-Bergman, S., Knowles, J. F., Woodhead, D. S., & Zinger, I. (2004). Effects of ionizing radiation exposure on plants, fish and mammals: relevant data

for environmental radiation protection. *Journal of Radiological Protection*, 24, A123 – A137.

Redlich, O., & Peterson, D. L. (1959). A useful adsorption isotherm. *Journal of Physical Chemistry*, 63(6), 1024 – 1024.

Roy, K., Mohapatra, P., Rawat, N., Pal, D., Basu, S., & Manchanda, V. (2004). Separation of ^{90}Y from ^{90}Sr using zirconium vanadate as the ion exchanger. *Applied Radiation and Isotopes*, 60, 621 – 624.

Saad, D. (2013). Development and application of functionalized polymeric materials for heavy metal ions recovery from industrial and mining wastewaters. A Thesis submitted to the Faculty of Science, University of Witwatersrand in fulfilment of the requirement for the degree of Doctor of Philosophy. Retrieved September 24, 2015 from wiredspace.wits.ac.za/handle/10539/14075

Saberi, R., Nilchi, A., Gramarodi, S., & Zarghami, R. (2010). Adsorption characteristic of ^{137}Cs from aqueous solution using PAN-based sodium titanosilicate composite. *Journal of Radioanalytical and Nuclear Chemistry*, 284, 461 – 469.

Saito, K., Tsuneda, S., Kim, M., Kubota, N., Sugita, K., & Sugo, T. (1999). Radiation-induced graft polymerization is the key to develop high-performance functional materials for protein purification. *Radiation Physics and Chemistry*, 54(5), 517 – 525.

Sangvanich, T., Sukwarotwat, V., Wiacek, R. J., Grudzien, R. M., Fryxell, G. E., Addleman, S. R., . . . , & Yantasee, W. (2010). Selective capture of cesium and thallium from natural waters and simulated wastes with copper ferrocyanide functionalized mesoporous silica. *Journal of Hazardous Materials*, 182, 225 – 231.

Saville, P. (2005). *Polypyrrole formation and use*. Defense R & D Canada - Atlantic, Canada, p. 50 DTIC Document.

Schwarz, H. E., Emel, J., Dickens, W., Rogers, P., & Thompson, J. (1990). *Water quality and flows: The earth as transformed by human action*. Cambridge University Press, Cambridge, UK.

Scienza, L. C., & Thompson, G. E. (2001). Preparation and Surface Analysis of PPY/SDBS Films on Aluminum Substrates. *Polímeros*, 11(3), 142 – 148.

- Sehaqui, H., Gálvez, M. E., Becatinni, V., cheng Ng, Y., Steinfeld, A., Zimmermann, T., & Tingaut, P. (2015). Fast and Reversible Direct CO₂ Capture from Air onto All-Polymer Nanofibrillated Cellulose-Polyethylenimine Foams. *Environmental Science and Technology*, 49(5), 3167 – 3174.
- Seid, L., Chouder, D., Maouche, N., Bakas, I., & Barka, N. (2014). Removal of Cd(II) and Co(II) ions from aqueous solutions by polypyrrole particles: Kinetics, equilibrium and thermodynamics. *Journal of the Taiwan Institute of Chemical Engineers*, 45(6), 2969 – 2974.
- Serrano, S., Garrido, F., Campbell, C.G., & Garcia-Gonzalez, M.T. (2005). Competitive sorption of cadmium and lead in acid soils of Central Spain. *Geoderma*, 124, 91 – 104.
- Setshedi, K. Z., Bhaumik, M., Songwane, S., Onyango, M. S., & Maity, A. (2013). Exfoliated polypyrrole-organically modified montmorillonite clay nanocomposite as a potential adsorbent for Cr(VI) removal. *Chemical Engineering Journal*, 222, 186 – 197.
- Shahabi, S., Najafi, F., Majdabadi, A., Hooshmand, T., Haghbin Nazarpak, M., Karimi, B., & Fatemi, S. M. (2014). Effect of gamma irradiation on structural and biological properties of a PLGA-PEG-hydroxyapatite composite. *The Scientific World Journal*, 2014, 1 – 9.
- Shahat, A., Awual, M. R., & Naushad, M. (2015). Functional ligand anchored nanomaterial based facial adsorbent for cobalt (II) detection and removal from waste samples. *Chemical Engineering Journal*, 271, 155 – 163.
- Shao, D., Hou, G., Li, J., Wen, T., Ren, X., & Wang, X. (2014). PANI/GO as a super adsorbent for the selective adsorption of uranium(VI). *Chemical Engineering Journal*, 255, 604 – 612.
- Sheha, R. R., & El-Khouly, S. H. (2013). Adsorption and diffusion of cesium ions in zirconium (IV) iodomolybdate exchanger. *Chemical Engineering Research and Design*, 91, 942 – 954.
- Şimşek, S., & Ulusoy, U. (2012). Uranium and lead adsorption onto bentonite and zeolite modified with polyacrylamidoxime. *Journal of Radioanalytical and Nuclear Chemistry*, 292(1), 41 – 51.
- Sips, R. (1948). On the structure of a catalyst surface. *Journal of Chemical Physics*, 16, 490 – 495.

- Sreeprasad, T. S., Maliyekkal, S. M., Lisha, K. P., & Pradeep, T. (2011). Reduced graphene oxide-metal/ metal oxide composites: Facile synthesis and application in water purification. *Journal of Hazardous Materials*, 186, 921 – 931.
- Srivastava, V. C., Mall, I. D., & Mishra, I. M. (2006). Equilibrium modelling of single and binary adsorption of cadmium and nickel onto bagasse fly ash. *Chemical Engineering Journal*, 117(1), 79 – 91.
- Stanković, V., Božić, D., Gorgievski, M., & Bogdanović, G. (2009). Heavy metal ions adsorption from mine waters by sawdust. *Chemical Industry and Chemical Engineering Quarterly/CICEQ*, 15(4), 237 – 249.
- Steeffel, C. I., Carroll, S., Zhao, P., & Roberts, S. (2003). Cesium migration in Hanford sediment: A multisite cation exchange model based on laboratory transport experiments. *Journal of Contaminant Hydrology*, 63, 219 – 246.
- Sun, Y., Shao, D., Chen, C., Yang, S., & Wang, X. (2013). Highly efficient enrichment of radionuclides on graphene oxide-supported polyaniline. *Environmental Science and Technology*, 47, 9904 – 9910.
- Tang, Y., Ma, Q., Luo, Y., Zhai, L., Che, Y., & Meng, F. (2013). Improved synthesis of a branched poly (ethylene imine)-modified cellulose-based adsorbent for removal and recovery of Cu(II) from aqueous solution. *Journal of Applied Polymer Science*, 129(4), 1799 – 1805.
- Tang, Z., Han, Z., Yang, G., & Yang, J. (2013). Polyethylenimine loaded nanoporous carbon with ultra-large pore volume for CO₂ capture. *Applied Surface Science*, 277, 47 – 52.
- Taty-Costodes, C.R., Fauduet, H., Porte, C., & Delacroix, A. (2003). Removal of Cd(II) and Pb(II) ions, from aqueous solutions, by adsorption onto sawdust of *Pinus sylvestris*. *Journal of Hazardous Materials*, B105, 121 – 142.
- Temkin, M. I. (1941). Adsorption equilibrium and the kinetics of processes on non-homogeneous surfaces and in the interaction between adsorbed molecules. *Zhurnal Fizicheskoi Khimii*. 15, 296 – 332.
- Thammawong, C., Opaprakasit, P., Tangboriboonrat, P., & Sreearunothai, P. (2013). Prussian blue-coated magnetic nanoparticles for removal of cesium from contaminated environment. *Journal of Nanoparticle Research*, 15(6), 1 – 10.

- Thomas, W. J., & Barry, C. (1997). *Adsorption technology and design*. Oxford and Boston: Butterworth-Heinemann, Oxford, pp 24 – 27.
- Todd, T., Mann, N., Tranter, T., Šebesta, F., John, J., & Motl, A. (2002). Cesium sorption from concentrated acidic tank wastes using ammonium molybdophosphate-polyacrylonitrile composite sorbents. *Journal of Radioanalytical and Nuclear Chemistry*, 254(1), 47 – 52.
- Tseng, R. -L., Wu, F. -C., & Juang, R. -S. (2010). Characteristics and applications of the Lagergren's first-order equation for adsorption kinetics. *Journal of the Taiwan Institute of Chemical Engineers*, 41(6), 661 – 669.
- Tumin, N. D., Chuah, A. L., Zawani, N., & Rashid, S. A. (2008). Adsorption of copper from aqueous solution by *Elais Guineensis* kernel activated carbon. *Journal of Engineering Science and Technology*, 3(2), 180 – 189.
- UN (United Nations) (2012). *Managing water under uncertainty and risk*. World Water Development Report 4 Paris: UNESCO Publishing. <http://unesdoc.unesco.org/images/0021//002156/215644e/pdf>
- UN (United Nations) (2004). *World Population to 2300*. United Nations, New York. www.un.org/esa/population/publications/longrange2/WorldPop2300final.pdf
- Unsal, E., Bahar, T., Tuncel, M., & Tuncel, A. (2000). DNA adsorption onto polyethylenimine-attached poly (p-chloromethylstyrene) beads. *Journal of Chromatography A*, 898(2), 167 – 177.
- UNSCEAR (United Nations Scientific Committee on the Effects of Atomic Radiation) (2008). *Sources and effects of ionizing radiation*. United Nations Publication, New York, 1, 223 – 233.
- UNSCEAR (United Nations Scientific Committee on the Effects of Atomic Radiation) (2000). Sources and effects of ionizing radiation. In *Report to the General Assembly with Scientific Annexes*. New York: United Nations.
- USEPA (United States Environmental Protection Agency) (2007). *Radiation Risks and Realities. Office of Radiation and Indoor Air*. EPA-402-K-07-006. www.epa.gov/radiation
- Vermeer, A. W. P., McCulloch, J. K., Riemsdijk, W. H., & Koopal, L. K. (1999). Metal ion adsorption to complexes of humic acid and metal oxides: Deviations from the additivity rule. *Environmental Science and Technology*, 33, 3892 – 3897.

- Valsala, T., Roy, S., Shah, J., Gabriel, J., Raj, K., & Venugopal, V. (2009). Removal of radioactive caesium from low level radioactive waste (LLW) streams using cobalt ferrocyanide impregnated organic anion exchanger. *Journal of Hazardous Materials*, 166(2), 1148 – 1153.
- Vincent, C., Hertz, A., Vincent, T., Barré, Y., & Guibal, E. (2014). Immobilization of inorganic ion-exchanger into biopolymer foams—application to cesium sorption. *Chemical Engineering Journal*, 236, 202 – 211.
- Vincent, T., Vincent, C., & Guibal, E. (2015). Immobilization of Metal Hexacyanoferrate Ion-Exchangers for the Synthesis of Metal Ion Sorbents- A Mini-Review. *Molecules*, 20(11), 20582 – 20613.
- Wampler, W. A., Rajeshwar, K., Pethe, R., Hyer, R., & Sharma, S. (1995). Composites of polypyrrole and carbon black: Part III. Chemical synthesis and characterization. *Journal of Materials Research*, 10(07), 1811 – 1822.
- Wang, S., Li, Z., & Lu, C. (2015). Polyethyleneimine as a novel dsorbent for anionic organic dyes on layered double hydroxide surface. *Journal of Colloid and Interface Science*, 458, 315 – 322.
- Wang, G., Liu, J., Wang, X., Xie, Z., & Deng, N. (2009). Adsorption of uranium (VI) from aqueous solution onto cross-linked chitosan. *Journal of Hazardous Materials*, 168(2), 1053 – 1058.
- Wang, J., & Chen, C. (2014). Chitosan-based biosorbents: Modification and application for biosorption of heavy metals and radionuclides. *Bioresource Technology*, 160, 129 – 141.
- Wang, S., Boyjoo, Y., Choueib, A., & Zhu, Z. H. (2005). Removal of dyes from aqueous solution using fly ash and red mud. *Water Research*, 39, 129 – 138.
- Weidlich, C., Mangold, K. -M., & Jüttner, K. (2001). Conducting polymers as ion-exchangers for water purification. *Electrochimica Acta*, 47(5), 741 – 745.
- WHO (2010). *Preventing diseases through healthy environments. Exposure to cadmium: A major public health concern*. World Health Organization. Retrieved April 15, 2016.
- WHO (2008). *Guidelines for drinking-water quality (electronic resource): incorporating 1st and 2nd addenda, vol. 1, recommendation*. World Health Organization. Retrieved May 30, 2017.

- Wojnárovits, L., Földváry, C. M., & Takács, E. (2010). Radiation-induced grafting of cellulose for adsorption of hazardous water pollutants: A review. *Radiation Physics and Chemistry*, 79(8), 848 – 862.
- Worch, E. (2012). *Adsorption technology in water treatment: Fundamental, processes and modelling*. Water de Gruyter GmbH & Co. KG, Berlin/ Boston.
- Wu, J., Xu, Q., & Bai, T. (2007). Adsorption behavior of some radionuclides on the Chinese weathered coal. *Applied Radiation and Isotopes*, 65, 901 – 909.
- Xin, Q., Fu, J., Chen, Z., Liu, S., Yan, Y., Zhang, J., & Xu, Q. (2015). Polypyrrol nanofibers as a high-efficient adsorbent for the removal of methyl orange from aqueous solution. *Journal of Environmental and Chemical Engineering*, 3, 1637 – 1647.
- Xiong, P., Chen, Q., He, M., Sun, X., & Wang, X. (2012). Cobalt ferrite-polyaniline heteroarchitecture: a magnetically recyclable photocatalyst with highly enhanced performances. *Journal of Materials Chemistry*, 22(34), 17485 – 17493.
- Yagub, M. T., Sen, T. K., Afroze, S., & Ang, H. M. (2014). Dye and its removal from aqueous solution by adsorption: a review. *Advances in Colloid and Interface Science*, 209, 172 – 184.
- Yang, L., Wu, S., & Chen, J. P. (2007). Modification of activated carbon by polyaniline for enhanced adsorption of aqueous arsenate. *Industrial and Engineering Chemistry Research*, 46(7), 2133 – 2140.
- Yang, S., Shao, D., Wang, X., Hou, G., Nagatsu, M., Tan, X., . . . , & Yu, J. (2015). Design of chitosan-grafted carbon nanotubes: evaluation of how the -OH functional group affects Cs⁺ adsorption. *Marine Drugs*, 13(5), 3116 – 3131.
- Yao, T., Cui, T., Wu, J., Chen, Q., Lu, S., & Sun, K. (2011). Preparation of hierarchical porous polypyrrole nanoclusters and their application for removal of Cr(VI) ions in aqueous solution. *Polymer Chemistry*, 2(12), 2893 – 2899.
- Yiacoumi, S., & Tien, C. (1995). Modeling adsorption of metal ions from aqueous solutions: I. Reaction-controlled cases. *Journal of Colloid and Interface Science*, 175(2), 333 – 346.
- Yürüm, A., Kocabas-Atakli, Z. Ö., Sezen, M., Semiar, R., & Yürüm, Y. (2014). Fast deposition of porous iron oxide on activated carbon by microwave heating and arsenic (V) removal from water. *Chemical Engineering Journal*, 242, 321 – 332.

- Zakharchenko, E., Mokhodoeva, O., Malikov, D., Molochnikova, N., Kulyako, Y., & Myasoedova, G. (2012). Novel sorption materials for radionuclide recovery from nitric acid solutions: solid-phase extractants and polymer composites based on carbon nanotubes. *Procedia Chemistry*, 7, 268 – 274.
- Zerriffi, H. (2000). *IEER Report: Transmutation- Nuclear Alchemy Gamble (Report)*. Institute for Energy and Environmental Research. Retrieved April 15, 2016.
- Zhang, L. I., Zhao, L. I., Yu, Y., & Chen, C. (1998). Removal of lead from aqueous solution by non-living *Rhizopus nigricans*. *Water Research*, 32(5), 1437 – 1444.
- Zhang, X., & Bai, R. (2002). Adsorption behavior of humic acid onto polypyrrole-coated nylon 6, 6 granules. *Journal of Materials Chemistry*, 12(9), 2733 – 2739.
- Zhang, Q., Pan, B., Pan, B., Zhang, W., Jia, K., & Zhang, Q. (2008). Selective sorption of lead, cadmium and zinc ions by a polymeric cation exchanger containing nano-Zr (HPO₃S)₂. *Environmental Science and Technology*, 42(11), 4140 – 4145.
- Zhang, Y., Li, Q., Sun, L., Tang, R., & Zhai, J. (2010). High efficient removal of mercury from aqueous solution by polyaniline/humic acid nanocomposite. *Journal of Hazardous Materials*, 175(1), 404 – 409.
- Zhao, Z. -Q., Chen, X., Yang, Q., Liu, J. -H., & Huang, X. -J. (2012a). Beyond the selective adsorption of polypyrrole-reduced graphene oxide nanocomposite toward Hg²⁺: Ultra-sensitive and-selective sensing Pb²⁺ by stripping voltammetry. *Electrochemistry Communications*, 23, 21 – 24.
- Zhao, Z. -Q., Chen, X., Yang, Q., Liu, J. -H., & Huang, X.-J. (2012b). Selective adsorption toward toxic metal ions results in selective response: electrochemical studies on a polypyrrole/reduced graphene oxide nanocomposite. *Chemical Communications*, 48(16), 2180 – 2182.
- Zhao, Y. G., Shen, H. Y., Pan, S. D., & Hu, M. Q. (2010). Synthesis, characterization and properties of ethenediamine Fe₃O₄ magnetic polymers for removal of Cr(VI) in wastewater. *Journal of Hazardous Materials*, 182(1-3), 295 – 302.
- Zhu, Y., Hu, J., & Wang, J. (2014). Removal of Co²⁺ from radioactive wastewater by polyvinyl alcohol (PVA)/chitosan magnetic composite. *Progress in Nuclear Energy*, 71, 172 – 178.

Zoleikani, L., Issazadeh, H., & ZareNezhad, B. (2015). Preparation of new conductive polymer nanocomposites for cadmium removal from industrial wastewaters. *Journal of Chemical Technology and Metallurgy*, 50, 71 – 80.

University of Malaya

LIST OF PUBLICATIONS AND PAPERS PRESENTED

LIST OF PUBLICATIONS RELATED TO THIS RESEARCH

1. **Olatunji, M.A.**, Khandaker, M.U., Amin, Y.M., & Mahmud, H.N.M.E. (2016). Cadmium-109 Radioisotope Adsorption onto Polypyrrole Coated Sawdust of *Dryobalanops aromatic*: Kinetic and Adsorption Isotherms Modelling. *PLOS ONE* 11(10). doi:10.1371/journal.pone.0164119
2. **Olatunji, M.A.**, Khandaker, M.U., Amin, Y.M., & Mahmud, H.N.M. (2016). Development and Characterization of Polypyrrole-Based Nanocomposite Adsorbent and Its Applications in Removal of Radioactive Materials. In Ibrahim, F. et al. (eds.). *IFMBE Proceedings*, 56, 30 – 35.
3. **Olatunji, M.A.**, Khandaker, M.U., & Mahmud, H.N.M.E. (2015). Influence of adsorption parameters on cesium uptake from aqueous solutions- a brief review. *RSC Advances*, 5, 71658 – 71683.

OTHER PUBLICATIONS DURING THE RESEARCH STUDY

1. Khandaker, M.U., Nasir, N.L.M., Asaduzzaman, Kh., **Olatunji, M.A.**, Amin, Y.M., Kassim, H.A.,, & Alrefae, T. (2016). Evaluation of radionuclides transfer from soil-to-edible flora and estimation of radiological dose to the Malaysian populace. *Chemosphere*, 154, 528-536.
2. Uwatse, O.B., **Olatunji, M.A.**, Khandaker, M.U., Amin, Y.M., Bradley, D.A., Alkhorayef, M., & Alzimami, K. (2015). Measurement of Natural and Artificial Radioactivity in Infant Powdered Milk and Estimation of the Corresponding Annual Effective Dose. *Environmental Engineering Science*, 32, 838 – 846.

3. Khandaker, M.U., **Olatunji, M.A.**, Shuib, K.S.K., Hakimi, N.A., Nasir, N.L.M., Asaduzzaman, Kh., ..., & Kassim, H.A. (2015). Natural radioactivity and effective dose due to the bottom sea and estuaries marine animals in the coastal waters around Peninsular Malaysia. *Radiation Protection Dosimetry*, 1 – 5. doi:10.1093/rpd/ncv243
4. Uwatse, O.B., **Olatunji, M.A.**, Khandaker, M.U., Amin, Y.M., Rahman, F.A., Thian-Khok, Y.,, & Horng-Sheng, L. (2015). Radiation dose to Malaysian infants from natural radionuclides via consumption of powdered Milk. *American Institute of Physics*, 1657, 120002.
5. **Olatunji, M.A.**, Uwatse, O.B., Khandaker, M.U., Amin, Y.M, & Faruq, G. (2014). Radiological study on newly developed composite corn advance lines in Malaysia. *Physica Scripta*, 89, 125002. <http://stacks.iop.org/1402-4896/89/125002>

LIST OF PAPERS PRESENTED AT INTERNATIONAL CONFERENCES

1. Removal of radioactive cobalt from low level radioactive waste effluents by modified electroactive conducting polymer: Effect of γ -irradiation on polymer capacity. Paper presented at the Innovation of Radiation Applications, University of Wollongong, Australia on April 20-22, 2017.
2. Remediation of radionuclides in wastewater by conducting polymer. Paper presented at the International Conference on Waste Management and Environment, Kuala Lumpur, Malaysia on August 20-22, 2015.
3. Development and Characterization of polypyrrole-based nanocomposite adsorbent and applications in the removal of radioactive materials. Paper presented at the International Conference for Innovation in Biomedical Engineering and Life Sciences, Putrajaya, Malaysia on December 6-8, 2015.